

View Article Online
View Journal

Journal of Materials Chemistry A

Materials for energy and sustainability

Accepted Manuscript

This article can be cited before page numbers have been issued, to do this please use: R. Al Hussami, M. Ghavipour, G. Nasser, C. Duah, S. Yousef and J. Kopyscinski, *J. Mater. Chem. A*, 2025, DOI: 10.1039/D5TA05195A.



This is an Accepted Manuscript, which has been through the Royal Society of Chemistry peer review process and has been accepted for publication.

Accepted Manuscripts are published online shortly after acceptance, before technical editing, formatting and proof reading. Using this free service, authors can make their results available to the community, in citable form, before we publish the edited article. We will replace this Accepted Manuscript with the edited and formatted Advance Article as soon as it is available.

You can find more information about Accepted Manuscripts in the <u>Information for Authors</u>.

Please note that technical editing may introduce minor changes to the text and/or graphics, which may alter content. The journal's standard <u>Terms & Conditions</u> and the <u>Ethical guidelines</u> still apply. In no event shall the Royal Society of Chemistry be held responsible for any errors or omissions in this Accepted Manuscript or any consequences arising from the use of any information it contains.



A Review of Methanol-to-Olefins Conversion over SAPO-34: Catalyst Design, Mechanisms, and Kinetics

Ralph Al Hussami a, Mohammad Ghavipour a, Galal Nasser, Chasty Duah, Shaza Yousef, and Jan Kopyscinski b

Department of Chemical Engineering, McGill University, 3610 University Street, Montreal, Quebec H3A 0C5, Canada

^a Equal contribution resulting in co-first authorship of persons involved.

^b To whom all correspondence should be addressed:

Tel.: +1 514 398 4276

jan.kopyscinski@mcgill.ca

Abstract

The methanol-to-olefins (MTO) process has gained significant attention as a promising alternative for light olefin production, particularly because traditional methods are energy-intensive and rely on a limited number of feedstocks. Methanol, on the other hand, is both abundant and can be sustainably derived, supporting the concept of a closed carbon cycle. This literature review combines three decades of key developments in the MTO process, with a focus on the role of SAPO-34, the catalyst which plays a critical part in achieving high selectivity for ethylene and propylene. The review begins by comparing the MTO process with existing olefin production technologies, followed by an overview of how the reaction mechanisms have developed over time, from early-stage concepts to the widely accepted hydrocarbon pool model. Kinetic models developed to describe the complex reactions involved in the MTO process are also examined. A significant part of this review is placed on catalyst design, including strategies for enhancing SAPO-34 performance through structural modifications, metal incorporation, and shaping techniques aimed at extending the catalyst's lifespan. This comprehensive review provides insights intended to inform future advancements in the efficiency and sustainability of MTO-based industrial applications.

Open Access Article. Published on 22 2025. Downloaded on 30.10.2025 01:47:29. -No This article is licensed under a Creative Commons Attribution-NonCommercial 3.0 Unported Licence.

Table of Contents

Abstract		
1	Introduction	4
2	MTO process	10
2.1	Process description & process flow diagram	10
2.2	MTO products and coke evolution	11
2.3	Reactor operating conditions	13
3	MTO reaction and deactivation pathways	15
3.1	Early studies: initial stages of light olefin production	16
3.1.1	Oxonium ylide mechanism	16
3.1.2	Carbene mechanism	17
3.1.3	Carbocationic mechanism	18
3.1.4	Free radical mechanism	19
3.1.5	Alkoxy chain growth route	20
3.2	Current studies: the 'hydrocarbon pool' concept	21
3.2.1	The Aromatic Cycle: The formation of polyalkylaromatics	22
3.2.2	The Aromatic Cycle: Mechanisms for light olefin formation	24
3.2.3	Evolution of Mechanistic Understanding & Developments	26
3.3	Deactivation pathways	34
3.4	Limitations of mechanistic studies	36
3.5	MTO reaction and deactivation kinetics	36
3.5.1	Limitations of the current kinetic approaches	40
4	Catalyst design and modification	45
4.1	Introduction to SAPO-34	45
4.2	Comparison of SAPO-34 vs. Other Zeolites	48
4.3	Characterization of SAPO-34	50
4.4	Synthesis of SAPO-34	54
4.4.1	Standard synthesis approach	54
4.4.2	Influence of Template	57
4.4.3	Influence of Silicon Content	62

4.4.4	Sub-micron SAPO-34 synthesis	
4.5	Hierarchical SAPO-34 synthesis by pre- and post-treatment methods	
4.5.1	Overview	71
4.5.2	Soft Template Addition	72
4.5.3	Hard Template Addition	73
4.5.4	Post-Treatment Desilication	75
4.6	Metal Promotion	77
4.7	Shaping of SAPO-34 Catalyst	86
4.8	Catalyst Design from an Industrial Perspective	89
5	Sustainability of Olefin Production Methods	92
5.1	Catalytic Efficiency for Emissions Abatement	92
5.2	LCA Considerations in Olefin Production	93
5.3	Cradle-to-Gate LCA Findings in Olefin Production	94
5.4	Energy Requirements in Olefin Production	97
5.5	Water Usage & Other Impact Categories in Olefin Production	98
6	Future Opportunities	101
7	Conclusion and Outlook	105
8	List of Abbreviations	108
Author Contributions		113
Conflicts of interest		113
Data Availability		
Acknowledgements		
References		

1 Introduction

Light olefins (ethylene and propylene) are often considered one of the key feedstocks for the petrochemical industry. These components take on the role as building blocks and are normally polymerized to form polyethylene and polypropylene, respectively ¹. The significant value of light olefins in today's society is due to the wide range of their derivatives' applications, including packaging, construction, synthetic fibers and coatings ². In terms of market trends, the demand for light olefins has escalated significantly in recent years (see Figure 1(A)). Fortifying this surge in the light olefins market, future projections seem to portray an even further intensified expansion, which further highlights the need to generate these valuable petrochemical products. Studies estimate that this market will achieve a compound annual growth rate of 5.58% by 2030, capable of generating a revenue of roughly 475.8 million US dollars in this timeframe ³.

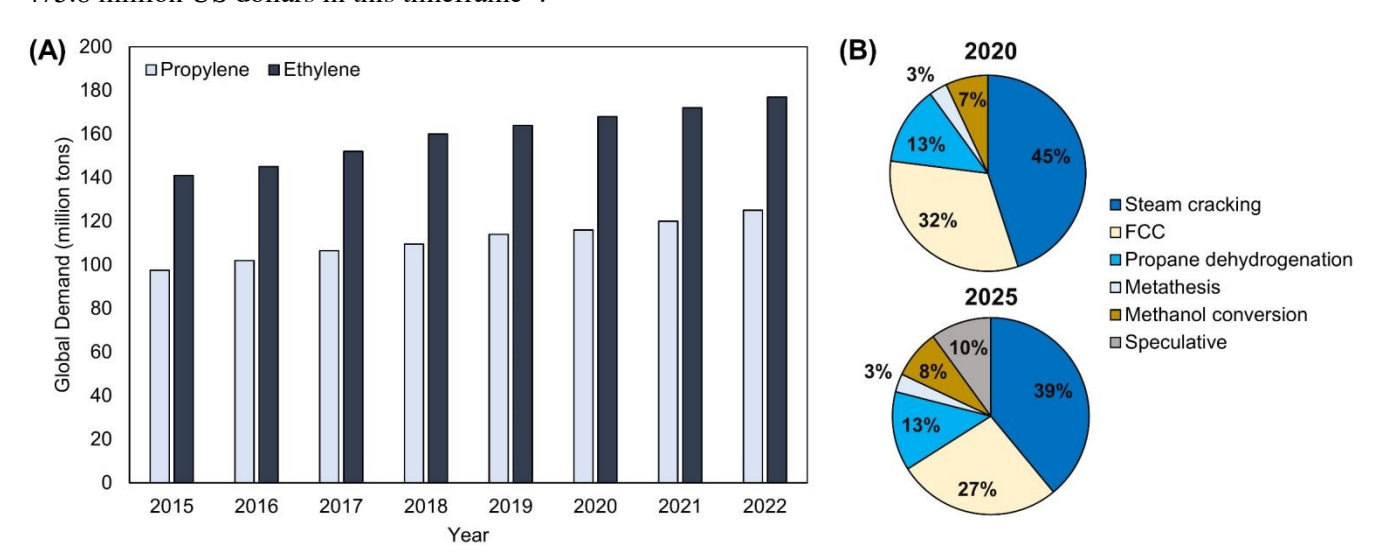


Figure 1 (A) Global ethylene and propylene demand (consumption) from 2015 to 2022. Adapted from reference ^{4,5} with permission from Statista, Copyright 2025. (B) Contribution of different processes towards global propylene production in early 2020 and end of 2025 (projected) ^{6,7}.

Light olefin production can occur through a wide array of different processes and technologies, however, traditional methods such as thermal (steam) cracking (SC) and fluid catalytic cracking (FCC) of hydrocarbons still remain the pillars of today's light olefin production industry (as seen in Figure 1(B), in the case of propylene production) ⁸. Steam cracking, the dominant technology in light olefin production (contributing to 30-50% of total global demand) ^{6,7,9–11} can have various feedstocks that are diluted with steam and undergo thermal decomposition/ pyrolysis at ~850 °C (at normal pressure of ~1.65 bar) in a tubular furnace and in the absence of oxygen ^{12,13}. The products subsequently formed via steam cracking are largely dependent on the choice of feedstock (as seen in Figure 2(A)) as well as reaction conditions. Typically, the conversion lies between 70 to ~95% for the different available feedstocks ¹⁴, where light compounds, like ethane, are more difficult to be cracked and possess a lower conversion. Pyrolysis gas (which contains primarily H₂, CH₄, CO and CO₂) contributes to a roughly 10-25 wt.%

yield amongst products 15 ; hence, steam cracking units remains a heavy threat to the environment, as they are responsible for the emission of more than 300 million tons of CO_2 per annum 16 .

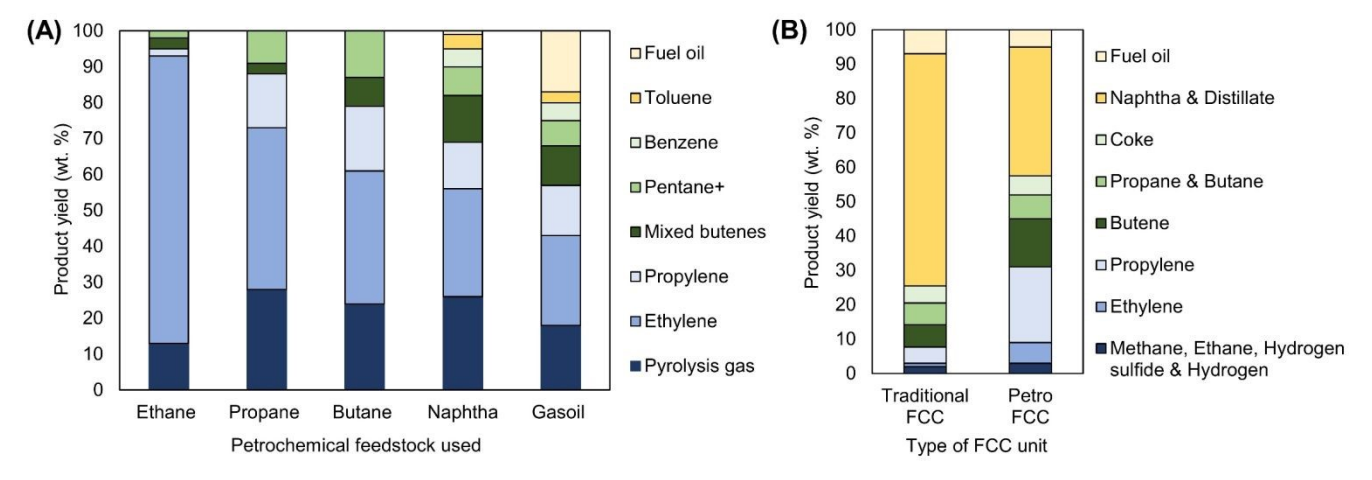


Figure 2 (A) Steam cracking product distribution (yield) for different petrochemical feedstock. Adapted from reference ¹⁷ with permission from Springer Nature, Copyright 2015. (B) Traditional FCC and PetroFCC product yields using VGO feedstock ¹⁸.

Fluid catalytic cracking (FCC), on the other hand, requires operating conditions of lesser severity (a lower reaction temperature of roughly 500 to 650 °C) due to the use of catalytic materials ¹⁹. The process can be manipulated to maximize gasoline, middle distillate, liquified petroleum gas (LPG), or lighter compounds by alteration of the feedstock used, type of catalyst, and operating conditions ²⁰. Nevertheless, it should be noted that, even if the process was adjusted to maximize the production of light compounds (e.g., by using technology licensed by UOP termed PetroFCC), the light olefin yield would still be in the range of 20 to 30 wt% ²¹ (see Figure 2 (B)). Besides the low yield of light olefins, another disadvantage associated with FCC could be substantial coke formation (4 to 6 wt%) that instigates rapid catalyst deactivation ²². Evidently, coke removal in the regenerator to reactivate the catalyst coincides with substantial CO₂ emissions.

Another process is dehydrogenation of ethane and propane, which requires the use of a hybrid catalyst – one that possesses both Brønsted and Lewis acidic sites (e.g. promoted platinum-based zeolite catalysts and promoted chromium-oxide) 23,24 . These processes typically take place between 535 and 650 °C, under pressures of 0.3 to 6 bar 25 . The maximum conversion of propane and ethane in industry are typically around 65% and 20%, respectively, with a selectivity of roughly 90% for propylene and ethylene (notable side products are methane, CO, and CO₂) 26,27 . Overall, the constraints of these processes include the use of costly and environmentally harmful catalysts, high energy consumption, thermodynamic limitations leading to low single-pass conversion, and restricted availability of feedstocks 28 .

In general, other than the disadvantages enumerated, since the available resources for these traditional cracking and light alkane dehydrogenation processes are limited and non-renewable (relying on either crude oil fractions or gas condensate (C_2^+)), these production routes would eventually have to be substituted. As a result, researchers are

continuing to look for alternative routes to synthesize light olefins, particularly those that possess a greater abundancy of resources and even renewable ones. Methanol to light olefins (MTO) process has started to become more commercially adopted worldwide in recent years, as the feed, methanol, can be generated from a wide range of different carbonaceous resources ^{29,30}. Natural gas reserves (154.7 billion metric tons available as of 2017 ³¹, which contain ~85 to 97% methane) and gas hydrate reservoirs (3000 billion metric tons, with an assumed 17 to 20% recovery rate, containing roughly 95 to 99% methane ^{32–34}), can be converted to syngas, and then ultimately to methanol for use in the MTO process. Reflecting on only methane as a feedstock (derived from either hydrate or natural gas), there are 10 times greater available resources for MTO compared to the ones for cracking and dehydrogenation processes ^{35,36}. Recently, much research has also been allotted towards investigating sustainable methanol production through both the direct and indirect conversion of carbon dioxide ^{37–40}. The indirect conversion of CO₂ to methanol has even been commercialized, with the first plant (George Olah) being introduced in Iceland in 2011 ^{41,42}.

Other than CO₂-derived methanol production, the development of green technologies revolving around a closed-loop carbon cycle has also added to the appeal of the MTO process. Carbon recycling in this context pertains to the indirect conversion of plastic wastes to methanol. Initially, plastic wastes are converted to synthetic gas via steam-reforming or partial oxidation, followed by the subsequent conversion of syngas to methanol, which ultimately can be utilized in the MTO process ⁴³. Furthermore, the promotion of carbon recycling can in turn help address the global waste management dilemma (especially with ever rising landfill sites and the negative environmental effects associated with incineration). It should be noted that a multitude of start-up firms have begun to take on the initiative of converting municipal solid waste (and residual biomass) into biofuels, methanol, and other value-added renewable chemicals ⁴⁴. With the aid of these feasible pathways for converting abundant resources to methanol, this value-added chemical has experienced an upsurge in production worldwide (Figure 3(A)) ⁴⁵. Subsequently, to further convert methanol to chemicals in even higher demand, Figure 3(B) demonstrates that the MTO process ranked as the highest consumption pathway of produced methanol globally (in 2021). This has led to the establishment of the MTO process in the petrochemical industry within the last two decades, contributing ~7% of global light olefin generation (see Figure 1(B)).

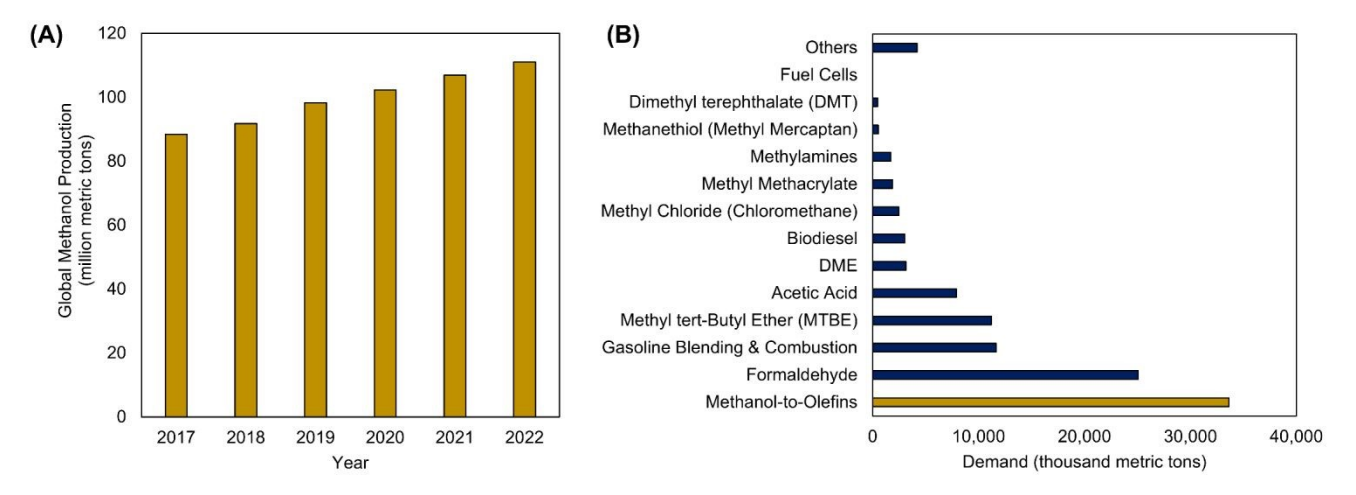


Figure 3 (A) Global methanol production between 2017 and 2022. (B) Global methanol demand by application in 2021. Adapted from reference ^{45,46} with permission from Statista, Copyright 2025.

The commercial introduction of the MTO process was first achieved by Union Carbide in 1981 ⁴⁷ by alteration of the catalyst of the methanol to gasoline process (MTG) (introducing exceptional shape-selective SAPO-34 as opposed to ZSM-5). The technology adopted by this research group, which is now patented by the Honeywell UOP/Norsk Hydro joint venture, remains the current most prevalent industrially-implemented MTO technology ⁴⁷. As of yet, SAPO-34 remains the most frequently used catalyst for the process, since it seems to drive peak catalytic performance relative to all other examined silicoaluminophosphate catalysts (as observed in Figure 4) ⁴⁸. Under optimal MTO reaction conditions, SAPO-34's relatively small pores (3.7 Å) ⁴⁹, medium acidity (~ 1 mmol g⁻¹) ⁵⁰⁻⁵² and high thermal stability (up to 1000 °C) ^{53,54} have been recognized as the key reasons for high initial feed conversion (~100%) and high selectivity towards light olefins (~80% total of C_2 ⁼ and C_3 ⁼) ⁵⁵⁻⁵⁷. The rather small pore size of SAPO-34 inhibits the diffusion of large hydrocarbon species out of the framework, with only smaller sized hydrocarbons (mainly light olefins) being capable of diffusing out of SAPO-34's cages, evidently explaining the selectivity towards these species.

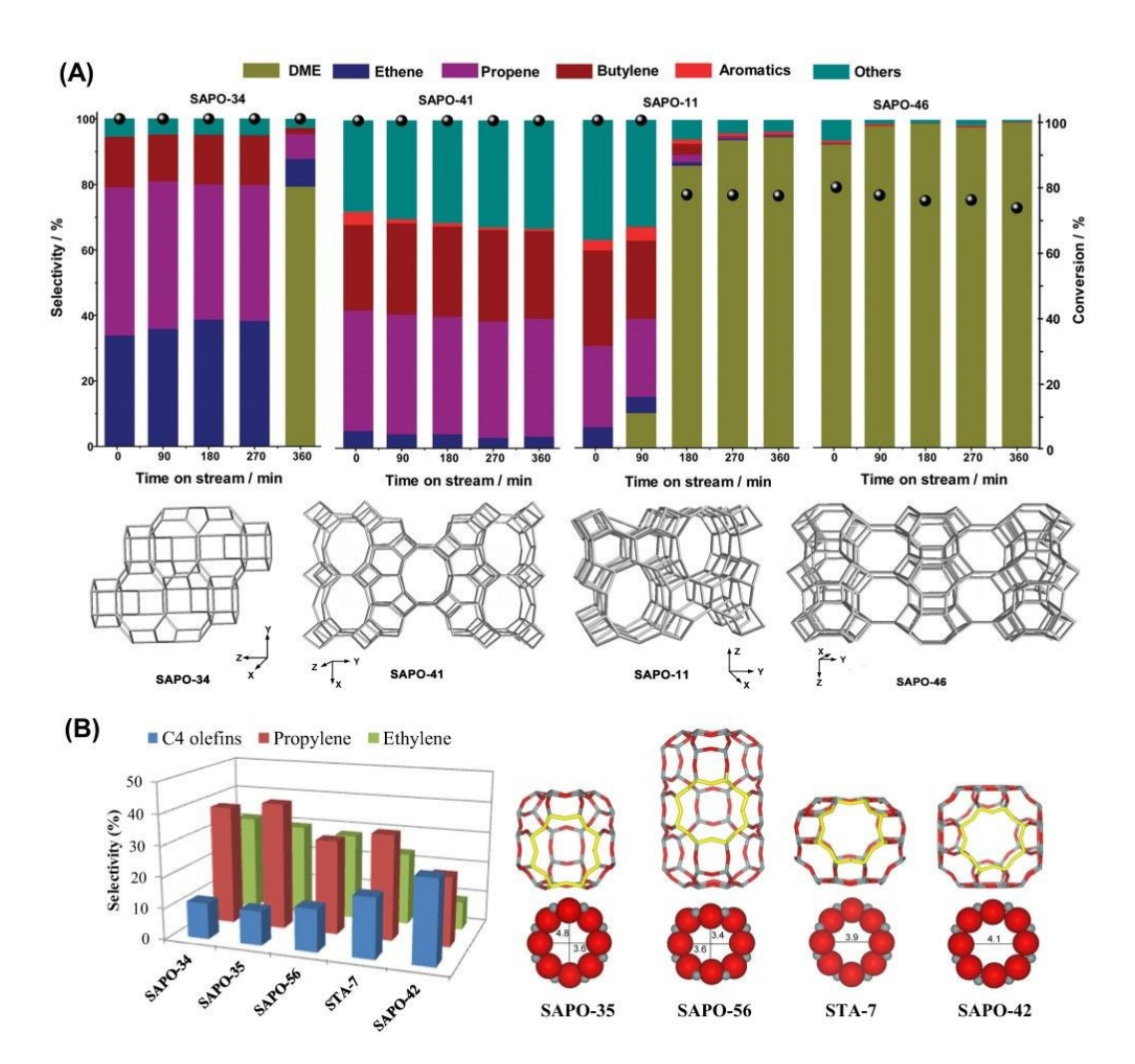


Figure 4 Product distribution obtained by application of different silicoaluminophosphate catalysts (alongside their topology structure) in the MTO reaction. (A) Parent SAPO-34 compared to SAPO-41, SAPO-11, and SAPO-46. Reaction conditions: T = 450 °C, p = 1 atm and Weight Hourly Space Velocity (WHSV) = 1 g_{MEOH} g_{Cat}^{-1} h^{-1} . Reproduced from reference ⁵⁸ with permission from American Chemical Society, Copyright 2015. (B) Parent SAPO-34 compared to SAPO-35, SAPO-56, STA-7 and SAPO-42. Reaction conditions: T = 400 °C, p = 1 atm, WHSV = 0.35 g_{MEOH} g_{Cat}^{-1} h^{-1} . Reproduced from reference ⁵⁹ with permission from Elsevier, Copyright 2017.

In terms of drawbacks, one major issue that still exists is the rather short catalyst lifetime that SAPO-34 encounters. Over time on stream, it has been experimentally validated that large multi-ring aromatic species (termed coke) build up inside and on the outer surfaces of the framework. These species block catalyst pores and in turn inhibit the diffusion of molecules, resulting in catalyst deactivation ^{60,61}. However, a variety of strategies at the lab scale (such as those discussed in Section 4) have been investigated to try and resolve this problem of pore blockage.

SAPO-34 is generally described as having "good hydrothermally stability", however studies show that prolonged exposure to steam at elevated temperatures gradually weaken its framework through hydrolysis of Si-O-Al and P-O-Al bonds⁶². Initially, the hydrolysis begins reversibly even at ambient temperature and extends into the MTO range (300 to%500 °C) ⁶³. Long-term exposure to moisture eventually causes irreversible hydrolysis, leading to

dealumination or desilication, loss of acidity, the formation of silanol defects, and in severe cases partial collapse or amorphization of the structure. Interestingly, coke deposits that form during the MTO cycle can temporarily protect the framework by shielding Brønsted acid sites from water, although they also block the pores and cause deactivation ^{62,64}.

Multiple studies identify critical temperatures where SAPO-34 stability rapidly decline. At around 400 °C, which is already within the MTO operating window, reversible hydrolysis sets in, and with time the framework starts to degrade. At higher temperatures, however, controlled steaming can have a stabilizing effect. Treatments at or above about 550 °C cause silicon to migrate within the lattice, which preserves microporosity and strengthens resistance to hydrolysis ⁶⁵. In contrast, steaming at lower temperatures such as at 400 °C can severely damage nanocrystalline SAPO-34. Beyond 700-800 °C, dealumination becomes extensive and the microporous structure collapses, while above 1000 °C the framework completely amorphizes into a glass-like state ^{66,67}.

These structural changes directly affect catalytic performance. Hydrolysis and dealumination reduce the number of active Brønsted sites, lowering conversion activity, while pore collapse hinders diffusion and accelerates coke-induced deactivation ⁶². To address these issues, several strategies have been developed. Controlled high temperature steaming at 550-600 °C can improve hydrothermal stability by restructuring the silicon environment. Acid-site passivation techniques such as silylation or temporary ammonia treatment reduce the vulnerability of framework bonds to hydrolysis ^{68,69}. Incorporating metal oxides like indium oxide, ceria, or magnesium into SAPO-34 has proven effective in redistributing acidity, creating mesoporosity, suppressing coke, and thereby extending catalyst lifetime and olefin selectivity ⁷⁰. Morphological engineering, such as synthesizing hierarchical or nanosized SAPO-34 (discussed in Section 4.4) can alleviate diffusion limitations and slow coking, though this often comes at the expense of intrinsic framework stability. On the operational side, strategies like mild water cofeeding and carefully controlled regeneration are used to moderate coke deposition and limit steam-induced degradation ⁶².

To date, research is continuously being allocated towards the redesign and modification of the catalyst in the hope of mitigating its short lifetime. Figure 5 demonstrates the surge in research that has been allocated towards MTO process over the last 30 years, which can project both the importance and emergence of this process as a means for sustainable light olefins production.

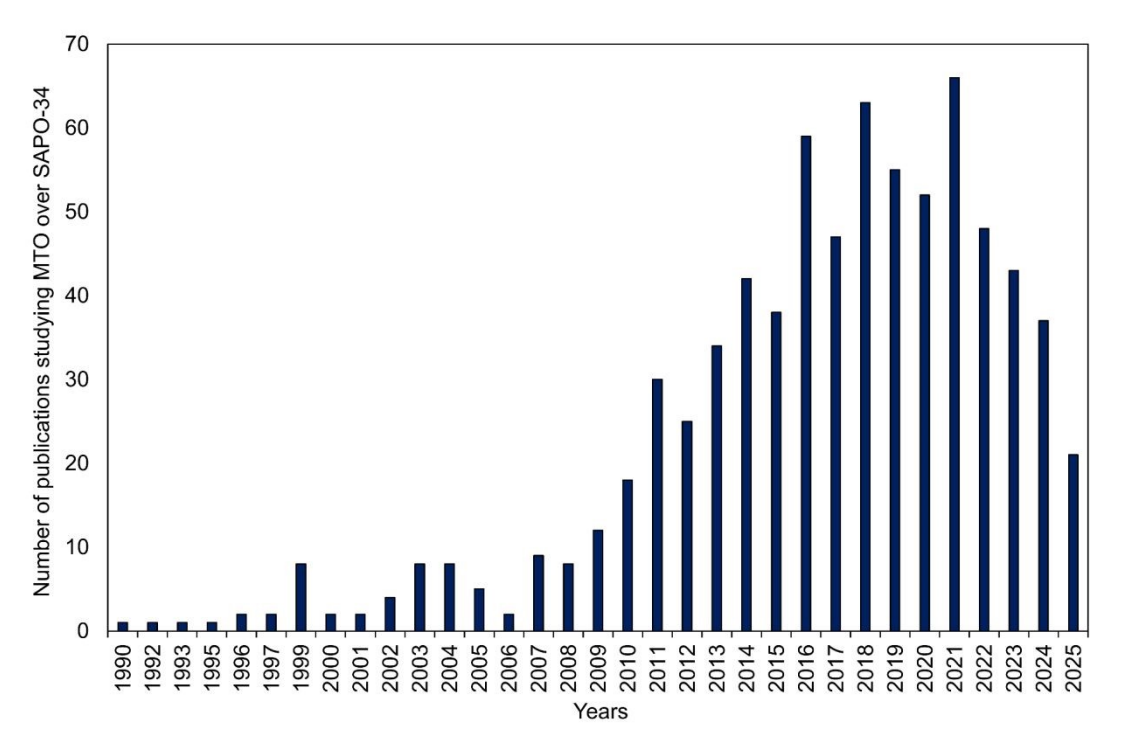


Figure 5 Number of publications related to methanol conversion to light olefins over SAPO-34 published per year from 1990 to 2025. Data collected from the Web of Science Core Collection⁷¹.

A bibliometric mapping image (Figure 6) has been formulated to decipher the most prominent terms and themes present in MTO-related articles between the years of 1999 and mid-2025. The size of the circles in the schematic correlates with the number of occurrences of a term. It seems there are two distinct clusters that correspond to (i) SAPO-34 synthesis and characterization (blue) and (ii) reaction and mechanistic studies (purple). The "reactor" seems to act as the interlinking concept between these cluster topics. The rationale lies in the fact that no matter whether a group is developing the catalyst's synthesis or studying the reaction mechanism and kinetics, conducting the activity test using a reactor is a vital step.

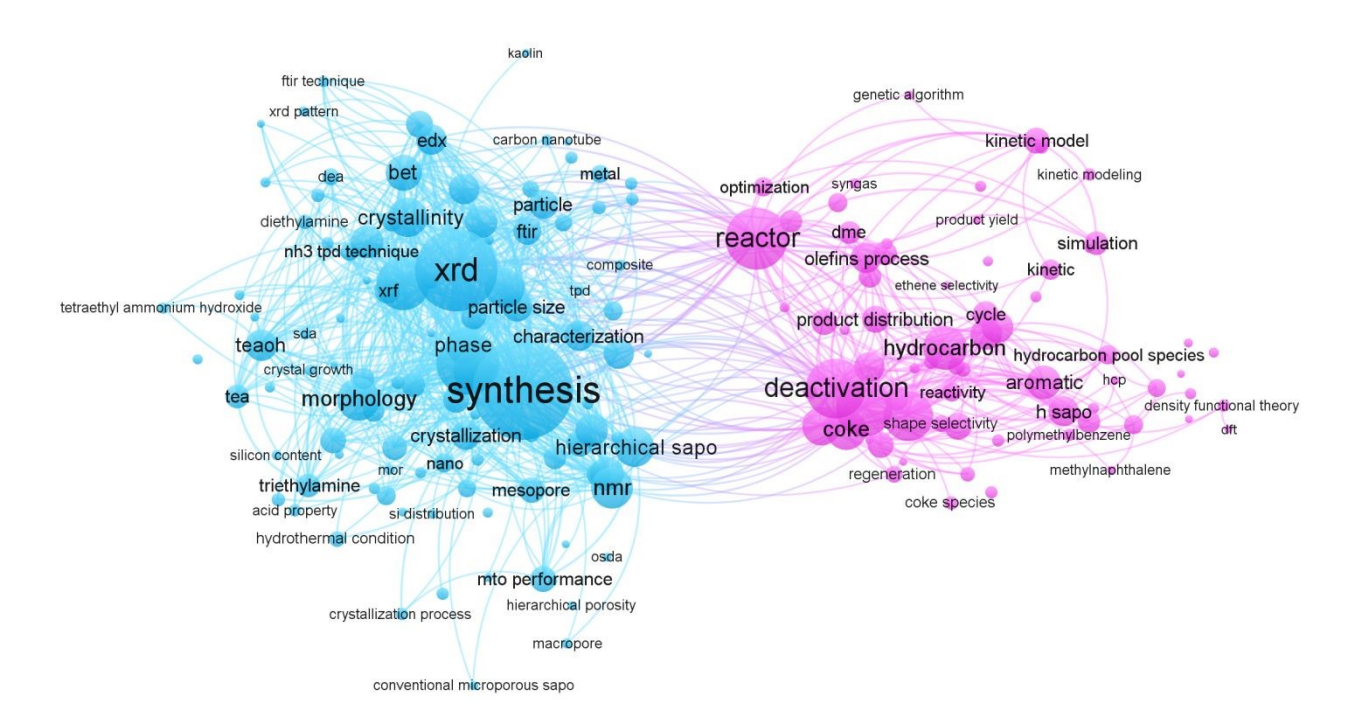


Figure 6 Bibliometric map generated by VOSviewer 72, based on 669 articles (keywords "MTO" and "SAPO-34") from the Web of Science Core Collection 71.

Considering all the justifications mentioned in the introduction regarding the importance of this process, alongside the extensive attention that has been brought to this topic from researchers worldwide in the last three decades (Figure 5), we were encouraged to conduct a comprehensive literature review on all the important aspects of this process. In the following sections, the literature review will be dedicated specifically to methanol conversion to light olefins over SAPO-34 catalyst. In detail, we will commence with a description of the process and the operating conditions that influence it, followed by an analysis of the reaction mechanism and deactivation pathways, reaction kinetics, and catalyst design and modification.

2 MTO process

2.1 Process description & process flow diagram

The simplified process flow diagram of the methanol conversion to light olefins process, based on the technology developed by the Honeywell UOP/Norsk Hydro joint venture, has been presented in Figure 7. Methanol diluted with 20 wt.% water is being warmed and vaporized by recovering heat from reactor effluent in E-101 heat exchanger. The methanol feed then passes through the feed distributor and fluidizes the fresh catalyst coming back from the regenerator. The regenerated catalyst (having a temperature of about 600 °C) heats up the feed to the reaction temperature (around 410 °C). The MTO reaction takes place in the reactor riser, and gaseous products along with the fluidized catalyst particles enter the disengagement section of the reactor. The higher cross-sectional

area of this section causes an instant drop in the gas velocity, which in turn triggers the fall of most of the catalyst into the dense phase catalyst section known as the catalyst inventory. A small portion of the catalyst, that is entrained in the gas phase, will be separated using multiple successive cyclones. Simultaneously, a portion of the catalyst is being transported to the generator to burn the partial coke formed via air. The reactor effluent is quenched (to remove the water and unreacted methanol) and then compressed to be directed to products separation and purification units. After caustic wash (to remove carbon dioxide) and drying (to remove the moisture), the gas passes through the de-ethanizer where ethylene, ethane, and lighter compounds are being separated from heavier ones. After the acetylene converter, the fuel gas (methane and hydrogen) will be removed, followed by ethylene purification. In the heavy compounds section, high-purity propylene is being produced, where C₄+ species are being sent to the olefin cracker to enhance the overall light olefin yield of the process ⁷³. The basic MTO process can yield 75-80% (carbon-based) ethylene plus propylene, 2-5% coke, 2-5% alkanes, and 0.5-1.0% Dimethyl Ether (DME), where the olefin cracker can improve the light olefin yield up to an extra 10%.

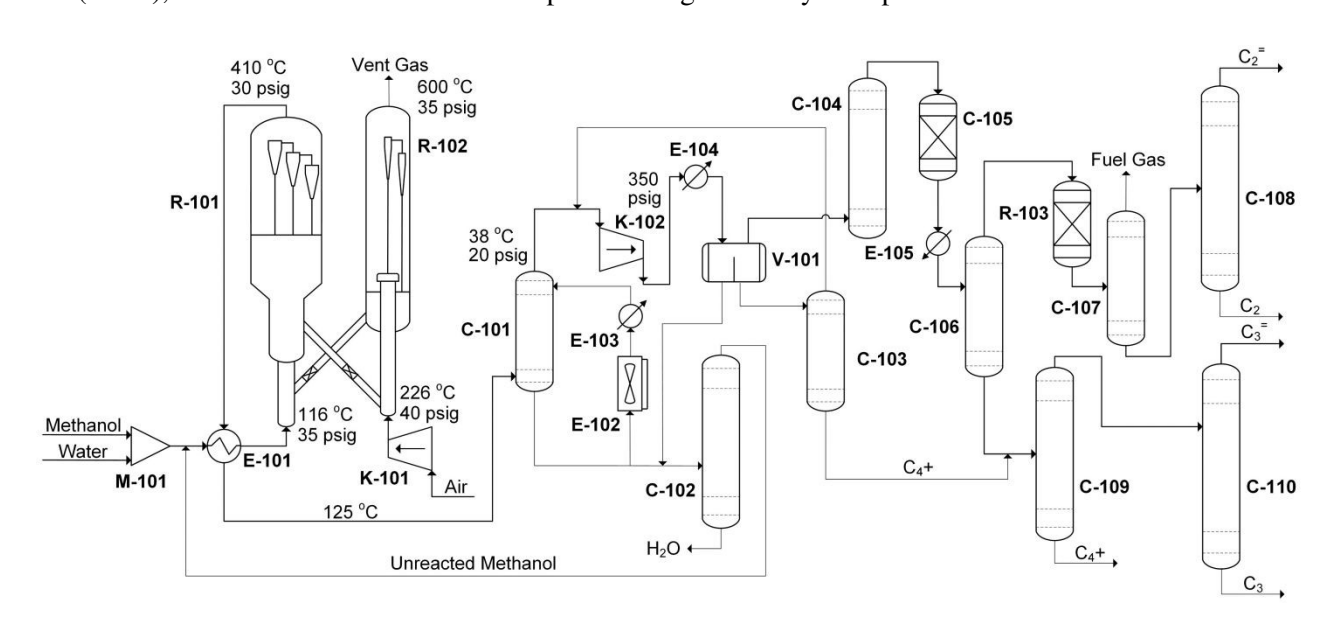


Figure 7 Process flow diagram of MTO process adapted from UOP co⁷⁴. Unit identification: M-101 Mixer; E-101 Heat Exchanger; R-101 Fluidized Reactor; R-102 Regenerator; K-101 Air Compressor; C-101 Quench Tower; E-102 Air-Cooled Exchanger; C-102 Water Stripper; K-102 Product Compressor; V-101 Phase Separator; C-103 Condensate Stripper; C-104 Caustic Scrubber; C-105 Gas Dryers; C-106 De-ethanizer; R-103 Acetylene Converter; C-107 De-methanizer; C-108 C₂ Splitter; C-109 De-propanizer; C-110 C₃ Splitter.

2.2 MTO products and coke evolution

In an industrial MTO unit, by employing a fluidized bed reactor with continuous regeneration of the catalyst, the coke content of the overall catalyst inventory within the reactor is maintained constant, resulting in a stable and unchanged product distribution. On the contrary, in a fixed bed reactor, due to gradual coke buildup, the products evolve over time on stream, shedding light on important phenomena. As illustrated in Figure 8 (A & B), gradual coke formation narrows the pores of the catalyst, which in turn makes the production of smaller molecules more

Open Access Article. Published on 22 2025. Downloaded on 30.10.2025 01:47:29.

C) EX-NO

This article is licensed under a Creative Commons Attribution-NonCommercial 3.0 Unported Licence.

favorable 75,76. As a result, selectivity towards methane, ethylene, and ethane is increasing, while the formation of heavier compounds such as propylene, butene, and C_5^+ olefins is being hindered. This continues until the formed coke completely blocks the pores of the catalyst, causing catalyst deactivation, where dimethyl ether (an intermediate) and unreacted methanol emerge. Interesting findings were revealed by the analysis conducted via Ghavipour et al. 76, who transformed a thermogravimetric analyzer into a TG reactor in the pursuit of performing live/in-situ measurements of coke generation during the MTO reaction over SAPO-34, in turn relating this to the products' evolution. As seen in Figure 8 (C & D), after weight reduction due to moisture desorption, the MTO reaction commenced by feeding 7 mol.% methanol in argon. Opposed to the speculation that the coke formation rate might be higher in the early stage of the reaction due to the higher number of active sites available, in reality, the coke formation gradually increases until it reaches the complete deactivation stage. According to Figure 8 (C), the group recorded a minor weight gain in the early stages of the reaction due to formation of entrained species such as hydrocarbon pool (HCP) autocatalytic intermediates. This was followed by moderate coke formation rate and subsequently enhanced coke formation towards the advanced times on stream (close to deactivation) due to the formation of poly-cyclic aromatic hydrocarbons. The group was able to approve this phenomenon using ¹³C NMR over partially and fully coked catalyst, explaining this through the schematic shown in Figure 8 (E & F). In the beginning of the reaction, as methanol molecules penetrate the catalyst pores, all the products, regardless of their sizes, can diffuse out. Conversely, as partial coke restricts the pores of the catalyst in advanced times on stream, methanol molecules still enter and light products exit, while heavier products become entrapped in the cavities and further grow. This causes faster coke formation in the later stages of the MTO reaction.

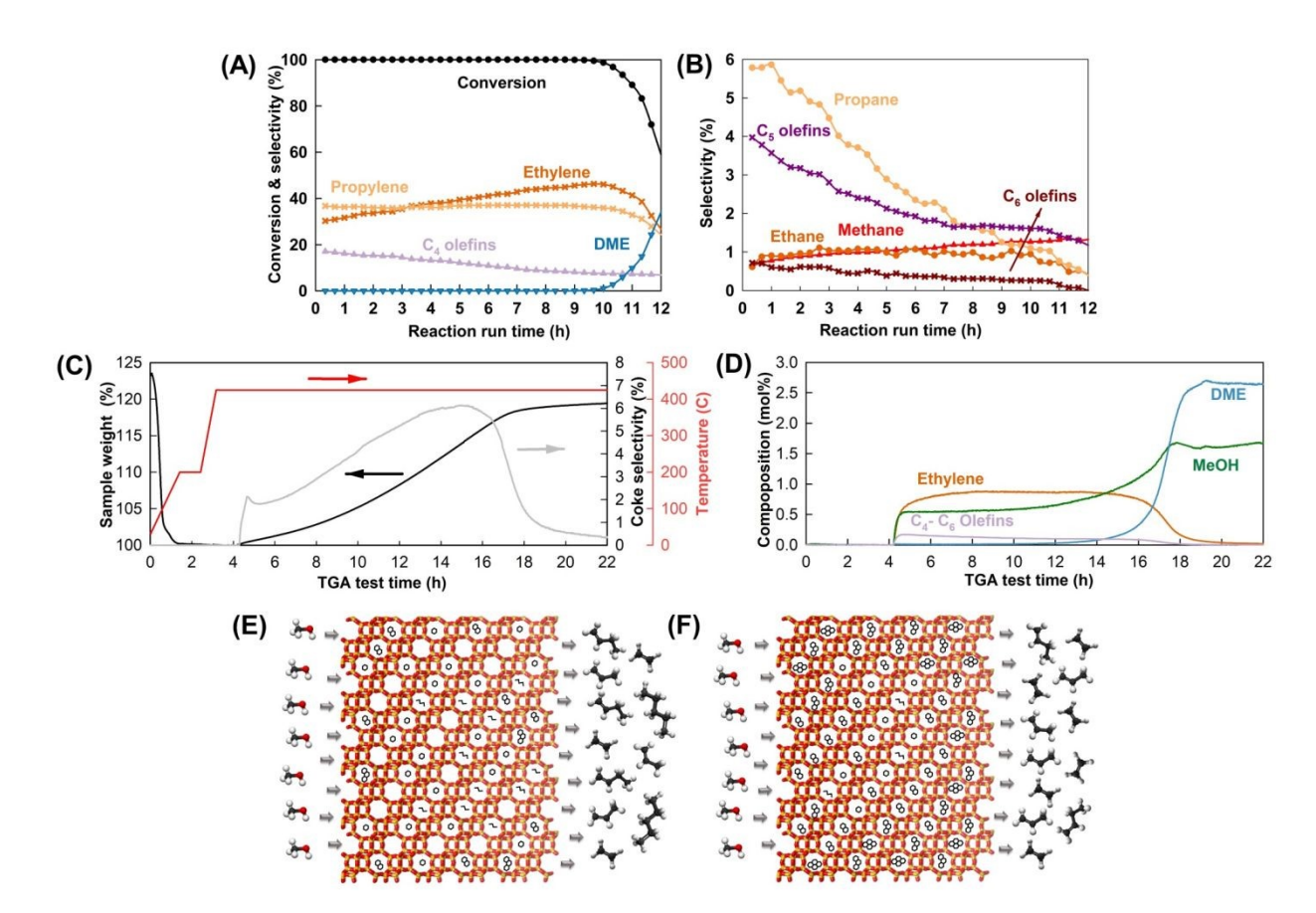


Figure 8 (A & B) Products distribution versus time on stream over SAPO-34 catalyst in the MTO reaction. Reaction conditions: temperature of 400 °C, atmospheric pressure, *WHSV* of 1 g_{MeOH} g_{Cat}⁻¹ h⁻¹, and methanol diluted with 20 wt.% water. (C & D) TGA-MS analysis: coke formation measurement using TGA and products distribution acquisition by MS. Reaction conditions: temperature of 400 °C, atmospheric pressure, *WHSV* of 1 g_{MeOH} g_{Cat}⁻¹ h⁻¹, and methanol diluted with 93 mol.% argon. (E & F) Coke evolution in the pores of the SAPO-34 catalyst in (E) the beginning of the activity run, and (F) in enhanced times on stream close to catalyst deactivation. Reproduced from reference⁷⁶ with permission from American Chemical Society, Copyright 2023.

2.3 Reactor operating conditions

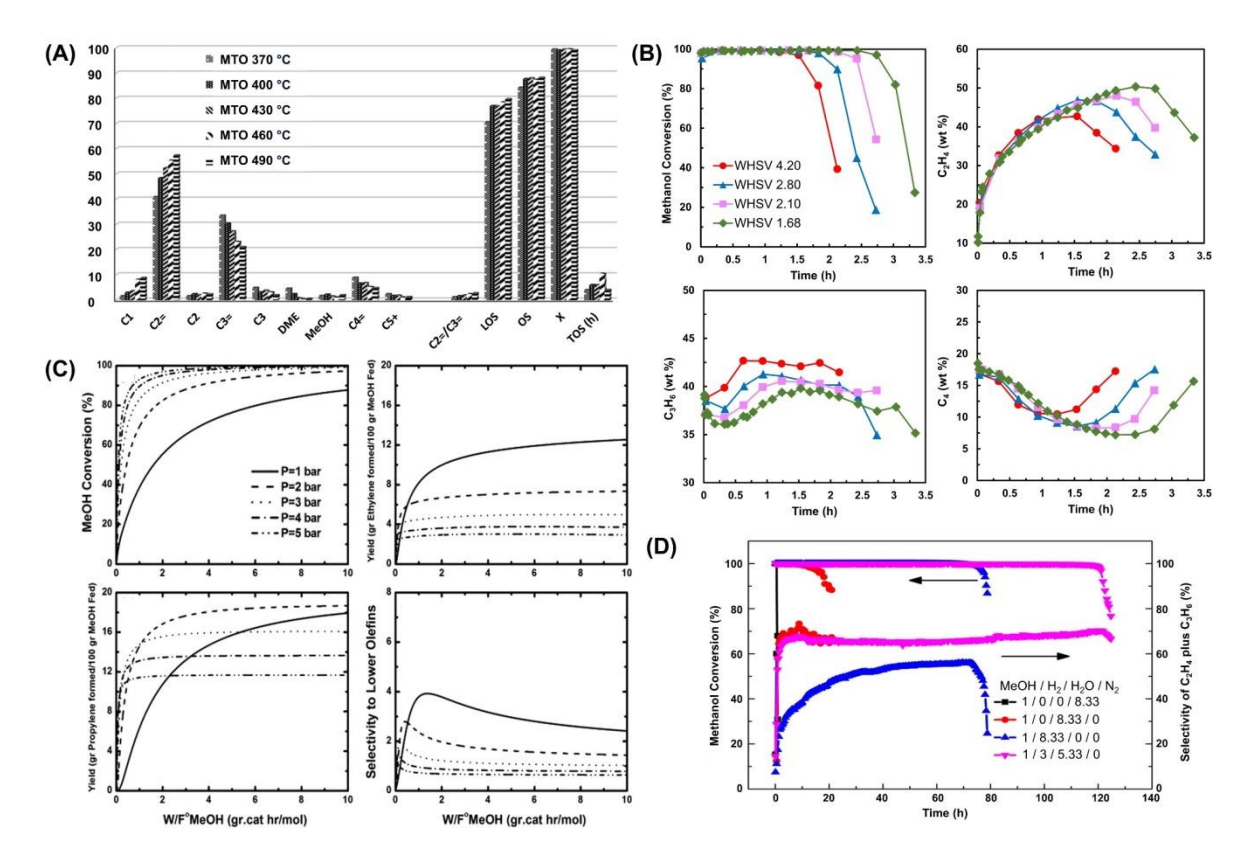


Figure 9 (A) Product distribution of MTO reaction over SAPO-34 catalyst at different *T*. Notation: *LOS* = light olefin selectivity, *OS* = olefin selectivity, *X* = conversion, *TOS* = time on stream. Reaction conditions: 0.1 barg pressure, *WHSV* of 1 g_{McOH} g_{Cat}⁻¹ h⁻¹, and methanol diluted with 20 wt.% water. Reproduced from reference ⁷⁸ with permission from Royal Society of Chemistry, Copyright 2016. (B) Effect of *WHSV* (in g_{McOH} g_{Cat}⁻¹ h⁻¹) on conversion of methanol, selectivity to ethylene, propylene, and butylene over time on stream reproduced from reference ⁸³ with permission from John Wiley and Sons, Copyright 2018. Reaction conditions: *T* of 450 °C, atm pressure, and methanol diluted with 20 wt.% water. (C) The effects of pressure alteration on methanol conversion, ethylene yield, propylene yield and selectivity towards light olefins. Reproduced from reference⁷⁹ with permission from Elsevier, Copyright 2011. Reaction conditions: *T* of 400 °C, *WHSV* of 12 g_{McOH} g_{Cat}⁻¹ h⁻¹, and methanol diluted with 69 wt.% water. (D) Synergistic effect between H₂O and H₂ on the catalytic performance of SAPO-34 in the MTO process. Reaction conditions: *T* of 450 °C, 40 bar, and *WHSV* of 4.0 g_{McOH} g_{Cat}⁻¹ h⁻¹. Reproduced from reference⁸⁴ with permission from American Chemical Society, Copyright 2019.

Other than operating temperature, one should consider the role that weight hourly space velocity (*WHSV*) may impose on catalytic activity. It has been found that the MTO reaction performs optimally under *WHSVs* of approximately 1 to 2 g_{MeOH} $g_{cat}^{-1}h^{-1}$ (as seen in Figure 9(B)) ^{80,85}. A *WHSV* below 1 g_{MeOH} $g_{cat}^{-1}h^{-1}$ has also been proven to reduce the total average selectivity of $C_2^{=}$ to $C_4^{=}$ species. This has been attributed to the longer residence time of species in the reactor, which can permit secondary reactions to take place and ultimately alter the product distribution ⁸⁰. The use of *WHSVs* larger than the aforementioned optimal range results in shortened catalyst active lifetime and, in even higher values, causes incomplete methanol conversion ⁸³.

Assuming this stipulated ideal *WHSV* has been employed, groups have also investigated the effect that reactor pressure may impose on MTO product distribution. Generally, it has been found that the optimal pressure, taking into account the combination of both *LOS* and feed conversion, lies between 1 to 2 bar ^{86,87}. A reactor pressure greater than this has been shown to negatively impact the average selectivity towards light olefins (see Figure

9(C)) and encourage greater deposition of coke instead ^{87,88}. This has been justified by the consequential increased residence time of reactants in the reactor, which encourages a greater likelihood of light olefins undergoing successive reactions to form byproducts. Furthermore, raising the pressure would favor the backward reaction in the conversion of, for instance, methanol to ethylene (from 2 to 3 moles of gas) or methanol to propylene (from 3 to 4 moles of gas), according to Le Chatelier's principle. It should be noted that, on the other hand, a pressure too low (keeping other factors, such as space velocity, constant) would result in reduced residence time of reactants, thus resulting in incomplete conversion of methanol over the catalyst active lifetime ⁸⁷.

Another important consideration is the impact feed composition may have on product distribution and catalyst lifetime. Studies have demonstrated that the use of diluents in the feed, such as water, decreases the partial pressure of methanol, which has correspondingly boosted selectivity towards light olefins and delayed catalyst deactivation ^{89,90}. Although nitrogen has been utilized as an alternative diluent, water is readily available, possesses a relatively higher heat capacity as a vapor (to carry away the heat of reaction), and has been shown to more effectively reduce the rate of coke formation and further improve catalyst utilization 91,92. Since water will tend to reversibly adsorb on catalyst acidic sites (primarily strong ones) due to its basic properties, it has been deemed to reduce the residence time of coke precursors adsorbed on such active sites as well as inhibit the coke-generating steps involving alkene monomers undergoing oligomerization and cyclization 91,93,94. Furthermore, problems involving product separation may arise when diluents other than water are employed⁹². Employing 70-80 mol% of water in the feed has proven to process roughly eight times more methanol (within the catalyst active period) than if the feed had consisted of only pure methanol 92. Exceeding this range (90 mol% water) has not been shown to significantly improve performance 95. It is important to note that addition of substantial amounts of water will result in occupation of the reactor volume, which consequently lowers the reactor's nominal processing ability. Besides, heating up the water to the reaction temperature and condensing the outlet water, despite the application of heat recovery methods, can result in heat loss and decreased energy efficiency. Hence, in the industrial application, feed water content is usually kept around 30 mol% (20 wt.% water in methanol) 74.

Other than the conventional use of water/nitrogen diluent in the feed, groups have also investigated the potential effects that other co-fed gases like hydrogen may impose on catalytic activity ^{84,96}. According to Figure 9(D), Zhao et al. ⁸⁴ reported that the SAPO-34 fed with pure methanol lasted for less than an hour; however, following hydrogen addition in the H₂/MeOH ratios of 8.3, the lifetime was substantially enhanced to around 80 hours. However, the light olefins were inevitably hydrogenated to alkanes, leading to a considerable drop in light olefins selectivity, from around 70% using pure methanol, to around 50% in the presence of hydrogen. Another group ⁹⁶ claimed milder reduction in light olefins selectivity in response to hydrogen addition (LOS of 76% for 0 H₂/MeOH

This article is licensed under a Creative Commons Attribution-NonCommercial 3.0 Unported Licence

molar ratio compared to LOS of 70.5% for 231 H₂/MeOH molar ratio) and over 70 times longer lifetime. Nonetheless, the reaction conditions that they employed (WHSV of 40 g_{MeOH} g_{cat}⁻¹h⁻¹ over only 4 mg of catalyst) seem to be far from the optimal range. Interestingly, the simultaneous presence of water and hydrogen in the feed seems to trigger a synergistic effect, leading to long lifetime without compromising LOS (see Figure 9(D)). Preceding studies have claimed that the fed H₂ may play a role in hydrogen transfer reactions and seemingly intercept the pathways that lead to the generation of deactivating multi-ring aromatic species. It was proclaimed that, under combined feeding of H₂ and H₂O ⁸⁴, heavy aromatic deposits that formed were likely to undergo hydrogenation catalyzed by SAPO-34 Brønsted acidic sites 97, followed by possible cracking (depending on the temperature employed). These species were declared to have likely reverted back to active intermediates and in turn decelerate the overall evolution of coke species 84. Periodic density functional theory (DFT) modelling that ensued focused on investigating these hydrogenation-based mechanistic claims that revolved around hydrogen cofeeding 98. It was uncovered that potential deactivation-inducing precursors such as formaldehyde and dienes, which have been claimed to drive the link between olefinic and aromatic dual cycles (see Section 4.3.1 on polyalkylaromatics formation), are selectively hydrogenated (i.e., at a higher rate) relative to desired light alkene species. Hence, the elimination of such potential aromatic precursors by hydrogenation, via high-pressure H₂ cofeeding, may be the plausible cause for the extended lifetime observed in the studies mentioned previously. Recently, the potential of undertaking MTO catalysis in the presence of syngas reagents (cofeeding a mix of H₂ and CO under high pressure) has been examined 99. However, under elevated methanol partial pressure, which begins to more closely resemble the MTO process, co-feeding CO (in both presence and absence of H₂) resulted in no clear improvement in any catalytic performance metric.

3 MTO reaction and deactivation pathways

The uncovering of the MTO mechanism has been and continues to be a challenge for researchers. Over the last 60 years, a vast number of mechanistic proposals have been put forward. The pathways that have gained increasing popularity over the years are depicted as a simplified schematic in Figure 10. In general, the elementary steps of the first C-C coupling (in the formation of light olefins) are still under debate. However, it has been widely accepted that early stage constructed light olefins are likely to undergo further reactions. These include hydrogen transfer, alkylation, cyclization, and aromatization to form the following species: paraffins, larger olefins, napthenes, and aromatics. The generation of large multi-ring aromatic species can, in turn, lead to the "coking" and hence the deactivation of the zeolite catalyst.

That being said, there still exists extensive discussion with regards to the reaction intermediates or active species leading to the previously mentioned hydrocarbon products. Some experimental evidence has ratified the hypothesis of dimethyl ether (DME) being an intermediate of the MTO reaction ^{100–102}. For instance, DME is the sole product observed following catalyst deactivation, which means it is produced over weaker acidic sites and may be formed and consumed over the active catalyst. In addition, feeding the reactor with DME instead of methanol results in almost the same product distribution, which raises the idea that DME can act as an active intermediate ¹⁰³. However, there are also mechanistic proposals that introduce other species as active intermediates, such as the free radical mechanism, the alkoxy chain growth route, and the hydrocarbon pool concept (which suggests polyalkylaromatics as active components). In the following sections, the most widely utilized mechanisms of the MTO reaction will be explored.

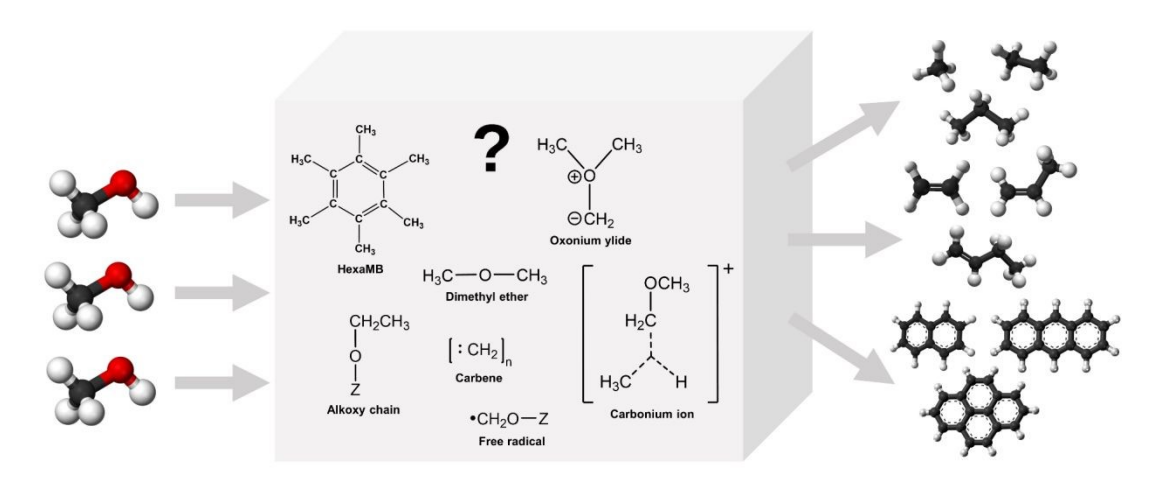


Figure 10 Simplified schematic of the MTO overall reaction.

3.1 Early studies: initial stages of light olefin production

The most probable path behind the first C-C bond formation has been the main topic of discussion for earlier studies conducted on the MTO process, lying primarily between the years of 1970 and 1990. A large number of mechanistic proposals have been put forward; however, the most widely discussed and relevant mechanisms have been relayed as follows.

3.1.1 Oxonium ylide mechanism

During early mechanistic research, the oxonium ylide mechanism (as seen in Figure 11) has received recognition as one of the viable paths for the formation of the initial C-C bond $^{104-106}$. It has been suggested that, in the presence of Brønsted acidic sites (H⁺) of zeolite catalysts, the initial step (A) consists of the dehydration of two methanol

molecules to a singular dimethyl ether (DME). This DME intermediate may interact with a Brønsted acidic site of the zeolite catalyst, to in turn form a dimethyl oxonium ion. These two preceding species can react further to produce a trimethyl oxonium ion (i.e., step B). This is then followed by a deprotonation step (C) of one of the methyl groups by a basic site, to in turn formulate a surface-associated dimethyl oxonium methyl ylide species. The subsequent step comprises of two options, either a Stevens rearrangement (step D) or an intermolecular methylation (step D'). Via the Stevens rearrangement, the ylide species is converted to a methylethyl ether (as well as a singular methanol molecule), which is then ultimately transformed to ethylene via a β -elimination step (E). On the other hand, with the intermolecular methylation (the second option), an ethyldimethyl oxonium ion forms. This is once again followed by a β -elimination step (E') to produce the ethylene species, while regenerating a DME molecule in this case. An isotope labelling study ¹⁰⁷ reached a conclusion that the intermolecular methylation (step D') is the preferred pathway in comparison to the potential 'Stevens rearrangement' (step D).

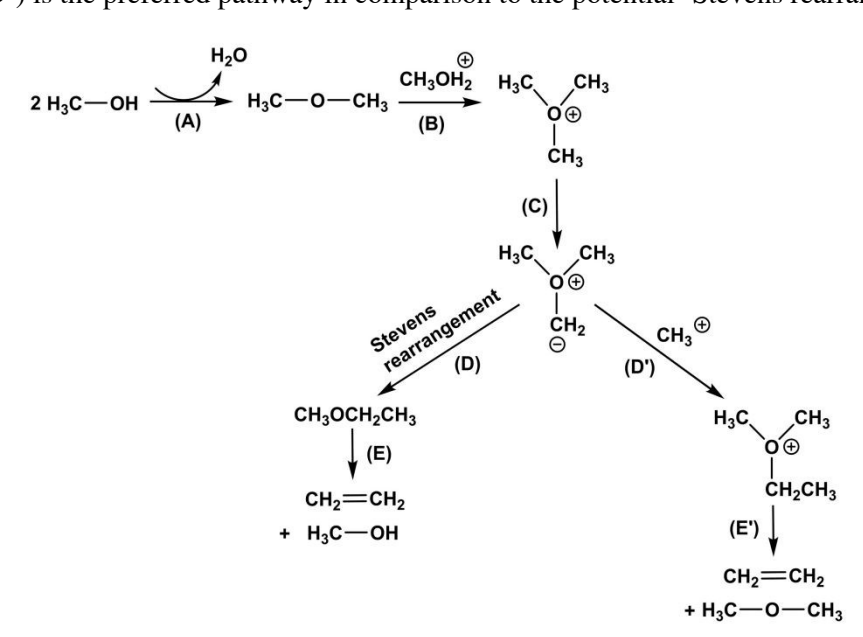


Figure 11 Oxonium vlide mechanism. Adapted from reference 104 with permission from the Royal Society of Chemistry, Copyright 2023,

3.1.2 Carbene mechanism

Another proposed route that may be responsible for early-stage light olefin production is commonly referred to as the 'carbene mechanism' (Figure 12) ^{108,109}. This mechanism commences via an initial α-elimination step (A), in which water and a carbene species form from the methanol reactant. This can then be followed by either polymerization of the carbene monomers to olefins (steps B and C), or via sp³ insertion of the carbene species in dimethyl ether or methanol molecules (step D). The newly generated intermediates can then undergo cleavage to form olefins, as well as regenerate water or alcohol species (step E).

$$H \xrightarrow{H_2} OH \xrightarrow{(A)} H_2O + [:CH_2]$$

$$(CH_2)_n \text{ For instance, } 2[:CH_2] \xrightarrow{(C)} CH_2 = CH_2$$

$$n[:CH_2] \xrightarrow{(D)} H_3C \xrightarrow{(C)} CH_2 = CH_2 + HOR$$

Figure 12 Carbene mechanism. Adapted from reference 108 with permission from Elsevier, Copyright 1981.

The search for supporting evidence behind carbene intermediacy was undertaken by isotope-labeling experiments involving ¹³C methanol, in the presence of propane, over HZSM-5 zeolites ¹¹⁰. Here, the resulting ratio of iso-over normal butane produced was substantially low (i.e., ~1 compared to 3.8 for the control run, which comprised a feed of only methanol and helium instead). This can provide evidence, as suggested by the authors, that the nature of the C₁ attacking species must be carbene-like. This is because insertion into a sp³ C-H bond (a mode of attack by carbene species) statistically leads to a low i/n butane ratio. This low ratio can also act to disprove the existence of both the 'oxonium ylide' and the to-be-introduced 'carbocationic' mechanisms (as the suggested paths for initial C-C bond formation), since such routes have been characteristically shown to display higher i/n butane ratios instead. It was also revealed that the produced butanes were singly labeled, which validated the direct methylation of propane via methanol.

3.1.3 Carbocationic mechanism

Some research groups have looked to the carbocationic mechanism as a possible path for initial C-C bond formation and early-stage light olefin production 111-113. Figure 13 portrays the elementary steps that comprise this mechanism. The pathway commences via the formation of dimethyl ether (from methanol) through a reversible dehydration step (A). Via protonation, dimethyl ether (i.e., a surface methoxyl) may be the provider of free methyl cations (step B), which could in turn react with another dimethyl ether molecule by addition to its C-H bond (step C). In turn, a carbonium transition state can form; its subsequent deprotonation (by the anionic zeolite catalyst) can lead to the production of methylethyl ether (methoxyethane) while regenerating the catalyst Brønsted acidic site (step D). The methylethyl ether can then ultimately transform to ethylene via a β -elimination step (E), like that seen in the final step for the 'oxonium ylide mechanism'. However, the more likely path instead involves the methoxyethane species further reacting with free methyl cations (from dimethyl ether in its protonated form) to in turn generate a pentavalent carbonium transition state (step F). This can then follow via deprotonation to produce methyl isopropyl ether (step G), which could finally eliminate methanol to produce propylene (step H). It could, though unlikely, repeat the cycle of methyl carbonium ion addition to form even larger olefins.

$$2 \text{ H}_{3}\text{C} - \text{OH} \xrightarrow{\text{(A)}} \text{H}_{3}\text{C} - \text{O} - \text{CH}_{3} \xrightarrow{\text{(B)}} \text{H}_{3}\text{C} - \overset{\text{(B)}}{\oplus} \text{CH}_{3}$$

$$(C) \qquad \qquad \text{(C)} \qquad \qquad \text{(C)}$$

Figure 13 Carbocationic mechanism. Adapted from reference 112 with permission from Elsevier, Copyright 1981.

It could be claimed that the C-H bond of DME (or methanol) may not be of sufficient nucleophilicity to undergo an attack by the electrophilic methyl cations (derived from dimethyl ether in its protonated form), as seen in step (C). Smith and Futrell ¹¹⁴ embarked on an investigation that assisted in providing an answer to this claim. The group undertook experiments in which they reacted methylcarbenium ion (CH₃+) with methanol. It was concluded that the reaction took place majorly (i.e., 80%) through intermediates structured as dimethyl-oxonium ion or protonated DME. However, according to the tandem ion cyclotron resonance mass spectrometer, C₂ species (such as ethylene) were not detected as part of the product distribution; rather, C₁ species were present. Hence, these observations can question the overall validity of the carbocationic mechanism in its capability for ethylene production.

A small portion of articles (during early mechanistic research) have proposed the participation of free radicals in the initial-stage production of light olefins ¹¹⁵⁻¹¹⁷, which have been depicted in Figure 14. Initially, a methanol molecule approaches a Brønsted acidic site of the zeolite catalyst, resulting in a dehydration reaction in which water and a surface methoxy group are formed (step A). Simultaneously, it has been declared that the interaction of methanol molecules on radicogenic sites of the catalyst lead to the generation of free methyl radicals 117. Consecutive reactions lead to the carbon chain buildup of these radical species. Subsequently, the methoxy group on the zeolite surface interacts with these radical carbonaceous species (such as an alkyl, alkoxyl, alkoxyl, to in turn form a radical intermediate (step B). Further interaction between this intermediate and the zeolite surface ultimately leads to the production of surface-bound carbene species i.e., methylene (step C). This can then be followed by polymerization of the carbene monomers to olefins (step D). A final step (F) involves the regeneration of the zeolite acidic site (ZOH).

$$H_{3}C-OH + ZOH \xrightarrow{(A)} CH_{3}OZ \xrightarrow{(B)} CH_{2}O-Z$$

$$CH_{2}O-Z \xrightarrow{(C)} ZO: :CH_{2} + ZO \xrightarrow{(F)} R^{\bullet} + ZOH$$

$$CH_{2}O-Z \xrightarrow{(C)} ZO: :CH_{2} + ZO \xrightarrow{(F)} R^{\bullet} + ZOH$$

Figure 14 Free radical mechanism. Adapted from reference 115 with permission from Elsevier, Copyright 1989.

Experimental evidence in support of the existence of free radical intermediates was presented by Clarke et al. 116. The group conducted experiments in which they reacted DME over H-ZSM-5 zeolite; using a spin trapping reagent with electron spin resonance (e.s.r.) analysis, free radicals were said to be detected during the reaction. Clarke et al. were also able to demonstrate that the source of these free radicals stemmed from small quantities of solid-state paramagnetic defects present in the zeolite, which were able to activate C-H bonds in DME (on ZSM-5 catalyst at ≥ 200 °C). Other tests were also performed using methanol fed over a catalyst comprising of 10 wt% MgO with 1 wt% Li₂O supported on a silica-alumina (13% wt. Al₂O₃). This was done to observe how methanol would interact with a catalyst that contained an abundance of both paramagnetic centers (Li⁺0⁻) and active sites (Brønsted acidic sites). The results demonstrated that the catalyst was able to readily convert methanol feed into both ethene and aromatics, with regards to tests in the range of 300 to 500 °C. According to the authors, these findings can provide evidence to support the notion that the 'free radical mechanism' and 'carbocationic mechanism' may be working in tandem in the generation of the initial C-C bond.

This article is licensed under a Creative Commons Attribution-NonCommercial 3.0 Unported Licence.

Open Access Article. Published on 22 2025. Downloaded on 30.10.2025 01:47:29.

Considering all previously discussed widespread mechanistic proposals presented during early research, the alkoxy chain growth route still remains the most simplified approach for the formation of the initial C-C bond ^{118,119}. According to Figure 15, the mechanism commences with a methanol molecule approaching an acidic site (i.e., the active site) of a zeolite catalyst. This results in a dehydration reaction in which a surface-associated methoxy group is formed in place of the active site, with water being eliminated (step A). A subsequent methanol molecule approaches the methoxy group, resulting in methylation of this species to generate a surface-associated ethoxy group instead (step B). Detachment of this ethyl group would ultimately form ethylene and regenerate the acid site in the process (step C). It should be noted that, despite the apparent simplicity associated with this approach, both research groups ^{118,119} declared that the growth of the alkoxy chain had not been previously observed or proven experimentally, which generates doubt as to its existence, relative to the previously discussed early stage proposals (Sections 3.1.1 to 3.1.4). To the best of our knowledge, there exists only limited research regarding experimental works (in the form of spectroscopic evidence) in support of the formation of surface alkoxide groups ¹²⁰.

Figure 15 Alkoxy chain growth route. Adapted from reference 119 with permission from American Chemical Society, Copyright 2003.

3.2 Current studies: the 'hydrocarbon pool' concept

As mechanistic research in the methanol conversion to olefins process developed, much research during the 1990s was allocated towards the understanding of a more novel parallel-type reaction concept i.e., the notion of the hydrocarbon pool (HCP). The initial formal suggestion of this concept was pronounced by Dahl and Kolboe ^{121,122}. Through the use of isotope labelling experiments, the authors were able to provide experimental evidence to back up the carbon pool idea they proposed. The experiments involved cofeeding ¹³C-methanol and ¹²C ethanol and propanol, simulating ethylene and propylene adsorbed on the surface of the SAPO-34 catalyst. In the case of the methanol and ethanol co-fed reaction, in view of the product isotopic distribution, propene and butene species were generated primarily from ¹³C, coming from methanol, rather than a combination of ¹³C and ¹²C. This can demonstrate that the produced hydrocarbons were not generated via successive methylations of ethylene, but instead via a sort of ambiguous 'carbon pool' mechanism. As research to uncover the details expanded into the later 2000s, the concept began to receive much recognition as the major contributor for both olefin formation as well as coke production for advanced times on stream ^{30,123–129}. With analysis of the species confined in catalyst

pores during the reaction, substantial amounts of polyalkylaromatics were detected. This finding spawned the idea that a pool of intermediate carbonaceous species exists, in which polyalkylaromatics (generally polymethylbenzenes) are the active centers. In this pool, a variety of elementary reaction steps, including chain extension, cyclization, and aromatization take place on linear chain aliphatic hydrocarbons (detected during early stages of MTO) ¹³⁰, in turn leading to the generation of aromatic species. As these aromatic species begin to alter and evolve, ethylene and propylene have been suggested to 'split off' as products. This in turn offers a path for light olefin generation, as opposed to the previously discussed ordinary formulation of these species (see Section 3.1). The HCP concept possesses two underlying mechanisms which are said to be generally responsible for light olefin formation. These are termed the exocyclic methylation route (i.e., the side chain mechanism) and the pairing mechanism (also commonly referred to as the expansion- contraction mechanism) ^{124–126}, which will be discussed, along with other noteworthy HCP means of light olefin formation, in the following section.

3.2.1 The Aromatic Cycle: The formation of polyalkylaromatics

As previously discussed, polyalkylaromatics are generally referred to as the core/active intermediates of the MTO hydrocarbon pool. Studies ^{127,131} have sought to experimentally validate the existence of these species over time on stream by investigating the organic deposits entrapped inside the pores and cages of SAPO-34 during both the reaction and deactivation periods. Specifically, the authors utilized a gas chromatograph equipped with a mass spectrometer detector (i.e., GC-MS analysis) and in-situ UV-visible spectroscopy, as well as ¹H magic-angle-spinning (MAS) and ¹³C cross-polarization MAS Nuclear Magnetic Resonance (NMR) spectroscopy. Analysis of the results proved that polymethylbenzenes (polyMBs) with 4–6 methyl groups, alongside polymethylnaphthalenes (polyMNs) with 2-4 methyl groups, are the key active components of the reaction period over SAPO-34 (as illustrated in Figure 16 (A)). Although such species are typically related to their capabilities in coke generation, groups ^{132,133} have used DFT modelling calculations to portray the potential of these species in assisting in the formation of light olefins within zeolite cages. In fact, one of the groups ¹³² provided a strategy to convert coke species to aforementioned naphthalenic species through steam cracking (i.e., passing hydrogen and steam over SAPO-34 catalyst) and uncovered a subsequent restoration of catalytic activity through boosted total light olefins selectivity.

In order to investigate the role that polyalkylbenzene (the first suggested active component) may play towards light olefin formation, it is crucial to first uncover how it could be initially generated. Wang et al. ¹³³ took on this task by using density functional theory (DFT) calculations to propose an energetically feasible reaction pathway from early-stage-constructed propylene into hexamethylbenzene (see Figure 16 (B), (C) and (D)). The group suggested that a singular propene molecule may undergo protonation (P1(a)) using an acid site of the zeolite

catalyst in close proximity, in turn generating 1-propyl carbenium ion. This intermediate can subsequently oligomerize (O1(a)) by reacting with another propene molecule, to form 2-hexyl carbenium ion. Deprotonation (D1(a)) of this ionic species can result in the production of 1-hexene. This may then be followed by a hydride transfer step (HT1(a)) between a zeolite surface-associated alkoxy (i.e., a methoxy) as the hydride acceptor, and 1-hexene as the hydride donor. This leads to the generation of a 1-hexene carbenium ion and an alkane (i.e., methane in this case). Subsequent cyclization (C1(a)) and deprotonation of the carbenium ion results in the formation of cyclohexene. A repetition of deprotonation and hydride transfer reactions (HT2(a) and HT3(a)) results in the production of benzene. Recurring methylation steps (M1-6(a)) ultimately leads to the formulation of hexamethylbenzene, which falls under the criteria as the active component of the HCP concept. The task of uncovering the route for polyalkylbenzene formation was also undertaken by Dai et al. 127, with the employment of hexene as the starting species for the mechanistic route (stating that their generation came about via the methylation of early-stage light olefins). As part of the proposed reaction pathway, initially, hexene species are protonated to form C_6^+ ions alongside C_6 -alkoxide. The skeletal isomerization of these carbenium ions could also be undertaken via alkylcyclopropane intermediates. However, the observed alkylcyclopropanes were found to be slightly less stable than hexenes, which could discourage the occurrence of such a route. The reaction pathway continues via a hydride transfer step, in which propene was selected to be the hydride-acceptor, leading to the formation of alkadienes from 3-methyl-1-pentene. The chain is then further propagated via subsequent methylation of the generated alkadienes. A repetition involving deprotonation and hydride transfer steps ultimately leads to the generation of polymethylbenzenes.

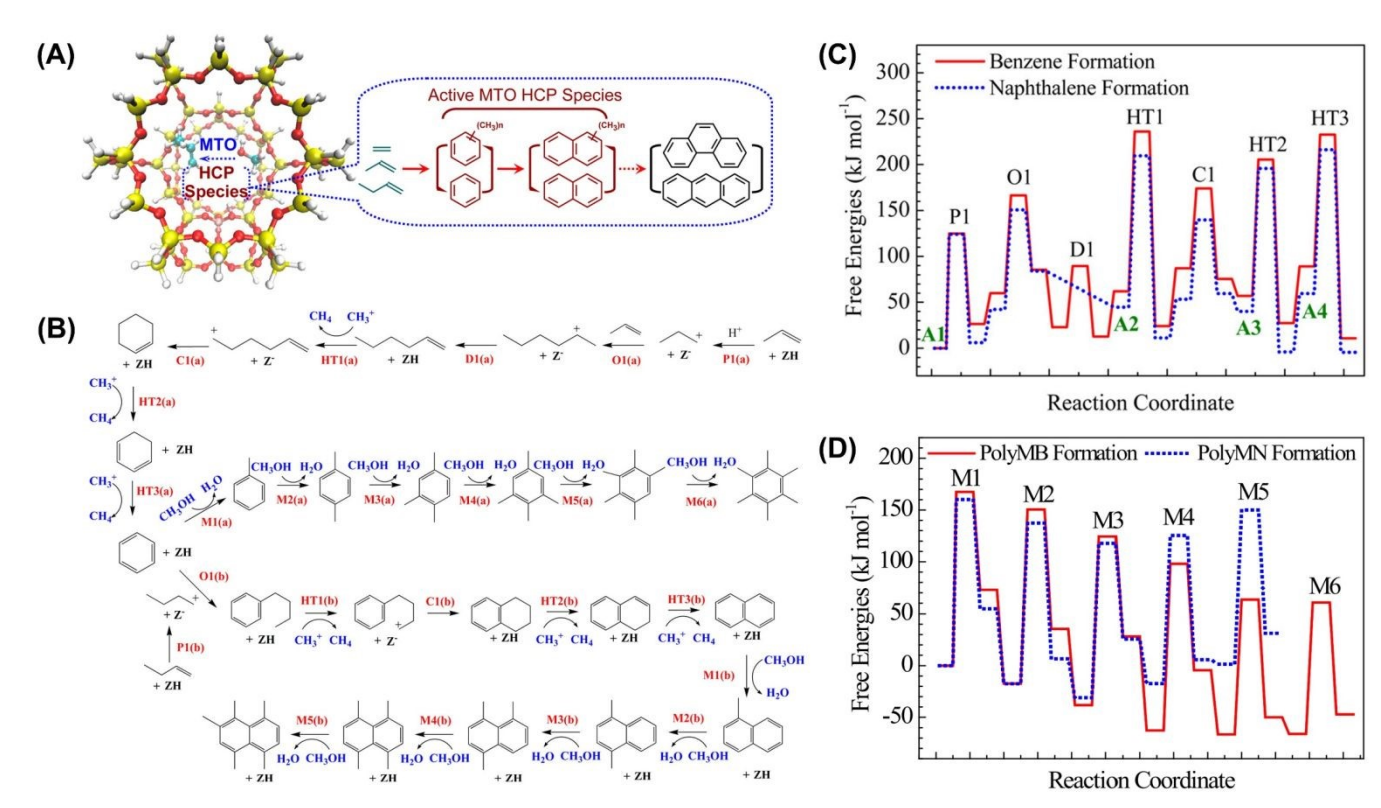


Figure 16 (A) The development of species present in the cages of the zeolite framework during the MTO reaction (atom coloring: yellow (Si), red (O), white (H), and pink (Al)). (B) Proposed mechanistic path for the formation of polymethylbenzene (polyMB) and polymethylnaphthalene (polyMN) during the MTO reaction over zeolite catalyst (ZH). (C) Free energy profiles for the generation of benzene and naphthalene (at 400 °C) during MTO over zeolite catalyst. In addition to the zeolite framework, adsorbed propene as well as benzene and butene (A1) are taken as the reference states for benzene and naphthalene production, respectively. States A2, A3, and A4 represent the methoxyl formation at the active site prior to hydride transfer reactions. (D) Free energy profiles for the generation of polyMB and polyMN (at 400 °C) during MTO over zeolite catalyst. In addition to the zeolite framework, adsorbed benzene and naphthalene are taken as the reference states for polyMB and polyMN, respectively. Reproduced from reference¹³³ with permission from American Chemical Society, Copyright 2016.

Referring to Figure 16 (B), (C) and (D), the formation of polymethylnaphthalenes (i.e., the other suggested active component of the hydrocarbon pool) has also been well documented and proven to be energetically feasible by the employment of DFT modelling. Taking benzene as the commencement point, this species has been suggested to initially react (step O1(b)) with a 1-butyl carbenium ion (which would have been previously generated via the protonation (P1(b)) of early-stage generated butene species). This would result in the formation of butylbenzene. Subsequently, a hydride transfer step (HT1(b)) may occur between a surface-associated methoxy group and butylbenzene, resulting in the production of a butylbenzene carbenium ion and a methane molecule. A 1,6cyclization and deprotonation step would lead to the generation of phenylcyclohexane (step C1(b)). A repetition of the deprotonation and hydride transfer reactions (HT2(b) and HT3(b)), followed by methylation steps (M1-5(b)), would ultimately result in the production of polymethylnaphthalene.

This article is licensed under a Creative Commons Attribution-NonCommercial 3.0 Unported Licence

The 'exocyclic methylation route', also commonly referred to as the 'side chain mechanism', is one out of the 2 central mechanisms under the HCP concept. To the best of our knowledge, this pathway was first proposed by Mole et al. ¹³⁴ during the early 1980s and has been subsequently modified ¹¹⁹. Over recent years, the side chain mechanism has received recognition as a means of explaining how light olefins may form within the MTO reaction 124-126,135,136. Figure 17 (A) provides a close examination of this mechanistic route over zeolite catalyst utilizing either polymethylbenzene (top row) or polymethylnaphthalene (bottom row), i.e., the previously mentioned active components of the hydrocarbon pool concept 133. Nonetheless, the mechanism proceeds in the same manner for both scenarios. Studying the case of the PMB cycle (top row), commencing with hexamethylbenzene, this species first undergoes gem methylation with methanol (M1) to form 1,1,2,3,4,5,6-heptmethylbenzenium cation (heptaMB+). Its subsequent deprotonation (D1) generates hexamethyl-methylene-cyclohexadiene (HMMC). The exocyclic double bond of HMMC reacts with an electrophilic methenium species (derived from a methanol molecule) to form an ethyl group on the benzenic ring (i.e., an extension of the benzenic species side chain) (M2). As suggested by a different group ¹²⁴, dealkylation of this ethyl group may take place, resulting in the formation of ethylene. However, there is the alternative possibility that deprotonation occurs instead (D2), which would regenerate the exocyclic double bond, forming hexamethyl-ethylene-cyclohexadiene. Further reaction with a methenium species (M3) leads to the formation of an isopropyl group attached to the benzenium cation. Dealkylation of this propyl group takes place via an internal hydrogen shift (E1), resulting in the formation of propylene. It should be noted that butene formation is highly unlikely to occur with respect to this mechanism due to steric hinderance ¹²⁴. Overall, groups ^{126,133} have backed up this mechanistic proposal as a plausible route for light olefin formation via the use of theoretical modelling DFT calculations (as seen in Figure 17 (B) and (C)).

Open Access Article. Published on 22 2025. Downloaded on 30.10.2025 01:47:29.

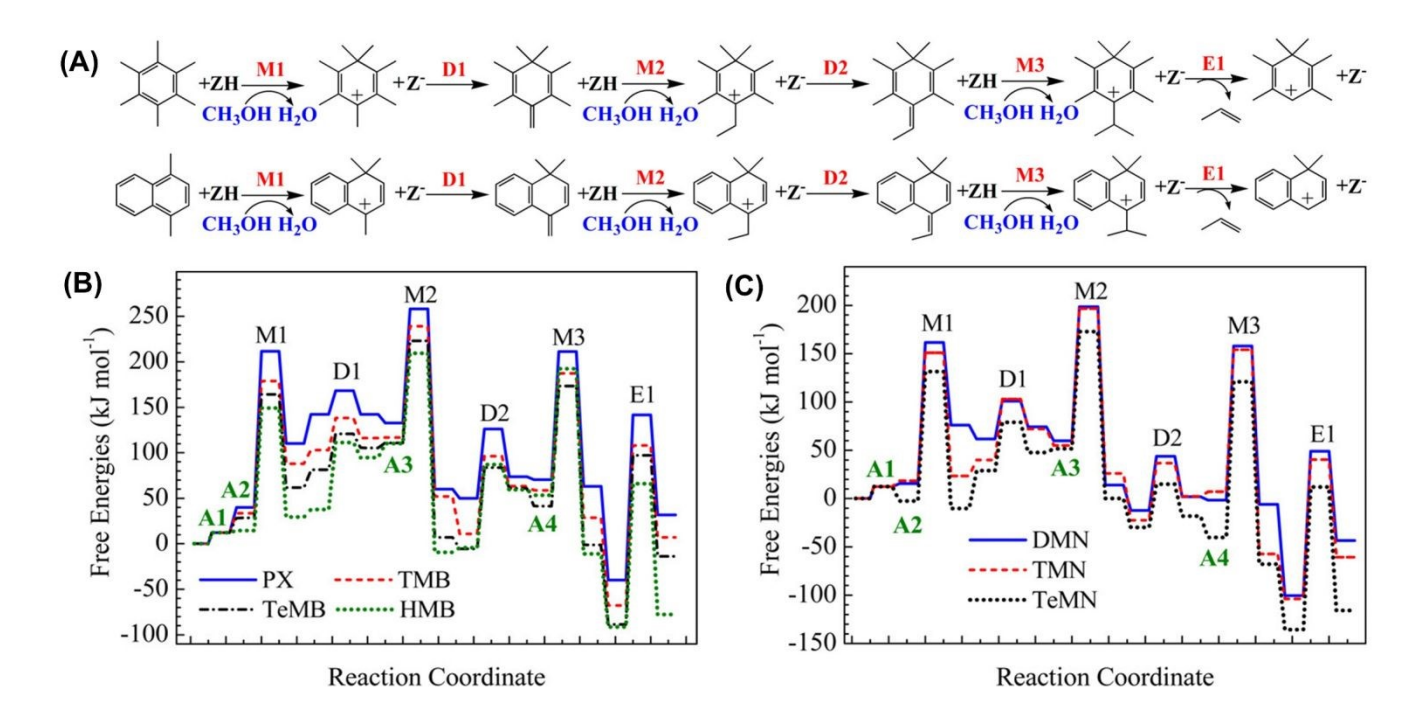


Figure 17 (A) Side chain mechanism via the top: polyMB cycle (commencing with hexamethylbenzene) and bottom: polyMN cycle (commencing with dimethylnapthalene) for the MTO reaction over zeolite catalyst. (B) Free energy profiles of the polyMB based side chain mechanism (at 400 °C) for different commencing polyMBs in the MTO reaction over zeolite catalyst. The commencing polyMBs studied are p-xylene (PX), 1,2,4-trimethylbenzene (TMB), 1,2,4,6-tetramethylbenzene (TeMB), and hexamethylbenzene (HMB). The zeolite framework, methanol and different polyMBs in gaseous phase are taken as the reference state. A1, A3, and A4 are the adsorption of methanol, while A2 is the additional adsorption of polyMB. (C) Free energy profiles of the polyMN based side chain mechanism (at 400 °C) for different commencing polyMNs in the MTO reaction over zeolite catalyst. The commencing polyMNs studied are 1,4-dimethylnaphthalene (DMN), 1,4,5-trimethylnaphthalene (TMN) and 1,4,5,8-tetramethylnaphthalene (TeMN). The zeolite framework, methanol and different polyMNs in gaseous phase are taken as the reference state. A1, A3, and A4 are the adsorption of methanol, while A2 is the additional adsorption of polyMN. Reproduced from reference¹³³ with permission from American Chemical Society, Copyright 2016.

The second major mechanistic route that falls under the HCP concept is commonly termed the expansioncontraction mechanism, or the paring mechanism. The introduction of this pathway came about in 1961 when Sullivan et al. ¹³⁷ sought to explain the formation of light olefins from polyalkyl benzenium ions. Since then, research fixating on this mechanistic proposal took flight, with many research groups agreeing on the viability of this path ^{124–126,136,138}. The generalized paring route can be observed in Figure 18 (A). The mechanism suggests alkyl side chain growth by ring contraction and expansion (as opposed to the alkylation steps involving methenium species of the side chain mechanism). Specifically, the six-membered ring (heptamethyl benzenium ion) is contracted to a five-membered ring (step A), followed by subsequent dealkylation of the isopropyl and isobutyl groups (which leads to the formation of propylene and isobutene, respectively). This can be seen in steps B', B, and C. The five-membered ring undergoes deprotonation and carbon atom interchange to in turn expand to a sixmembered ring (steps D and F). Methylation involving methanol leads to the ultimate formation of hexamethylbenzene (hexaMB) (steps E and G). This process is then repeated as hexaMB is converted back to the starting species (heptamethyl benzenium ion) via gem methylation with methanol (step H). Isotope labelling

This article is licensed under a Creative Commons Attribution-NonCommercial 3.0 Unported Licence

Open Access Article. Published on 22 2025. Downloaded on 30.10.2025 01:47:29.

experiments conducted by Bjørgen et al. ¹³⁹ promoted the idea that the paring mechanism may be the dominant route in olefin formation over zeolite catalysts. Precisely, the group reacted ¹³C-methanol and ¹²C-benzene over H-beta zeolite catalyst. In turn, methylbenzene species (comprised of a ¹²C-benzene ring) with ¹³C methyl groups were generated. The gas-phase product isotopic distribution provided evidence in support of the existence of the paring mechanism. A great portion of the propene product molecules contained carbon atoms (¹²C) from the benzene ring, which is in line with the notion of the ring contraction-expansion of the paring mechanism. Furthermore, as seen in Figure 18 (B), one study ¹³⁶ utilized DFT-based modelling to analyze the most crucial reaction steps of the paring mechanism (i.e., up to ethylene formation (step B')). It was uncovered that the paring mechanism may be an energetically feasible pathway for certain zeolite catalysts (such as H-ZSM-5), but it was argued that in the case of H-SAPO-34, the side chain mechanism seems to be more favorable in comparison (due to both the less favorable kinetics and thermodynamics of the B' step).

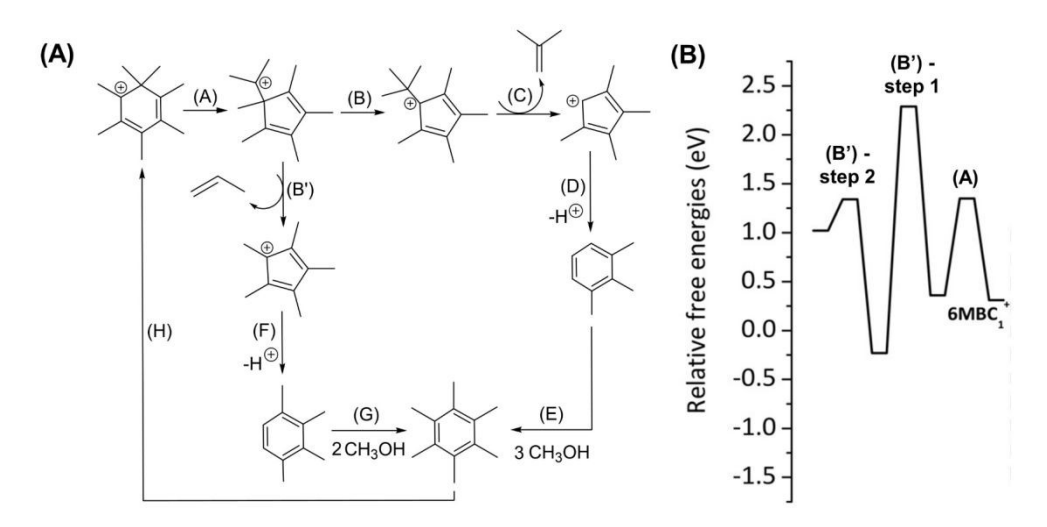


Figure 18 (A) Paring mechanism via the polyMB cycle for the MTO reaction over zeolite catalyst. Adapted from references ¹²⁴ and ¹²⁵ with permission from Elsevier, Copyright 2005 and John Wiley and Sons, Copyright 2009 respectively. (B) Free energy profile of the most crucial steps of the polyMB based paring mechanism (at 452 °C), initiated from the most favorable gem-methylated carbenium intermediate (6MBC₁+) over H-SAPO-34. The energy reference is the free energy of the adsorbed gem-methylated carbenium intermediate (ZO⁻-6MBC₁+) alongside three gas-phase methanol molecules.

Adapted from reference¹³⁶ with permission from American Chemical Society, Copyright 2021.

Hence, overall, in terms of the two key mechanisms ('side chain' and 'expansion- contraction'), the articles studied have suggested that both are likely to take place, but that it is largely dependent on the zeolite's acid site strength, leading to the favoring of one over the other ^{124–126}. From a theoretical perspective, as dictated by Olsbye et al. ¹²⁴, the side chain mechanism could be favored over the expansion-contraction mechanism by utilizing a zeolite catalyst with active sites of relatively low acidic strength.

3.2.3 Evolution of Mechanistic Understanding & Developments

Overall, with consideration of Table 1, the following conclusions can be made as to the preferred mechanistic pathway adopted by SAPO-34 in the MTO conversion process. To commence, it is important to reiterate that the

ournal of Materials Chemistry A Accepted Manuscrip

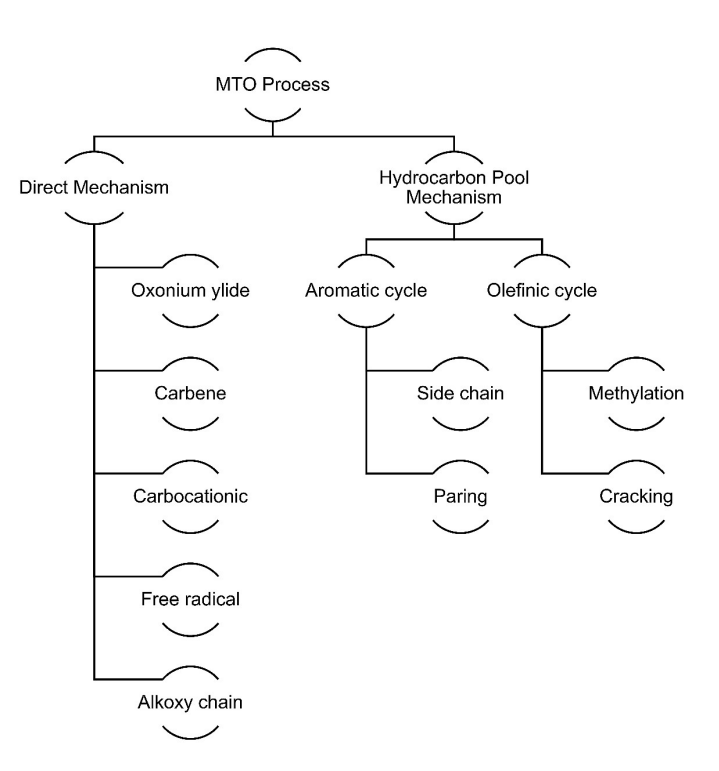


Figure 19 MTO process classification chart of mechanistic concepts.

Table 1 Supporting and opposing evidence for major proposed MTO mechanistic pathways.

Table 1 Supporting and opposing evidence for major proposed WTO mechanistic pathways.					
Mechanistic Pathway	Supporting Evidence	Opposing Evidence			
Direct mechanism 1: Oxonium ylide mechanism	 In the study conducted by Sayed¹⁴⁰, IR spectroscopy (1000-4000 cm⁻¹) of CH₃OH over HZSM-5 was used to support an oxonium-based mechanism. This involved higher ethers (methylethyl, methylisopropyl, methyl-t-butyl) that decompose to ethene, propene, and isobutene. Two observations were observed by the author that provide the key evidence: (1) after DME consumption, methanol bands reappear (O-H stretch at 3675 cm⁻¹, C-O stretch at 1033 cm⁻¹) despite a DME feed, suggesting reversible oxonium intermediates; and (2) a loss of DME bands (1102 cm⁻¹ C-O stretch, 1178 cm⁻¹ CH₃ rock), which coincides with the growth of a C=C band at 1650 cm⁻¹, consistent with DME-to-alkene conversion. In the study presented by Olah et al¹⁴¹., GC and GC-MS analysis were carried out to investigate the mechanism of the conversion of methanol/dimethyl ether, with particular emphasis on how the initial C-C bond forms. Labeling experiments strongly indicated the formation of initial trimethyloxonium ions, followed by the production of oxonium ylides (i.e., methylenedimethyloxonium ylide) via proton abstraction. The authors claimed that, ultimately, the cleavage of oxonium ion intermediates results in the formation of ethylene and dimethyl ether. 	 The study by Sayed¹⁴⁰ was conducted for MTG/HZSM-5 conversion. Considering the key differences between ZSM-5 and SAPO-34 (ZSM-5 being more acidic in nature, holding a larger average pore size, and possessing MFI topology relative to CHA topology), it could be argued that the oxonium ylide mechanism, while applicable for ZSM-5, may not be as dominant in MTO over SAPO. The focus of the study by Olah et al¹⁴¹ is on bifunctional acid-base catalyst systems, which possess no shape selectivity of zeolites. Hence, the mechanistic details presented by this study on the oxonium ylide may also not be fully applicable to MTO over SAPO, due to this clear discrepancy in catalyst system utilized. 			
Direct mechanism 2: Carbene mechanism	 Chang et al ¹⁴². provided evidence obtained from ¹³C isotope-labeling experiments showing the existence of carbenoid C₁ species during methanol reactions over HZSM-5 zeolites. It was ultimately concluded that these species are partly involved in the initial C-C bond formation process in the methanol conversion process. 	- In the study by Chang et al ¹⁴² ., it was claimed that the reactions of olefins over zeolites can be explained partly by classical carbenium ion mechanisms. The group claimed this lead to alkanes and aromatics and in turn, catalyst deactivation. However, the precise mechanism of initial C-C bond formation from methanol,			

- The study presented by Minova et. al¹²⁰ proposes a carbene coupling reaction pathway for olefin formation from surface methoxy groups. The group claimed that insertion of surface carbene-like species into adjacent surface methoxy groups is a key step in the induction period of MTO over SAPO-34. This was supported by spectroscopic evidence utilizing synchrotron FTIR microspectroscopy coupled with mass spectrometric analysis.
- involving carbene species, was not presented, which makes the claimed involvement of these species still subject to speculation. Another point of consideration is the fact that this paper was conducted over a more acidic, larger pore size zeolite (ZSM-5) as opposed to SAPO-34.

- In the study presented by Nagy et al. ¹⁴³, ¹³C-NMR and gas chromatography analysis presented data suggesting that a carbenium ion mechanism was highly probable in methanol conversion reactions. The group claimed that the involvement of carbenium ions led to the presence of alkanes and ethylene under the reaction conditions reported.
- The report conducted by Minova et al.¹²⁰ presents experimental evidence in the form of spectroscopic studies, stating that methoxy cations also play an important role (alongside previously discussed carbene-like species) as intermediates during the MTO process over SAPO-34.
- A computational study by Lesthaeghe et al.¹⁴⁴ also claims the involvement of carbenium ions in methanol to olefins conversion. The group reports that the zeolite framework is able to assist in stabilizing carbenium ion species, thereby reducing the energy barriers associated with mechanistic steps involving their formation and presence. Furthermore, the group reported that the CHA topology of SAPO-34 and SSZ-13 was best able to stabilize cationic species as opposed to other studied zeolite topologies (i.e., MFI).
- The study by Nagy et al.¹⁴³ focuses on the conversion of methanol on H-ZSM-5 in the presence of carbon monoxide. Hence, it could be argued that the discrepancy in the feed (i.e., not pure methanol fed) and the choice of catalyst system (ZSM-5 as opposed to SAPO-34) makes the evidence less reliable when applied to the traditionally conducted MTO process over SAPO-34.
- Although the study by Lesthaeghe et al.¹⁴⁴ provided valuable insight into the role of carbenium ions in methanol to olefins conversion, the group does not provide experimental findings to back up the computationally-directed claims presented in the paper.

Direct mechanism 4: Free radical mechanism

This article is licensed under a Creative Commons Attribution-NonCommercial 3.0 Unported Licence

Open Access Article. Published on 22 2025. Downloaded on 30.10.2025 01:47:29.

- Clarke et al.¹⁴⁵ studied the mechanistic pathway of dimethyl ether over H-ZSM-5 zeolite, and in turn detected the presence of free radicals by using a spin trapping reagent with e.s.r. analysis. The group thereby provided evidence that free radicals are involved in the initial C-C bond forming step and exist as important intermediates for the ultimate production of both alkenes and aromatics.
- The study by Clarke et al. 145 remains valuable for its mechanistic insights into the involvement of free radical species in hydrocarbon conversion. However, the focus of the study is on the reaction of dimethyl ether over H-ZSM-5 zeolite, with the goal to produce alkene and aromatic hydrocarbons. Hence, as with other previously mentioned studies, the applicability of these mechanistic details to MTO over SAPO-34 could be questioned.

Direct mechanism 5: Alkoxy chain growth route

- Researchers¹²⁰ have validated the presence of surface alkoxy species during the methanol conversion process, through the use of spectroscopic evidence. The group claims that such alkoxy species (primarily methoxy species) are the core intermediates during the induction period of the MTO process, and exist amongst the pool of other pre-mentioned hydrocarbon species (e.g., carbocationic species).
- Computational research by Ke et al.¹⁴⁶ has also provided partial evidence for the likely existence of alkoxy species during the MTO process. The group utilized microkinetic simulations in a three-site model to claim the existence of these species as intermediates in the reaction.
- To the best of our knowledge, there exists limited research papers¹²⁰ containing experimental evidence in support of this direct route. The majority of MTO mechanistic studies mention the possible existence of these species as intermediates during the induction period, but relative to the HCP concept, the alkoxy chain growth route is of much lower significance.

HCP Mechanism 1: Aromatic cycle

- A study by Mole et al. ¹⁴⁷ provided evidence (in the form of ¹³C and ²H isotope labelling experiments) for the existence of the aromatic cycle of the hydrocarbon pool concept. The group targeted their efforts on validating the side chain mechanism of the aromatic
- In the study by Mole et al. ¹⁴⁷, the authors state that the experimental evidence collected implies alternative or additional pathways within the aromatic cycle (such as ring expansion/contractions in addition to the side chain

This article is licensed under a Creative Commons Attribution-NonCommercial 3.0 Unported Licence

Open Access Article. Published on 22 2025. Downloaded on 30.10.2025 01:47:29.

cycle for light olefin formation. It was ultimately revealed via these experiments that the side chain mechanistic scheme is viable. The mechanism implies that the carbon of the methyl group of a methylaromatic compound should be eventually incorporated into ethylene. This was validated by the labelling experiments where conversion of methanol, in the presence of toluene (with ¹³C situated in the toluene methyl group), led to the capture of ¹³C labelled ethylene.

- A study by Lesthaeghe et al¹⁴⁴ also provided valuable insight on the aromatic cycle of the HCP concept, focusing on methanol to olefins conversion over ZSM-5 zeolite. The group's theoretical computations verified that the side chain mechanism on methylbenzenes over zeolite catalysts is a plausible reaction scheme in the formation of ethene from methanol. On the other hand, the paring mechanism of the aromatic cycle (focusing on ring expansion/contraction) has been shown to favour the production of propene or isobutene. Overall, the group claims that the aromatic cycle is a dominant mechanistic concept of the MTO process.
- A study by Li et al. ¹⁴⁸, involving ¹³C-labeling pulse experiments, indicated that the aromatic based hydrocarbon pool mechanism was the most dominant reaction route of methanol conversion over SAPO-34. The group studied a variety of zeolites, including SAPO-34, H-ZSM-5 and H-ZSM-22, concluding that SAPO-34 in particular favours the aromatic cycle, with the zeolite holding enough spaces in its framework to accommodate large aromatic intermediates.

- mechanism). Specifically, it was stated that the group's interpretations should be regarded as a working hypothesis rather than a rigorously established mechanism. Hence, the complexity of the HCP mechanistic scheme can make it difficult to establish an exact and dominant path.
- In the study by Lesthaeghe et al¹⁴⁴, it is important to note that the group faced some bottlenecks in uncovering the most energetically favourable route for ethene formation via the side chain mechanism. It was found that the main issue (energetically speaking) existed in the elimination steps of ethene. Hence, determining the exact route with lowest energy barriers for olefin formation is not always a straightforward process, especially given the pool of simultaneous reactions taking place in the aromatic cycle. Moreover, it should be noted that this study was conducted over H-ZSM-5 and not SAPO-34; hence, as with previously mentioned studies, the applicability of certain mechanistic details may be questioned given the discrepancies in acidity and pore size between the two zeotypes.
- The study by Li et al.¹⁴⁸ demonstrates that zeolite type plays a large role in determining the route adopted within the hydrocarbon pool mechanism. Due to the space confinement discrepancies that exist between zeolites of different structural topologies, this alters the type of hydrocarbon pool species that are most dominant. Overall, this once again highlights the complexity involved in determining the exact aromatic-based path adopted for the MTO process.

HCP Mechanism 2: Alkene cycle

- A study by Gong et al. ¹⁴⁹ presents the existence of the alkene (olefinic) cycle of the hydrocarbon pool concept. Spectroscopic evidence conducted by the group elucidates the fact that both the aromatic and olefinic cycle exist in the hydrocarbon pool concept as a dual cycle mechanism that simultaneously occurs. It was concluded that the extent to which each of the two cycles dominate depends on the treatment of the zeolite.
- A study by Ke et al. 146 performed simulations in a three-site model to study the MTO conversion in industrially relevant H-SAPO-34 zeolite under a wide range of operating conditions. Via a combination of DFT calculations and microkinetic simulations, the group confirmed the presence of a dual cycle concept (involving both the olefinic cycle and aromatic cycle) within the global hydrocarbon pool framework in the MTO process. The group concluded that the reaction conditions implemented affected the extent to which each cycle dominates. Specifically, it was uncovered that the aromatic-based cycle dominated in MTO
- The study conducted by Gong et. al ¹⁴⁹ focuses on the effect of steamed ZSM-5 zeolite on the reaction mechanism for the methanol-to-hydrocarbons process. Hence, this discrepancy in catalyst system and treatment approach implies that the mechanistic details may not be directly applicable.
- The study by Ke et al. 146 provides valuable insight into the mechanistic details of the hydrocarbon pool framework- specifically capturing the dual cycle concept and the relative dominance of each cycle under different operating conditions. However, it should be noted that this study is still highly theoretical/computational. Hence, there still exists a greater need for more complementary studies bringing experimental validation of the recently proposed dual cycle notion.

- An article by Yu et al¹⁵⁰ provided experimental validation of the existence of the dual cycle concept over SAPO-34 in the MTO process. Via the employment of a ¹²C/¹³C-methanol isotope switching experiment, the group were able to acknowledge the existence of both an aromatic-based cycle and alkene-based cycle taking place during the bulk of the MTO reaction process. The detailed reaction route was highly dependent on types of organic species most dominant in the catalyst framework at different times on stream. It was uncovered by the group that during the efficient reaction period, the aromatics-based cycle existed as the dominant of the two. However, during both the induction and deactivation periods, the olefinic-based cycle contribution grew larger.

This article is licensed under a Creative Commons Attribution-NonCommercial 3.0 Unported Licence

Open Access Article. Published on 22 2025. Downloaded on 30.10.2025 01:47:29.

In recent years, researchers have focused their efforts on understanding the factors that influence the mechanistic pathways involved in methanol conversion over zeolite catalysts, particularly with regard to schemes that fall under the HCP concept. The dominant route, in terms of the likelihood of formation of specific HCP intermediates (e.g., Polymethylbenzenes (PMBs) vs Polymethylnapthalenes (PMNs)), and subsequent production of light olefins utilizing these intermediates, seems to depend highly on the zeolite catalyst acidity, topology, and reaction conditions in place.

Commencing with acidity, researchers ¹⁵¹ have placed great emphasis on the tuning of hydrocarbon pool intermediates by alteration of this parameter. Using GC-MS and NMR methods, it has been uncovered that SAPO-34 with lower Brønsted acid site density (i.e., by utilizing a SiO₂/Al₂O₃ molar ratio of 0.2 in the starting gel) were found to favor the promotion of PMBs as active hydrocarbon pool species as opposed to PMNs. This was justified by the suppression of intermolecular hydrogen transfer reactions, which are needed for the growth of PMBs into polycyclic aromatics, such as PMNs and beyond. It should be noted that researchers ¹⁵¹ have discerned that alterations in SAPO particle size (i.e., morphological changes), unlike acidity changes, has a much smaller impact on the product distribution. Hence, this indicates that particle size as a parameter holds little to no impact on the favoring of a PMB or PMN-based HCP route for olefin formation.

Researchers ¹⁵² have also investigated the effects of zeolite topology on the mechanistic route adopted for olefin formation from methanol. DFT and ab initio calculations conducted on the paring mechanism (a key mechanism of the aromatic cycle of the HCP concept) for different zeolite topologies, such as MFI (H-ZSM-5), AFI (H-SSZ-24) and CHA (H-SAPO-34), demonstrated a clear favoring of this mechanism over the CHA (H-SAPO-34) zeolite. Differences in pore size amongst the different topologies were ascribed to play a major part in determining the likelihood of the paring mechanism to take place. The researchers justified that zeolites with larger pore sizes (such as ZSM-5) were able to better accommodate the mobility of heptaMB+ (a key intermediate of the paring

This article is licensed under a Creative Commons Attribution-NonCommercial 3.0 Unported Licence.

Open Access Article. Published on 22 2025. Downloaded on 30.10.2025 01:47:29.

mechanism), encouraging the adsorbate to rearrange and achieve more favorable transition state structures, which possessed generally higher free energy of adsorbed states. Hence, higher overall energy barriers for the paring mechanism were observed over larger pore zeotypes like ZSM-5, making it less favourable to occur relative to small-pore ones like SAPO-34.

Lastly, researchers have also demonstrated the effect that chosen reaction conditions can impose on the mechanistic route adopted for methanol conversion over SAPO-34 catalyst. As discussed in Chapter 2 (the MTO Process), it is well established, through experimental validation, that alterations in process operating parameters (such as temperature) play a large role in determining the product distribution ^{153–155}. However, some researchers have taken the next step of investigating how this effect occurs. This has been achieved by both analyzing the species developed during the reaction period (upon changes in reaction conditions) via in-situ and/or operando experimental techniques, as well as by applying modelling/computational-based methods. Commencing with one of the most important operating parameters, researchers have 156 demonstrated (via the use of operando UV-vis spectroscopy and methanol pulse experiments) that alterations in the process temperature can highly impact the nature of active and deactivating species formed during MTO over SAPO-34, thereby shifting the mechanistic pathway adopted to form olefins. Researchers ¹⁵⁶ have observed that for the lower MTO process temperature range of 300 °C and 325 °C, the active HCP species are primarily highly methylated benzene carbocations (and low amounts of methylated naphthalene carbocations species), which have been found to favour the selectivity towards propylene formation. At this low temperature range, these methylated naphthalene species were found to act as deactivating species, since catalyst deactivation was caused by the gradual filling and eventual blocking of micropores by these species. At a greater temperature condition of 350 °C, the active species consist of a mixture of both highly methylated benzene carbocations and methylated naphthalene carbocations. A higher MTO process temperature range of 400 °C and 500 °C has been found to preferentially promote methylated naphthalene carbocations as the primary active HCP species (and low amounts of highly methylated benzene carbocations). which has been found to favour the formation of ethylene. At this high temperature range, the Methylated naphthalene carbocation species only act as active species. However, these species do eventually give rise to the production of phenanthrene/anthracene (polycyclic) aromatic deposits (both neutral and carbocationic species). which are then mainly responsible for the deactivation by pore blockage at the higher temperature range.

Besides temperature, researchers ¹⁵⁷ have also investigated how other operating conditions shape the mechanistic pathways of the MTO process over SAPO-34. Microkinetic simulations, involving more than 300 elementary steps, have revealed that pressure (*p*) and water-to-methanol feed ratio (*x*) also play significant roles in determining the route taken by the hydrocarbon pool (HCP). Before addressing these effects, it is important to note that recent studies on the HCP concept have begun to support the existence of a dual-cycle mechanism taking place (see Figure 20). This involves the well-documented aromatic-based cycle (driven by polymethylbenzenes (PMBs) and polymethylnaphthalenes (PMNs) as key active intermediates, producing light olefins via side-chain and paring

mechanisms) as well as the existence of an olefinic-based cycle (in which heavier olefins act as reactive intermediates and form lighter olefins through successive methylation and cracking steps). This represents a rather recent development to the original claims of a stand-alone, single aromatic-based cycle within the HCP concept. Hence, considering this, researchers are now beginning to determine how operating conditions affect both (i) the extent to which these two major cycles of the HCP occur, as well as (ii) the specific trends observed within each cycle. Commencing with the former, it can be seen that the overall rate of methanol conversion is dominated by the aromatic-based cycle at high temperatures, low pressures, and low water-to-methanol feed ratios. In contrast, the inverse trends cause the olefinic-based cycle to become dominant, often proceeding 1-5 orders of magnitude faster than the aromatic-based cycle. Regarding the latter, it can be seen that distinct selectivity trends emerge within each cycle ¹⁵⁷. For the aromatic-based cycle, the paring mechanism is favoured at high temperatures, low pressures, and low water content, leading to higher propylene selectivity relative to ethylene, whereas the sidechain mechanism is promoted under the opposite conditions, increasing ethylene formation. On the other hand, in the olefinic-based cycle, low temperatures and high pressures favor propylene formation (i.e., the opposite trend to the aromatic-based paring mechanism). However, high water content favors ethylene formation, mirroring the aromatic side-chain mechanism. Overall, considering that the reaction conditions in place both affect the relative dominance of each cycle and the cycle-specific selectivity trends, the following two conclusions can be made. Firstly, propylene formation is more consistently associated with the dominant cycle under its optimal conditions. Under higher T, lower p, and lower x, the dominant aromatic-based cycle favors propylene formation via the paring mechanism. Inverse reaction conditions dominates the olefinic cycle, which then tends to also favor propylene formation under those conditions. Secondly, with regards to ethylene formation, it seems that although ethylene can be favored within either cycle under certain conditions, those conditions in place do not usually coincide with those in which the ethylene-producing cycle dominates overall conversion. This demonstrates the overall dominance of propylene formation, relative to ethylene formation, under almost all operating conditions set.

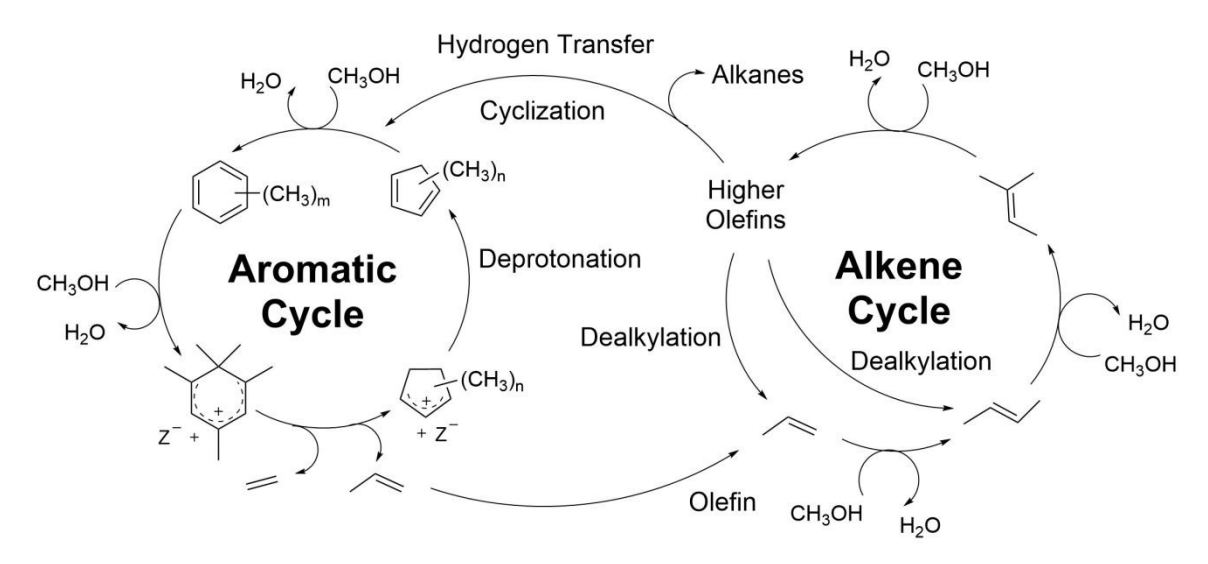


Figure 20 Simplified Mechanistic Scheme of the Dual Cycle Concept of the Hydrocarbon Pool Mechanism. Reproduced from reference ¹⁵⁸ from Académie des Sciences, Copyright 2018.

Although it has been appropriate to uncover how the MTO mechanism (and henceforth, product distribution) alters as a function of the set operating conditions, it is of even greater value to understand how the mechanism takes place under specific, industrially relevant conditions. As outlined in Chapter 2 (MTO Process), the commercial fluidized-bed reactors typically operate at ~400 °C, near-atmospheric pressure (~1 bar), and with a water-to-methanol feed ratio of about 1:1 (molar). Under these conditions, researchers ¹⁵⁷ have shown that the olefinic-based cycle of the hydrocarbon pool (HCP) strongly dominates, with the simulated methanol conversion rate exceeding that of the aromatic-based cycle by more than forty-fold, closely reproducing experimental conversion values. With regards to the cycle-specific selectivity, under these conditions, microkinetic simulations demonstrate that the dominant olefinic cycle favours propylene formation relative to ethylene, with a roughly one order of magnitude higher formation rate. Altogether, these findings highlight the critical role of the olefinic-based HCP cycle in governing MTO conversion over H-SAPO-34 under industrially relevant conditions.

3.3 Deactivation pathways

The consensus amongst articles regarding coke formation is that the mechanism commences with polyalkylnaphthalene. This group of molecules are said to undergo molecular rearrangement, ring expansion and aromatization, which leads to the formation of multi-ring aromatics, as seen in Figure 22. Ultimately, these heavy aromatics (so-called coke) block zeolite catalyst pores, preventing the diffusion of reactant molecules (methanol) towards active sites and resulting in catalyst deactivation ^{133,159}. The nature of such coke species can be visually observed in Figure 21, which demonstrates the results of a gas chromatography–mass spectrometry (GC-MS) analysis conducted over deactivated SAPO-34 catalyst, with the species beyond 11 minutes retention time indicative of the type of compounds responsible for deactivation.

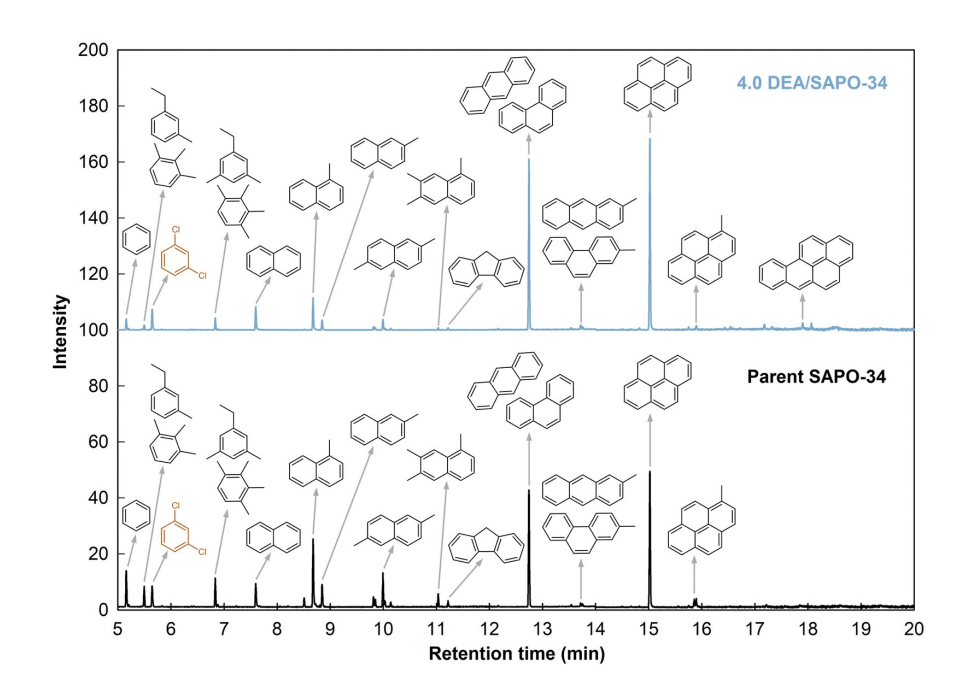


Figure 21 GC-MS analysis of coke species formed over deactivated SAPO-34 catalyst (directed with tetraethylammonium hydroxide (TEAOH)) and deactivated SAPO-34 catalyst post-treated with 4.0 molar diethylamine (DEA) aqueous solution. Reproduced from reference¹⁶⁰ with permission from Royal Society of Chemistry, Copyright 2023.

Interestingly, as multi-ring aromatics begin to form, the necessary hydride transfer reactions between intermediate species and surface-associated methoxy groups leads to the formation of methane molecules (see Figure 22). Thus, this can provide a justification as to why methane and coke production seem to rise concurrently during the MTO reaction, since the hydride transfer step (which generates methane) is necessary for the building up of aromatic rings to form coke species. Figure 22 also illustrates the free energy profile associated with the mechanistic scheme developed for the formation of anthracene and phenanthrene (i.e., types of multi-ring aromatics that constitute coke) ¹³³. The conducted DFT modeling indicated that anthracene and phenanthrene production in zeolite cages is kinetically more difficult relative to the generation of benzene and naphthalene. Moreover, the free energy barriers of methylation and olefin elimination steps in the previously discussed polymethylnapthalene (poly(MN)) based side chain mechanism are much lower in comparison to the hydride transfer reactions for anthracene and phenanthrene formation. Hence, it can be concluded that (poly)MB and (poly)MN are more likely to assist in the formation of olefins, the more favourable pathway, rather than simply build up to form polycyclic aromatics. In other words, these species take on more of a role as the active components of the hydrocarbon pool mechanism, rather than being the precursors for inactive species.

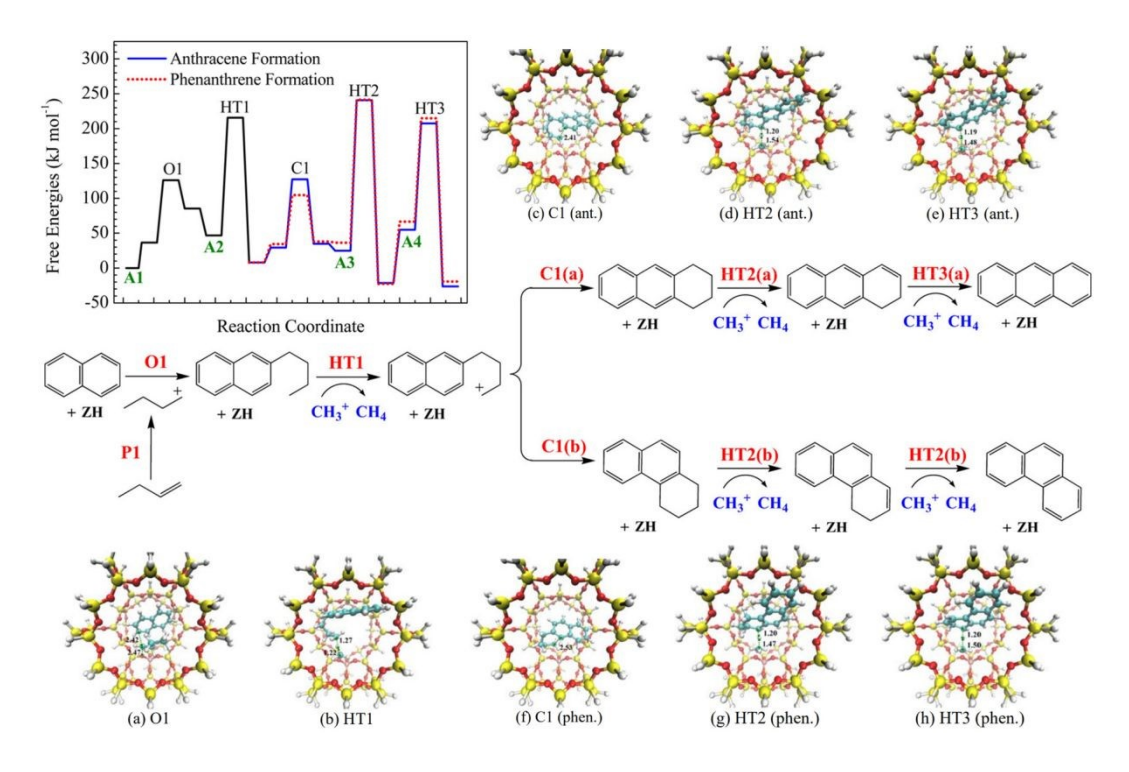


Figure 22 Proposed mechanistic path for the formation of polycyclic aromatic species (anthracene and phenanthrene) during the MTO reaction over zeolite catalyst. The top left plot presents the free energy profile for both anthracene (ant.) and phenanthrene (phen.) production (at 400 °C) in the MTO reaction over zeolite catalyst. In addition to the zeolite framework, naphthalene and adsorbed butene (A1) are taken as the reference state for the formation of

anthracene and phenanthrene. A2, A3, and A4 represent methoxyl generation at the active site prior to the hydride transfer reactions. For each of the elementary steps, the optimized transition states have been presented schematically. Notation: O1 refers to oligomerization, HT1–HT3 refer to hydride transfer reactions, and C1 is for the 1,6-cyclization. Atom colorings: yellow (Si), red (O), white (H), pink (Al) and blue (C). Bonding distances are presented in Å. Reproduced from reference¹³³ with permission from American Chemical Society, Copyright 2016.

3.4 Limitations of mechanistic studies

Although much progress has been made towards uncovering the mechanisms of the methanol conversion to olefins reaction, the individual steps amongst a majority of these mechanisms are somewhat vague, and do not normally possess the detail needed to be termed as elementary steps. Furthermore, a majority of the mechanisms presented have been generalized for different types of zeolites (such as mordenite, H-ZSM-5, and SAPO-34), which may not be accurate considering differences in acidity, topology, and pore sizes. In reality, these factors that distinguish one zeolite catalyst from another could largely affect the activation energies associated with elementary steps, and in turn influence the mechanistic route adopted. Research to explain how some zeolites may favor one path over another is quite limited and has only recently emerged 136. With DFT calculations of van der Waals dispersive corrections, one group ¹³⁶ concluded that the 'side chain mechanism' acts as the major reaction pathway over H-SAPO-34, whereas the H-ZSM-5 catalyst was shown to favor the paring route instead. Furthermore, according to the generalized HCP mechanism, polyalkylaromatics, which are deemed the active intermediates for light olefin production, are themselves being produced from light olefins, which seems counterintuitive. To the best of our knowledge, there still exists a lack of comprehensive studies that compare the elementary steps and energy activation barriers of initial light olefin production and desorption i.e., referring to early time on stream, with that of further olefin reconstruction to create polyalkylaromatics and late-stage light olefins. Furthermore, as has been touched upon in this section, it is clear that research groups are in agreement that aromatic species such as benzene and naphthalene play a dual role in both olefin and coke formation. However, up to the present day, mechanistic studies struggle to uncover the ways to fine-tune the mechanism in order to prevent or largely limit the pathway of coke production, while instead promoting olefin formation from these active intermediates. This remains at the forefront of future work in the field of MTO and its reaction mechanism. Lastly, research groups have begun to reveal superior ways to modify the catalyst synthesis procedure in order to achieve superior catalytic performance in the MTO reaction, involving the pre-treatment, post-treatment, and mixed templating of the catalyst (which will be discussed further in Section 4). As of now, mechanistic studies have largely focused on detailing the reaction route associated with the traditionally prepared SAPO-34 catalyst; hence, investigations into the potential mechanistic alterations associated with catalyst modification are yet to be fully revealed.

3.5 MTO reaction and deactivation kinetics

As seen by the highly varied and complex mechanistic scheme that constitutes the MTO reaction (discussed in Section 3), no kinetic model from research until present day has been able to fully encapsulate MTO's extensive reaction network. Research groups that have delved into the field of MTO kinetics (with SAPO-34 as the catalyst) have largely presented simplified lumped kinetic models that are derived from reaction schemes comprising a small number of steps. Iterative approaches were tried and tested until model predictions of MTO performance were comparable to that of the experimental data. Different approaches at developing these models have been utilized, ranging from the use of simple power laws to the application of the Langmuir-Hinshelwood (LH) approach. For a detailed insight into the specific reaction and deactivation kinetic models utilized, kinetic parameters, and rate expressions used by different research groups, consult the Supplementary Information. One example can be taken from Fatourehchi et al. 161 who utilized both LH and power law kinetic models to derive their rate equations. The developed simple mechanism consisted of five reaction steps (which can be seen in Table 2), involving the adsorption of methanol on the surface of the zeolite (in place of a Brønsted acidic site), followed by the formation of a surface-associated dimethyl ether, which could subsequently desorb or instead convert to light olefins. With use of the LH formulation, it was assumed that the reactant methanol molecules were able to adsorb on the surface of the catalyst, diffuse in close proximity to the surface, and in turn react with surface associated molecules. Evidently, the generated products on the surface are assumed to desorb into the fluid phase without constraint. Other than the LH mechanism, all other possible paraffinic products were lumped together as a singular species, and the corresponding reaction rate expression was formulated as a simple power law. Reaction steps 3 to 5 were presumed to be rate-determining. The group established this via an iterative approach of altering the assumed rate-determining steps, and in turn comparing the predictions from a variety of suggested rate models with experimental data.

Table 2 Reaction mechanism and final reaction rate expressions used to describe the MTO process over SAPO-34 catalyst, based on both Langmuir-Hinshelwood and power law kinetic models ¹⁶¹.

Reaction pathway*	Rate expressions**
$MeOH + Z \overset{k_m}{\underset{k'_m}{\rightleftharpoons}} MeOH \cdot Z$	_
$2 \operatorname{MeOH} \cdot Z \underset{k'_d}{\rightleftharpoons} \operatorname{DME} \cdot \operatorname{Z} + \operatorname{H}_2\operatorname{O} + \operatorname{Z}$	_
$DME \cdot Z \overset{k_r}{\to} DME + Z$	$r_r = \frac{k_r K_d K_m^2 p_{MeOH}^2}{p_w (1 + K_m p_{MeOH} + (K_d K_m^2 p_{MeOH}^2 / p_w))}$
$DME \cdot Z \xrightarrow{k_e} C_2 H_4 + H_2 O + Z$	$r_e = \frac{k_e K_m^2 p_{MeOH}^2}{P_w (1 + K_m p_{MeOH} + (K_d K_m^2 p_{MeOH}^2 / p_w))}$

This article is licensed under a Creative Commons Attribution-NonCommercial
$$3.0$$
 Unborted Ficence. Substate the control of difference and the cataly data, t , wein the control of the

$$\begin{split} \text{DME} \cdot \text{Z} + \text{MeOH} \cdot \text{Z} &\overset{k_p}{\to} \text{C}_3 \text{H}_6 + 2 \text{H}_2 \text{O} + 2 \text{Z} \\ & - \\ & r_p = \frac{k_p K_d K_m^3 p_{MeOH}^3}{p_w (1 + K_m p_{MeOH} + (K_d K_m^2 p_{MeOH}^2 / p_w))^2} \\ & - \\ & r_{Paraffin} = k_{Paraffin} p_{Paraffin}^n \end{split}$$

With regards to the detailed studies seen in the Supplementary Information (e.g., Table S5), some groups considered coke formation as part of their reaction rate expressions, as it influences the products distribution substantially $^{100,162-164}$. Accordingly, one group 162 formulated a kinetic model and included the coke-dependent parameter by using a thermogravimetric reactor and measuring the coke content over time on stream. Both rate expressions, involving feed consumption (methanol and dimethyl ether, lumped as MDOH) and rate of production of different species i, contains the parameters a' and a_i , which, respectively, are indicative of the catalyst activity and the dependency of each species production on the coke content (see Table 3). The group tested a range of catalyst activity functions (a') and found that the exponential function provided the best fit for the experimental data, justified by its higher correlation coefficient (0.9965). This catalyst activity expression is a function of only the coke content (C), determined by the TGA. The coke content C in turn is a function of the temperature C, time C, weight hourly space velocity C0.

Table 3 MTO reaction pathways and rate expressions, with inclusion of a coke dependency term ¹⁶².

Decation motherways	Rate ex	kpressions**
Reaction pathway*	Rate of consumption of species A (MDOH)	Rate of production of species i
	$r_{\mathrm{A}} = a' \cdot r_{\mathrm{A0}} = a' \cdot k_{\mathrm{A}}^{0} e^{-\left(\frac{Ea_{\mathrm{A}}}{RT}\right)} p_{\mathrm{A}}$	$r_{\rm i} = a' \cdot r_{ m A0} \cdot lpha_{ m i} = a' \cdot k_{ m A}^{0} e^{-\left(rac{E lpha_{ m A}}{RT} ight)} p_{ m A} \cdot lpha_{ m i}$
$MDOH \xrightarrow{k_1} CH_4$	$r_{\rm A}=a'\cdot k_{\rm A}^0 e^{-\left(\frac{Ea_{\rm A}}{RT}\right)}p_0y_{\rm A}$	$r_{\mathrm{i}} = a' \cdot k_{\mathrm{A}}^{0} e^{-\left(\frac{Ea_{\mathrm{A}}}{RT}\right)} p_{0} y_{\mathrm{A}} \cdot \alpha_{\mathrm{i}}$
$MDOH \xrightarrow{k_2} C_2H_4$ $MDOH \xrightarrow{k_3} C_3H_6$	$r_{\rm A} = a' \cdot k_{\rm A}^0 e^{-\left(\frac{Ea_{\rm A}}{RT}\right)} p_0 \cdot \frac{1 - X}{1 + X \cdot \sum_{\rm i} \alpha_{\rm i} + \frac{N_{\rm N_2}}{F_{\rm A} \cdot t_p}}$	$r_{\rm i} = \alpha' \cdot k_{\rm A}^0 e^{-\left(\frac{Ea_{\rm A}}{RT}\right)} p_0 \cdot \frac{1 - X}{1 + X \cdot \sum_{\rm i} \alpha_{\rm i} + \frac{N_{\rm N_2}}{F_{\rm A} \cdot t_p}} \cdot \alpha_{\rm i}$
$MDOH \xrightarrow{k_4} C_4H_8$	Where, catalyst acti	vity function: $a' = e^{-\beta C}$
$MDOH \xrightarrow{k_5} C_n H_m^{***}$	$C = C_0 \left(1 - e^{\left\{ \left[a + b \left(\frac{T}{1000} \right) + \right] \right\}} \right)$	$c\left(\frac{T}{1000}\right)^{2} + d\left(\frac{T}{1000}\right)^{3} + f \cdot p \cdot WHSV \cdot t$
	Where, stoichiometric coefficien	t function: $\alpha_i = x_i (e^{u_i \cdot c} + z_i) \cdot e^{v_i/T}$

^{*}Reaction pathway presented as simplified unbalanced reactions (side products omitted). MDOH refers to the lumped species of MeOH and DME.

^{*}Reaction rate constants (k_j) are in units of mol $g^{-1}h^{-1}$, except for $k_{Paraffin}$, which is in units of mol $g^{-1}h^{-1}$ bar⁻ⁿ (where n = 0.31). Z in the reaction expressions refer to the zeolite active site.

^{**} r_i refers to the rate of species i production (mol g⁻¹ h⁻¹). K_j refers to the equilibrium constant for a reaction j. p_w and p_{MeOH} refer, respectively, to the partial pressure (bar) of water and methanol in the feed.

^{**} N_{N_2} refers to the molar flow rate of N_2 (mol h^{-1}). F_A is the molar flow rate of methanol feed (mol min⁻¹). t_p is the pulse duration (min). p_A and p_0 respectively refer to the partial pressure of compound A (MDOH) and the initial total system pressure (both in MPa).

R is the gas constant (8.314 J mol⁻¹ K⁻¹). C is the weight percentage of coke on the catalyst in $g_{coke}/100 g_{Cat}$. C_0 is the final coke content on the catalyst in

Overall, considering the dependence of product distribution on catalyst coke content, feed dilution, and temperature (as explained in Section 2), a universal and acceptable kinetic model should consider all the aforementioned influential parameters. In addition, the activity tests used to estimate the kinetic rate constants ought to be conducted under conditions that closely resemble industrial or realistic settings. Regrettably, some of the kinetic studies overlooked the influence of catalyst coke content on products' distribution ⁵⁶ ¹⁶¹ ¹⁶⁵, while others conducted the experimental tests under unrealistic conditions such as with a heavily diluted feed with water ⁵⁶ (as opposed to the industrial case of 20 wt.% dilution with water 73). A few points need to be highlighted here concerning the derivation of a kinetic model. Firstly, to simulate a differential reactor with limited conversion, a very high WHSV must be employed, but one should be aware that SAPO-34 catalyst tends to deactivate quite rapidly upon exposure to these conditions. Hence, utmost attention should be given to not collect data over partially deactivated catalyst. Intermittent (pulse) flow of feed could be a possible solution. Secondly, since the methanol conversion to light olefins reaction is not thermodynamically limited and backward reactions are not probable, the dependence of the methanol conversion rate on its concentration can be mirrored by different levels of dilution using an inert gas instead of products. However, the diluent should not block the active sites or alter the reaction mechanism; thus, water is not a suitable fit, as one group 165 varied the water content in the feed from 0 to 75 wt.% and observed an influence of water dilution on the rate of each specific species' production. Besides this, to accurately mimic the actual reaction conditions, the diluent should impose similar molecular diffusion resistance as the actual products of the reaction (i.e., with regards to methanol penetrating into the pores). For instance, methanol diffusion in the presence of dominant MTO products such as ethylene, propylene, and butylene is not similar to methanol in argon. Table 4 summarizes the parameters and specifications of proposed kinetic models so once can assess the alignment of these models with these considerations.

Table 4 Evaluation of the proposed kinetic models for the MTO reaction over SAPO-34.

T(°C)	$WHSV \\ (g_{MeOH} \\ g_{Cat}^{-1}h^{-1})$	Dilution (wt. % of diluent in the feed)	Rate equation type	Produced and lumped species considered	Coke formation or deactivation consideration	Ref.
400 - 450	10.7 - 37.2	69 wt% water	Power law	$\begin{aligned} & DME, CH_4, C_2H_4, C_3H_6, \\ & C_4H_8, C_5H_{10}, CO, CO_2, \\ & C_2H_6 \end{aligned}$	The effect of coke was not considered	56

^{***} C_nH_m refers to rest of hydrocarbons (i.e., $C_5^=$ and paraffins).

400 - 550	57 - 2558	Helium as diluent, N/A wt%	Power law	C_2H_4 , C_3H_6 , C_4H_8 , C_5H_{10} , C_6H_{12} Lumped species: oxygenates (MeOH + DME), paraffins	Coke was included as a parameter <i>C</i> , referring to the wt% of coke on the catalyst	100
375 — 425	3.2 - 12.8	36 wt% water	Mainly Langmuir— Hinshelwood approach, minority being power law	MeOH \cdot Z, DME \cdot Z, C_2H_4 , C_3H_6 Lumped species: paraffins	The effect of coke was not considered	161
375 — 475	7.08 - 35.91	Nitrogen as diluent, N/A wt%	Power law	CH ₄ , C ₂ H ₄ , C ₃ H ₆ , C ₄ H ₈ Lumped species: MDOH (MeOH + DME), and rest of hydrocarbons (paraffins, except CH ₄ , and C ₅ *)	Coke was included as a function of the final coke content, temperature, time, <i>WHSV</i> , and methanol partial pressure	162
350 — 475	2.27 - 100	0 - 75 wt% water	Power law	C_2H_4 , C_3H_6 , C_4H_8 Lumped species: oxygenates (DME + MeOH) and rest of hydrocarbons (paraffins and C_5H_{10})	The effect of coke was not considered	165
450	1 - 500	~0.02 wt% Helium	Power law	CH_4 , C_2H_4 , C_3H_6 , C_3H_8 , coke Lumped species: C_4 (C_4H_8 + C_4H_{10}), C_5 (C_5H_{10} , C_5H_{12} , and paraffins)	Coke was included as a function of time	163
400 - 470	31.7 - 339.4	~69 wt% water	Power law	CH_4 , C_2H_4 , C_3H_6 , C_3H_8 , C_4H_8 Lumped species: MDOH (MeOH + DME), C_4 (C_4H_{10} + 1,3-butadiene), and C_5^+ (includes C_2H_6)	A deactivation rate was introduced (in terms of grams of catalyst that deactivates per unit time)	166
450	1.68 - 8.40	20 - 60 wt% water	Power law	C_2H_4 , C_3H_6 Lumped species: C_4	Coke was included as a function of time, the maximum coke content, methanol feed concentration, WHSV, and the density of the catalyst bed	164
400 - 490	1.5 - 3	40 - 70 wt% water	Langmuir- Hinshelwood- Hougen- Watson approach	DME, CH ₄ , C ₂ H ₄ , C ₂ H ₆ , C ₃ H ₆ , C ₃ H ₈ , C ₄ H ₈ , C ₄ H ₁₀ , C ₅ H ₁₀ , H ₂ , CO, CO ₂	The effect of coke was not considered	167

			Langmuir-		A catalyst activity	
			Hinshelwood-	$DME, CH_4, C_2H_4, C_2H_6,$	function was introduced	
400 - 500	3 - 6	N/A	Hougen-	$C_3H_6, C_3H_8, C_4H_8, H_2,$	as a function of	168
			Watson	CO, CO_2	temperature, time and	
			approach		WHSV	

Note on commercial conditions: WHSV of 2-3 g_{MeOH} $g_{Cat}^{-1}h^{-1}$; T of 400-450 °C; methanol dilution with 20 wt.% water ⁷³.

It should be noted that some research groups have also begun to fixate on the kinetics surrounding the steam/air regeneration process of SAPO-34 in MTO ^{169–171}, as a means of de-coking the spent catalyst. Although this lies beyond the scope of the present review, it remains an interesting topic of discussion from an industrial perspective.

3.5.1 Limitations of the current kinetic approaches

Considering the diverse variety of kinetic models discussed (see Table 4), the next step is to understand why such discrepancies exist and determine which models best capture the MTO process under realistic operating conditions. Commencing with the former, discrepancies among the models stem largely from one of the main areas: the considered assumptions, the mathematical simplifications made, and the experimental setup utilized. The first major discrepancy exists in the extent of lumping of the feed (i.e., assumptions regarding the feed composition). Some models treat methanol and DME as separate reactants 172,173, while others have taken the approach of lumping the two species ^{174,175}. The discrepancy lies in the fact that some articles choose to pursue a mathematically simpler approach with the consideration that DME exists in quasi-equilibrium with methanol. However, the realistic and more accurate approach, yet more complex one, is to still model the two species independently, since the operating conditions in place may shift the equilibrium, resulting in the lumping method being an oversimplification. Overall, this discrepancy exists depending on how researchers choose to weigh accuracy relative to simplicity of the model. The second major discrepancy exists in the reaction mechanistic scheme utilized, in the development of the reaction rate expressions, and henceforth, the kinetic model. Some groups have used a simple power law approach for their model formulation^{172,174–179}, while others follow a more complex Langmuir-Hinshelwood (L-H) model^{180,181}. Some groups have also adopted a mixture of the two approaches¹⁸². The reason behind differences in kinetic model type is primarily due to alterations in objectives regarding mathematical simplicity and data availability. For instance, adopting the power law approach allows for simple empirical fitting, with the goal of achieving fast, reactor-scale applicability. However, adopting approaches such as L-H or microkinetic-based models is more computationally expensive and complex, but allows for greater fundamental accuracy and mechanistic insight. The third major discrepancy lies in the level of product species lumping that takes place in formulation of the kinetic model. Research groups either take the route of lumping product species into groups such as light olefins or paraffins 174,175,177,178,182, whereas others choose to model products completely unlumped and individual from one another^{172,180,181}. As with the previously discussed discrepancy, these lumping differences arise from differences in research group objectives regarding simplicity and mechanistic reliability. The lumping approach allows for easier modelling, mathematically speaking, but simultaneously sacrifices on detailing

fundamental mechanistic insights. The fourth discrepancy between different kinetic models is whether researchers have addressed the issue of catalyst deactivation via coke formation. Some researchers include deactivation dynamics in the form of coke deposition in the model^{175–178}, while others choose to neglect it^{174,172,181,182}. The reasons for use vs. lack of integration of deactivation lies primarily in the researcher's objectives. One such objective exists in the complexity vs simplicity trade-off with regards to inclusion vs exclusion, respectively, of coke-based parameters. Another objective lies in the focus of the study, if the goal is to have fundamental kinetic insight (focusing on early stages of the process before the onset of deactivation) or if the goal is to have greater practical relevance (in which coke formation becomes inevitable). The fifth and last discrepancy of kinetic models lies in the chosen operating range in which these models are applicable to. The choice of operating condition depends on the researcher's purpose once again for formulating the model, i.e., trying to create models suitable for fixed-bed, lab-scale conditions, or to instead derive the model applicable for industrially based conditions (fluidized bed with a wider pressure and temperature range). This explains the wide range of operating conditions employed by different research groups^{174,177}.

Now having considered the discrepancies that exist between model types and the reasons therefore, it is hereby appropriate to critically assess which type of models are most transferable and applicable under realistic MTO conditions. From our understanding, it is clear that highly mechanistic microkinetic-based models (i.e., founded on microkinetic schemes that detail hundreds of steps) are able to provide thorough fundamental insight. However, such models are highly complex, which limits their industrial relevance and makes them impractical for largescale reactor simulations. On the other hand, the choice of a simple power law approach lacks the capabilities to accurately predict and replicate experimental results, especially under wide or varying conditions. Hence, it seems that the most transferable approach is that of a Langmuir-Hinshelwood-type model, which possesses some detail of mechanistic insight but isn't as complex and computationally expensive as microkinetic models. The most transferable LH kinetic approach would incorporate deactivation kinetics within their model in the form of coking parameters, to reflect the reality of commercial MTO operation. The model should also be applicable to operating conditions typical of realistic MTO conditions, which means accounting for water co-feeding, and under operating ranges close to 400 °C and 1 bar. In terms of the degree of lumping of the feed and products, a semi-lumped LH based model is recommended. However, it is essential to note that a great degree of lumping can lead to a model that is able to describe overall conversion trends reasonably well, but is unlikely to be fully reliable for predicting detailed product evolution. This is because coke formation in SAPO-34 does not affect all reaction pathways for the different products equally. Thus, simple, heavily lumped models (which often treat deactivation as a single decay factor) are only able to capture the decline in activity, but cannot accurately predict the product distribution over time on stream (especially given the true complexity of the hydrocarbon pool mechanism for MTO over SAPO-34). Hence, for lumped models to be more transferable, they need to include a variety of deactivation effects explicitly stated, instead of a single empirical decay multiplier. This should be done in order to capture and validate experimental data over long time periods on stream, the route-specific nature of coking (e.g., the olefin-based vs

aromatic-based cycle of the HCP concept), and any alterations in product distribution due to coke buildup in micropores. Thus, lumped models that include activity factors tied to coke mass and are route-specific (e.g., separate activities for olefin-based vs. aromatic-based hydrocarbon-pool pathways) would be most transferable to commercial MTO application, but validity must still be confirmed by comparing model predictions to long-time experimental industrial datasets across a wide range of operating conditions.

This article is licensed under a Creative Commons Attribution-NonCommercial 3.0 Unported Licence.

Open Access Article. Published on 22 2025. Downloaded on 30.10.2025 01:47:29.

Reflecting the need for catalyst deactivation dynamics in achieving a transferable kinetic model, one should consider the difficulties of including coking parameters and in turn seek solutions to mitigate such issues. Hence, to begin, the main challenges most models face in integrating deactivation dynamics in kinetic models will be discussed as follows. The first challenge in modeling these reactions is due to the complexity of the hydrocarbon pool concept, i.e., referring specifically to the dual-cycle mechanism in which the MTO process takes place. This mechanism consists of two parallel, autocatalytic cycles: an olefin-based cycle and an aromatic-based cycle, which operate simultaneously, and in turn complicate the modeling of catalyst deactivation. This is because the aromatic cycle exhibits both activating and deactivating roles. While certain aromatic species, i.e., polymethylbenzenes, are active intermediates, others, such as polymethylnaphthalenes, while also active for light olefin formation, can grow into larger, polyaromatic species that cause deactivation. This dual role of some key intermediates makes it difficult to model deactivation dynamics accurately¹⁸³. Overall, this complexity often necessitates oversimplifying the process by reducing the number of HCP-based elementary steps. A second major challenge in modeling deactivation dynamics is the nature of coke formation and deposition. Coke is composed of multi-ring aromatics of varying sizes, from simple two-ring structures to extensive multi-ring species. Hence, this diversity in size leads to differences in the sites of coke deposition. Smaller coking molecules may develop within the internal cages of the catalyst, whereas larger coke molecules may accumulate more on the external surface. This variability in deposition location, which is directly affected by the size of coke, can result in a spectrum of diffusional effects that are both location-dependant and product-dependant, presenting one of the primary challenges in accurately modeling this coke forming process. It is clear from research¹⁸³ that the accumulation of coke on the catalyst, and the type of coke species that forms, plays a crucial role in both methanol conversion and product selectivity. However, existing kinetic models still struggle to represent mathematically the effects of coke deposition, location and coke type associated with the MTO process over SAPO-34. A third major challenge for modelling deactivation dynamics is the rapidity and transient nature in which SAPO-34 catalyst deactivates. Specifically, deactivation of SAPO-34 in MTO is a highly transient process, which exhibits a strong dependence on time rather than progressing at a steady state. Unlike reactions that can be adequately described with time-independent rate constants under steady-state assumptions, in SAPO-34, product distribution evolves continuously as a function of both coke composition and distribution within the zeolite. Since it is difficult to track in real time, this rapid and fluctuating deactivation nature complicates its accurate integration into a kinetic model¹⁸³. Hence, taking the prementioned into account, most kinetic models struggle to properly include all the pertinent factors in a way that accurately describes deactivation tendencies, resorting to lumped or simple models.

Open Access Article. Published on 22 2025. Downloaded on 30.10.2025 01:47:29.

Addressing the problems of accuracy and oversimplification in MTO kinetic modelling, modern studies have begun to incorporate Machine Learning (ML) techniques to achieve a more reliable approach. One way researchers¹⁸⁴ have done so is by design of an Artificial Neural Network (ANN) to model catalyst deactivation. After validation of the fidelity of the hybrid model, by comparing simulated results with experimental kinetic data, it was observed that ANNs enhance the simulation of deactivation dynamics as they are able to more accurately capture the nonlinear relationships between activity and altering operating conditions. Rather than relying on direct coke deposition data over time on stream, the ANN implicitly accounts for coke formation and pore blockage by learning from experimental trends of activity decay. This way, the ANN works as a surrogate model for catalyst activity decline, replacing detailed mechanistic coke models. Its output triumphs that generated by simple lumped kinetic models, in turn yielding a hybrid model that is mechanistically interpretable and flexible enough to capture real deactivation behaviour. Another promising ML approach is the use of Relevance Vector Machine (RVM) modelling, which widely uses industrial data sets for optimal operation of the MTO process at a commercial level¹⁸⁵. RVM assists in predicting the yield distribution of main products given operating conditions, providing both mean and uncertainty estimates. The connection between kernel parameters and the predicted mean and variance is analyzed to make the model interpretable. While research acknowledges that coke deposition and catalyst deactivation affect yields, RVM is used primarily as a probabilistic yield predictor for process optimization, not as a direct mechanistic model of SAPO-34 deactivation.

Overall, although research on enhancing our knowledge of the kinetics of the MTO process has been promising, especially with the recent emergence of machine-learning-assisted approaches 184,185, there still exist some limitations to provide a clearer fundamental understanding. One such factor is the consideration of how diffusion limitations, transport restrictions, and mass transfer phenomena take place inside the small CHA cages of SAPO-34 during the MTO process, which in turn would affect the apparent kinetics, deviating from the intrinsic kinetics of elementary steps. The growth of the hydrocarbon pool and aromatic species within these small cages can introduce diffusion limitations, leading to slower-than-expected reaction rates. Such transport restrictions can lead to coke precursors building up near pore openings and promoting secondary reactions, which is usually not accounted for by intrinsic kinetic models. Hence, kinetic models that ignore such diffusion limitations, due to coke buildup in pores, tend to underestimate deactivation rates. Some studies have begun to delve into the effects of diffusion explicitly within their kinetic models by coupling intracrystalline mass transport with reaction networks, thereby forming a simulated dataset better in agreement with experimental data, especially during later stages of time on stream (i.e., the deactivation period). Researchers have employed reaction-diffusion models using Maxwell-Stefan transport (intraparticle) theory, for MTO on SAPO-34, using the dual-cycle mechanism, with the effect of coke formation on diffusion and adsorption accounted for 186. Generally, studies 186–188 have concluded that both reaction site loss and internal diffusion limitations (which increase with coke accumulation in pores over time on stream) slow down apparent kinetics, reducing rates observed experimentally relative to computed intrinsic elementary-step rates (where diffusion effects are neglected). Specifically, the reduced effective diffusivities due

to coke growth create a recurring loop that accelerates deactivation, in turn further slowing down the observed kinetics of the process. As deactivating species build up in pores, this slows down diffusion and increases local residence of such species, which leads to the buildup of even more coke and even slower diffusion as a result (i.e., a positive feedback loop). Studies have shown that effective diffusion coefficients reduce by up to four orders of magnitude during deactivation as pores are blocked- especially for larger hydrocarbons¹⁸⁶. These larger intermediates get trapped within the CHA cages, causing intraparticle resistances and in turn shifting product selectivity primarily to smaller compounds such as ethylene, which can diffuse out of the crystal more smoothly¹⁸⁸. These pre-mentioned diffusion-controlled, apparent product selectivity shifts cannot be easily captured by lumped kinetic models, which generally neglect such effects. Overall, despite the progress within this research direction of the kinetics of the MTO process, it seems that the development of multiscale models, comprising of both intrinsic reaction rates and transport phenomena inside SAPO-34's cages, still remains open for development- in order to obtain a highly accurate model to describe the MTO process under industrially relevant conditions.

This article is licensed under a Creative Commons Attribution-NonCommercial 3.0 Unported Licence

Open Access Article. Published on 22 2025. Downloaded on 30.10.2025 01:47:29.

4 Catalyst design and modification

4.1 Introduction to SAPO-34

SAPO-34 is a microporous silicoaluminophosphate that possesses a topology analogous to that of the naturally occurring silico-aluminate chabazite (CHA) zeolite. The structure consists of a three-dimensional pore system of alternating D6R (double-six rings) cages and large CHA cavities (~9.4 Å in diameter) that are accompanied by smaller eight-ring (8r) windows/pore openings (3.8 Å). The 3D structure of SAPO-34 has been depicted in a variety of manners. Its molecular sieving capabilities makes SAPO-34 suitable for applications in the MTO process, allowing for the diffusion of the primarily desired C₂ and C₃ olefinic products out of its framework. In comparison to the neutral aluminophosphate (AlPO₄-34) structure, which predominantly consists of alternating Al-O-P bonds, SAPO-34 possesses a similar framework, one in which primarily phosphorous atoms (of PO₄ tetrahedra) are substituted by silicon ^{189–192}. This is considered the first (and well-acknowledged) substitution mechanism (SM1), which forms Si (4Al) (isolated) structures; however, the second potential mechanism (SM2) involves the double substitution of neighboring Al and P by Si atoms, generating island-based entities i.e., Si (nAl) (*n* ranging from 3 to 0) ^{190–192}. Overall, the incorporation of Si⁴⁺ for P⁵⁺ (SM1 route) yields a negatively charged framework; hence, protons (as additional cations) with Brønsted acid properties are introduced into the structure as part of bridging hydroxyl groups (i.e., Si-OH-Al) for total charge compensation ^{190–192}. These ultimately play a major role as the active sites for the MTO reaction.

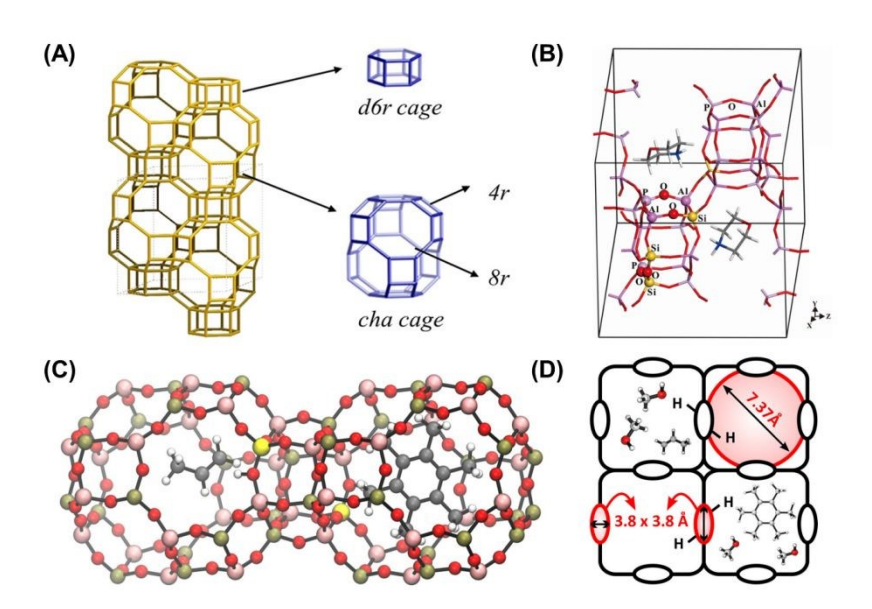


Figure 23 (A) SAPO-34 (CHA type framework) topology structure alongside the composite building units. Reproduced from reference¹⁹³ with permission from John Wiley and Sons, Copyright 2018. (B) Geometry-optimized SAPO-34 structure, with the four O connectivities indicated (Si-O-Si, Si-O-Al, Si-O-P, and Al-O-P). Reproduced from reference ¹⁹⁴ with permission from American Chemical Society, Copyright 2018. Here, the Si-O-Si species exists due to the presence of an Si island configuration. The illustrated Si-O-P linkage, which may be generated via the SM I mechanism, has not been experimentally observed. (C) H-SAPO-34 cell with two adjacent cages containing hydrocarbon pool species adapted from. Color code: Al (pink), P (green), Si (yellow), O

urnal of Materials Chemistry A Accepted Manuscrip

(red), H (white), C (gray). (D) H-SAPO-34 pore system demonstrating the large cages connected via 8-ring windows. Reproduced from reference 195 with permission from American Chemical Society, Copyright 2025.

SAPO-34 molecular sieves are primarily synthesized using a hydrothermal method due to its effectiveness and simplicity. However, alteration of the types of precursors utilized in synthesis (as well as the overall procedure used) has shown to have varied effects on particle shaping, capable of generating particles that are sheet-like 196,197 and micro-spherical 196,198

Overall, since SAPO-34 suffers from relatively rapid deactivation as a result of pore blockage by organic species, there exists the need to uncover methods to prolong catalyst lifetime 60,61. Hence, Table 5 summarizes the key scientific and technological challenges in SAPO-34-based MTO catalysis, with mitigation strategies and future directions for such work. Furthermore, as will be seen in the following sections, research groups have begun to improve catalyst performance by employing techniques during synthesis as a means of reducing particle size (to shorten the molecular diffusion pathway) as well as introducing secondary meso- and macro-pores, resulting in a hierarchical SAPO structure (to facilitate intra-particle diffusion). Furthermore, procedures involving template/OSDA (organic structure directing agent) alteration alongside modifications in silicon content (which directly impacts active site content) have also been utilized to improve catalytic activity. Figure 24 summarizes the activity performance of optimum catalysts developed by over 35 research groups via utilization of the aforementioned techniques. Light olefins' selectivity and catalytic lifetime, the two most important metrics of acceptable catalytic performance, have been depicted. Since the methanol weight hourly space velocity can largely affect the catalyst's lifetime and varies largely from one article to another, to draw a fair comparison amongst the articles, a universal term 'methanol processing ability' was defined. This term describes the amount of methanol (in grams) that can be processed over 1 gram of catalyst over its lifetime (until conversion drops to 90%). Overall, the highest average light olefin selectivity that can be achieved generally falls in the range of 80-85 mol%, while the greatest methanol processing ability was recorded to be close to $30 \, \mathrm{g}_{\mathrm{MeOH}} \, \mathrm{g}_{\mathrm{Cat}}^{-1}$. Although the datapoints related to each technique are scattered throughout the graph, in summary, the creation of a hierarchical structure and submicron synthesis seem to be the most efficient routes for SAPO-34 activity improvement.

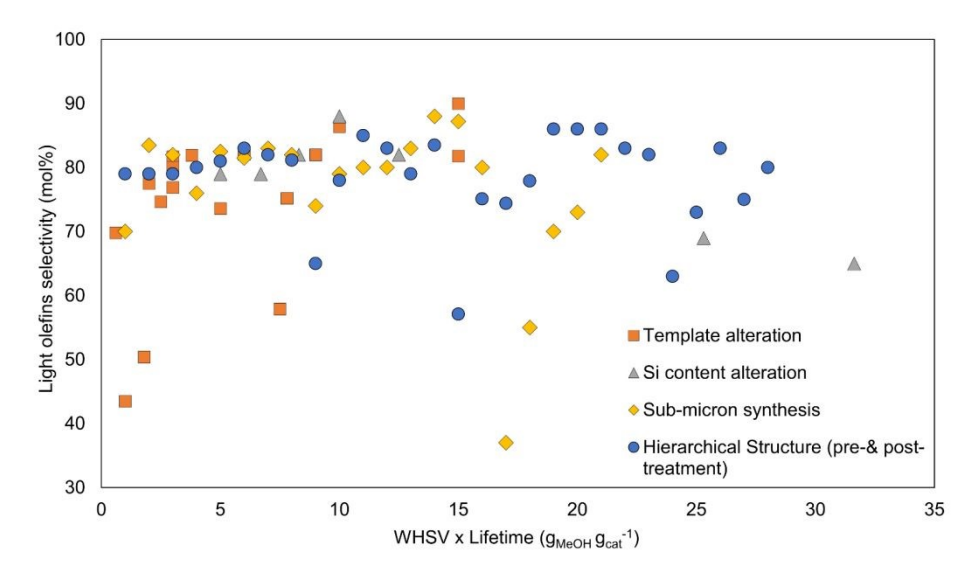


Figure 24 Catalytic performance of SAPO-34 catalysts synthesized by employing different techniques for the MTO reaction. The data points refer to all references within sections 4.4 to 4.5

Table 5 Summary of core scientific and technological challenges in SAPO-34-based MTO catalysis, with mitigation strategies and future directions.

Category	Challenges	Description & Impact	Current Mitigation Strategies	Potential Research Direction
Scientific (Catalyst-level)	Rapid Deactivation via coke formation	Large multi-ring aromatics (coke) accumulate in pores and on surfaces, blocking active sites and reducing lifetime to hours in lab tests. This lowers conversion/ selectivity over time and correlates with unwanted methane production via hydride transfer.	Hierarchical structures via templating or desilication to improve coke tolerance (2-6x lifetime extension); metal promotion (e.g., Zn) to alter acidity and suppress coke precursors (See sections 4.4-4.5).	Explore CO ₂ co-feeding to inhibit coke deposition (e.g., via ZnCeZrO _x /SAPO-34 dual catalysts); integrate AI-driven modeling for predictive coke management ¹⁹⁹ .
	Diffusion limitations in small pores	SAPO-34's 3.7 Å CHA cages enable high light olefin selectivity (~80%) but restrict larger hydrocarbon diffusion, leading to uneven coke buildup (faster at pore mouths) and mass transfer issues.	Sub-micron/nanosheet synthesis to shorten diffusion paths; hierarchical meso/macropore introduction (See sections 4.3.4-4.4).	Particle size control via advanced synthesis (e.g., reducing to <100 nm for better acid site utilization); combine with in-situ spectroscopy for real-time diffusion monitoring ²⁰⁰ .
	Acidity imbalance and silicon distribution	Medium acidity (~1 mmol g ⁻¹) is optimal, but high Si content creates islands promoting side reactions/aromatization; low Si reduces active sites, affecting initial conversion (~100%).	Tune Si/Al ratio (0.2-0.3) via templates (e.g., TEAOH); metal doping (e.g., Zn ²⁺) for Brønsted/Lewis acid synergy (See sections 4.3.2-4.3.3, 4.5).	Theoretical studies on Zn-modified SAPO-34 for diene formation; hybrid catalysts with oxides like In ₂ O ₃ -ZrO ₂ for acidity optimization ^{201,202} .

Open Access Article. Published on 22 2025. Downloaded on 30.10.2025 01:47:29.

Technological	Short lifetime	Industrial fluidized beds	Shaping into	H ₂ co-feeding or alternative
(Process- & Industry- Level)	requiring frequent regeneration	need continuous coke burnoff, but this is energy- intensive, emits CO ₂ , and risks framework damage (hydrothermal instability).	microspheres/extrudates for better fluidization; mild steam regeneration (400-500°C) to gasify coke (See sections 2.1, 4.6).	regenerants for lower- energy cycles; scale up hydrothermal-stable variants ²⁰³ .
	Scalability of catalyst synthesis/modifications	Lab-scale hierarchical/metal-modified SAPO-34 improves performance but faces reproducibility issues, high template costs, and inconsistent Si distribution at scale.	Solvent-free/microwave-assisted synthesis; binder optimization in shaping (See section 4.3-4.4).	Commercial-scale templating (e.g., soft/hard) for cost reduction; integrate with upstream methanol from CO ₂ /plastics for closed-loop economics ²⁰⁴ .
	Energy intensity and economic viability	High temperatures (400-460°C) promote coking/alkanes; integration with feed production (e.g., from CO ₂) adds separation costs, limiting vs. steam cracking.	Diluents like water to reduce partial pressure; process optimization (WHSV 1-5) (See sections 2.3).	Direct syngas-to-olefins to bypass methanol step; techno-economic analyses for CO ₂ -derived feeds ¹⁹⁹ .

4.2 Comparison of SAPO-34 vs. Other Zeolites

Given that the MTO process can employ a wide variety of microporous catalysts, each material's framework and composition can strongly influence its performance. Silicoaluminophosphate molecular sieves like SAPO-34 have been identified as benchmark MTO catalysts due to their exceptional light olefin selectivity²⁰⁵. By contrast, traditional aluminosilicate zeolites such as ZSM-5 exhibit different product distributions and stabilities. To contextualise SAPO-34's performance against the other readily available options, Table 6 summarises key characteristics against some representative MTO catalysts.

Table 6 Comparison of Selected MTO Catalysts (Structure, acidity, selectivity, products, and stability)

Catalyst & Acid strength topology		Light olefin selectivity	Main byproducts	Lifetime categorization	Ref.	
SAPO-34 (CHA, 3D small-pore, 8- MR)	Mild (silicoalumino- phosphate)	High (primarily C ₂ -C ₃ olefins)	Minimal heavies (no aromatics or C_{3+} , only minor C_4 hydrocarbons)	Short (rapid coke build-up in cages; deactivates in minuteshours)	206–208	
SAPO-18 (AEI, 3D small-pore, 8- MR)	Mild, weaker than SAPO-34 (silicoalumino- phosphate)	High (comparable C ₂ -C ₃ olefins to SAPO-34)	Minimal heavies (no aromatics, similar to SAPO-34)	Moderate (improved diffusion and slightly weaker acidity extend lifetime vs. SAPO-34)	209	
SAPO-35 (LEV, 2D small-pore, 8- MR)	Moderate, stronger than SAPO-18	High (comparable C ₂ -C ₃ olefins to SAPO-34)	Mainly light olefins initially; rapid formation of heavy coke/aromatics later	Short (deactivates quickly; conversion drops sharply within ~100 min)	209	
ZSM-5 (MFI, 3D medium-pore, 10-MR)	Moderate (aluminosilicate)	Moderate (significant C_2 - C_3 olefins, but	Substantial aromatics and C_{5+} olefins (gasoline-range	Long (hours of operation; larger pores streamline coke	207	

		lower than	byproducts from larger 10-	exit, so deposits are mainly on	
		SAPO-34)	MR channels)	external surface)	
ZSM-22 (TON,	Strong	Low (mostly	Predominantly C ₆₊ olefins;	Negligible (cannot sustain	207
1D medium-pore,	(aluminosilicate)	heavier C ₃₊	negligible aromatics (DME	MTO activity; 1D pores	
10-MR)		olefins)	formed instead of olefins	prevent hydrocarbon pool;	
			after prolonged operation)	olefin production only	
				observable in brief initial	
				period	

MR = membered ring (aperture size of micropore); C_2 - C_3 = ethylene/propylene range. AEI, LEV, TON is a framework type code assigned by International Zeolite Association.

As depicted in the table above, SAPO-34 stands out for its high selectivity for light olefins (primarily propylene and ethylene) while suppressing the formation of heavier hydrocarbons^{206–208}. This arises from its small chabazite (CHA) cages, which favour C_2 - C_4 olefin products and exclude larger molecules; consequently, SAPO-34 produces minimal aromatics or C_{5+} by-products under MTO conditions²⁰⁷. In addition to its structure, the milder acidity associated with SAPO-34's silicoaluminophosphate composition also provides mild acid sites that limit secondary reactions like oligomerisation or hydrogen transfer (that could form paraffins or aromatics)²¹⁰.

On the other hand, the ZSM-5 zeolite is a medium-pore catalyst with larger channels (10-membered ring) 207 . Although it can achieve notable methanol conversion with a fair amount of C_2 - C_3 olefins, its selectivity to light olefins is lower than SAPO-34's as a direct consequence to its more dispersed MFI channels, serving as a gateway to the formation of bulkier hydrocarbons 207 . As such, ZSM-5 permits the generation of aromatics (such as benzene, toluene, and xylenes) 211 that cannot form in SAPO-34's constrained cages. Consequently, a significant fraction of the carbon in the MTO reaction is converted into aromatic and gasoline-range byproducts 207,211 . Therefore, although ZSM-5 can be utilized for methanol-to-olefins, it compromises olefin yield for the generation of heavier products due to selectivity constraints.

One crucial consideration is that of catalyst stability (reported as the time-on-stream before deactivation) which markedly varies between these materials. For instance, as reported previously, the opportunity cost of employing SAPO-34 for its high olefin selectivity is its limited catalyst lifetime²¹². SAPO-34's CHA cages tend to trap hydrocarbon intermediates as core reactions are being undergone, and the buildup of polymethylbenzene species (otherwise known as the "hydrocarbon pool") eventually leads to rapid coke deposition inside the cages, which then blocks available active sites for subsequent cycles²¹². Consequently, SAPO-34 tends to deactivate relatively quickly in fixed-bed applications (without regeneration). As discussed in Section 2.1, this is alleviated in industry by using SAPO-34 in fluidized-bed reactors that have continuous regeneration. Nevertheless, at the particle level, SAPO-34's active lifetime per cycle is relatively short. On the other hand, ZSM-5 generally offers a longer operational time under MTO operating conditions²¹³. This is because its larger MFI channels allow for more polyaromatic coke precursors to migrate out of its micropores; as a result, coke then forms on the external surface

Researchers have also opted to explore other small-pore SAPO catalysts in the pursuit of improved MTO performance, such as SAPO-18²⁰⁹. With structural similarities to SAPO-34, the AEI framework is reminiscent of the CHA structure due to its large cages that can be accessed through 8-ring windows, which similarly yield high selectivity towards light olefins. However, the orientation of the double six-ring unit in SAPO-18 is different, and it often features slightly lower acidity (depending on silicon content), which can influence diffusion and coking behaviour. In a study by Huang et al²⁰⁹, SAPO-18 demonstrated excellent MTO performance with high olefin yield and stability (maintained over 6000 minutes on stream with co-fed syngas before deactivation). While this test involved a bi-functional setup (and the presence of hydrogen in syngas), it suggests that inducing modifications in SAPO-18 can prolong catalyst life²⁰⁹. On the other hand, SAPO-35 (LEV framework) is another 8-ring small-pore silicoaluminophosphate that is a direct example of topology affecting stability. Similar to SAPO-18, SAPO-35 has cages accessible through 8-MR windows of similar size. However, unlike SAPO-18 (which has a threedimensional structure), SAPO-18's LEV structure forms a 2D channel system with more restricted connectivity. This poorer diffusivity in SAPO-35 leads to faster coke saturation, which was observed in MTO testing (contrasted with SAPO-18)²⁰⁹. These comparisons are critical to elucidate how not all small-pore frameworks are made equal, characteristics like cage connectivity and surface openness can impact the delicate balance between olefin selectivity and catalyst longevity.

This article is licensed under a Creative Commons Attribution-NonCommercial 3.0 Unported Licence.

The case of ZSM-22 is one that depicts how necessary an appropriate pore structure is to sustain MTO catalysis. ZSM-22 is a 10-MR zeolite just like ZSM-5, though it has a one-dimensional channel system with no inherent structural intersections²⁰⁷. Its shape-selective environment is so hindered that the classic hydrocarbon pool mechanism, which is a necessary intermediary step to arrive at the MTO reaction, cannot easily be sustained²⁰⁷. In practice, only dimethyl ether (DME) is obtained as the primary product, where any light olefins obtained from ZSM-22 originated from either impurity phases or reactions on external acid sites, rather than through a sustained, stable catalytic cycle in the micropores of the zeolite²⁰⁷. Furthermore, ZSM-22's products are skewed more towards non-aromatic C_{6+} olefins when activity is present, and virtually no aromatics are produced due to its severe spatial constraints²⁰⁷. Thus, this inherent inability of ZSM-22 to sustain any MTO conversion illustrates the importance of having at least a 2D or 3D channel system to form methanol. In addition, the structure must not only be balanced between small pore openings in a way to allow for olefin production but also host a sufficiently connected network to alleviate coke buildup.

The alternative catalyst choices presented above exhibit some advantages over SAPO-34 such as catalyst longevity and stability, though this is at the expense of producing heavier hydrocarbons and unwanted by-products. Thus, with process-driven intentions, it is evident that SAPO-34 is the most pertinent for the MTO application.

4.3 Characterization of SAPO-34

X-ray diffraction (XRD) is typically the first characterization tool employed for crystalline-structured catalysts to verify that the desired phase has been formed via peak matching of the sample with that of its reference pattern. Depending on the choice of synthesis procedure and template/structure directing agent utilized, competing phases (SAPO-5, -11, and -18) may present in combination with the main SAPO-34 structure ^{214–216}.

Another common characterization technique is physisorption analysis, widely used tools to measure surface area and pore volume, as well as the relevant contribution of macro, meso and micropores. SAPO-34 normally exhibits an adsorption isotherm akin to that of the type I curvature ²¹⁷. Recent attempts to enhance mass transfer, by introducing meso- and macro-pores into the SAPO-34 structure (subsequently termed hierarchical), has led to isotherm patterns that are a combination of both type I and IV ^{218,219}.

Scanning electron microscopy (SEM), a technique used to observe morphology, has shown that SAPO-34 generally possesses a cube-like particle morphology ^{220,221}, with particle sizes ranging from the hundreds of nanometers ^{222,223} to tens of microns ^{224,225}. However, research groups have demonstrated that by alteration of synthesis precursors as well as the procedure used, different types of SAPO-34 particle morphologies are possible (such as spherical and sheet-like particle) ^{196–198}. SEM images may be utilized in tandem with an image-analyzing software to visually determine and quantify the particle size distribution ^{226,227}. The morphological characterization of multi-phase materials is generally conducted via the analysis of the back scattered electrons (BSE) emitted by the sample in a scanning electron microscope ²²⁸. Heavier elements (i.e., elements possessing a greater number of protons/ Z-number) are able to generate more BSEs, and in turn appear brighter, relative to lighter elements ²²⁹. Hence, this presents as a useful tool when performing the morphological analysis of SAPO-34 catalyst modified with secondary metal species to assess the distribution of the promoted metal in the SAPO-34 structure.

In order to investigate the bulk elemental composition of a produced catalyst, the most commonly employed methods are inductively coupled plasma (ICP) spectroscopy and X-Ray fluorescence (XRF) spectroscopy. The ICP-based technique can operate in a variety of manners depending on the spectroscopy method utilized (e.g., mass spectrometry (MS) and atomic emission spectroscopy (AES)). Conducting an analysis of the bulk elemental composition can be highly valuable, as the acidity of the catalyst is a function of the number of silicon atoms present within the sample ²³⁰. Moreover, with respect to in-situ metal incorporation as well as promotion via wet impregnation (which involves washing steps as opposed to dry impregnation), it is important to uncover the quantity of secondary metal species that were able to retain in the final solid catalyst ²³¹. When choosing the type of bulk elemental analysis tool to employ on SAPO-34, it is important to consider the difficulties involved in

X-Ray photoelectron spectroscopy (XPS) and scanning electron microscopy with energy dispersive X-Ray spectroscopy (SEM-EDXS) are the techniques typically utilized in the revelation of a catalyst's surface elemental composition. With the aid of these techniques, it is possible to locally specify the composition of visuallydistinguished phases of the sample ^{235,236} while bulk composition analysis gives an average composition of all phases presented in the specimen. In the case of metal-modified SAPO-34, depending on the procedure of secondary metal promotion (i.e., impregnation based vs. in-situ metal incorporation), the distribution of these participating metals may be different on the outer surface as opposed to the bulk, and could play a different role with regards to catalytic capabilities ^{237,238}.

This article is licensed under a Creative Commons Attribution-NonCommercial 3.0 Unported Licence.

Fourier transform infrared spectroscopy (FTIR) is often used to further assist in deciphering and verifying the elemental environments present in a sample. This technique can be used to identify the chemical bonds present in the SAPO structure; however, it may fail to reveal the entire environment narrative. For instance, in the case of comparing secondary metal promoted SAPO-34 to its parent H-SAPO-34, no substantial differences are visible between the samples' spectrums which could set them apart ²³⁹. The same peaks are observable for these calcined samples, present at roughly 499 cm⁻¹, 637 cm⁻¹, 725 cm⁻¹ and 1,098 cm⁻¹ in the fingerprint region, as well as peaks at 1,638 cm⁻¹ and 3,400 cm⁻¹. These are respectively assigned to T-O bending of Si tetrahedra, T-O bending in 6membered rings, T-O-T symmetric stretching, asymmetric stretching of TO₄ tetrahedra, -OH vibration (water absorbed on SAPO samples), and bridging hydroxyl (Si-OH-Al) groups (i.e., the active sites) ^{239–242}. Minor peaks at 3675 cm⁻¹ and 3743 cm⁻¹ have also been observed, which, respectively, can correspond to P-OH and Si-OH weak hydroxyl groups ^{240,242,243}.

Nuclear magnetic resonance (NMR) spectroscopy is also another commonly employed tool in the field of catalysis, where it can determine the types of environments prevalent in a catalyst structure. With respect to ²⁹Si-NMR, five different peaks close to -90.5, -94.4, -99.6, -104.3 and -109.8 ppm are often observable, respectively corresponding to environments of Si(4Al) (i.e., isolated Si), and silica islands such as Si(3Al,Si), Si(2Al,2Si), Si(Al,3Si) and Si(4Si) ^{244–246}. Generally, it has been observed that the greater the amount of silicon incorporated into the SAPO framework, the more likely the formation of Si islands in comparison to isolated Si environments ²⁴⁷. A general consensus amongst research groups exists in that the formation of primarily isolated silicon

This article is licensed under a Creative Commons Attribution-NonCommercial 3.0 Unported Licence.

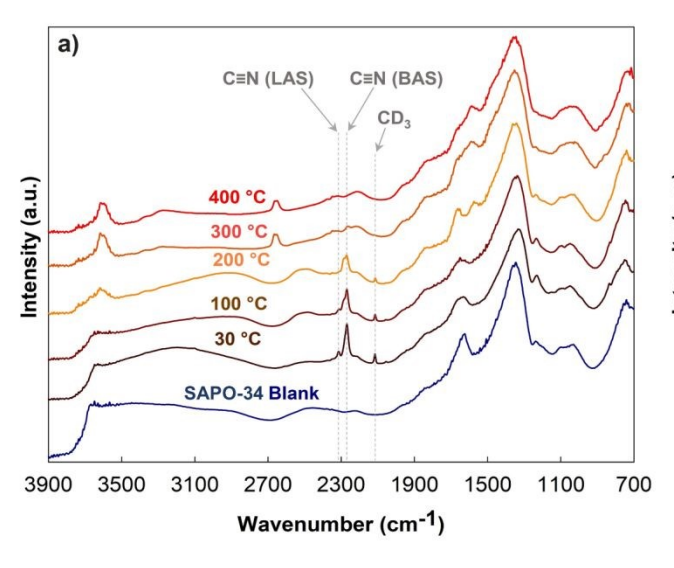
environments (as opposed to Si islands) is more desirable from a catalyst activity standpoint, which is often justified by the lower acidity strength associated with isolated Si sites 248,249 . 27 Al-NMR spectroscopy is also another technique generally employed in studies, where two peaks are visible near roughly 35 to 39 ppm and -7 to -21 ppm, which respectively correspond to tetrahedral framework aluminum (main source of Brønsted acid sites) and octahedral aluminum species (main source of Lewis acid sites) $^{51,250-253}$. Some research groups have also reported a weak signal close to 15 ppm due to penta-coordinated Al atoms 253,254 , which these groups have also attributed to being Lewis acid sites 255 . With respect to 31 P-NMR, a singular peak is usually present at roughly -28 ppm, which has been suggested to correspond to tetrahedral phosphorus in the SAPO framework 256,257 .

As mentioned previously, the primary drawback associated with the MTO reaction is catalyst deactivation due to coke formation, which occurs inevitably over time on stream. The development of coke species leads to blockage of catalyst pores, resulting in rapid decline in methanol feed conversion and reduced light olefins selectivity ^{60,61,258–260}. Ample research has focused on deciphering the mechanistic pathways responsible for coke formation ^{133,261}, as well as uncovering ways to limit its generation rate ^{262,263}. Therefore, tools such as thermogravimetric analysis-temperature programmed oxidation (TGA-TPO) have been utilized by researchers as a means to quantify the coke content over deactivated SAPO catalysts ^{222,264}. Generally, the weight reduction observed in the temperature range of 50 to 200 °C corresponds to the desorption of water from the sample, whereas a second weight depletion is observed gradually between 200 to 600 °C and can be attributed to the combustion of coke species from the catalyst sample ^{222,233,265}.

Other than identifying the coke generation rate, deciphering the types of species that constitute coke can provide a broader perspective on coke analysis. For instance, the identification of coke species that are distinctly responsible for ultimate pore blockage may provide further insight into the deactivation mechanistic sequence. One method to accomplish this involves analysis of coke species in deactivated catalyst via ¹³C or ¹H nuclear magnetic resonance (NMR) spectroscopy ^{54,266,267}. Although this technique does not necessarily analyze the detailed structure of the species contained in coke, it can still provide an indication of the type of functional groups present. Groups who have utilized this method have indicated that coke species are largely aromatic-based as opposed to linear chain aliphatic compounds ^{266,267}.

For a more in-depth analysis of the structure of coke species, a technique involving gas chromatography-mass spectrometry (GC-MS) may be utilized instead, which depicts coke species as ranges of multi-ring aromatics ^{84,268,269}. Here, the deactivated catalyst may be digested in hydrofluoric acid, with the hydrocarbon phase extracted using dichloromethane (CH₂Cl₂)⁸⁴. The organic compounds can be subsequently injected into the GC as a means of separating the different coke species by their retention time, which can then be analyzed via MS successively. Although this technique may seem promising with regards to structural identification, there lies some inconsistencies between the types of coke species entrained in deactivated SAPO-34 reported by research groups. One group was able to analyze and identify insoluble hydrocarbons (up to 55 C atoms in size) within coke species

Since the active site for the MTO reaction is well known to be the Brønsted acid site (i.e., the bridging hydroxyl groups, Si-OH-Al) over the catalyst, acidity measurements play an important role in catalyst characterisation. The easiest and most commonly used tool in the determination of acidic site quantity and strength is NH₃ temperature programmed desorption (TPD) ^{252,271,272}. This tool generally provides two peaks that correspond to weak sites (combination of Lewis and Brønsted sites) and strong sites (primarily Brønsted) in ranges of 150 to 200 °C and 350 to 450 °C, respectively ^{273–275}. FTIR spectroscopy goes beyond by distinguishing between the two types of acidic sites (Lewis and Brønsted) over the catalyst using a prob molecule. Choosing the probe molecule regarding SAPO-34 is quite challenging. Pyridine, having a molecular kinetic diameter of 5.33 Å, is not able to penetrate the small pores of SAPO-34 (pore size of 3.7 Å) and cannot be used as the probe molecule ²⁷⁶. NH₃-FTIR is not viable either, as the region where the vibrational modes of ammonia adsorbed on Lewis centers and Brønsted ones (LAS at 1625 cm⁻¹, and BAS related peaks at 1457 and 1405 cm⁻¹ ²⁷⁷) interferes with the characteristic peaks related to SAPO-34 framework in the range of 500-1700 cm⁻¹. Therefore, deuterated acetonitrile (CD₃CN) was employed by one research group ⁷⁶. The C≡N stretching vibration of CD₃CN, interacting with BAS and LAS, appears within the 2100-2500 cm⁻¹ where no interference exists. The CD₃CN-FTIR test provides a qualitative analysis. In order to study the acidic sites quantitatively, CD₃CN-TPD was also conducted and related to the CD₃CN-FTIR test ⁷⁶. According to Figure 25, since the LAS-related peak almost disappeared at around 100 °C, the low temperature peak that has appeared in the CD₃CN-TPD test can be attributed to both LAS and BAS while the other two peaks at higher temperatures are almost solely related to Brønsted acidic sites. Overall, it can be said that the majority of acidic sites presented over SAPO-34 are BAS rather than LAS.



This article is licensed under a Creative Commons Attribution-NonCommercial 3.0 Unported Licence.

Open Access Article. Published on 22 2025. Downloaded on 30.10.2025 01:47:29.

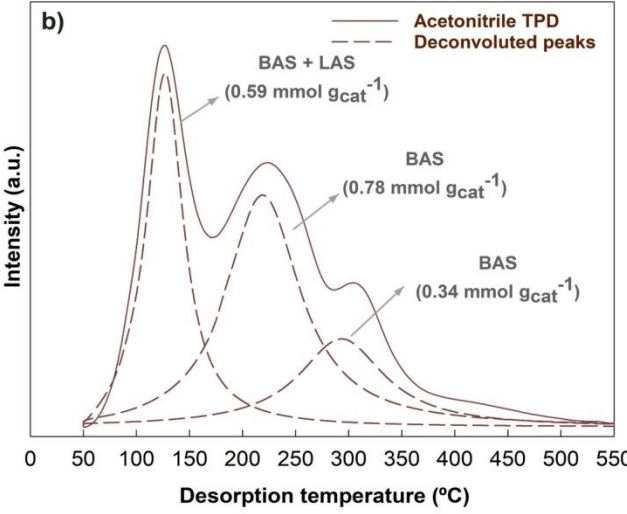


Figure 25 a) Temperature-dependent DRIFT spectra of SAPO-34 catalyst saturated with CD₃CN (blank sample is without CD₃CN). b) Deuterated acetonitrile temperature programmed desorption (CD₃CN-TPD) over SAPO-34 and deconvolution of the peaks. Reproduced from reference⁷⁶ with permission from American Chemical Society, Copyright 2023.

4.4 Synthesis of SAPO-34

4.4.1 Standard synthesis approach

The synthesis of SAPO-34 zeolites typically involves mixing the precursors of the main constituent elements, specifically silicon, aluminum, and phosphorus. In addition to these primary components, other chemicals such as organic structure-directing agents (OSDAs), commonly referred to as templates, alkaline metals used as mineralizing agents, and water as solvent play a crucial role in the synthesis process. The selection, type, and concentration of these chemicals are critical factors that significantly influence the physicochemical properties of the resulting SAPO-34, including its crystallinity, particle size, morphology, and catalytic performance. These variables directly affect the catalytic efficiency and stability of SAPO-34 in the MTO reaction, highlighting the importance of optimizing the synthesis parameters. The following sections will discuss and summarize the different parameters influencing the synthesis of SAPO-34, while in this section we focus on the basic steps involved in the synthesis of SAPO-34.

The synthesis of SAPO-34 was first reported by the Union Carbide Corporation (UCC) in the early 1980s as part of a broader study on SAPO (silicoaluminophosphate) molecular sieves ²⁷⁸. UCC researchers successfully developed a series of SAPO materials, including SAPO-34, by incorporating silicon into aluminophosphate frameworks, which led to the creation of novel molecular sieves with unique properties. This breakthrough was significant as it expanded the range of available microporous materials, combining the benefits of both zeolites and aluminophosphates. The original synthesis method involved the hydrothermal crystallization of a gel containing sources of silicon, aluminum, and phosphorus, along with organic structure-directing agents (OSDAs), which played a crucial role in defining the framework and pore structure of SAPO-34. After this innovative research, many different versions of the synthesis protocol have been developed. These variations have allowed for further adjustment of SAPO-34 properties, such as pore size, acidity, and thermal stability. As a result, SAPO-34 has become a versatile catalyst in different applications, including the MTO process.

To this day, the hydrothermal synthesis approach exists as the most commonly used procedure for the generation of SAPO-34 molecular sieves ^{189,279}. The synthesis commences by gel formation via the mixing of different precursors (i.e., sources of Al, P and Si) and the template (commonly tetraethylammonium hydroxide (TEAOH)). This is followed by the crystallization step, typically conducted in a Teflon-lined stainless-steel autoclave at 175-215 °C, with the total period of crystallization typically lasting ~24 hours ^{189,280}. The subsequent steps utilized in

the final formulation of SAPO-34 are the separation of the solid from the liquid phase (via filtering or centrifugation), followed by drying and calcination (550-600 °C for 4-5 h to remove volatile organic compounds, i.e., the template) ^{189,280}. Typically, the resulting catalyst particles exhibit a cube-like morphology ^{220,221} (as shown in the SEM images in Figure 28), with sizes ranging from hundreds of nanometers ^{222,223} to tens of microns ^{224,225}.

Other synthesis approaches have been explored for the preparation of SAPO-34, each offering unique advantages and challenges. Among these, the dry-gel conversion method involves using a minimal amount of solvent, making it an eco-friendly approach that reduces waste and allows for the precise control of crystal size and morphology²⁸¹. The two-step crystallization method involves an initial low-temperature aging step, followed by crystallization at higher temperatures. This staged process helps in controlling the nucleation and growth phases separately, leading to better control over the final crystal size and shape ²⁸². Ionothermal synthesis, which utilizes ionic liquids as both solvents and structure-directing agents, offers a unique pathway to synthesizing SAPO-34 without the need for traditional organic templates²⁸³. Ultrasonic synthesis uses ultrasonic waves to induce cavitation in the precursor solution, promoting rapid nucleation and crystallization. This technique not only shortens synthesis time but also enhances the dispersion of reactants, leading to more uniform crystal growth²⁸⁴. Microwave synthesis uses microwave radiation to directly heat the precursor mixture, significantly speeding up the crystallization process compared to conventional hydrothermal methods. This approach allows for rapid heating and uniform temperature distribution, leading to faster reaction kinetics and the formation of well-defined crystalline structures. The ability to fine-tune the microwave power and reaction time provides additional control over the final properties of SAPO-34 ²⁸⁵.

Figure 26 summarizes the main steps involved in these different synthesis protocols, highlighting the unique characteristics of each method. Subsequently, Table 7 provides a detailed comparison of the gel compositions and other important details pertaining to each synthesis procedure. This summary overview serves as a valuable resource for researchers, guiding them in selecting the most suitable synthesis route based on the desired properties of SAPO-34. By understanding these synthesis methods, researchers can replicate the procedures with greater precision, reducing the time and effort required while ensuring consistent and high-quality SAPO-34 synthesis, thus allowing them to focus on advancing their core research objectives.

This article is licensed under a Creative Commons Attribution-NonCommercial 3.0 Unported Licence.

Open Access Article. Published on 22 2025. Downloaded on 30.10.2025 01:47:29.

Figure 26 Illustration of the summary of the main steps involved in the synthesis of SAPO-34 using different synthesis protocols.

Table 7. Summary of the common synthesis protocol with the physical properties of the produced SAPO-34.

Synthesis protocol	Gel composition	Crystallization temperature (°C)	Crystallization time (h)	Particle size (µm)	Morphology	Ref.
Hydrothermal	0.5(TEA) ₂ O: 0.6SiO ₂ : Al ₂ O ₃ : P ₂ O5: 52H ₂ O	200	168	-	-	278
Dry gel	1.0Al ₂ O ₃ : 1.0P ₂ O ₅ : 0.6SiO ₂ : 1.8TEAOH: 77H ₂ O	180	3-24	0.045 - 0.075	Cube-like shape	286
Two-step Crystallization	Al ₂ O ₃ : 0.6SiO ₂ : P ₂ O ₅ : 0.5TEAOH: 65H ₂ O	Step 1: 130-150 Step 2: 180	Step 1: 4 Step 2: 10	0.55 - 0.32	Cube-like shape	282
Ionthermal synthesis	-	130-200	3 - 48	1 - 10	Spherical and cubic ^a	283
Microwave synthesis	1.0A ₁₂ O ₃ : 1.0P ₂ O ₅ : 0.6SiO ₂ : 6TEAOH: 110H ₂ O	150	7 - 20	0.01 - 0.1	Plate-like shape	285
Ultrasonic synthesis	1.0Al ₂ O ₃ : 1.0P ₂ O ₅ : 0.6SiO ₂ : 2.0TEAOH: 70H ₂ O	200	1.5 (15) ^b	0.05	Sphere-like shape	284

^aThe morphology varies with the type of ionic liquid. ^bSonication time in minutes.

4.4.2 Influence of Template

Alteration of the organic structure directing agent (i.e., a vital component in zeolite synthesis) is one method that has been investigated with the intention of modifying the catalyst structure to ultimately enhance activity and overall performance (see Table 8 summary). This notion has also been investigated by research groups with the aim of reducing the costs associated with catalyst synthesis. This is because TEAOH, the primary template used in micron-sized pure SAPO-34 synthesis, imposes a high cost. Hence, cheaper templates such as morpholine (MOR), triethylamine (TEA), dipropylamine (DPA), piperidine, and diethylamine (DEA) have also been employed 85,287. However, the economic benefit of individually applying the latter three templates may be offset by the consequences imposed on the catalyst, such as larger particle size, decreased crystallinity, and generation of impurities or competing phases, which can ultimately worsen catalytic performance 288,289. To combat this,

This article is licensed under a Creative Commons Attribution-NonCommercial 3.0 Unported Licence.

Open Access Article. Published on 22 2025. Downloaded on 30.10.2025 01:47:29.

recently, research has been devoted to synthesizing SAPO-34 via a mixed template approach, which involves the idea of initial nucleation of pure SAPO-34 crystals via TEAOH followed by further crystal growth using one of the cheaper template alternatives ^{288,290-292}. Thus, by implementation of this method, one can achieve more cost-effective SAPO-34 synthesis without having to compromise on phase purity and particle size. In fact, the use of the mixed template synthesis method has been shown to introduce new catalyst intergrowth structures that makes internal active sites more accessible to reactants, reducing the rate of blockage of pore openings by coke species, thereby prolonging catalyst lifetime ⁷⁶.

It is well known that single template usage of TEAOH can generate pure SAPO-34 phase void of other competing phases or irregularities. However, it is important to be attentive to the pH of the gel during synthesis, since, depending on the template's specific basicity strength, different quantities should be added to remain within an acceptable pH range for the commencing gel ⁷⁶. The consequences of this can be seen in one group that employed identical synthesis procedures for alternating single template samples and surprisingly observed the SAPO-5 impurity phase while using TEAOH ²⁹⁰. The use of a mixed template, specifically a combination of MOR and TEAOH, leads to a reduction in particle size and a change in morphology to a spherical type formed by the aggregation of nano-sized crystals. The mixed template approach allows for a better balance of acidic sites, which is crucial for MTO reaction. The presence of both templates in different concentrations can optimize the distribution and strength of the acidic sites, leading to improved catalytic performance in the MTO reaction as shown in Figure 27.

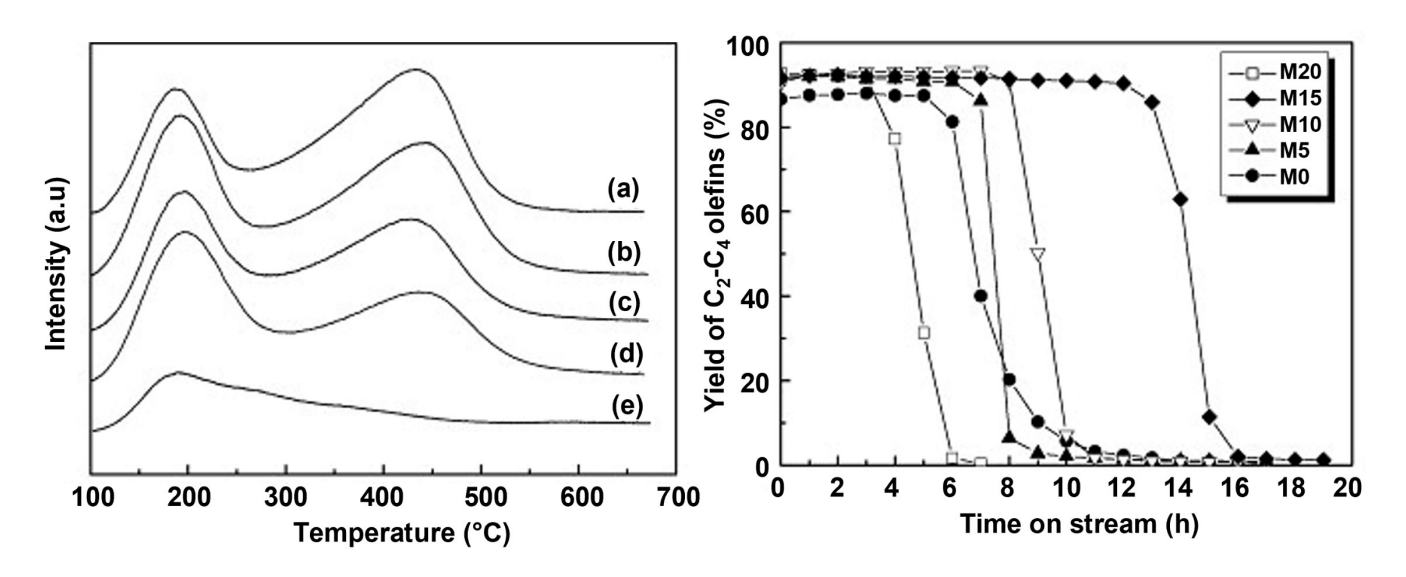


Figure 27 (Left) NH₃-TPD (a) M20, (b) M15, (c) M10, (d) M5, and (e) M0, and (Right) yield of C2-C4 olefins with time on stream over SAPO catalyst prepared at different compositions of MOR and TEAOH templates. "M" stands for mixed template, and the number following refers to the degree of mixing, where M0 and M20 mean only TEAOH and MOR were used, respectively. Reprinted from reference ²⁹⁰ with permission from Elsevier, Copyright 2007

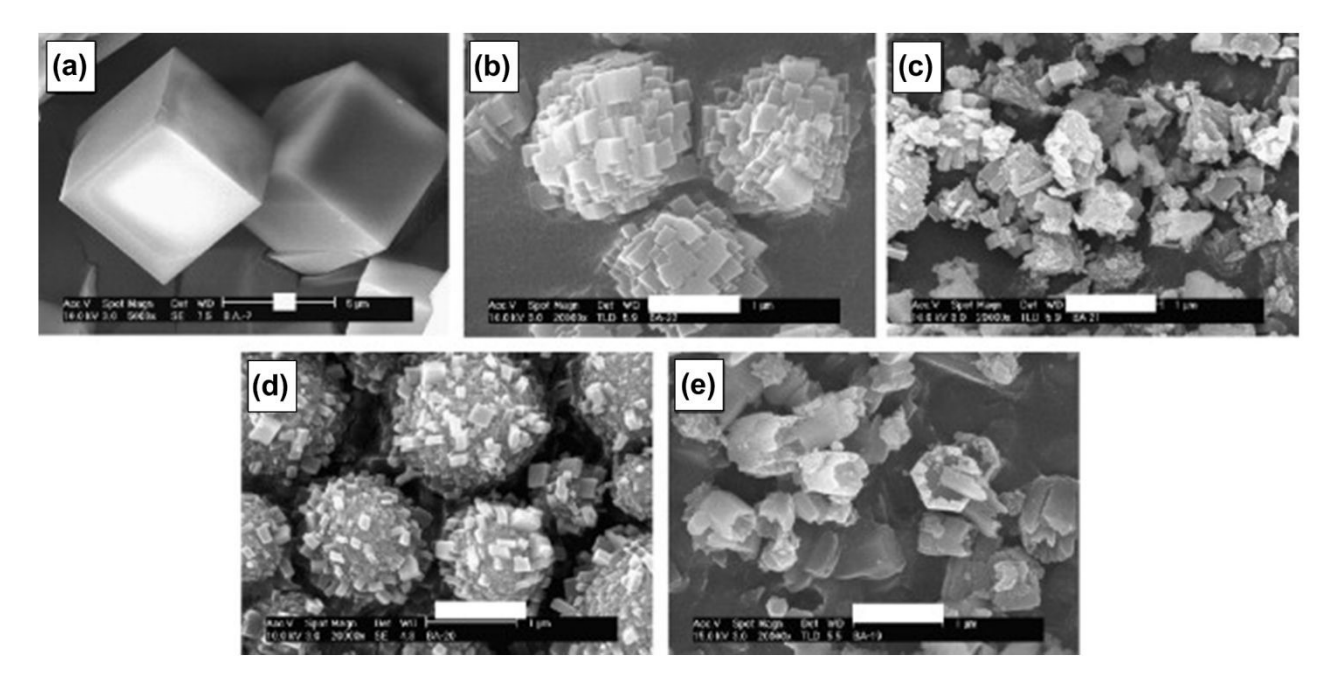


Figure 28 SEM images elaborating the influence of the combined templates on the morphology and SAPO-34 (a) M20, (b) M15, (c) M10, (d) M5, and (e) M0. Bars correspond to 1 µm. Reprinted from reference ²⁹⁰ with permission from Elsevier, Copyright 2007.

With regards to the a cheaper templates (e.g., DEA and TEA) as a substitute for TEAOH, these typically introduce impurity phases such as SAPO-5 and SAPO-11 ^{288,289}, as well as undesired amorphous phases, which can be a major factor (along with the previously discussed catalyst particle size) in the downfall of catalytic activity of these samples, as can be seen in Figure 29. For instance, the use of piperidine as an organic structure directing agent (OSDA) in catalyst synthesis generated a crystalline product that was a combination of different SAPO family structures (specifically SAPO-17, SAPO-20, and SAPO-35) in tandem with the desired SAPO-34 phase ²⁸⁷.

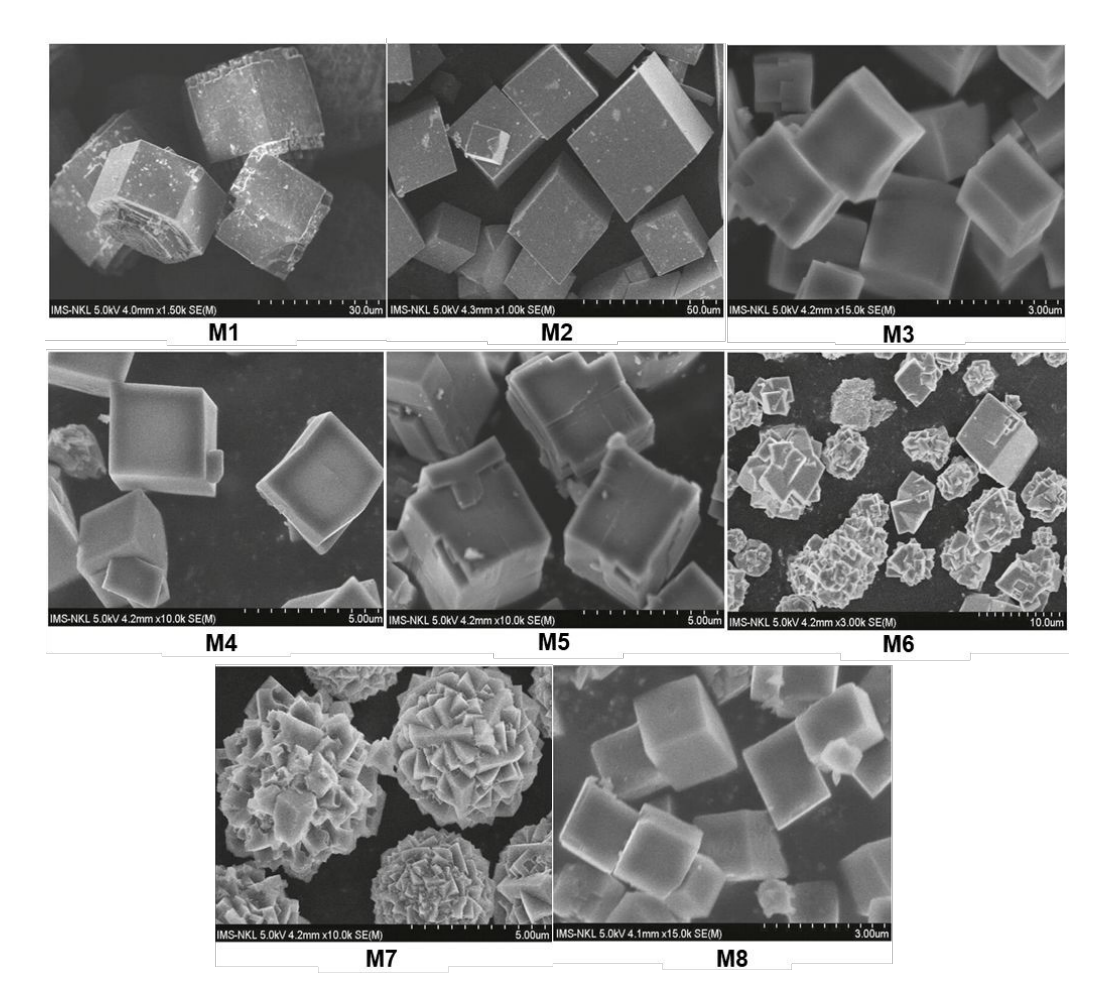


Figure 29 Influence of different types of templates and their combination on morphology and purity of SAPO-34: (M1) TEA, (M2) MOR, (M3) TEAOH, (M4) 3MOR:1TEAOH, (M5) 3TEA:1TEAOH, (M6) 3MOR:1TEA, (M7) 1MOR:1TEA, (M8) 3MOR:3TEA:1TEAOH. Reproduced from reference 288 with permission from John Wiley and Sons, Copyright 2019.

Furthermore, based on the literature, alteration of the template undoubtedly influences the Si incorporation amount and mechanism, resulting in different acidities, despite having the same starting gel composition. Although one group ²²⁴ reported that the higher the portion of TEAOH (using the MOR-TEAOH mixed-template catalyst) can result in lower catalyst acidity, in the majority of cases, no clear trend with regards to acidity could be established, with the results highly fluctuating between the different synthesized catalysts ^{293,294}.

Table 8. Summary of the effect of different templates on phase purity, morphology, and catalytic activity.

-			Ope	rating Co	onditions	Morphol	ogy	Ac	tivity	Re
Sample	Templates	Phase	T(°C)	p (atm)	$WHSV \\ (g_{MeOH} g_{Cat}^{-1} \\ h^{-1})$	Shape	Particle size (μm)	Stability (h)	Olefins Selectivity (C ₂ -C ₄)	_
S-1	TEA	СНА	400	1	1.2	Cuboids	~20	< 0.5	~ 70	85
S-2	ТЕАОН	СНА	400	1	1.2	Plate-like	0.5×0.3	6.5	~90	85
S-3	Methylami ne (MA)	СНА	400	1	1.2	Cuboids	~10	1.5	~85	85
S-4	Dipropyl amine (DPR)	СНА	400	1	1.2	Typical cube-like rhombohedra	20 × 20 × 5	2.5	~80	85
S-5	DEA	СНА	400	1	1.2	Cuboids	~10	~1	~65	8:
SAPO-34, SAPO-20, SAPO-35, SAPO-17	Piperidine	CHA formed at optimum Piperidine/Al ₂ O ₃ = 1.1, otherwise impurities phases exist	300	2.5	N/A	Pseudo-cubic crystals	5-30	N/A	N/A	28
M1-M8	MOR/TEA OH/ TEA	CHA over MOR, TEAOH or combination of the three templates	N/A	N/A	N/A	M1 (hexagonal and plate-like morphology), M2- M3 (cubic), M6- M7 (cube-like agglomerated to sphere), M8 (cubes)	M1: 10-20, M2: 20-45, M3: 3-8, M6: 5-7, M7: 5-7, M8: 3	N/A	N/A	28
M0	MOR: TEAOH (0:1)	SAPO-5 (92%) + SAPO-34 (8%)	250- 500	1	1	Typical hexagonal of SAPO-5	< 1	6.2	60.2*	29
M5	MOR: TEAOH (0.25:0.75)	СНА	250- 500	1	1	Spherical with nano-cubes aggregate	-	7.2	76.3*	29
M10	MOR: TEAOH (0.5:0.5)	СНА	250- 500	1	1	Irregular shape	Submicron	8.7	82*	29
M15	MOR: TEAOH (0.75:0.25)	СНА	250- 500	1	1	Spherical aggregates of nano-sized cubes	1	14	81.8*	29
M20	MOR: TEAOH (1:0)	СНА	250- 500	1	1	Cubes	5–20	2.7	81.9*	29
SP34-X (X=1-0)	MOR/TEA OH	For x>0.4 CHA, otherwise impurities exist.	425	1	2	Cubes	1-0.5	5.5	91.8	21
A,b,c,d,f, g	ТЕАОН	CHA at higher TEAOH concentration, otherwise SAPO-5	170- 220	N/A	N/A	Cuboids	~1	N/A	N/A	21

^{*}Yield of C₂-C₃ olefins.

This article is licensed under a Creative Commons Attribution-NonCommercial 3.0 Unported Licence.

Open Access Article. Published on 22 2025. Downloaded on 30.10.2025 01:47:29.

4.4.3 Influence of Silicon Content

Due to the strong correlation that exists between silicon content and its incorporation mechanism in SAPO-34's crystalline structure with the amount and strength of generated Brønsted acidic sites (BAS), a large number of studies have adjusted the Si quantity in the commencing catalyst synthesis gel to decipher the optimal acidity that can result in superior catalyst performance $^{131,295-297}$. According to 29 Si NMR analysis illustrated in Figure 30, starting with a low Si content in the gel (up to an SiO₂/Al₂O₃ ratio of roughly 0.2), the Si incorporation mechanism is mainly dominated by SM1 (P atom substitution for Si), resulting in so-called isolated Si (i.e., Si(4Al)). However, when employing a higher amount of Si in the commencing gel, the Si incorporation mechanism is also comprised of SM2 (simultaneous adjacent Al-P pair substitution by two Si atoms), leading to Si-rich (island-like) environments (Si(nAl), n = 0-3) 298 .

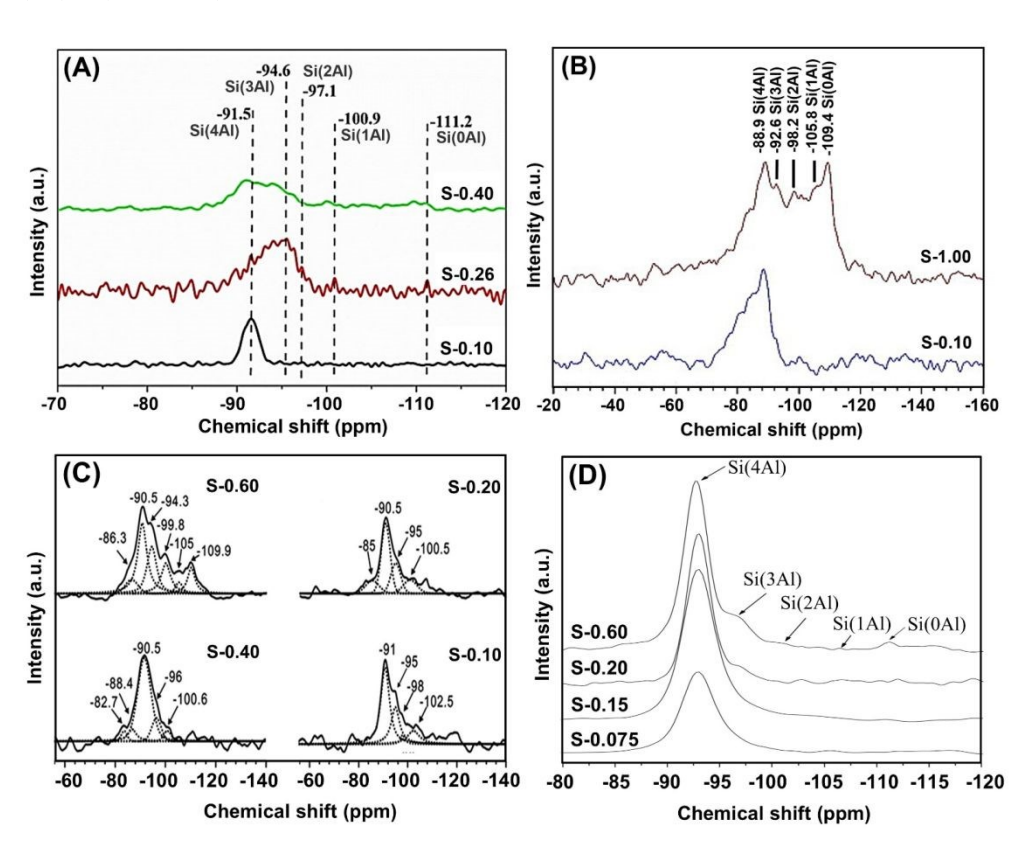


Figure 30 ²⁹Si NMR spectrum for SAPO-34 (S-*x*) samples, where *x* stands for different SiO₂/Al₂O₃ ratios. (A) Reproduced from reference ²⁹⁶ with permission from Elsevier, Copyright 2019 (B) Reproduced from reference ²⁸⁰ with permission from Elsevier, Copyright 2008 (C) Reproduced from reference ²⁹⁹ with permission from Royal Society of Chemistry, Copyright 2014. (D) Reproduced from reference ³⁰⁰ with permission from Elsevier, Copyright 2008.

The general observation, according to literature ^{131,296}, is that the larger the Si content incorporated into the bulk catalyst structure, the greater the total number of Brønsted acid sites generated – although there is the possibility that a portion of Si forms as an extra-framework amorphous silica phase. This trend occurs up to the point in which isolated Si environments begin to transform into island-like configurations. It is worth mentioning that the number

of BAS per incorporated Si is lower for Si islands relative to isolated Si environments. As a result, the trend shifts to either stagnation 131 or slight depletion 296 in overall acidic site amount, as seen for the larger Si-containing samples in the NH₃ temperature programmed desorption (TPD) results of different research groups (Figure 31).

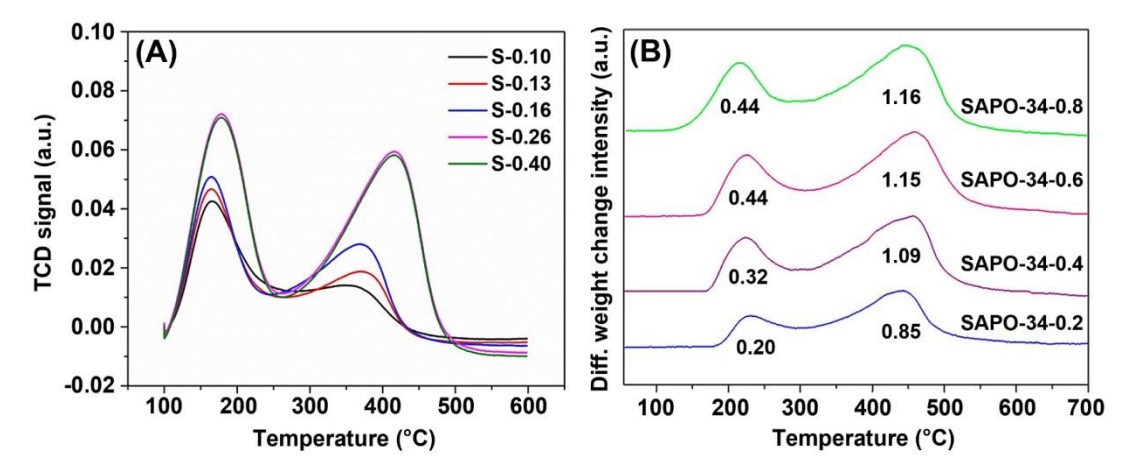


Figure 31 NH₃ temperature programmed desorption of SAPO-34(-x) samples with different SiO₂/Al₂O₃ (x) ratios. (A) Reproduced from reference ²⁹⁶ with permission from Elsevier, Copyright 2019 and (B) Reproduced from reference 131 with permission from American Chemical Society, Copyright 2018. The values beneath the peaks of (B) refer to acidic site density in mmolNH₃ g_{Cat}⁻¹.

By employing this Si alteration method, groups have found that the optimal starting SiO₃/Al₂O₃ molar ratio, with the aim of achieving superior catalyst lifetime, exists between 0.2 and 0.3, as seen in Figure 32 131,296,301. With regards to light olefin selectivity, on the other hand, the greatest value was attained utilizing SAPO-34 of low acid site density (with an SiO_2/Al_2O_3 molar ratio between 0.1 to 0.2 in the gel) 131,296,302 , which possesses a framework structure of primarily isolated silicon environments (see Figure 30). It has been generally found that exceeding the SiO₂ to Al₂O₃ molar ratio of roughly 0.2 to 0.3 results in an excess of strong Brønsted active sites, which can facilitate both aromatization of cycloalkanes, along with intermolecular hydrogen transfer reactions between polymethyl-benzenes/naphthalenes (PMBs and PMNs) and light olefins ²⁶⁶. In turn, this can amplify the formation rate of polycyclic aromatic compounds (as well as paraffinic species), ultimately resulting in much more rapid catalytic deactivation. The resulting decreased number of PMBs/PMNs, which are active components of the hydrocarbon pool mechanistic concept, can also result in a concurrent depletion of light olefin production. Furthermore, samples constructed with too large a silicon content in the gel have been found to possess dense cubic crystals with little to no macroporous cracks, relative to low Si-containing samples which seem to contain hollow, thin-walled SAPO crystals with a large range of pore sizes (meso- and macro-, in addition to micro-pores) ²⁹⁶. Macro-pore presence in SAPO-34 can permit the diffusion of reactant and product species, despite the formation of coke (which initially blocks only micro-porous pathways). Hence, the elimination of such macrocracks in high Si-containing samples can partly be blamed for the shortening of catalyst lifetime. On the other hand, moving below the optimal SiO₂/Al₂O₃ range of 0.2-0.3 can result in a catalyst that does not possess the

required number of acidic/active sites to sustain long-term light olefin production. Once coke species begin to develop on this limited number of active sites, no further sites would be available for the adsorption and subsequent reactions involving further reactant methanol molecules. Although lower Si-containing samples (i.e., a lower SiO₂/Al₂O₃ ratio such as 0.1-0.2) is beneficial for light olefin production, as it suppresses the hydrogen transfer and aromatization reactions leading to coke, it is still important to introduce enough silicon during the gel stage of synthesis to ensure an adequate active site density in the SAPO framework to achieve time-extended methanol conversion ²⁹⁶. Overall, the effects of Si content alteration on SAPO-34 acidity and activity in the MTO reaction have been detailed in Table 9.

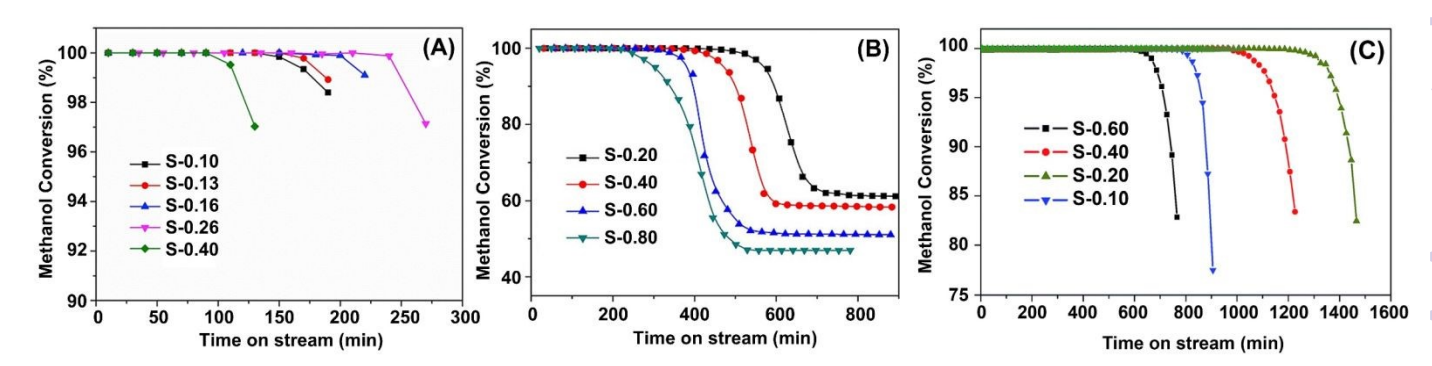


Figure 32 Methanol conversion activity test results for SAPO-34 (S-x) samples, where x stands for different SiO₂/Al₂O₃ ratios. (A) At 450 °C and WHSV of 3 g_{MeOH} g_{Cat}⁻¹ h⁻¹. Reproduced from reference ²⁹⁶ with permission from Elsevier, Copyright 2019. (B) At 425 °C and WHSV of 1 g_{MeOH} g_{Cat}⁻¹ h⁻¹. Reproduced from reference ¹³¹ with permission from American Chemical Society, Copyright 2018. (C) At 400 °C and WHSV of 2 g_{MeOH} g_{Cat}⁻¹ h⁻¹. Reproduced from reference ²⁹⁹ with permission from Royal Society of Chemistry, Copyright 2014.

The acidic strength of the proton attached to the bridging hydroxyl group (Si-OH-Al) can be highly affected by the electronegativity of the first and second shells of neighboring molecules ³⁰³. The higher the electronegativity of the surrounding atoms, the stronger the acidity of the Brønsted site (noting that the electronegativity of Al, Si, and P are 1.61, 1.90, and 2.19, respectively). Comparing the first and second shell of neighboring atoms for the isolated silica (Si (4Al)(8P)) and the silica island (Si (1Si 3Al)(3Si 5P)), the first neighboring shell of silica island is more electronegative (due to the presence of one Si instead of one Al). Taking this into account, it has been widely inferred that BAS associated with Si islands possess greater acidic strength than those with isolated environments ³⁰³, and consequently, catalysts possessing higher silica islands are prone to faster deactivation. However, it seems that the lower electronegativity of the second neighboring shell of the silica island has been overlooked (due to the presence of three Si instead of three P atoms). Thus, to correctly assess the strength of the acidic sites, an aggregate effect of the first and second shells should be considered ⁷⁶. Overall, there still exists the need for an exclusive study to properly address the matter.

Table 9. Summary of the influence of altering the Si content on SAPO-34 acidity and activity in the MTO reaction.

Catalyst	Si/Al ratio	Acid density (mmol g ⁻¹)	Lifetime (min.) ¹	Olefins (C ₂ -C ₃) S (%)	Note	Ref.
SAPO-34-0.2 0.4		1.05	351	~ 87	The Si content did not affect phase purity, morphology, particle size, or surface area.	266
SAPO-34-0.4	0.8	1.41	287	~ 82	Acid density increased with the increase of Si/Al ratio.	
SAPO-34-0.6	1.2	1.59	245	~ 79	Stability enhanced with lower Si/Al ratios.	
SAPO-34-0.8	1.6	1.60	173	~ 79		
S-34(8)	0.8	-	120	~ 92*	A lower Si/Al ratio require higher concentration of template to obtain a pure CHA phase. SEM micrographs showed plate-like morphology.	295
S-34(6)	0.6	-	120	~ 94*	The crystallite size decreased with the increase of silicon content.	
S-34(4)	0.4	-	<30	$\sim 87^*$		
S-0.10	0.2	0.92	160	~ 84	Samples with lower Si (S-0.10, S-0.13, S-0.16) contents formed AEI impurities beside the CHA phase. Low Si content leads to thin-wall cube crystals with macropores.	296
S-0.13	0.26	1.00	170	~ 84	High Si content results in more solid crystals without macropores.	
S-0.16	0.32	1.16	220	~ 82	Medium Si content produces hollow crystals with a more integrated surface. The increase in Si content also leads to a transformation from	
S-0.26	0.52	2.04	240	~ 84	a hollow structure to a dense phase and a change in surface structure. The higher the Si content, the denser the crystal structure becomes, and the surface becomes more integrated	
S-0.40	0.80	2.04	110	~ 78	without visible macroporous cracks.	
S-0.50	1	2.13	-	-		
SAPO-34(0.3)	0.6	2.64	~1400	~90*	Increasing the Si content generally leads to smoother and more cubic-like particles, while lower Si content can result in	297
LaAPSO-34(0.1)	0.2	-	~1500	~88*	the formation of amorphous particles and rougher surfaces. The Si/Al ratio affects the crystallinity of the catalysts.	
LaAPSO-34(0.2)	0.4	1.92	~1000	~90*	The ShArrano affects the crystallinity of the catalysts.	
LaAPSO-34(0.3)	0.6	1.29	~2100	~93*		
LaAPSO-34(0.4)	0.8	-	~1900	~93*		
LS	0.06	-	-	-	Si content influenced the crystallinity of SAPO-34.	
LMS	0.13	-	-	-	Si content affected the weak acid sites, which was linked to	301
MS	0.22	-	-	-	the degree of crystallinity. Weak acid sites had no role in the MTO reaction.	
MHS	0.36	-	-	-	Hydrocarbon yield was maximum over the low medium	
HS	0.50	-	-	-	silicon content (LMS) sample.	

Lifetime was considered when the conversion dropped to lower than 100%.

4.4.4 Sub-micron SAPO-34 synthesis

Obtaining SAPO-34 morphology with reduced particle size is highly desired due to its contribution in prolonging catalyst lifetime ^{61,304}. Groups have declared that smaller particles can increase the exposure and accessibility of active sites as well as enhance the mass transfer properties of the catalyst. This also implies a shortened diffusion

^{*}C₂-C₄ olefins selectivity.

Chemistry A Accepted Manuscrip

Journal of Materials

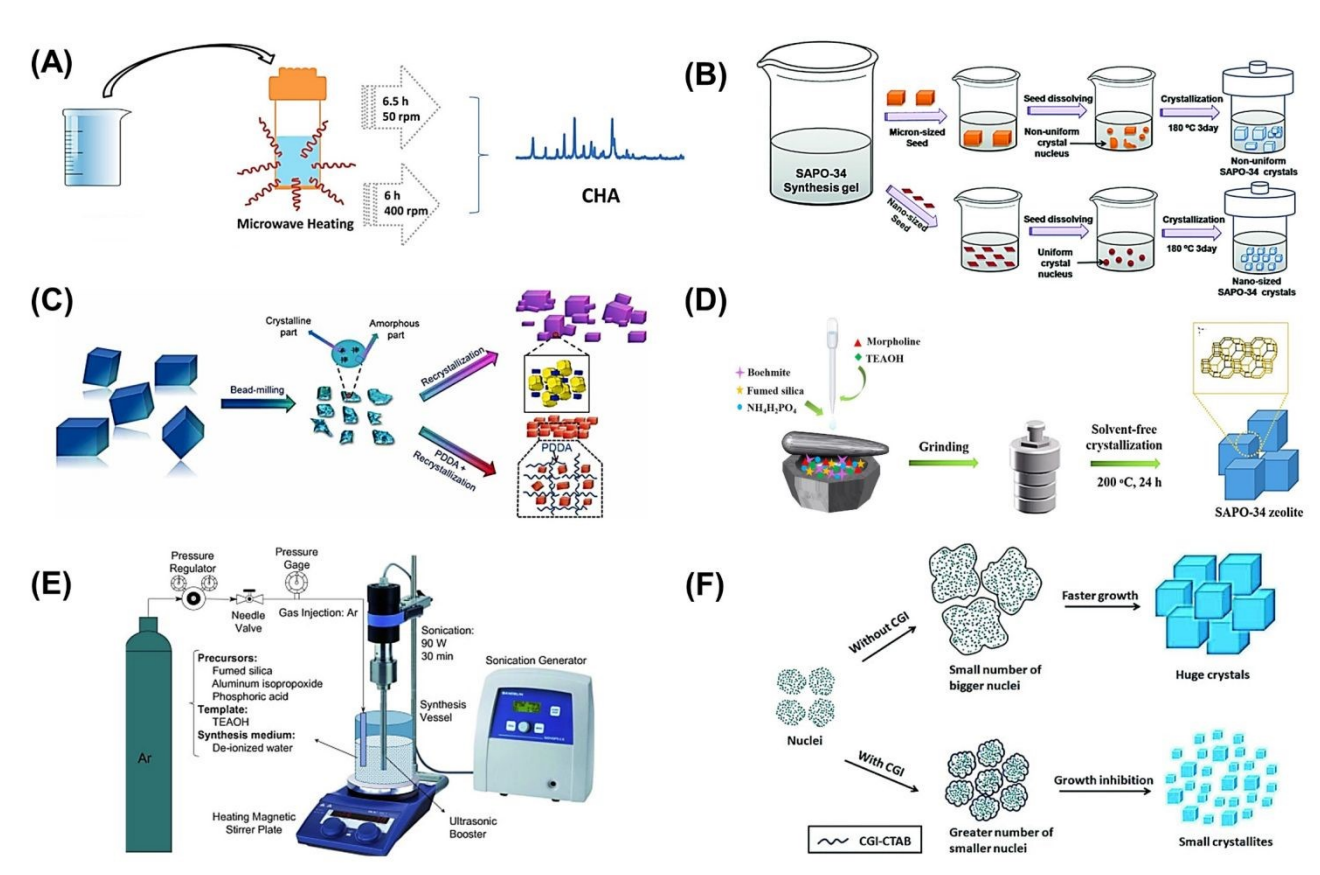


Figure 33 Sub-micron SAPO-34 synthesis techniques: (A) Microwave-assisted hydrothermal synthesis reproduced from reference 305 with permission from American Chemical Society, Copyright 2019; (B) Seed-assisted synthesis reproduced from reference 306 with permission from Royal Society of Chemistry, Copyright 2017; (C) Post-synthesis milling and recrystallization reproduced from reference 307 with permission from Elsevier, Copyright 2022; (D) Solvent-free hydrothermal synthesis reproduced from reference 308 with permission from MDPI, Copyright 2021; (E) Sonochemical-based synthesis reproduced from reference 309 with permission from Elsevier, Copyright 2014; (F) Crystal growth inhibitors (CGIs) involved synthesis reproduced from reference 310 with permission from Royal Society of Chemistry, Copyright 2018.

Microwave-assisted hydrothermal synthesis is one such method that has been deemed capable in synthesizing nanocrystalline SAPO-34 catalysts relative to the conventional hydrothermal method i.e., 0.075-0.15 μm (see Figure 34(A)), compared to its parent of a few microns 304,305,311. This approach, involving microwave irradiation of the synthesis gel under static conditions, allowed for the reduction in crystallization time to only a few hours and more homogeneous nucleation of particles, yielding SAPO particle morphologies that were thin, smaller, more plate/sheet-like, and uniform. This ultimately resulted in roughly 50 to 60% enhanced catalyst lifetime (alongside maintained light olefin selectivity), justified by reductions in the diffusion pathway and residence time of the reactant and product species in the micro-pores of the catalyst ³¹².

Seed-assisted synthesis is an alternative technique that has been employed for the generation of higher surface area, nano-sized SAPO-34 (range of 0.2-0.7 µm as seen in Figure 34(B)) ^{222,306}, which has displayed both a 4-fold enhanced catalytic lifetime and an improved average light olefin selectivity in the MTO reaction ^{306,313–315}. In brief, this method operates via the addition of pre-constructed SAPO-34 seed crystals to the initial synthesis gel, followed by the normal hydrothermal synthesis approach ³¹⁶. The seed crystals, which partially dissolve in the gel, take on the role as surfaces or nuclei for newly growing crystals. As a result, one study ³¹³ demonstrated that this method allowed for rapid nucleation, which effectively reduced the time for synthesis, as well as decreased the consumption of template (OSDA) by up to 52%, which was deemed to lower synthesis costs.

Alternatively, the generation of SAPO-34 nano-particles (0.05–0.35 μm in size, as seen in Figure 34(C), relative to the parent of a few μm) has been achieved through the use of a top-down approach known as post-synthesis milling and recrystallization ^{307,317,318}. In turn, implementation of this technique brought about improved MTO catalytic performance in terms of both lifetime (a 5-fold enhancement) and LOS ³¹⁸. This method commences with synthesized SAPO crystals that are crushed via bead milling (such as using a planetary ball mill with water as a dispersing phase), followed by crystallinity recovery via hydrothermal recrystallization (utilizing an aluminophosphate solution). The use of X-ray photoelectron spectroscopy (XPS) in one study revealed that milling followed by post recrystallization resulted in decreased Si content on the surface of SAPO particles relative to the bulk interior ³¹⁸. Hence, other than the reduction in particle size, this decrease in particle surface acidity could suppress the hydrogen transfer and aromatization reactions responsible for coke formation, retaining the interior active sites as accessible.

Solvent-free hydrothermal synthesis, also termed dry gel conversion, exists as another method employed for the generation of nano-sized SAPO-34 crystals (in the range of 0.075 to 0.5 μ m, as seen in Figure 34(D)) ^{286,308,319–321}. This method can operate either by evaporating the solvents contained in the final catalyst gel prior to the hydrothermal step ³²², or alternatively, grinding and mixing the required precursors in absence of a solvent entirely ³⁰⁸. In order to achieve a desirable H_2O/Al_2O_3 ratio, a certain quantity of water may potentially be introduced into the dry precursor, which is then followed by the typical hydrothermal portion of the synthesis ³²². From an

economic standpoint, an evident benefit of solvent-free hydrothermal synthesis is that it allows for significantly reduced template consumption. In addition, it is owed significantly reduced time for crystallization, with ~6 h of synthesis until fully crystalline SAPO-34 is successfully attained ^{286,320,321}. Nano-sized catalysts constructed via this methodology possess a hierarchical structure containing mesopores (in addition to the traditional microporous pathways) due to the stacking of nanocrystals, which has been claimed to enable the mass transfer of reactant and product species ³²². Overall, the implementation of this method has resulted in prolonged catalyst lifetime (roughly two to four-fold increase) with equivalent to slightly greater light olefins selectivity, relative to that under the conventional hydrothermal method 320-322.

Sonochemical-based synthesis is introduced as another technique utilized in the construction of SAPO-34 nano-

catalysts (in the range of 0.05 µm to 0.45 µm, as seen in Figure 34(E)) ^{57,227,323,324}. This method involves the use of ultrasonic irradiation (rather than mechanical stirring) during the aging step, followed by a shortened hydrothermal step to minimize the overall growth of the crystal nuclei. Due to the chemical effects ultrasonic waves impose (as a result of acoustic cavitation phenomena in the solution), the rate of nucleation is enhanced while the agglomeration of particles is diminished, resulting in a catalyst with a larger total and external specific surface area than the traditionally prepared parent counterpart. Due to the reduced residence time of hydrocarbon species in nano-catalyst particles (i.e., as a result of shorter intracrystalline diffusion length), sono-synthesized catalysts have displayed reduced coke generation rate, and thus prolonged activity (roughly two-fold), alongside a similar product distribution to the conventionally prepared parent SAPO-34 (displaying a 2 µm average particle size) 323. Lastly, some groups have utilized crystal growth inhibitors (CGIs) during synthesis such as polyethylene glycol (PEG) (see Figure 34(F)), polyoxyethylene lauryl ether (Brij-35), methylene blue (MB), and surfactant cetyltrimethylammonium bromide (CTAB)) 310,325. This method consists of the addition of one or more of these compounds as either the final precursor(s) or prior to template addition during the gel stage of SAPO synthesis. The added inhibitors are generally removed during the final calcination step. On the other hand, the CGIs are suggested to interact with reactive sites of inorganic precursors in solution, such as to give rise to enhanced rates of nucleation. This ensues by the adsorption of CGIs onto the external surface of generated nuclei, allowing for their separation, and thus lowering the rate of crystal growth. Overall, this results in the formulation of a larger number of smaller-sized crystals, without imposing any significant structure-directing effects during the generation towards the final catalyst framework (i.e., no clear major presence of competing phases). This method has resulted in catalysts with a much larger BET surface area than the conventionally prepared parent catalyst. A study that

investigated the use of CTAB during SAPO-34 synthesis found that the optimal resulting catalyst, sized between

Open Access Article. Published on 22 2025. Downloaded on 30.10.2025 01:47:29.

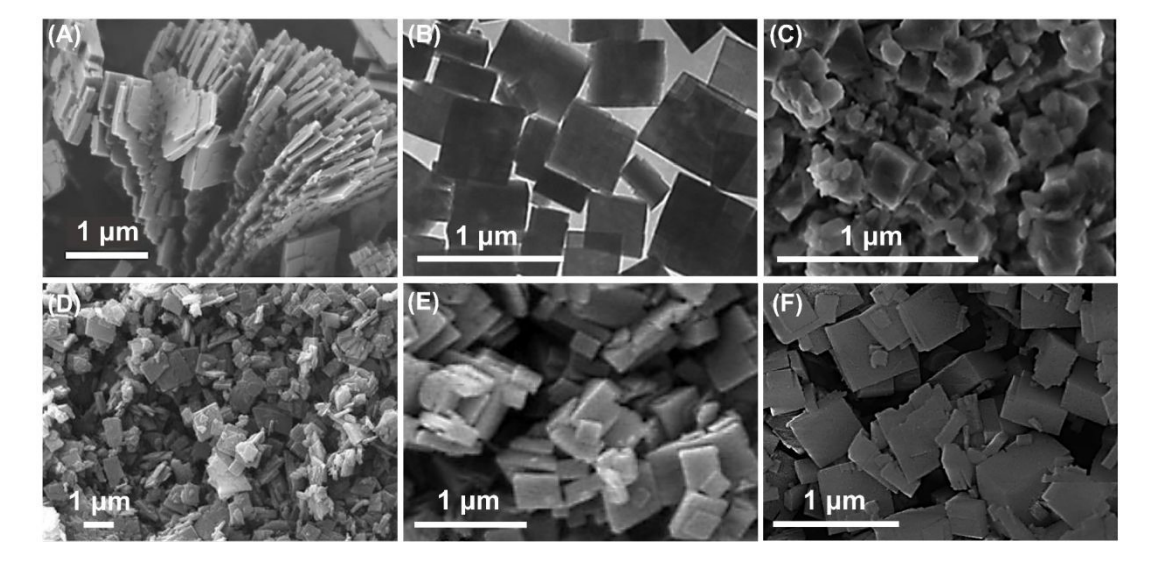


Figure 34 SEM/TEM images of the catalysts prepared via different sub-micron SAPO-34 synthesis techniques: (A) Microwave-assisted hydrothermal synthesis reproduced from reference ³¹² with permission from Royal Society of Chemistry, Copyright 2014; (B) Seed-assisted synthesis reproduced from reference ³¹⁴ with permission from Royal Society of Chemistry, Copyright 2015; (C) Post-synthesis milling and recrystallization reproduced from reference ³¹⁸ with permission from Royal Society of Chemistry, Copyright 2014; (D) Solvent-free hydrothermal synthesis reproduced from reference ³²⁰ with permission from Springer Nature, Copyright 2016; (E) Sonochemical-based synthesis reproduced from reference ⁵⁷ with permission from Elsevier, Copyright 2014; (F) Crystal growth inhibitors (CGIs) involved synthesis reproduced from reference ³²⁵ with permission from American Chemical Society, Copyright 2008.

Although nano-sized SAPO-34 has proven useful in enhancing catalyst performance in the MTO reaction, the aforementioned synthesis methods generally still face issues involving low yield, higher production costs, and serious difficulties concerning scale-up. Hence, a comprehensive cost-benefit analysis of each technique seems to still be required to truly assess whether the benefits of improved catalyst performance outweigh the costs associated with these synthesis procedure adaptations. Furthermore, only a limited number of groups have investigated the effect of combined application of these methods, e.g., the hydrothermal approach involving seed assistance followed by dry gel conversion ³²⁰. A detailed exploration of the possible synergistic effects of multiple technique integration (in a singular synthesis procedure) seems yet to be undertaken.

Table 10. Summary of different approaches of Sub-micron SAPO-34 synthesis and their effect on SAPO-34 properties and activity in the MTO reaction.

Approach	Approach Particle Morphology		Activity	Note	Ref.
	Size	Shape	-		
	(µm)				
Microwave- assisted approach	0.02 - 1	Flaky, nano- spherical, and cubic	Catalytic activity was linked to particle size. It was maximum over flake-like particles, followed by nano-sphere, submicron cube, and micron cube.	Particle size and shape vary with temperature, time, and source of Si precursor.	304

			Coke formation was minimised with decreasing particle size.		
Microwave- assisted approach	0.1 - 0.2	Sphere-like	Catalysts demonstrated 100% methanol conversion for 120 minutes and a total light olefins selectivity of ~85%.	Spherical particles agglomerated to form a flake-like shape.	269
Microwave- assisted approach	0.075 - 0.01	Varies between sphere- and cube-like	The study is limited to synthesis only, and the authors examined different parameters that affect crystallinity and morphology.	Morphology and particle size were strongly influenced by microwave exposure time. Microwave power delivery affected phase purity and morphology.	311
Microwave- assisted approach	0.01 - 0.1	Plate-like	MW-assisted synthesized SAPO-34 exhibited a longer lifetime of up to 13 hours, compared to 8 hours with conventional heating. It also displayed higher initial olefins selectivity; however, after 3 h of TOS, all catalysts exhibited very similar olefins selectivity, reaching around 90% at all temperatures tested.	Microwave irradiation favored lower levels of Si incorporation and thus lower acidity. It led to a significant variation in crystal shape and size compared to conventional heating, resulting in smaller size, shorter crystallization time, specific plate-like morphology, and conversely lower surface area.	285
Seed-assisted synthesis	0.2 - 0.5	Cube-like	Methanol conversion was enhanced with the use of different-sized seeds. The smaller the crystal size of the seed, the smaller the SAPO-34 produced, leading to more effective catalytic activity & higher overall conversion rates and LOS compared to conventional SAPO-34.	Seed-assisted synthesis of SAPO-34 reduced the crystal size to a range of 0.2–0.5 µm from 50-10 µm. This method also caused larger external surface areas than those obtained from conventional SAPO-34.	222
Seed-assisted synthesis	0.035 - 0.1	Varies between sphere- and cube-like	The study analyzed the effect of the template and seed content on SAPO-34 synthesis. These factors significantly influenced the textural properties of SAPO-34. However, the analysis of the selected samples was inconclusive regarding the impact of seed content on catalytic activity due to simultaneous changes in more than one factor.	Small particles (0.035-0.1 µm) agglomerated to form larger particles. The introduction of seed in the synthesis reduced the use of OSDA by 50%.	313
Seed-assisted synthesis	0.2	Nano-sheets	Since the seed-assisted method did not change the particle size and merely reduced the synthesis time to 20 min, there was no obvious effect on the catalytic activity.	Using seeds accelerated crystallization of SAPO-34 significantly compared to methods without seeds. With seeds, the zeolite crystallized in just 10 minutes, while conventional methods could take over 40 minutes with low yields.	314
Seed-assisted synthesis	0.3 - 0.8	Cube-like	The nano-sized seed -assisted hierarchical SAPO-34 exhibited a catalytic lifetime of up to 586 minutes, four times longer than that of the conventional micron-sized	The seed-assisted method is instrumental in achieving high yields, enhanced structural properties, and superior catalytic	315

			microporous catalyst. Its selectivity for ethylene and propylene reached 85.0%, a 10% improvement from conventional microporous SAPO-34 zeolites.	performance of SAPO-34 zeolites. It reduced the particle size by one-tenth of that of conventional SAPO-34 zeolite.	
Post-synthesis milling	0.05 - 0.15	Cube-like	Micro and nanoscale SAPO-34 catalysts achieved 100% methanol conversion. However, the lifetime of the bead-milled sample extended from around 65 to 140 minutes, increasing to approximately 290 minutes through porogen-assisted recrystallization. The catalysts had similar total olefin selectivity, but the bead-milled catalysts were more selective towards ethylene and less towards butylene.	The bead-milling process effectively reduces the particle size from 20 µm to 0.05-0.15 µm, enhancing the material's properties for catalytic applications.	307
Post-synthesis milling	0.05 - 0.35	Cube-like	After milling and recrystallization, the catalytic lifetime of the recrystallized SAPO-34 was significantly extended from 38 minutes to 224-258 minutes. The selectivity for ethylene and propylene increased from 71.6% to 82.6%. Additionally, the selectivity to propane was reduced from 6.3% to 0.6%.	Milling and subsequent recrystallization not only improved particle size and shape, but also enhanced the catalytic performance of SAPO-34 in the MTO reaction, leading to longer catalyst lifetimes and higher selectivity for desired olefins.	318
Solvent-free hydrothermal synthesis	10 - 30	Cubic	Conversion of methanol to olefins in SAPO-34 synthesised using the solvent-free method was found to be comparable to catalytic performance using the conventional hydrothermal method.	Hierarchal macro- and mesopores of 0.1-3 μm and 0.005-0.05 μm were also found in the cubic crystals, which was attributed to the presence of macro- and meso-structures in the starting materials.	326
Sonochemical- based synthesis	0.05	Spherical	The study is limited to synthesis only, and the authors examined different parameters that affect crystallinity and morphology.	Sonochemically prepared SAPO-34 was obtained in only 1.5 h, a significant improvement from the 24 h attributed to the conventional hydrothermal method. The former was found to be a much faster & efficient method to synthesise SAPO-34 nanocrystals.	324
Crystal growth inhibitors	0.02 - 0.2	Cubic rhombohedral	Catalytic lifetime increased by 1.5 times when an inhibitor was used in comparison to conventionally synthesised SAPO-34. It was concluded that higher Si content in SAPO-34 gave rise to more acidic sites, thereby leading to higher conversion & superior selectivity towards light olefins.	The addition of the inhibitor was deemed ineffective at suppressing intergrowth (given instances of unsuccessful modification and large crystallite size). It was found that the time of inhibitor addition to SAPO-34 is critical to attaining hierarchal structures.	327

4.5 Hierarchical SAPO-34 synthesis by pre- and post-treatment methods

4.5.1 Overview

Another strategy that has been utilized by research groups to conquer fast catalyst deactivation by coking involves the introduction of secondary macro- and meso-pores to naturally microporous SAPO-34. This fundamental creation of a new level of porosity consequently results in a hierarchical structure ³²⁸⁻³³¹. While micropores enable the molecular sieving process of SAPO-34, to maintain a high selectivity to light olefins, these secondary macro- and meso-pores can improve the mass transfer properties of the catalyst. They can keep interior active sites accessible to reactants despite progressive coke blockage of micropores over time, thereby prolonging catalyst lifetime. To achieve this, research groups have employed a variety of bottom-up (pre-treatment) and top-down (post-treatment) synthesis methods, which have been described in more detail in the subsequent sections. Pre-treatment methods generally involve the addition of secondary soft or hard templates into the catalyst gel during synthesis. Generally speaking, these will burn during calcination, leaving behind macro- and meso-sized pores within catalyst particles that depend on both the size and morphology of these secondary templates. On the contrary, the top-down method involves (generally chemically selective) post-treatment of the synthesized catalyst via the employment of acid or alkali-based etching agents that results in somewhat preferential extraction of framework cations ^{218,332,333}.

In general, although bottom-up methods have generally been successful in preparing hierarchically structured catalysts, they may pose some drawbacks worth mentioning ³³². Firstly, since the process of combustion (through calcination) is generally required for template removal and simultaneous creation of desired meso-pores, this results in a sacrificial loss of potentially expensive template, in the case that no recovery-based methods are viable. Secondly, a significant quantity of heat and water may be generated during the thermal decomposition of the mesoporogen agents, which could potentially contribute to the destabilization of the catalyst framework. Overall, while top-down methods may be substituted in place of bottom-up as they are more economically favorable and less complicated ³³⁴, it should be mentioned that they may yield their own consequences as well. For instance, the preferential extraction of framework cations (i.e., dealumination or desilication), during chemically selective acid or alkali post-treatment, may trigger a loss in catalyst mass. This could subsequently hinder the catalyst's acidic (active) properties, and thus its potential regarding catalytic performance ^{332,335}. It should also be noted that the etching post-treatment time and concentration (intensity) utilized are parameters that should be carefully considered and optimized to achieve superior catalytic performance. If chosen inadequately, its effects may be either too minimal (resulting in no significant introduction of meso-/macro-sized secondary pores) or over-bearing (yielding an unstable and demolished SAPO crystalline framework) ³³³. Various instances of either approach will

be discussed extensively in the following sections. Furthermore, Table 11 has been provided to summarize the different approaches of Hierarchical SAPO-34 synthesis and their effect on SAPO-34 properties and activity in the MTO reaction.

4.5.2 Soft Template Addition

With regards to soft templates, one that is commonly employed is the organosilane surfactant [3-(trimethoxysilyl)propyl]-octadecyldimethyl-ammonium chloride (i.e., TPOAC) ^{272,336}. This secondary template has been observed to adopt a dual role as a mesopore-generating agent and an alternative silica source precursor (alongside tetraethyl orthosilicate (TEOS) ²⁷²) during synthesis. Due to the surfactant's adsorption behavior with regards to SAPO precursors, it has been also stated to possess crystal growth-inhibiting capabilities (see Figure 38(A), displaying the spherical agglomeration of nanosheet-like crystals for the pre-treated catalyst). The resulting catalyst has displayed an improved catalyst lifetime (two to four-fold) as well as maintained comparable 272 to enhanced 336 selectivity (by $\sim 10\%$) towards light olefins (relative to its conventionally prepared parent counterpart). However, it can be argued that that the use of organosilane surfactants as secondary templates is a relatively expensive approach 335,337. Therefore, another largely explored soft template includes the use of cost-effective polyethylene glycol (PEG) in a variety of molecular weights ^{338–342}. This compound has demonstrated similar capability in formulating hierarchical SAPO-34 catalysts with intracrystalline micro-, meso-, and macro-porosity (see Figure 38(B)). The resulting catalysts generated via this soft template have exhibited two to six times higher catalytic lifetime, alongside comparable to 10% improvement in light olefins selectivity. PEG employment has been shown to trigger a conflicting mix of either greater ³⁴⁰ or lower ³³⁹ concentration of strong acidic (primarily Brønsted) sites; however, groups have generally reported a depletion in average Brønsted acidic strength upon its use (with reference to PEG of higher molecular weight i.e., 2000-4000 g mol⁻¹)

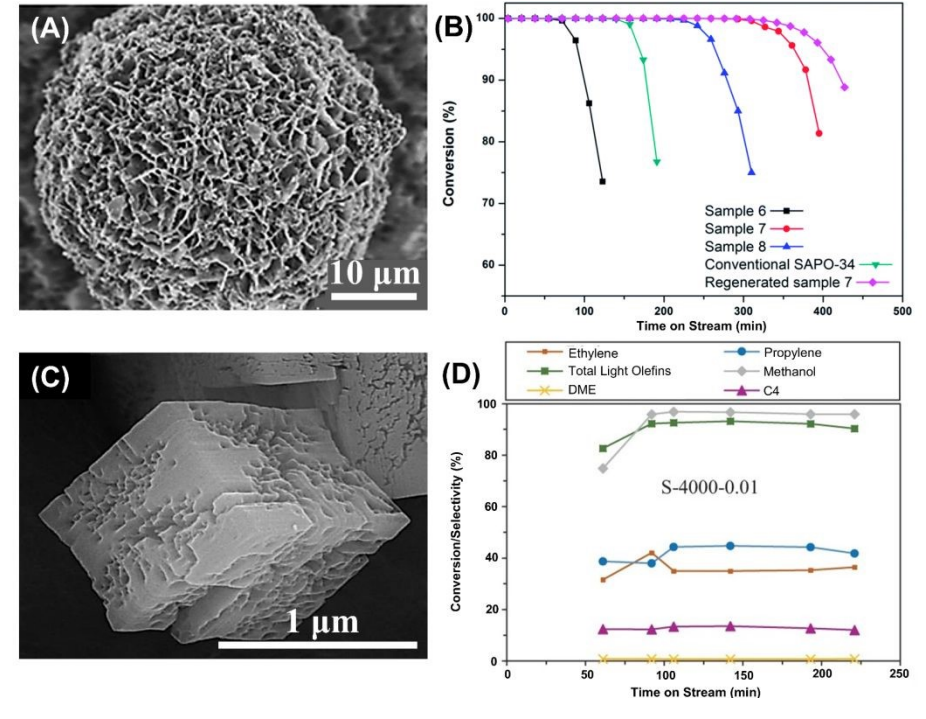


Figure 35 SEM images and Time on Stream results of catalysts (fixated on one particle) produced via application of different soft templating treatment techniques: (A) TPOAC as a secondary (soft) template; (B) Methanol conversion variation with time-on-stream over samples 6, 7, 8, conventional SAPO-34 and regenerated sample 7. Experimental conditions: WHSV = 3 g_{McOH} $g_{Cat}^{-1}h^{-1}$, T = 450 °C, catalyst weight = 300 mg. Reproduced from reference ²⁷² with permission from Royal Society of Chemistry, Copyright 2015; C) PEG as a secondary (soft) template; (D) Light olefin selectivities, methanol and DME conversions over the hierarchical SAPO-34 catalyst variation with time on stream for sample S-4000-0.01 with experimental conditions: T = 425 °C, P = 1 atm, WHSV = 2.3 g_{McOH} $g_{Cat}^{-1}h^{-1}$, catalyst weight = 2 g. Reproduced from reference ³⁴⁰ from Springer Nature, Copyright 2021.

4.5.3 Hard Template Addition

Aside from the soft templates mentioned previously, the use of hard (solid) structure directing agents has been used as an alternative approach by groups to introduce mesoporosity in SAPO-34 crystals. Here, groups have primarily investigated the use of carbon nanoparticles and nanotubes as secondary (hard) templates added during the culmination of the gel stage of catalyst generation (prior to the crystallization step) ^{335,337}. Then, as previously touched upon, the combustion of these secondary templates during calcination is ultimately responsible for the mesopore generation seen in the catalyst structure. One group that investigated the use of carbon nanoparticles as a hard template demonstrated its ability in enhancing the catalyst external surface area and increasing the total pore volume, but the structures formulated were cavity-like rather than interconnected pores. This would have seriously hindered the catalyst mass transfer properties and internal diffusivity, and also limited the accessibility of reactant species to internal active sites ³³⁷. In turn, the resulting catalyst displayed no significant improvement in catalytic performance (i.e., with regards to lifetime and light olefins selectivity) relative to the parent catalyst. In order to alleviate the previously mentioned issues associated with nanoparticle templating, carbon nanotubes have been utilized instead as an alternative secondary template 335,337. With respect to Figure 38(C), its implementation has led to the generation of mesoporous channels (of varying diameters and orientation) which

urnal of Materials Chemistry A Accepted M

Open Access Article. Published on 22 2025. Downloaded on 30.10.2025 01:47:29.

connect the inner section of the catalyst to the external surface. This has resulted in a three-dimensional multi-pore network, rather than simple cave-like and unconnected pores. This approach demonstrated prolonged catalytic lifetime in the MTO reaction with only slightly lower light olefins selectivity relative to the conventionallyprepared sample 335. However, the slight reduction in LOS could be argued to be related to the greater collapse of the SAPO crystalline framework structure, which could hinder its molecular sieving capabilities.

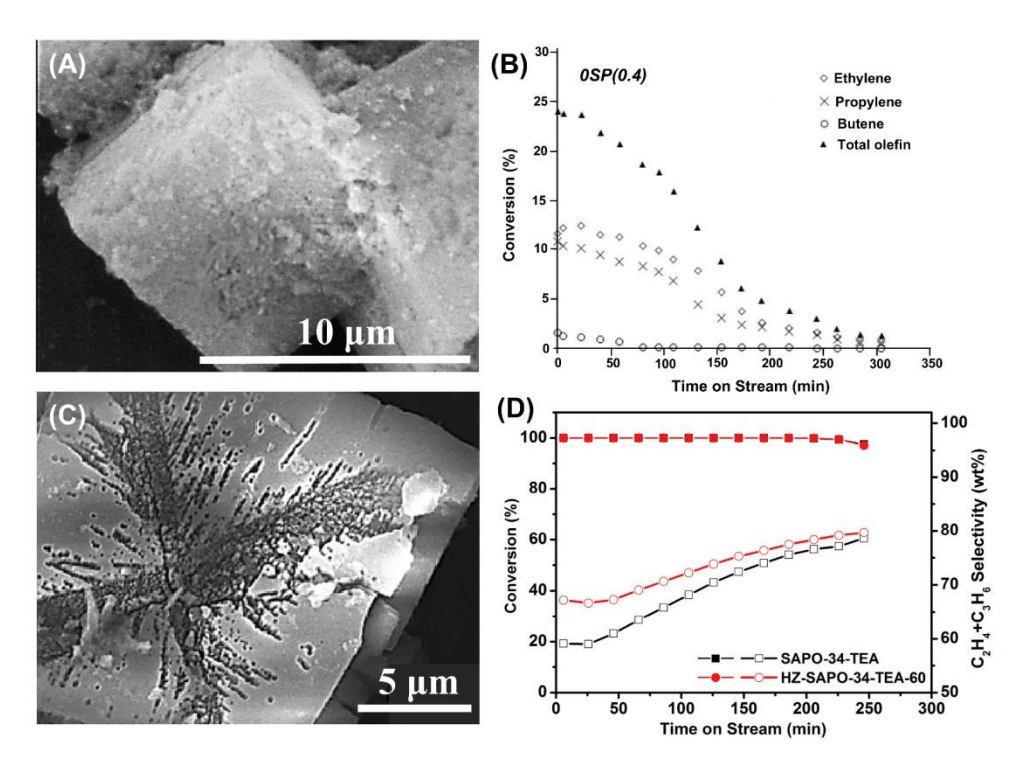


Figure 36 SEM images of the catalysts (fixated on one particle) produced via application of different hard templating treatment techniques: (A) Carbon nanotube as a secondary (hard) template; (B) Yields of ethylene, propylene, butene, and total olefins (C2-C4) with time on stream over SAPO-34 catalyst 0SP(0.4). Reproduced from reference 335 with permission from Elsevier, Copyright 2016; (C) HF-NH₄F mixed aqueous solution as an acid-based etching agent; (D) Methanol conversion (solid symbols) and selectivity of C₂H₄ plus C₃H₆ (hollow symbols) during the MTO reaction over the initial sample and the sample treated with a mixed HF-NH₄F solution for SAPO-34-TEA (WHSV=2 g_{MeOH} g_{Cat}⁻¹h⁻¹, T=400 °C). Reproduced from reference ²¹⁸ with permission from Elsevier, Copyright 2016.

4.5.4 Post-Treatment Desilication

Chemically selective etching (specifically desilication) of SAPO-34 catalysts has been undertaken under ultrasonic conditions via a fluoride medium post-treatment route involving an HF-NH₄F mixed aqueous solutions ^{218,332}. The resulting post-treated catalysts (prepared individually with one of MOR, TEA or TEAOH as micropore generating agents ²¹⁸) displayed the desired hierarchical-like structure (see Figure 38(D)) with slightly reduced average Brønsted acidic site strength, in turn performing better in terms of average light olefins selectivity (by ~2%). In terms of catalyst lifetime, one study displayed a range of worse (by 25-30%) to comparable values for post-treated samples compared to the parent counterparts ²¹⁸. This was largely attributed to the observed SAPO crystallinity depletion alongside insufficiency in the number of catalyst active sites due to reduced strong (primarily Brønsted)

acidic site quantity. By contrast, another group 332 observed a slightly enhanced lifetime (less than 2-fold) of their treated samples, despite having a similarly large reduction in active site (BAS) concentration. Other than fluoridebased post-treatment, etching using TEAOH aqueous solution is another procedure that has been employed for the preparation of hierarchical SAPO-34 crystals ³³³. The resultant catalysts displayed double the catalyst lifetime while maintaining the average LOS relative to the parent catalyst. However, the concentration of strong acidic sites (as well as strength) was reported to have increased over treated samples, which seems to conflict with the observed and expected preferential desilication upon treatment 160. Generally, the choice of etching agent is crucial when it comes to controlling the preparation of hierarchical SAPO-34. For instance, the use of sodium hydroxide instead as a basic etching agent in the post-treatment of SAPO-34 has been observed to lead to a substantial reduction in crystallinity and selectivity remove phosphorus from the bulk structure, yielding amorphous aluminosilicate ³⁴³. Another important consideration is the time duration associated with etching post-treatment, which has also been partly investigated by groups with regards to its effect on catalyst properties ^{218,332}. It was uncovered that increased treatment time resulted in reduced SAPO-34 crystallinity, more deeply etched crystals, larger secondary pores, and greater desilication (which resulted in decreased Brønsted acidic site concentration).

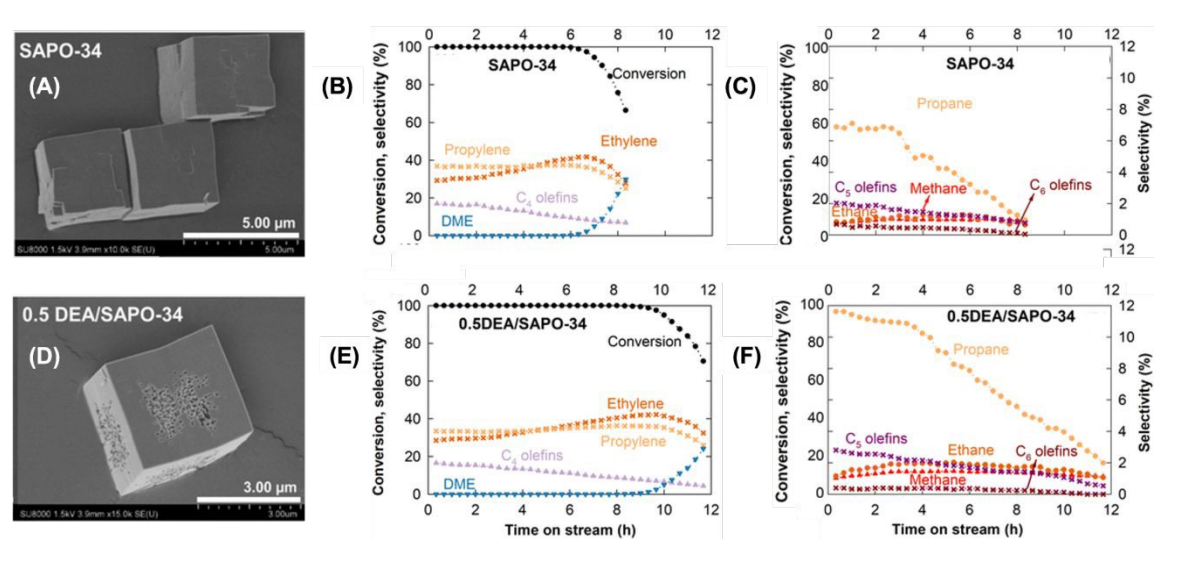


Figure 37 (A) SEM image of the parent catalyst. (B) Methanol conversion and (C) products' selectivity versus time on stream for parent SAPO-34. (D) SEM image of the treated catalyst. (E) Methanol conversion and (F) selectivity versus time on stream for over 0.5 DEA/SAPO-34. Temperature 400 °C, atmospheric pressure, and at a WHSV of 1 g_{McOH} g_{Cat}⁻¹ h⁻¹. Reproduced from reference ¹⁶⁰ with permission from Royal Chemistry Society, Copyright 2023.

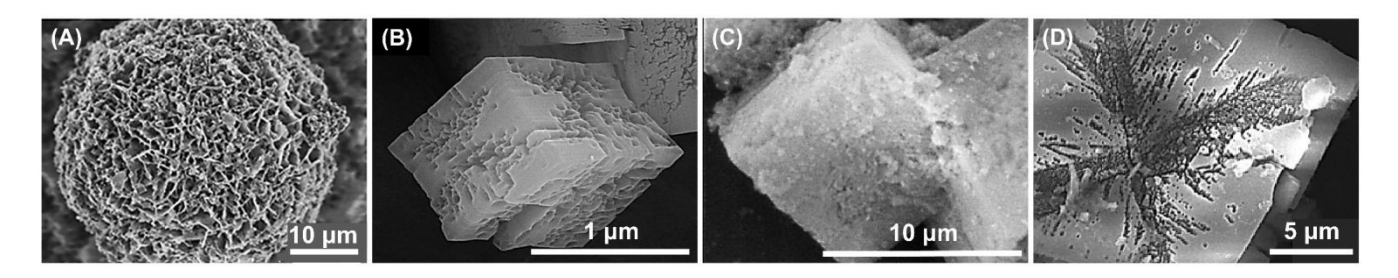


Figure 38 SEM images of the catalysts (fixated on one particle) produced via application of the different pre- and post-treatment techniques: (A) TPOAC as a secondary (soft) template. Reproduced from reference ²⁷² with permission from Royal Society of Chemistry, Copyright 2015; (B) PEG as a secondary (soft) template. Reproduced from reference ³⁴⁰ from Springer Nature, Copyright 2021; (C) Carbon nanotube as a secondary (hard) template. Reproduced from reference ³³⁵ with permission from Elsevier, Copyright 2016; (D) HF-NH₄F mixed aqueous solution as an acid-based etching agent. Reproduced from reference ²¹⁸ with permission from Elsevier, Copyright 2016.

Table 11: Summary of different approaches of Hierarchical SAPO-34 synthesis and their effect on SAPO-34 properties and activity in the MTO reaction

Approach	Particle morphology	Activity	Reaction Conditions	Note	Ref.
Soft Template (TPOAC)	Spherical agglomeration of nanosheet-like crystals	2–4-fold increase in catalyst lifetime; comparable to ~10% improved light olefins selectivity (LOS).	$WHSV = 3 g_{MeOH} g_{Cat}^{-1} h^{-1},$ $T = 450 ^{\circ}C, catalyst$ $weight = 300 mg$	Acts as mesopore- generating agent and silica source; relatively expensive	213, 276
Soft Template (PEG)	Intracrystalline micro-, meso-, and macro-porosity	2–6-fold increase in catalyst lifetime; comparable to ~10% improved LOS.	WHSV = 2.3 $g_{MeOH} g_{Cat}^{-1} h^{-1}$, T = 425 °C, $p = 1$ atm, catalyst weight = 2 mg	Cost effective; variable Brønsted acid site concentration depending on molecular weight.	338– 342
Hard Template (Carbon Nanoparticles)	Cave-like, unconnected pores	No significant improvement in Lifetime or LOS.	Not specified	Limited mass transfer due to the unconnected pores.	275, 277
Hard Template (Carbon Nanotubes)	Interconnected mesoporous channels	Prolonged lifetime; slightly lower LOS	Not specified	Forms 3D multi-pore network; slight framework collapse may affect sieving.	275, 277
Post-treatment Desilication (HF-NH ₄ F)	Hierarchical structure	Comparable to 25-30% worse lifetime; ~2% improved LOS	WHSV = 2 h ⁻¹ , T = 400 °C	Reduced Brønsted acid site strength; crystallinity depletion affects performance.	218 332
Post-treatment Desilication (TEAOH)	Hierarchical structure	2-fold increase in lifetime; maintained LOS	WHSV = 1 $g_{MeOH} g_{Cat}^{-1} h^{-1}$, $T = 400 ^{\circ}\text{C}, p = 1 \text{ atm}$,	Increased acid site concentration; conflicts with expected desilication effects.	160 333

4.6 Metal Promotion

Metal modification of SAPO-34 has also been examined with regards to its effect on catalytic performance and activity. To the extent of our knowledge, the following metals have been utilized for SAPO-34 promotion in MTO centered studies: Co, Ni, Fe, La, Ce, Y, K, Ag, Ca, Cu, W, Mg, Mn, Ge, Zn, Ti, and Zr ^{231,233,239,241,344–360}. These articles have attempted different methods of promoting parent SAPO-34 catalyst with metal, ranging from in-situ

The in-situ metal incorporation approach typically involves adding a specific quantity of metal salts during the gel synthesis phase, prior to hydrothermal crystallization ^{231,233,241,344,346–349,351,352,354,355}. This generally leads to the integration of metal atoms into the SAPO-34 framework. The impregnation method ^{239,344–346,350}, on the other hand, involves the addition of metal solutions to already-prepared SAPO-34 catalyst. This results in metal atoms being largely deposited onto the catalyst surface (with only slight incorporation into the framework) via capillary force (dry approach) or diffusion (wet approach) from the metal salt solution. A minority of articles have also looked to a simple physical mixing/blending method for metal promotion ^{345,353,356}. This typically comprises of the mixing of already-synthesized SAPO-34 sample with the metal salt, where these components are often mechanically grinded together. Amongst these techniques, in-situ metal incorporation is the most widespread method utilized by research groups for metal promotion because of its superiority in uniform metal distribution (see Figure 39 (A) & (C)) and its capability of retaining SAPO-34's high surface area. Alternatively, impregnation usually leads to metal agglomerates (Figure 39 (B) & (D)) and SAPO pore blockage ³⁴⁴.

This article is licensed under a Creative Commons Attribution-NonCommercial 3.0 Unported Licence

Open Access Article. Published on 22 2025. Downloaded on 30.10.2025 01:47:29.

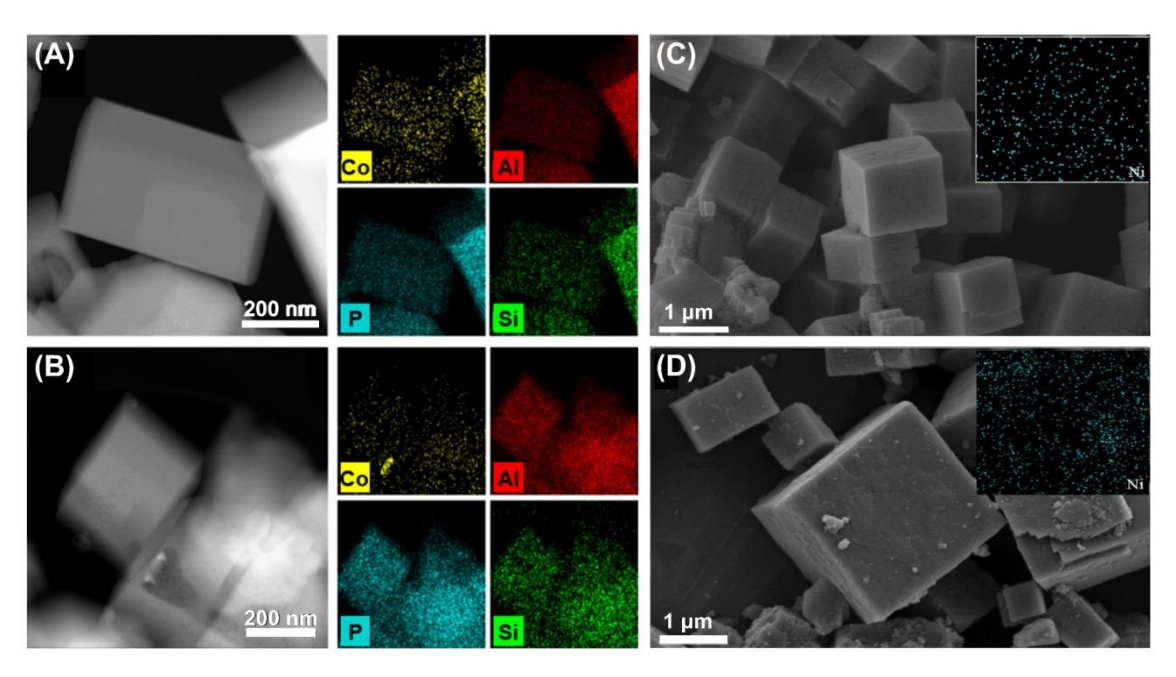


Figure 39 (A) & (B) High-angle annular dark-field (HAADF) scanning TEM and energy-dispersive X-ray spectroscopy (EDS) elemental mapping images of (A) Co-incorporated SAPO-34 and (B) Co-impregnated SAPO-34. Reproduced from reference 236 with permission from Elsevier, Copyright 2019. (C) & (D) SEM and EDS elemental mapping images of (C) Ni-incorporated SAPO-34 (using a template assisted approach) and (D) Ni-impregnated SAPO-34. Reproduced from reference ²³⁹ from Springer Nature, Copyright 2021.

Table 12 compares the application of different metals utilized for SAPO-34 promotion. The synthesis method involved, the type of metal used, the gel formula, along with the reaction conditions and activity performance for the promoted catalysts as well as the parent sample (to provide a fair comparison) has been presented. Generally,

it has been claimed that metal promotion is able to both extend the catalyst lifetime and boost light olefins selectivity, relative to unmodified parent SAPO-34. With reference to the tabulated studies, there exists some clear trends with regards to the optimal type of metals utilized. For instance, several articles have demonstrated that non-transition metals (i.e., rare earth metals such as La, Ce and Y, alkali metals, such as K, and alkaline earth metals, such as Ca) have displayed superior catalytic performance in relation to the studied transition metals (i.e., Fe, Co, Ni, Ag, Cu and W) ^{231,345-347}. Specifically, these non-transition metals have surpassed the other candidates in the domains of catalyst lifetime and total light olefins selectivity, as well as lower overall methane formation. Upon review, out of the wide range of metals studied, it has also been detected that certain metals were able to facilitate the selective formation of specific olefins over others. For instance, Ni-incorporated SAPO-34 demonstrated greater selectivity to ethylene as opposed to propylene ^{231,344,352}. On the other hand, La-modified SAPO-34 displayed the contrary, favoring propylene production instead ^{231,345}. However, it should be noted that the justifications for such selective formation of specific light olefins remain immature and are yet to be thoroughly explained.

A small portion of articles investigated the effect of metal loading on catalytic performance 241,350,351,354 . A majority of the articles have tried a 0.05-0.08 Me/Al₂O₃ ratio in the initial gel 231,346,348,355,357 , while some groups have tested lower values (0.005-0.01) 233,349,350 , and some higher (around 0.1-0.12) 351,353 . Some studies 350,351 have fixated on deciphering the optimum loading amount and have found that the metal content has a crucial effect on the promoted catalyst performance, but it should be noted that this optimum metal content cannot be generalized to all metals and could vary from one metal to another. However, it seems that exceptionally small loadings (relative to the other components in the gel) are required to achieve enhanced performance 350 . Nevertheless, with such small loadings, one can question how much of a role the metal can truly play. It can even be argued as to whether the introduction of metals is truly the driving force behind any positive results seen, since it seems that the greater the loading, the poorer the performance.

Table 12 Summary of the key parameters and results from metal promoted SAPO-34 studies.

Metal	Comment/ Synthesis technique	Gel formula (molar) $ (Al_2O_3/P_2O_5/SiO_2/ \\ T/H_2O/Me)^{\alpha} $	Catalyst formula $(molar)$ $Al_a P_b Si_c M_d$	Methanol Processing ability* $(g_{MeOH} \ g_{Cat}^{-1})$	Average light olefins selectivity** (mol %)	Reaction Conditions	Ref
		1 Al ₂ O ₃ / 1 P ₂ O ₅ / 0.4				WHSV=	
_	Parent SAPO-34	SiO ₂ / 1 TEAOH/	$Al_{0.485}P_{0.405}Si_{0.108}$	7.9	N/A	$5.00 \; h^{-1}$	344
		1 MOR/ 60 H ₂ O				Reaction T:	

_	Hierarchical SAPO-34	1 Al ₂ O ₃ / 1 P ₂ O ₅ / 0.4 SiO ₂ / 1 TEAOH/ 1 MOR/ 60 H ₂ O	$Al_{0.474}P_{0.423}Si_{0.101}$	10.4	N/A	400 °C MeOH: 19 mol%	
Co	Hierarchical + Insitu metal incorporation	1 Al ₂ O ₃ /1 P ₂ O ₅ /0.4 SiO ₂ /1 TEAOH/ 1 MOR/60 H ₂ O/0.08 Co	$Al_{0.480}P_{0.426}Si_{0.079} \\ Co_{0.014}$	15.8	N/A	Water: 81 mol%	
	Hierarchical + Impregnation	1 Al ₂ O ₃ /1 P ₂ O ₅ /0.4 SiO ₂ /1 TEAOH/ 1 MOR/ 60 H ₂ O	$Al_{0.481}P_{0.409}Si_{0.093} \\ Co_{0.016}$	13.3	N/A	_	
Ni	Hierarchical + Insitu metal	1 Al ₂ O ₃ /1 P ₂ O ₅ / 0.4 SiO ₂ /1 TEAOH/ 1 MOR/ 60 H ₂ O/ 0.08 Ni	$AI_{0.482}P_{0.421}Si_{0.087} \\ Ni_{0.009}$	14.2	N/A	_	
	Hierarchical + Impregnation	1 Al ₂ O ₃ /1 P ₂ O ₅ /0.4 SiO ₂ /1 TEAOH/ 1 MOR/ 60 H ₂ O	$AI_{0.489}P_{0.405}Si_{0.090} \\ Ni_{0.015}$	8.3	N/A	_	
_	Parent SAPO-34	1 Al ₂ O ₃ /1 P ₂ O ₅ /0.4 SiO ₂ /1.1 TEAOH/ 0.9 MOR/ 60 H ₂ O	$Al_{0.481}P_{0.407}Si_{0.112}$	8.0	N/A		
Fe	In-situ metal incorporation	1 Al ₂ O ₃ / 1 P ₂ O ₅ / 0.4 SiO ₂ / 1.1 TEAOH/ 0.9 MOR/ 60 H ₂ O/ 0.05 Fe	$Al_{0.467}P_{0.386}Si_{0.139}$ $Fe_{0.008}$	9.0	N/A	_	
Co	In-situ metal incorporation	1 Al ₂ O ₃ /1 P ₂ O ₅ /0.4 SiO ₂ /1.1 TEAOH/ 0.9 MOR/60 H ₂ O/ 0.05 Co	$Al_{0.468}P_{0.385}Si_{0.135}$ $Co_{0.012}$	11.0	N/A	$WHSV =$ 2.46 h^{-1} Reaction T:	
Ni	In-situ metal incorporation	1 Al ₂ O ₃ /1 P ₂ O ₅ /0.4 SiO ₂ /1.1 TEAOH/ 0.9 MOR/60 H ₂ O/ 0.05 Ni	$\begin{array}{c} {\rm Al}_{0.478}P_{0.381}{\rm Si}_{0.138} \\ \\ {\rm Ni}_{0.003} \end{array}$	10.0	N/A	425 °C MeOH: 19 mol% Water: 81 mol%	231
La	In-situ metal incorporation	1 Al ₂ O ₃ /1 P ₂ O ₅ / 0.4 SiO ₂ / 1.1 TEAOH/ 0.9 MOR/ 60 H ₂ O/ 0.05 La	$Al_{0.470}P_{0.378}Si_{0.137}$ $La_{0.015}$	15.0	N/A		
Се	In-situ metal incorporation	1 Al ₂ O ₃ / 1 P ₂ O ₅ / 0.4 SiO ₂ / 1.1 TEAOH/ 0.9 MOR/ 60 H ₂ O/ 0.05 Ce	$Al_{0.472} P_{0.380} Si_{0.132}$ $Ce_{0.016}$	17.0	N/A		
_	Parent SAPO-34	N/A	$Al_{0.448}P_{0.352}Si_{0.200}$	4.9	81.0		345

La	3 wt% La loading, solid-state ion exchange Liquid phase ion	N/A N/A	N/A La _{0.002}	5.6	84.5	$WHSV = 2.10$ h^{-1} Reaction T:	
Y	exchange 3 wt% Y loading, solid-state ion exchange	N/A	N/A	5.8	85.0	450 °C MeOH: 25 mol% Water:	
-	Liquid phase ion exchange	N/A	Y _{0.003}	4.7	81.9	75 mol%	
-	Parent SAPO-34	1 Al ₂ O ₃ / 1 P ₂ O ₅ / 0.6 SiO ₂ / 9 DEA/ 110 H ₂ O	$Al_{0.460}P_{0.364}Si_{0.176}{}^{\text{\tiny Y}}$	12.0	85.0	WHSV= 6.00 h ⁻¹	
Fe	In-situ metal incorporation	1 Al ₂ O ₃ /1 P ₂ O ₅ /0.6 SiO ₂ /9 DEA/110 H ₂ O/ 0.05 Fe ₂ O ₃	$Al_{0.335}P_{0.325}Si_{0.114}$ $Fe_{0.227}{}^{\text{Y}}$	36.0	10.0	Reaction <i>T</i> : 450 °C MeOH:	346
K	Ion exchange -wet impregnation	N/A	N/A	60.0	90.0	30 mol% Water:	
Ag	Ion exchange -wet impregnation	N/A	N/A	17.0	91.0	70 mol%	
-	Parent SAPO-34	1 Al ₂ O ₃ / 1.15 P ₂ O ₅ / 0.55 SiO ₂ / 2 TEAOH/ 110 H ₂ O	$Al_{0.526}P_{0.357}Si_{0.117}{}^{\gamma}$	7.3	40.3	<i>WHSV</i> = 4.85 — h ^{−1}	
Ca	In-situ metal incorporation	1 Al ₂ O ₃ / 1.15 P ₂ O ₅ / 0.55 SiO ₂ / 2 TEAOH/ 110 H ₂ O/ 0.007 CaO _x	$Al_{0.544}P_{0.308}Si_{0.141}$ $Ca_{0.007}{}^{\gamma}$	9.7	58.7	Reaction <i>T</i> : 350 °C	347
Cu	In-situ metal incorporation	1 Al ₂ O ₃ / 1.15 P ₂ O ₅ / 0.55 SiO ₂ / 2 TEAOH/ 110 H ₂ O/ 0.007 CuO _x	$Al_{0.541}P_{0.341}Si_{0.116}$ $Cu_{0.002}{}^{\gamma}$	8.9	49.0	MeOH: 5 mol% Helium:	347
W	In-situ metal incorporation	1 Al ₂ O ₃ / 1.15 P ₂ O ₅ / 0.55 SiO ₂ / 2 TEAOH/ 110 H ₂ O/ 0.007 WO _x	$Al_{0.537}P_{0.326}Si_{0.130}$ $W_{0.007}{}^{\gamma}$	5.7	40.9	95 mol%	
-	Parent SAPO-34	1 Al ₂ O ₃ / 1 P ₂ O ₅ / 0.6 SiO ₂ / 1 TEAOH/ 1 MOR/ 60 H ₂ O	$Al_{0.58}P_{0.29}Si_{0.12}{}^{\gamma}$	N/A	1.8^{μ}	$WHSV = 8.70 \text{ h}^{-1}$	
Ni	In-situ metal incorporation	1 Al ₂ O ₃ / 1 P ₂ O ₅ / 0.6 SiO ₂ / 1 TEAOH/ 1 MOR/ 60 H ₂ O/ 0.05 NiO	$Al_{0.50}P_{0.31}Si_{0.19}$ $Ni_{0.005}{}^{\gamma}$	N/A	7.8 ^µ	 Reaction <i>T</i>: 400 °C MeOH: 19 mol% 	348
Mg	In-situ metal incorporation	1 Al ₂ O ₃ / 1 P ₂ O ₅ / 0.6 SiO ₂ / 1 TEAOH/ 1	$\begin{array}{c} Al_{0.36} P_{0.44} Si_{0.20} \\ \\ Mg_{0.006} {}^{\text{Y}} \end{array}$	N/A	4.0 ^µ	Water: 81 mol%	

		MOR/ 60 H ₂ O/ 0.05						
		MgO						
		1 Al ₂ O ₃ / 1 P ₂ O ₅ /0.30						
_	Parent SAPO-34	SiO ₂ /2.0 TEAOH/50	N/A	15.8	85.0			
		H ₂ O						
	In-situ metal	1 Al ₂ O ₃ / 1 P ₂ O ₅ /0.30				WHSV=		
Co	incorporation	SiO ₂ /2.0 TEAOH/50	$Co_{0.003}$	11.0	87.0	0.48 h^{-1}		
	(Method 1)	$\rm H_2O/0.007CoO$				— Reaction T:		
	In-situ metal	1 Al ₂ O ₃ / 1 P ₂ O ₅ /0.30				400 °C		
Mn	incorporation	$SiO_2/2.0$ TEAOH/50	$Mn_{0.003}$	25.0	86.0	MeOH:	349	
	(Method 1)	$H_2O/0.005~{\rm MnO}$				5 mol%		
	In-situ metal	1 Al ₂ O ₃ / 1 P ₂ O ₅ /0.30	NI: in a constant					
	incorporation	SiO ₂ /2.0 TEAOH/50	Ni incorporation ~	9.6	85.0	Nitrogen: 95 mol%		
N T:	(Method 1)	H ₂ O/ 0.007 NiO	0			93 mor%		
Ni	In-situ metal	1 Al ₂ O ₃ / 1 P ₂ O ₅ /0.10						
	incorporation	SiO ₂ /2.0 TEAOH/50	$Ni_{0.003}$	17.3	85.0			
	(Method 2)	H ₂ O/ 0.01 NiO						
		1 Al ₂ O ₃ / 1 P ₂ O ₅ / 0.6				WHSV=		
_	Parent SAPO-34	SiO ₂ / 2 TEAOH/ 70	$Al_{0.381}\ P_{0.477}\ Si_{0.142}\ ^{\text{Y}}$	119.1	90.0	$14.3 \ h^{-1}$		
		H_2O				Reaction T: 400		
						°C	350	
	Impregnation	1 Al ₂ O ₃ / 1 P ₂ O ₅ / 0.6	$Al_{0.380}P_{0.480}Si_{0.137}$			МеОН:		
Ce	(Optimal: 0.5 wt%	SiO ₂ / 2 TEAOH/ 70		214.5	91.0	30 mol%		
	CeO ₂ loading)	H ₂ O / 0.012 CeO ₂	$\mathrm{Ce}_{0.002}$ Y			Water:		
						70 mol%		
		1 Al ₂ O ₃ / 1 P ₂ O ₅ / 0.2				WHSV=		
_	Parent SAPO-34	SiO ₂ / 0.7 TEAOH/ 1.1	$Al_{0.501}\ P_{0.425}\ Si_{0.074}\ ^{\gamma}$	N/A	82.0	$3.5 \ h^{-1}$		
		DEA/ 50 H ₂ O				Reaction T:		
						450 °C	251	
	In-situ metal	1 Al ₂ O ₃ / 1 P ₂ O ₅ / 0.1	$Al_{0.503}\ P_{0.436} Si_{0.048}$			MeOH:	351	
Ge	incorporation	SiO ₂ / 0.7 TEAOH/ 1.1	$Ge_{0.013}$ $^{\gamma}$	N/A	84.0	27 mol%		
	(Optimal: 0.1 mol	DEA/ 50 H ₂ O/ 0.1				Water:		
	GeO ₂ loading)	GeO_2				73 mol%		
		4 11 0 14 7 0 10 1				WHSV=		
	D (C1DC 21	1 Al ₂ O ₃ / 1 P ₂ O ₅ / 0.4	N1/4	15.0	00.1	$4.0 \ h^{-1}$		
_	Parent SAPO-34	SiO ₂ /2 TEAOH/70	N/A	15.3	80.1	Reaction T:		
		H_2O				450 °C		
						MeOH:	233	
AgP	In-situ metal	1 Al ₂ O ₃ / 1 P ₂ O ₅ / 0.4	4 DW *			36 mol%		
	in commonstion	$SiO_2/2$ TEAOH/ 70	$AgPW_{0.009}^{\delta}$	32.7	92.3	Water:		
W	incorporation	H ₂ O / 0.010 AgPW				water:		

_	Parent SAPO-34	1 Al ₂ O ₃ / 1 P ₂ O ₅ / 0.3 SiO ₂ / 1 TEAOH/ 50 H ₂ O	$Al_{0.503}P_{0.347}Si_{0.151}$	7.0 [△]	N/A	WHSV=			
Fe	In-situ metal incorporation	1 Al ₂ O ₃ / 1 P ₂ O ₅ / 0.3 SiO ₂ / 2 TEAOH/ 50 H ₂ O/ 0.075 FeO	$Al_{0.509} P_{0.351} Si_{0.137}$ $Fe_{0.002}$	4.5 ^{\triangle}	N/A	1.00 h ⁻¹ Reaction <i>T</i> : 425 °C	352		
Со	In-situ metal incorporation	1 Al ₂ O ₃ / 1 P ₂ O ₅ / 0.3 SiO ₂ / 2 TEAOH/ 50 H ₂ O/ 0.075 CoO	$Al_{0.506}P_{0.329}Si_{0.162}$ $Co_{0.004}$	8.0℃	N/A	MeOH: 15 mol% Nitrogen:			
Ni	In-situ metal incorporation	1 Al ₂ O ₃ / 1 P ₂ O ₅ / 0.3 SiO ₂ / 2 TEAOH/ 50 H ₂ O/ 0.075 NiO	$Al_{0.494} P_{0.361} Si_{0.143} $ $Ni_{0.001} $	5.0℃	N/A	85 mol%			
_	Hierarchical SAPO-34	1 Al ₂ O ₃ / 0.8 P ₂ O ₃ / 0.4 SiO ₂ / 2.0 TEAOH/ 50 H ₂ O	N/A	16.7	82.3				
	Physical mixing (Interpellet) Physical mixing (Intrapellet- AL i.e., not calcined mixture)	1 Al ₂ O ₃ / 0.8 P ₂ O ₅ / 0.4 SiO ₂ / 2.0 TEAOH/ 50 H ₂ O/ 0.11 ZnO	N/A	15.0	82.4	$WHSV = 10.0 h^{-1}$ Reaction T :			
ZnO		1 Al ₂ O ₃ / 0.8 P ₂ O ₅ / 0.4 SiO ₂ / 2.0 TEAOH/ 50 H ₂ O/ 0.11 ZnO	N/A	9.2	84.0	500 °C MeOH: 85 mol% Nitrogen:	353		
	Physical mixing (Intrapellet-HY i.e., calcined mixture)	1 Al ₂ O ₃ / 0.8 P ₂ O ₅ / 0.4 SiO ₂ / 2.0 TEAOH/ 50 H ₂ O/ 0.11 ZnO	N/A	8.4	83.7	15 mol%	15 mol%	15 mol%	
_	Parent H-SAPO- 34-L (sample with relatively large crystals)	1 Al ₂ O ₃ / 1 P ₂ O ₅ / 0.3 SiO ₂ / 2.0 TEAOH/ 52 H ₂ O	$Al_{0.52}P_{0.34}Si_{0.14}{}^{\gamma}$	11.7	65.0	$WHSV = 10.0 \text{ h}^{-1}$ Reaction T :			
Ti	In-situ metal incorporation (Optimal: TiO ₂ loading in 0.006 relative molar ratio)	1 Al ₂ O ₃ / 1 P ₂ O ₅ / 0.3 SiO ₂ / 2.0 TEAOH/ 52 H ₂ O/ 0.006 TiO ₂	$Al_{0.56}P_{0.31}Si_{0.13}$ $Ti_{0.00034}{}^{\gamma}$	30.0	78.0	400 °C MeOH: 77 mol% Nitrogen: 23 mol%	354		
	Parent SAPO-34	N/A	N/A	9.5□	80.5	WHSV=			
	Wet Impregnation	N/A	Co _{0.0176}	7.0□	76.7	2.0 h ⁻¹			
Со	Template- assisted method	N/A	Co _{0.0024}	10.0 [△]	81.3	Reaction <i>T</i> : 400 °C MeOH:	239		
Ni	Wet Impregnation	N/A	Ni _{0.0175}	7.5□	78.2	35.7 mol%			

	Template- assisted method	N/A	Ni _{0.0028}	11.0□	80.4	Nitrogen: 64.3 mol%	
	Wet Impregnation	N/A	Zn _{0.0178}	6.5□	82.5	_	
Zn	Template- assisted method	N/A	Zn _{0.0050}	9.5□	77.5	_	
Ni	In-situ metal incorporation	1 Al ₂ O ₃ / 1 P ₂ O ₅ / 0.6 SiO ₂ / 1 DEA/ 70 H ₂ O/ 0.05 NiO	$\begin{array}{c} {\rm Al}_{0.470}P_{0.380}Si_{0.130} \\ \\ {\rm Ni}_{0.02}{}^{\gamma} \end{array}$	2.5	88.0	$WHSV = 0.4 \text{ h}^{-1}$ $= \text{Reaction } T$	
Mn	In-situ metal incorporation	1 Al ₂ O ₃ / 1 P ₂ O ₅ / 0.6 SiO ₂ / 1 DEA/ 70 H ₂ O/ 0.05 MnO	$\begin{array}{c} Al_{0.480}P_{0.390}Si_{0.120} \\ \\ Mni_{0.01}{}^{\gamma} \end{array}$	4.2	94.0	400 °C MeOH: 30 mol%	355
Mn & Ni	In-situ metal incorporation (bimetallic)	1 Al ₂ O ₃ / 1 P ₂ O ₅ / 0.6 SiO ₂ / 1 DEA/ 70 H ₂ O/ 0.05 NiO/ 0.05 MnO	$\begin{array}{c} Al_{0.380}P_{0.420}Si_{0.170} \\ Ni_{0.02}Mni_{0.01}{}^{\text{Y}} \end{array}$	2.5	85.0	Water: 70 mol%	
-	Parent SAPO-34	N/A	$Al_{0.411}P_{0.485}Si_{0.105}$	8.3	60.0	$WHSV = 1.0 \text{ h}^{-1}$ Receipt To	
Co	In-situ metal incorporation, milling and recrystallization (Optimal: 0.003 mol in relative molar ratio)	N/A	$\begin{array}{c} {\rm Al}_{0.472}P_{0.415}{\rm Si}_{0.086} \\ \\ {\rm Co}_{0.027} \end{array}$	11.8	65.0	Reaction <i>T</i> : 350 °C MeOH: 83.5 mol% Water: 16.5 mol%	241
	Parent SAPO-34	1 Al ₂ O ₃ / 0.8 P ₂ O ₅ / 0.6 SiO ₂ / 2.5 MOR/ 80 H ₂ O	$Al_{0.43}P_{0.43}Si_{0.14}$	12.3	79.0	$WHSV = 2.0 \text{ h}^{-1}$	
t- ZrO ₂	Physical blending method	N/A	$Al_{0.41}P_{0.41}Si_{0.18}$	28.4	82.0	Reaction T: 380 °C	356
(Tetra gonal-phase zircon ia)	Hydro-thermal surface coating modification method	N/A	$Al_{0.42}P_{0.40}Si_{0.18}$	37.3	82.0	MeOH: 50 mol% Water: 50 mol%	
	Parent SAPO-34	1 Al ₂ O ₃ / 1 P ₂ O ₅ / 0.6 SiO ₂ / 3 TEA/ 50 H ₂ O	$Al_{0.470}P_{0.351}Si_{0.178}$	5.5	77.0	$WHSV = 2.0 \text{ h}^{-1}$	
Zn	In-situ metal incorporation	1 Al ₂ O ₃ / 1 P ₂ O ₅ / 0.6 SiO ₂ / 3 TEA/ 50 H ₂ O/ 0.04 Zn(NO ₃) ₂ · 6H ₂ O	$\begin{array}{c} Al_{0.448}P_{0.339}Si_{0.198} \\ \\ Zn_{0.015} \end{array}$	8.5°	80.0	Reaction T: 425 °C MeOH: 50 mol% Water:	357

Open Access Article. Published on 22 2025. Downloaded on 30.10.2025 01:47:29.

Journal of Materials Chemistry A

50 mol%

Some articles have partially supported the idea of metal-promoted catalysts performing similarly to or even worse than the parent SAPO-34. One study 349 reported that the metal-modified catalysts possessed lifetimes shorter (for Co-SAPO-34) and similar (in the case of Ni-SAPO-34) to the parent catalyst, without considerable changes in light olefins selectivity. Another study 346 explored the effect of Fe-incorporated SAPO-34 and found that the selectivity towards C₂ and C₃ olefins (under optimal conditions) was notably small due to substantial methane formation, particularly in comparison to the parent catalyst. Deterioration of catalytic performance by secondary metal addition has also been reported using the impregnation technique. Co-, Ni- and Zn-impregnated SAPO-34 catalysts in one study 239 demonstrated significantly shortened lifetime relative to the parent catalyst with worse or comparable LOS. This inferior performance due to metal addition has also been observed in other circumstances, such as La- and Y- impregnated 345 and physically-blended ZnO modified samples 353. A comprehensive study conducted by Ghavipour et al. 361, in which 20 different metal promoted catalysts were tested, found that the majority of the catalysts suffered from a loss in crystallinity, which ultimately resulted in inferior catalytic performance.

Overall, by observing the results of the conducted research in metal modification of SAPO-34, clear contradictions can be spotted. Even while employing similar metals, opposing catalytic performances have been reported. For instance, in the case of Ni-incorporated SAPO-34, there have been reports of significantly improved ³⁴⁸, unchanged ³⁴⁹, and slightly worsened ²³⁹ light olefins selectivity (relative to the parent catalyst). This demands a comprehensive discussion on the justifications provided by these articles in support of superior or inferior catalytic activity of the promoted catalysts. In this regard, some articles have claimed that the addition of secondary metal precursors enhances the nucleation, resulting in smaller crystals that have better mass transfer characteristics and can last longer within the reaction ³⁵¹. Alternatively, introduction of new mesopores into the structure due to secondary metal addition has also been claimed to be one of the underlying factors for superior catalytic performance ³⁴⁷, although the mechanism for the formation of these mesopores has not been clarified. One study ³⁶⁰ has applied a

^{*} Methanol processing ability = $WHSV \left(g_{MeOH} g_{Cat}^{-1} h^{-1} \right) \times \text{(time taken to go to 80\% MeOH conversion) (h)}$

^{**} Average light olefin selectivity = $\frac{\text{Amount of methanol converted to C2 \& C3 on average (mol)}}{\text{Amount of methanol converted on average (mol)}} \times 100\%$

⁷ The surface composition was only measured/ provided (i.e., by XPS or SEM-EDS)

^µ An alternative definition for light olefin selectivity was utilized: specified as the ratio of the sum of produced ethylene and propylene to undesirable products (others hydrocarbon).

^a For references ³⁵², ²³⁹ & ³⁵⁷, none of the catalysts reached 80% conversion. The methanol processing ability was instead computed using the time taken to reach 95% conversion.

 $^{^{\}delta}$ The numerical value presented depicts the molar ratio of AgPW to Al₂O₃ (i.e., not with respect to all the precursors).

distinct metal modification method termed hydrothermal surface coating, which resulted in elimination of the external active sites by tetragonal zirconia crystals addition. Subsequently, the group claimed that this may reduce the build-up of coke at the entry of SAPO-34 pores. In turn, the lack of pore blockage would lead to a greater diffusion of reactant methanol molecules over time on stream, which has resulted in doubled catalyst lifetime. However, this statement does not seem to be completely valid, since the acidic sites that lie beneath the exterior neutralized layer are still active and can block the pores by coke build-up. Apart from that, the majority of metal promoted articles ^{231,344,346,348,350} stated that lowering the quantity of Brønsted acidic sites via substitution of Si (as opposed to the other SAPO elements) by the added metal ^{231,344,346-348} hinders the evolution of coke precursor formation reactions, while retaining an acidity level sufficient for the dehydration steps to light olefins. Thus, overall, this results in the decreased production of alkanes (specifically methane) and multi-ring aromatic species (the precursors of coke), leading to a delay in pore blockage in which the diffusion of species can continue to transpire (i.e., prolonged catalytic activity).

Despite the consensus amongst these articles in support of this rationale, there still lies some ambiguities that need to be addressed. Firstly, these articles are quick to suggest that the decrease in acidity acts as the primary justification, when this alteration can be achieved by a more facile approach: reducing the silica content in the starting gel. This should in turn question the need to use secondary metals entirely, since they seem to increase costs unnecessarily when a more economic approach may be utilized instead.

Secondly, it should be noted that research groups have previously investigated the effect of silica content alterations on catalytic performance ^{131,296}. They arrived at the conclusion that the optimal SiO₂/Al₂O₃ ratio, concerning catalyst lifetime, lies between 0.2 to 0.3. This silica content range is generally adopted by the aforementioned articles in the preparation of their parent catalyst. Hence, metal atom promotion (which causes acidity and silica content to fall below optimum levels) cannot appropriately explain why improved catalytic performance is achieved.

Finally, metal modification usually results in a worsening of physicochemical properties, such as a loss in both surface area and crystallinity; in turn, this finding further contradicts the idea that metal promotion can yield enhanced results. Nonetheless, assuming the legitimacy that improved performance may be achieved via secondary metal introduction, a fundamental justification for this may still need to be uncovered. It is possible that the promotion of metal with regards to the SAPO framework may in some way affect Brønsted acidic sites and/or influence the mechanistic route taken (by altering the activation energy barriers of elementary steps). There may even lie the possibility of metal atoms acting as new active sites themselves in addition to Brønsted acidic sites.

Similarly, one article ³⁵³ observed intermediate formaldehyde formation due to ZnO promotion and hypothesized that formaldehyde is able to facilitate ethylene production and simultaneously convert active hydrocarbon pool species into inactive carbon deposits. However, none of these articles, including the previously mentioned one, examined how the secondary metals could participate in the reaction mechanism. Although, utilizing SEM-EDX, one study ³⁶¹ was able to separate different secondary metal modified catalysts into specific categories (see Figure 40) i.e., those that illustrated complete metal incorporation, partial metal incorporation, and no incorporation whatsoever. Such analysis may be useful for future work in determining if some metals that do incorporate into the crystalline framework play a role (a positive or negative one) in the reaction mechanistic scheme for light olefin production, or simply play no significant role in the case when incorporation did not occur (i.e., when metals emerged as an amorphous phase instead). Hence, the role of secondary metals in the mechanistic scheme for the MTO reaction remains an area open to further exploration. For example, a recent study employed molecular dynamics (MD) simulations to provide mechanistic insights into interatomic interactions associated with coke suppression and enhanced olefin selectivity in mixed metal oxide-modified SAPO-34 catalysts ³⁶². However, to gain a more comprehensive understanding, complementary approaches such as density functional theory (DFT) calculations or other more exhaustive characterization techniques are still needed.

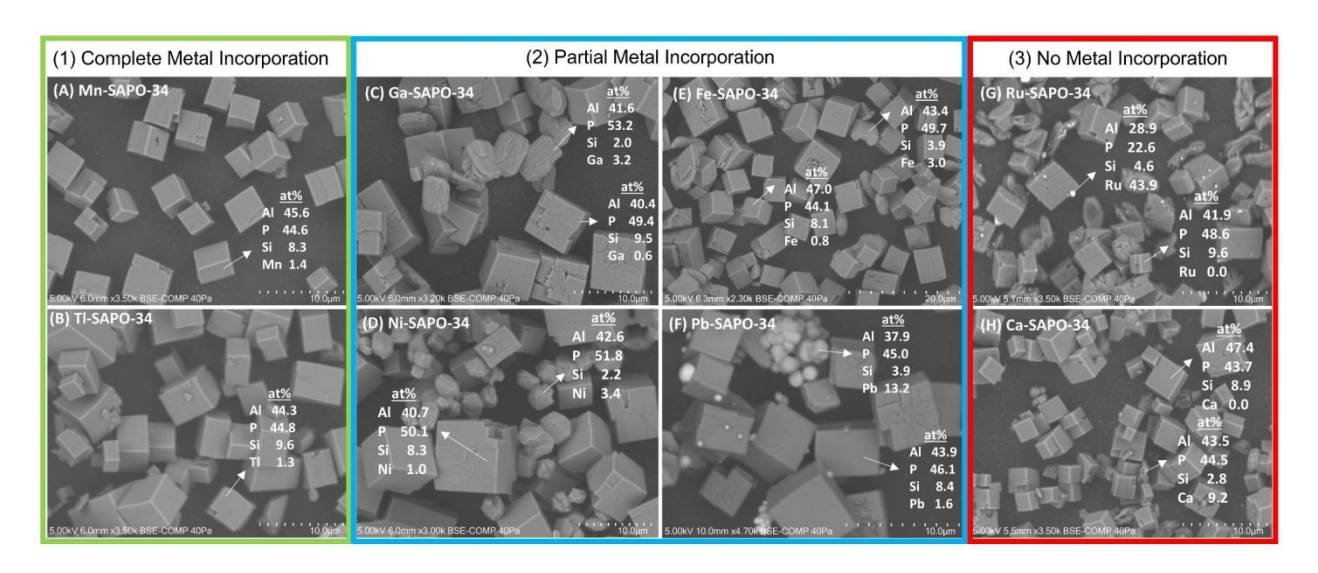


Figure 40 SEM with SEM-EDX results overlayed with respect to different secondary metal-promoted SAPO-34 catalysts. The results have been categorized as follows: Complete metal incorporation consisting of (A) Mn-SAPO-34 and (B) Tl-SAPO-34; Partial metal incorporation consisting of (C) Ga-SAPO-34, (D) Ni-SAPO-34, (E) Fe-SAPO-34, and (F) Pb-SAPO-34; No incorporation consisting of (G) Ru-SAPO-34 and (H) Ca-SAPO-34.

Reproduced from reference 361 from John Wiley and Sons, Copyright 2024.

In summary, research groups have demonstrated that metal modification, considering the method of promotion, the metal loading, and the type of metal, can pose completely different effects on SAPO-34 catalytic performance

(which can range from worsening, improving or unsubstantial effects). Nonetheless, the explanation as to why specific metals perform better than others still remain relatively immature.

4.7 Shaping of SAPO-34 Catalyst

Since SAPO-34 suffers from rapid deactivation by inevitable coke generation, the only practical industrial-scale solution is the employment of a fluidized bed reactor accompanied by continuous regeneration of spent catalyst (see MTO process section 2). That being said, catalyst particles entrained in the gas phase must be collected using multi-stage cyclones to then be directed to the regenerator. Hence, in order to ensure that this catalyst-collecting procedure using cyclones is both feasible and efficient, the SAPO-34 catalyst should be present in the form of agglomerates of cubic crystals sized generally between 50 to 100 micron ³⁶³. Since the conventional (lab-scale) hydrothermal method generates particles in the size of a few micron, the larger desired SAPO-34 particle size for fluidized-bed application is traditionally achieved through the employment of an adhesive agent (binder) such as silica or alumina, followed by spray drying of the catalyst. However, the issue with this customary method is that the binder utilized has the capability to alter the physicochemical properties of the catalyst (potentially worsening catalytic performance), block catalyst pores, substantially reduce the total catalyst surface area, as well as make catalyst particles in the core of the agglomerates inaccessible to reactant species. Hence, groups have begun to investigate an alternate catalyst-shaping strategy by mounting SAPO-34 crystals over pre-synthesized microspherical supports made of alumina, silica, or aluminosilicates (i.e., Kaolin, as seen in Figure 41(A)) 364-368. To achieve this, the microspheres are placed within the initial catalyst gel prior to the hydrothermal (i.e., SAPO crystallization) phase, followed by all other conventional steps. The benefits of this technique include the fact that firstly, microspheres are inexpensive, and secondly, catalyst mounting on the outer surface of microspheres ensures that no part of the precious catalyst is wasted (unlike the binder-spray drying approach). Although this acts as a suitable alternate method, it still faces a crucial problem of not being able to achieve thorough adherence and high loading of SAPO particles onto microspheres. For instance, when α-Al₂O₃ was used as the microsphere support, the SAPO-34 formation was even on the outer surface but the content was low (6.5 wt%) ³⁶⁶. In another case, the employment of silica microspheres resulted in an uneven distribution of SAPO-34 crystals (see Figure 41(B)) ³⁶⁶. This depicts the importance of attempting to choose a suitable support material and corresponding synthesis procedure to achieve successful catalyst mounting. Furthermore, to deal with these previously mentioned issues, one approach has involved the pre-treatment of microspheres. In one study, Kaolin microspheres were treated with NaOH aqueous solution of increasing concentration to increase its surface roughness, in pursuit of enhancing SAPO-34 loading on the external surface (see Figure 41 (C - F)) ³⁶⁴. Another tactic involves supplying the silica

Open Access Article. Published on 22 2025. Downloaded on 30.10.2025 01:47:29.

and alumina required for SAPO-34 synthesis from the support itself (i.e., in-situ SAPO/Kaolin catalyst) as a means for successful SAPO-34 crystal adhesion, which resulted in up to 22 wt% SAPO-34 loading ³⁶⁵. Another group ³⁶⁸ who grew SAPO-34 crystals on γ-Al₂O₃ microspheres introduced a new microwave-assisted synthesis approach, and were thus able to load up to even higher relative quantities, 31 and 44 wt%, when mounting SAPO-34 directed with TEAOH and TEA templates, respectively. However, it is to be noted that procedures to introduce better adhesion between the microsphere support and catalyst still remains an area of study to be developed further. In terms of catalytic activity, it has been generally observed that SAPO-34 over microspheres are better performing relative to spray-dried samples (which deactivate much more rapidly) due to a more developed mesoporous structure ^{365,366,368}. Relative to the parent SAPO-34 catalyst, one group ³⁶⁴ reported 9 times longer activity over their SAPO/Kaolin sample (treated with 4 wt.% NaOH solution- as seen in Figure 41(E)), but in the absence of a distinct and well-established justification. It could be argued that, in the best-case scenario (i.e., a successful mounting of SAPO-34, with unaltered physicochemical properties, over the support), SAPO/microsphere catalyst should exhibit similar to slightly enhanced activity relative to the conventionally prepared SAPO-34 catalyst ³⁶⁸. Overall, Table 13 has been provided to summarize the different SAPO-34 shaping methods and their corresponding effects on structure, characteristics and MTO activity.

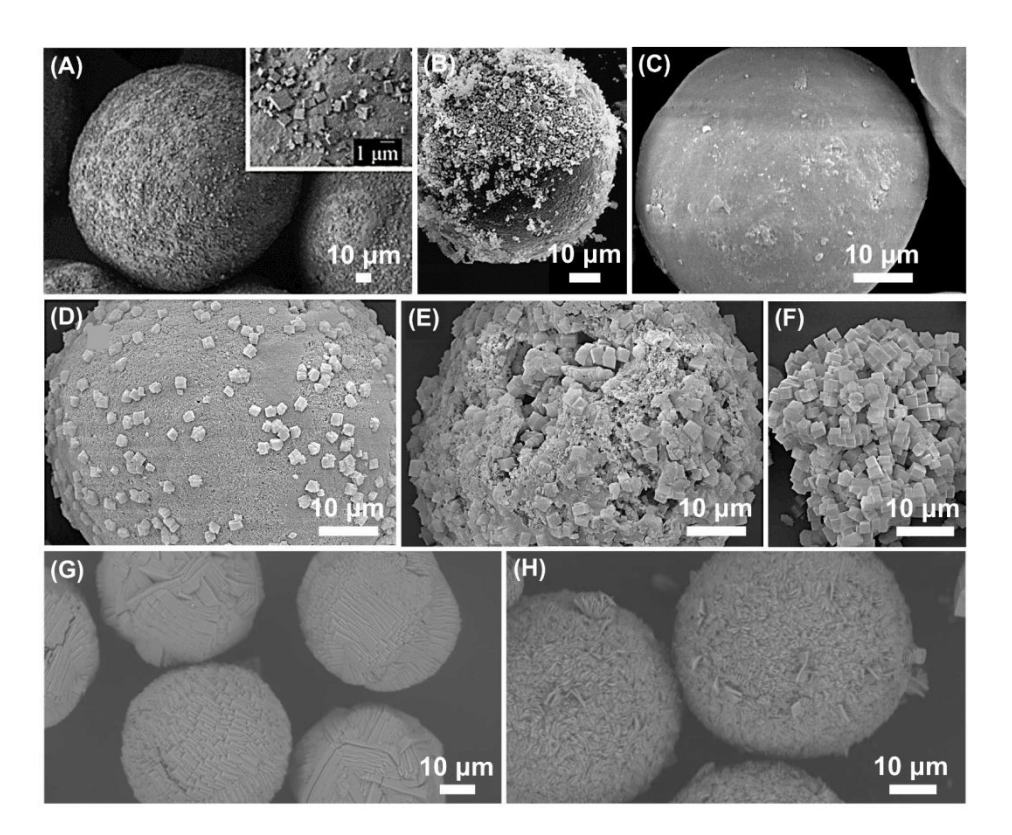


Figure 41 SEM images depicting the morphology of SAPO-34 mounted on different microspheres: (A) SAPO-34/kaolin microsphere reproduced from reference ³⁶⁵ with permission from Elsevier, Copyright 2010; (B) SAPO-34/silica microsphere reproduced from reference ³⁶⁶ with permission from Elsevier, Copyright 2008. (C – F) SAPO-34 on calcined kaolin microspheres treated with NaOH solutions of (C) 2, (D) 4, (E) 10, (F) 14 wt.% concentrations

reproduced from reference 364 with permission from American Chemical Society, Copyright 2011. (G) TEAOH-directed SAPO-34 crystals on γ -Al₂O₃ microspheres. (H) TEA-directed SAPO-34 crystals on γ -Al₂O₃ microspheres. Reproduced from reference 368 with permission from Elsevier, Copyright 2024.

Table 13: Summary of SAPO-34 Shaping Methods: Structure, Characteristics and MTO Activity

Shaping	Structure	Characteristics	Activity	Additional Remarks	Ref
Method	Description				
Spray-dried	Agglomerates	Binder (silica or alumina)	Rapid deactivation; lower	Binder may block pores,	
SAPO-34	of cubic crystals	used to form the agglomerates	activity compared to	reduce surface area, and	
	between 50-100	of cubic crystals	microsphere-supported	limit core accessibility	363
	μт		SAPO-34		
Parent SAPO-	Cubic crystals	Conventional hydrothermal	Baseline activity;	Limited by small particle	
34	in the size of a	synthesis product	deactivates faster than	size for fluidized bed	
	few μm		microsphere-supported	applications	363
			catalysts.		
SAPO-34 on α-	SAPO-34	Even SAPO-34 distribution,	Not specified; expected	Low loading limits	
Al_2O_3	crystals	low loading (6.5 wt%)	similar to slightly	catalytic efficiency.	
	mounted on 50-		enhanced activity vs.		366
	100 μm		parent		
	microspheres				
SAPO-34 on	SAPO-34	Uneven SAPO-34 distribution	Not specified; expected	Uneven distribution	
Silica	crystals		similar to slightly	reduces effectiveness	
Microspheres	mounted on 50-		enhanced activity vs.		366
	100 μm		parent		
	microspheres				
SAPO-34 on	SAPO-34	Enhanced loading due to	9 times longer activity	NaOH treatment (4 wt%)	
Kaolin	crystals	NaOH-treated surface	than parent SAPO-34	improves adhesion;	364
Microspheres	mounted on 50-	roughness		developed mesoporous	266
(NaOH-	100 μm			structure	366
treated)	microspheres				
SAPO-34 on	SAPO-34	In-situ synthesis, up to 22	Better performance than	Supplied silica/alumina	
Kaolin	crystals	wt% SAPO-34 loading	spray-dried	from support; improved	
Microspheres	mounted on 50-			adhesion.	365
(In-situ)	100 μm				
	microspheres				

SAPO-34 on γ-	SAPO-34	High loading (31-44 wt%)	Similar to slightly	Microwave-assisted	
Al_2O_3	crystals	with TEAOH/TEA templates	enhanced activity vs.	synthesis enhances	
Microspheres	mounted on 50-		parent; better than spray	loading; mesoporous	368
(Microwave-	100 μm		dried	structure	
assisted)	microspheres				
assisted)	microspheres				

4.8 Catalyst Design from an Industrial Perspective

The MTO process has been successfully commercialized in several large-scale plants around the world. For instance, Dalian Institute of Chemical Physics (DICP) and its partners developed the DMTO (Dalian MTO) technology with capacities exceeding 600 kt of olefins per year^{369,370}. UOP and Total also developed the UOP/Hydro MTO process, operating with a fluidized-bed reactor and regeneration system tailored for the SAPO-34 catalyst. These commercial efforts demonstrate the maturity of the technology and emphasize the need for robust, scalable, and cost-effective catalyst designs to meet the demands of continuous high-throughput operations. Yet, much effort on the lab scale is still ongoing for the catalysts development.

The innovation in catalyst development should be translated into an industrial application; however, it requires a comprehensive evaluation of several factors beyond the catalytic activity. The lab-scale studies focus on optimizing SAPO-34 catalysts for activity and selectivity under controlled conditions, while industrial viability critically depends on the economic feasibility of raw materials, catalyst synthesis routes, mechanical robustness under reactor conditions, long-term regenerability, and alignment with sustainable and green chemistry principles. The different synthesis routes should be further examined from an industrial perspective. This should include, for instance, the green synthesis route, the mechanical and chemical stability of hierarchical and metal-promoted SAPO-34 catalysts, and trade-offs between activity and likelihood of scaling up the catalysts. The integration of these perspectives would assist in designing catalysts that are not only highly active but also scalable, durable, and align with sustainability concerns, which facilitate bridging the gap between academic research and practical industrial deployment.

A major challenge in commercializing SAPO-34 is related to the catalyst production costs. The traditional hydrothermal synthesis, which we discussed earlier in detail, is widely adopted in industry; however, it utilizes the expensive templates, TEAOH, which significantly increases catalyst cost. Fortunately, the mixed template method could mitigate this by combining cheaper amines (e.g., MOR and DEA) with minimal TEAOH. This has been studied and has effectively reduced template consumption and associated costs while still producing nanocrystalline and high-performance SAPO-34^{371,372}. Moreover, the expensive TEAOH is reduced by introducing a pre-synthesized SAPO-34, known as seeds-assisted crystallization, into the synthesis gel to provide nucleation centers, allowing less OSDA to be used while still obtaining pure SAPO-34 ^{373,374}. Seeded syntheses not only reduce template cost but also accelerate crystallization and can yield smaller crystals with improved MTO

performance. Therefore, the mixed-template and seed-assisted methods are cost-effective, which reduces the scalability cost.

The dry gel method is an eco-friendly method for synthesizing SAPO-34 in the absence of solvent with a minimal amount of water. This leads to high concentrations of ingredients, including the OSDA, which promotes rapid nucleation and the formation of smaller crystals³⁷⁵. The dry gel method produced nano SAPO-34 crystals using the TEAOH template, which are significantly smaller than those from traditional hydrothermal methods³⁷⁶. Similarly, the combination of TEAOH with MOR yielded SAPO-34 nanoparticles (under 500 nm) in just 6 hours, much faster than the 1-2 days typically required³⁷⁷. Moreover, the dry gel method enhances crystallization yield, which minimizes unconverted "waste gel," reduces wastewater generation, and aligns with green chemistry principles by lowering the use of water and other ingredients, including OSDA³⁷⁸. However, the industrial scalability remains a challenge to ensure uniform heating and hydration of a large amount of dry gel.

The ionothermal synthesis utilizes ionic liquids as solvents and templates, which eliminating the need for OSDA. For instance, SAPO-34 can be synthesized using 1-ethyl-3-methylimidazolium bromide (EMIM)Br in the absence of OSDA^{379,380}, leading to green chemistry advantages. This method reduces costs by avoiding expensive templates and eliminating the high-temperature calcination step needed to remove organics, thus saving energy and reducing CO₂ and NO_x emissions³⁷⁴. We refer to this method as OSDA-Free, however, it worth mentioning that this method is different than the well-known OSD-Free CHA synthesis^{381–384}. Although ionic liquids are still not cheap (but less expensive than OSDA), however, they are recyclable, supporting waste minimization, with biodegradable solvents like choline chloride being explored for SAPO synthesis. This process generates minimal wastewater that aligns with green chemistry principles. However, challenges remain, including the high risk of impurities, which may necessitate mild processing steps³⁸⁵. Scalability is another concern, as handling viscous ionic liquids and crystal separation may require specialized equipment. Despite these challenges, advancements in ionothermal synthesis, including the production of hierarchical porous SAPO-34, indicate a promising future for green, sustainable scaling, provided that ionic liquid recycling and process efficiency are effectively managed²⁸³.

Microwave heating accelerates the SAPO-34 synthesis, improves crystal size uniformity, reduces the time from ~ 48 hours to about two hours, and producing SAPO-34 cube particles ~100 nm³^{75,386,387}. This method enhances throughput and lowers costs due to its efficient energy use. Moreover, it allows for better morphology control in crystal formation. In regard to the activity test, microwave-synthesized SAPO-34 shows equal or improved performance, as seen in longer catalyst lifetimes. However, scalability remains a challenge for larger reactors, but advances may enable rapid, energy-efficient SAPO-34 production at scale, justifying equipment costs.

In summary, each synthesis method involves trade-offs in cost, physicochemical properties, performance, and scalability. Hydrothermal is proven on an industrial scale, but uses expensive templates or yields larger crystals if cheap templates are used. Mixed-template and seed methods mitigate template cost and improve crystal size, with minimal changes needed to existing hydrothermal processes. Dry-gel conversion and concentrated gel methods

Open Access Article. Published on 22 2025. Downloaded on 30.10.2025 01:47:29.

Metal promotion of SAPO-34, especially with rare earths like La^{3+} and Ce^{3+} , can significantly extend catalyst lifetime by moderating acidity and suppressing coke formation. Comparative studies rank lifetime improvement as Ce > La > Co > Ni > Fe > undoped SAPO-34³⁸⁸. La/Ce dopants typically double or triple cycle length and enhance light-olefin selectivity while reducing methane formation ^{388,389}.

La and Ce form non-volatile oxides, maintaining stability under high-temperature regeneration (up to ~750 °C) and reinforcing framework integrity ³⁹⁰. The main risks are sintering and loss of dispersion, especially when metals are introduced via post-synthesis impregnation, whereas in-situ substitution or ion exchange better anchors dopants and preserves crystallinity. Excessive loading may also introduce secondary phases or over-cracking, which can degrade lifetime if not controlled ³⁸⁸. Leaching is negligible under dry, gas-phase MTO conditions; rare-earth dopants remain stable during attrition-prone cycling ³⁹¹. While promoters can slightly shift product distribution, for example, La favoring propylene over ethylene, these changes are minor compared to the overall benefit of prolonged catalyst life³⁸⁸. In industrial settings, dopant choice and incorporation methods must also preserve the mechanical integrity of catalyst particles³⁹².

In industry, SAPO-34 powders must be shaped (e.g., spray-dried with binders, please refer to section 4.7) into robust, millimeter-scale particles to withstand thermal cycling and fluidized-bed abrasion. Attrition resistance depends on crystal size, binder material, and morphology. Optimal designs use ~0.5–5 μm crystals with alumina binders, which typically yield stronger particles than silica ^{393,394}. Metal additives can influence mechanical integrity (e.g., Ni/Cs incorporation may weaken particles) while hierarchical structuring or binderless pelletization can improve strength without heavy binder dilution³⁹⁵.

Table 14 Comparison of different SAPO-34 synthesis methods for industrial scaling up feasibility.

Synthesis Method	Relative Catalyst Cost	Industrial Feasibility	Effect on SAPO-34
Conventional Hydrothermal	High cost if using expensive OSDA.	Excellent scalability. Well-established in the industry.	Produces highly crystalline SAPO-34. Large crystals and stable SAPO-34. Minimum structure damage if properly calcined.
Mixed- Template Hydrothermal Method	Lower cost: a portion of the costly OSDA is replaced with a cheaper one.	High scalability; uses the same autoclave setup as conventional.	Reduced crystal size. improving diffusional stability. Stable catalyst compared to conventional SAPO-34.
Seed- Assisted Method	Lower cost: it saves up to ~40% of OSDA.	High scalability and ensure phase purity.	Seeds yield smaller crystals and suppress impurities.

DOI: 10.1039/D5TA05195A

formation of a secondary phase.

	Seeds require preparation but can be recycled.		No loss of framework stability; it improves crystallinity at lower template usage.
Dry-Gel Conversion Method	Low cost: minimal solvent and high yield. Reduces template and energy per unit product.	Good scalability; eliminates handling of large liquids but requires uniform steam distribution. High flexibility to adopt simple synthesis equipment.	Yields small, plate-like crystals with hierarchical porosity ³⁹⁶ . These have high structural integrity and improved coke resistance.
Ionothermal (OSDA-free)	Potentially low cost: no OSDA and recyclable ion liquids.	Moderate scalability; requires handling of viscous ion liquid and catalyst separation. Recycling ion liquid is crucial for sustainability and waste minimization.	Produces triclinic SAPO-34; slightly different crystal habit ³⁸⁰ . Higher framework stability; low calcination temperature. ³⁸⁵
Microwave- Assisted	Moderate cost with the advancement in microwave equipment. Faster crystallization and lower energy consumption.	Scale-up is challenging; limited by microwave penetration and uniformity in large volumes. Dedicated microwave reactors are needed for industrial throughput.	Produces uniform nanocrystalline SAPO-34, crystals may need binders for mechanical strength (see next section).
Ultrasonic- Assisted Method	Low-to-moderate cost: uses standard equipment plus ultrasonic transducers. Reduce synthesis time and thus energy.	Scalable in principle; large ultrasonic reactors exist (e.g. sonochemical tanks). Multi-point sonication may be required for uniform large batches.	Produces ultra-small crystals (~50 nm) ²⁸⁴ Enhanced catalyst life compared to conventional. As with microwave, nano-SAPO-34 needs to be formed into larger particles for use.
Metal promotion of SAPO-34	A higher cost compared to the metal-free approach.	Scalable and the dopant selection and loading method are crucial for mechanical stability ³⁹² .	Tune the catalyst acidity, enhancing stability and selectivity ^{388,389} , ³⁹⁰ . Metals sinter and lose dispersion. High metal concentration may cause the

5 Sustainability of Olefin Production Methods

5.1 Catalytic Efficiency for Emissions Abatement

The negative environmental externalities arising from the production of base chemicals are significant, specifically with regards to petrochemicals such as olefins³⁹⁷. In particular, the olefin industry comprises 30% of total direct CO₂ emissions produced from chemical plants^{398,399}, making this sector one of the most pertinent for consumption reduction. When considering the evolution of this industry, from 2000-2016, CO₂ emissions decreased by 29.4% per tonne of ethylene generated in China. This implies process improvements and efficiency advancements in a leading region of olefin production. However, it is coupled with ever-expanding industry growth and, as such, increased overall emissions⁴⁰⁰. Thus, it is crucial to account for emissions across Scope 1 (direct, on-site process and combustion), Scope 2 (indirect from purchased electricity/steam), and Scope 3 (all other value-chains

upstream and downstream)⁴⁰¹. This helps ensure that olefin production can be assessed, quantified, and ultimately produced in a sustainable manner³⁹⁷.

Catalyst design, then, can inherently tackle reductions across Scopes 1, 2, and 3 respectively by abating emissions through enhanced process efficiency and reduced energy demand⁴⁰². Catalysts can directly abate Scope 1 emissions by enhancing selectivity, which create pathways that bypass by-product formation and reduce CO₂ generation entirely⁴⁰². Taking an example of the development of SAPO-34 catalysts for the methanol-to-olefin process^{400,403}, this on-site enhancement would lead to direct improvements across Scope 1 by enhancing methanol-to-olefin conversion and selectivity, thereby reducing the likelihood of GHG byproducts. Broadly speaking, however, an increase in catalytic efficiency could also allow for the integration of cleaner energy sources, thus decreasing the prospect of indirect CO₂ produced, which would then address Scope 2 emissions⁴⁰². Finally, innovations in catalyst design could also propel significant improvements across Scope 3 emissions which are thought to be the most polluting in industry, and simultaneously the most difficult to track⁴⁰⁴. By improving upon feedstock conversion and product yield, optimised catalysts can shave off upstream burdens, while also tackling embodied emissions downstream and enabling greener end-of-life practices⁴⁰⁵.

As such, the need for continuous improvement and process optimisation is further exacerbated by issues of commercial attractiveness and technical feasibility, which present hurdles to transitioning away from conventional, fossil-derived olefin production³⁹⁷. One study by Reznichenko et al³⁹⁸ conceptualises a colour scheme of olefin production technologies not unlike that of the "hydrogen rainbow"⁴⁰⁶. They differentiate between feedstocks stemming from coal (brown), oil and gas (grey), biomass (green), and recycled plastic (pink), considering also the cases of carbon capture and storage (CCS, purple) and carbon capture and utilisation (blue)³⁹⁸. By coupling an analysis of both olefin production technology and its feedstock, the sustainability and circularity of the process can be more comprehensively understood.

5.2 LCA Considerations in Olefin Production

Regarding the emissions drawn from olefin production processes, process feedstock is of paramount importance, from its sourcing, to its purification, to its eventual conversion⁴⁰⁷. This choice of feedstock in olefin production is predominantly governed by resource availability and price, where Europe and Asia are more petroleum and coal based, whereas light hydrocarbons take the fore in North America and the Middle East⁴⁰⁰. Irrespective of this regional variability, which inherently affects the preferred technology employed, steam cracking is regarded as the benchmark and most widely adopted production route in the olefin production industry, with coal-based processes largely explored due to their vast adoption in regions like China^{399,408}.

As with all life cycle assessments (LCAs), it is important to note that direct comparisons may either vary tremendously, or their results cannot be compared entirely. This can be attributed to 5 main LCA factors: functional unit, allocation method, system boundaries, region, and year of study⁴⁰⁰. Evidently, the functional unit, system boundaries, and allocation method provide the reference frame against which LCA results can be compared⁴⁰⁹. The year of study is directly related to the assessment method and database, given that new aggregates and benchmarks are established in tandem with their database sources⁴¹⁰. Finally, given the availability of different technology and resources across the world, this creates inherent discrepancies in embodied emissions across the processes' value chains - particularly when considering energy use and provision sources (Scope 2), as well as overall supply chains and their counterparts like transportation (Scope 3)^{409,410}.

A critical facet to LCAs available in literature is that of co-products and their allocation. When comparing the two key processes of steam cracking vs. MTO, steam cracking yields valuable co-products (such as propylene, but alongside other hydrocarbons and fuel gas/oil), whereby some environmental impacts are shared^{411,412}. Conversely, MTO is regarded as a more targeted production method in the context of LCAs, with olefins and water and/or heat as the primary byproducts⁴¹¹; this concentrates more detriment per unit olefin, if there are no major by-products among which to distribute the process' impact. In addition, the allocation of functional unit can vary by entirely different scales (namely, mass, energy, or economic), which can skew results by tens of percentage points³⁹⁸. For example, Zhao et al⁴¹¹ allocated approximately 29% of steam cracking impact to propylene (which was the main product in their study), whereas in another study by Lv et al.⁴¹² only 15% was allocated, which justifies the subsequently reported CO₂/ton disparities - even though both studies were conducted using a mass basis. Thus, caution must be heeded when drawing comparisons across LCAs from different sources, particularly when involving different functional unit bases and allocation methods.

5.3 Cradle-to-Gate LCA Findings in Olefin Production

Generally, studies have found that coal-based MTO has a significantly higher cradle-to-gate CO₂ footprint (i.e., per amount of olefin product produced) than traditional steam (naphtha- or ethane-fed) cracking^{398,400,413}. Furthermore, when considering the MTO process specifically, natural gas-based production tends to fare better than its coal-fuelled counterpart^{398,400,414–416}. In particular, the product of interest that is typically examined for these light olefin applications is either ethylene or propylene, given their prevalence in industry^{398,414}. Various studies have considered offsetting upstream emissions by modifying the methanol carbon source to coke-oven gas^{417,418} or methane⁴¹⁹, all of which have been reported to reduce CO₂ emissions. Another widely considered environmental

For instance, comparing these routes, Chen et al⁴¹⁶ found that the following olefin production method had the most environmental and commercial potential in China, albeit a historically coal-abundant and -dependent region: production and importing of methanol sourced from American natural gas/shale gas to obtain ethylene. This natural gas-to-ethylene (NTO) route was determined to have the highest "eco-efficiency" when compared against oil-to-ethylene (OTO, sourced from imported crude oil from the Middle East) and coal-to-ethylene (CTO, locally sourced coal within China)⁴¹⁶. The concept of eco-efficiency (E/E) - considering the product's added value against its environmental detriment⁴²⁰, proved how NTO outperformed the other two methods in both economics and emissions⁴¹⁶. As such, NTO was found to generate a larger net value than OTO (by 25%) and CTO (by 7.8%), as well as lower GHG emissions (4% less than OTO and 60% less than CTO) - making its eco-efficiency higher by 30.2% and 176.6% than OTO and CTO, respectively⁴¹⁶. Even when pairing the CTO system with a CCS unit hosting a 50% capture rate - though its emissions did decrease by a significant 20% - the CTO-CCS system's emissions remained considerably higher than the OTO and NTO systems considered⁴¹⁶.

Corroborating these conclusions is a study by Xiang et al⁴⁰⁰, which highlighted the differences between ten production routes: steam cracking of mixed petroleum (PSC), steam cracking of conventional natural gas (NSC), steam cracking of shale gas (SSC), catalytic pyrolytic process (CPP), coal to olefins via methanol-to-olefins (CMTO), natural gas to olefins via methanol-to-olefins (NMTO), CO₂ to olefins via methanol-to-olefins (CO₂-MTO), biomass to olefins via methanol-to-olefins (BMTO), coal to olefins via Fischer-Tropsch to olefins (CFTO), and biomass to ethylene via ethanol-to-ethylene (BETE). In this studyl⁴⁰⁰, PSC was taken as the emissions baseline (due to its industrial prevalence) at 1.7 tCO₂ per tonne of ethylene produced. Benchmarked against this, the other two steam cracking processes investigated (NSC and SSC) were found to modestly reduce emissions by 23.5% and 17.7%, respectively 1400. Conversely, CPP released 94.1% more tCO₂ than PSC, making it ~2.4x more polluting than steam cracking 1400. On the other hand, the MTO options varied drastically. NMTO (natural gas-based) emitted nearly 2x as much CO₂ as PSC, whereas CMTO (coal-based) was 5x more emitting than PSC, with CFTO (coalbased via Fischer-Tropsch) peaking at 12x more emissions than the baselinel⁴⁰⁰. By stark contrast, CO₂-MTO was almost carbon-neutral (101.2% decrease compared to benchmark), while BMTO (biomass-based) was carbonnegative at -1.3 tCO₂ per tonne of ethylene produced (176.5% decrease)l⁴⁰⁰. When paired with CCS integration, BMTO had the lowest emissions contribution at -8.2 tCO₂, while CMTO and CFTO (coal-based) emissions demonstrated 55.2% and 36.9% reductions - though this marginal improvement was not drastic enough to make the coal-based MTO processes competitive, as they were still the most carbon-intensive options by far. With the

"green" synthesis routes (biomass-based and/or coupled with CCS) making up the emissions rear, and the coal-based ("brown") methods at the fore, it is evident that low-carbon technologies present the most sustainable MTO pathways, whereas coal-fuelled production carries a substantial environmental premium^{398,400}. This reinforces the idea that the carbon burden of olefin production - especially for the MTO process - hinges on feedstock choice and the progression beyond and away from coal-based processes.

Another cradle-to-gate study by Zhao et al⁴²¹ similarly compared major olefin production methods, analysing the following four: catalytic cracking (CC), steam cracking (SC), coal-to-olefins (CTO), and coal-to-propylene (CTP). Among these, CC was owed the lowest footprint, with 22.5% less GHG emissions than SC, whereas CTO and CTP produced emissions that were 5.8x and 7.6x higher (respectively) than CC. This was also reflected by the trend observed in the primary energy demand, where CTO consumed the most energy, followed by CTP and SC, while CC again performed the best. For the two top polluters (CTO and CTP), over 88% of emissions arose from the production processes themselves, which encompass many stages such as air separation, coal gasification, methanol synthesis, and MTO/MTP. Most significantly, coal gasification alone gave rise to 67.72% and 60.79% of the GHG emissions in CTO and CTP, respectively. However, when adopting CO₂ capture, GHG emissions were found to decrease by 32.4% and 26.1% - though energy usage spiked by 2.6% and 3.6% - for CTO and CTP, respectively. This further propels the notion that coal-based production processes are disproportionately carbonand energy-intensive - and while advancements like CCS can certainly curb their environmental detriment, coal's unfavourable performance warrants phase-out.

A 2022 compilation by Reznichenko et al³⁹⁸ presented one of the most comprehensive cradle-to-gate comparisons of olefin production methods, tabulating all the cases explored in previously mentioned studies and more. This analysis unsurprisingly revealed similar findings: the "brown" (coal-to-olefins MTO) baseline was the most emissions-intensive (even when compared to other coal conversion processes different than MTO), at a hefty maximum of 8.65 tCO₂/t olefin³⁹⁸. Yet again, coal-powered processes proved more detrimental than their "grey" counterparts' emissions peaks - with 2x more CO₂ generated than conventional naphtha steam (4.5 tCO₂) and 2.5x more than condensate-based cracking (3.4 tCO₂)³⁹⁸. Conversely, including CCS units ("purple") into coal-based MTO lowered emissions by 66% (to 2.63 tCO₂); though this was a notable change, it still trailed behind several non-fossil alternatives³⁹⁸. It is evident that - solely considering the MTO process alternatives - circular routes hold the most promise. With the low-value waste stream of black liquor sourced as a methanol feedstock, a "green" MTO route led to a 75% decrease in emissions (to 2.17 tCO₂), whereas a "blue" Power-to-X approach to olefins, starting from atmospheric CO₂ and using DAC, had carbon-negative performance (-1.5 tCO₂), 117% lower than the coal-MTO benchmark - albeit with ~2x higher energy demand³⁹⁸. This study³⁹⁸ echoed the same findings as discussed earlier: coal-based MTO is currently the least sustainable in industry - though this can be abated through

the incorporation of renewable or waste-derived methanol feed, making it a low-carbon or even carbon-negative route.

Other technologies like bioethanol to ethylene ("green") have demonstrated high sensitivity to upstream intermediate production emissions, such as those related to farming biomass, fertilisers, and transportation³⁹⁸. As such, the emissions associated with their olefin production vary drastically - from being carbon-negative⁴²² to netpositive and even highly net-positive⁴²³. Some of these studies depict how these sources' intrinsically sustainable nature can be eroded by biogenic emissions in pre-processing during upstream stages. However, though drawing from various LCAs can relay highly variable results in the literature, most realistic scenarios depict a near 35-45% reduction compared to traditional naphtha-based cracking, thus performing better than both steam cracking ("grey") and coal-MTO ("brown")³⁹⁸.

Similarly, different LCAs report mixed results for the recycled plastic ("pink") route, depending on the accounting method employed. For instance, when considering a direct process basis to produce ethylene from waste, pyrolysis with steam cracking was carbon-intensive in nature, relaying 3 tCO₂ of reported emissions, which was not much improved from traditional naphtha cracking³⁹⁸. However, common LCA practice is to adopt a "differential credit" system - accounting for the abated emissions of this route insofar as waste incineration is avoided (which would have been the fate for the plastics involved). Doing so alleviated the footprint across the process' life cycle drastically, amounting to 50% lower GHG than the original naphtha route³⁹⁸. In other words, this "pink" recycled plastic feedstock paves the way for closing the carbon loop on polymers ⁴²⁴, where the CO₂ that would have been emitted by the disposal or burning of waste is harnessed for new value-added products. Comparable environmental benefits for this waste-to-methanol-to-olefin (WMO) process are also disclosed by Salah et al ⁴²⁴, who express how this route can achieve meaningful GHG reductions in the so-called "linear" fossil economy. It must be noted, however, that this path was made viable by modelling a cleaner electricity mix (ideally renewable sources such as wind energy)⁴²⁵, necessarily also at the large-scale to avoid burden shifting to other impact categories (namely, eutrophication, particulate matter formation, acidification, and resource use) ⁴²⁶.

Overall, though the differences in regional energy sources and efficiencies across cradle-to-gate studies are vast, naphtha steam cracking is said to produce roughly 0.8-2.1 tons of CO₂ emissions per ton of olefin produced, an immense difference from the whopping 5.2-11.5 tons arising from coal-based MTO ⁴²⁷. Though both processes are very well-established in industry, they face imminent obsoletion without addressing their environmental implications. Steam cracking is anticipated to remain omnipresent in industry for another 10-20 years; to remain as such, however, mid-term improvements of optimised cracker efficiency and feedstocks from recycled ("pink") and renewable ("green") sources are crucial. Long-term advancements in cracker electrification propel this shift³⁹⁸, as electrified crackers can achieve up to a 92% reduction in emissions relative to today's furnaces (assuming a carbon-free electricity supply) ⁴²⁸. On the other hand, the best-case MTO scenarios outperform steam cracking

when methanol is sourced from low-carbon pathways like biomass or waste, resulting in nearly net-zero or even net carbon-negative GHG footprints (depending on the feed)⁴²⁹. Growth in this regard is predominantly staggered by technological or economic immaturity - especially for "green" and "blue" MTO solutions still at lab- or pilot-scale - when choosing to opt for less carbon-intensive feedstocks⁴³⁰. Therefore, bio-based methanol sources cannot singlehandedly replace fossil feed at scale - at least in the near-short term³⁹⁸. As for coal-powered processes, eventual phase-out or decarbonisation is unequivocally pertinent, though increased policy support and infrastructural changes are needed to accommodate for CCS ("purple") solutions³⁹⁸.

5.4 Energy Requirements in Olefin Production

A key environmental consideration - especially when benchmarking technologies and feedstocks across various studies - is that of energy requirement. When investigating olefin production, the conversion of methane or coal into methanol and then to olefins involves multiple reaction steps, where energy content of the feed is expended and efficiency losses are realised in stages such as syngas production, methanol synthesis, and the MTO reaction itself ⁴³¹. On the other hand, steam-cracking has been dubbed more energy-efficient due to its one-step nature and direct olefin yield - albeit endothermic ⁴³¹ and energy-intensive, where crackers typically require furnace temperature between 750-1100 °C ⁴³². The disparity in energy requirement between these two conventional routes is equally as ingrained in literature as that in emissions - where multiple studies report notable differences between the energy demand of coal-based MTO (150-156 GJ/ton olefin) and steam cracking (54-66 GJ/ton olefin) ^{421,433} again demonstrating the shortcomings in coal-powered MTO.

As a proposed fix to coal-based MTO, the caveat with CO₂-to-olefins is their immense energy requirement - and, as such, the high capital and operational costs. Power-to-X routes are energy-intensive, particularly due to electrolysis and CO₂ conversion steps. For example, Flores-Granobles et al.⁴⁰⁸ found that a two-step CO₂-to-methanol-to-olefin process would require ~59 GJ (16.3 MWh) of electricity per ton of olefin produced, which is roughly 5x higher than the conventional cracking benchmark used. Similarly, Reznichenko et al.³⁹⁸ noted that it is not viable to satisfy the global light olefin demand of 200 Mt/year solely through the CO₂-MTO production method, as it would require 644 GW of renewable electric power (roughly half of the United States' overall grid capacity of 1280 GW) ⁴³⁴. This immense scale of renewable energy deployment poses a towering economic viability barrier. Thus, the only two scenarios in which these routes could compete with petrochemicals today is either through 1) strong carbon pricing, subsidies, or policies, or 2) the adoption of wide-scale renewable energy to the degree of abundance and affordability ³⁹⁸.

Looking towards the prospect of a fully decarbonised olefin industry, a mixed-market solution may prove ideal to accommodate regional strengths, financing hurdles, and technological barriers. For instance, e-crackers can be

employed in steam cracking solutions, whereas other green fuels can be used to feed MTO units presently available in industry ³⁹⁸. In tandem, the proposed circular carbon storage ("purple") and utilisation ("blue") solutions can be further developed, while also accelerating the integration of renewable energy into local grids³⁹⁷.

5.5 Water Usage & Other Impact Categories in Olefin Production

Beyond GHG emissions and energy requirements, other environmental considerations are also considered to provide a more holistic overview of how different technologies and materials interact with both human life, the natural environment, and available resources. These are referred to as midpoint impact categories, all of which are related to an endpoint that is encompassed by an area of protection. As illustrated in Figure 42 below⁴³⁵, the selection of impact categories in most comprehensive LCAs spans across all three major nodes of protection - Human Health, Natural Environment, and Natural Resources.

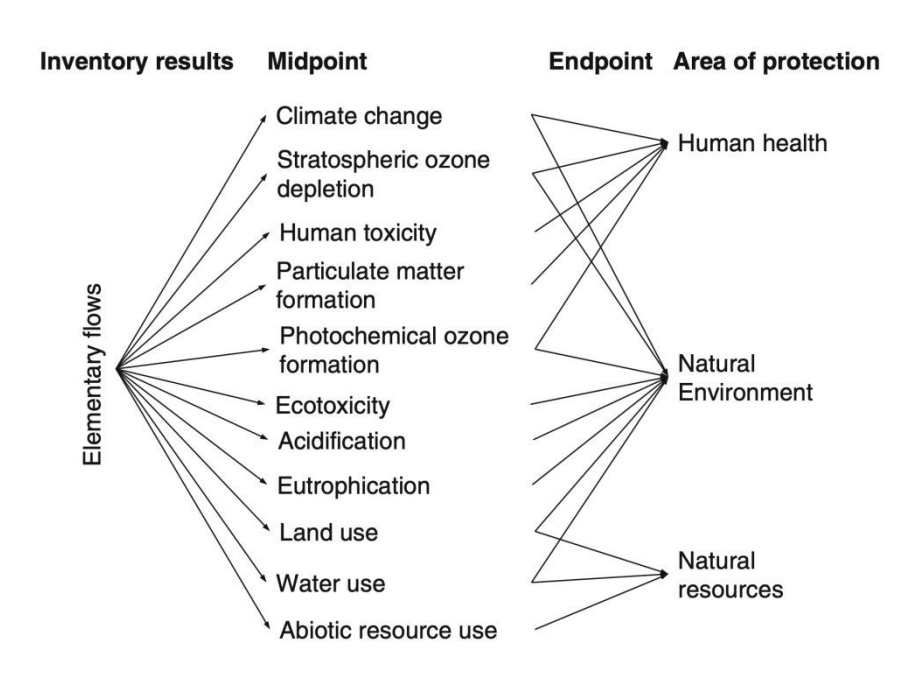


Figure 42 Framework of environmental midpoint impact categories illustrating their relation to the areas of protection. Reproduced from reference 435 from Springer Nature, Copyright 2015.

To contextualise the results that will be disclosed across multiple LCAs, a definition for each impact category will be provided. An extensive discussion was provided on climate change in an earlier analysis - which is primarily measured in terms of GHG emissions (CO₂-equivalent units) - defined as a greenhouse gas-driven radiative forcing (or global warming), leading to sea level rise, extreme weather, and ecological disruptions, and impacting both human health and the natural environment⁴³⁵. Ozone depletion involves chlorofluorocarbons (CFCs) and halocarbons, which reduce the ozone layer and increase UVB radiation; this direct causation of skin cancer, cataracts, and ecosystem loss also similarly affects both human health and the natural environment. Human toxicity evolves from health damages due to chemical exposure (outdoor, indoor, occupational, and in consumer products)

across populations and over time, with direct impact on human health. Particulate matter formation encompasses the generation of primary and secondary particles, leading to respiratory concerns that are connected directly to human health⁴³⁵. Photochemical ozone formation accounts for the ozone (or O₃) that is formed by NOx and NMVOC emissions, causing both respiratory effects and crop (and greater ecosystem) damage, linking both to human health and the natural environment. Ecotoxicity assesses the damage from chemical exposure via effects on species across trophic levels, ultimate harming the natural environment⁴³⁵. Acidification describes the ecosystem damage that arises specifically from emissions (namely - CO₂, N, and S compounds) causing acidification across terrestrial, freshwater, and marine ecosystems, which directly impacts the natural environment. Eutrophication refers to the ecosystem change that is driven by the production and release of excess nitrogen and phosphorus, leading to nutrient oversupply that disrupts natural pre-existing ecosystems and ultimately affects the natural environment⁴³⁵. Land use reflects the disruptions from human land occupation and transformation, including the loss of biodiversity, which also affects the natural environment⁴³⁵. Water use captures the impacts of water consumption, which can deprive ecosystems and human users of available water supplies, linking to both the natural environment and human health⁴³⁵. Finally, abiotic resource use concerns the depletion of non-living resources such as metals, minerals, fossil and nuclear energy, and flow energy sources like wind, which directly links to natural resources⁴³⁵.

Among these categories, water depletion metrics are recurring figures of sustainability in the context of olefin production ⁴³⁶. The previously mentioned comparative study by Chen et al.⁴³⁷ revealed that the process water consumption of coal-to-olefins (CTO) was the worst of the three methods considered - 2.3x higher than NTO (natural gas-to-olefin) and 3.3x higher than OTO (oil-to-olefin). Revisiting the study by Lv et al.⁴³³, the authors also emphasised a similar trend across four propylene production routes: coal-to-olefins (CTO), propane dehydrogenation (PDH), steam cracking (SC), and catalytic cracking (CC). As expected, water consumption was highest in CTO, averaging 35.4 tons of water per ton of propylene produced - attributed to its intensive cooling and gasification operations⁴³³. Furthermore, the three other impact categories of eutrophication, acidification, and respiratory inorganics also peaked with CTO - the latter two arising predominantly from electricity and steam input⁴³³. On the other hand, the reason why eutrophication was heavily skewed towards CTO was because of its direct nitrogen emissions⁴³³- which has the most immediate effect on eutrophication potential⁴³⁵- reaching levels approximately 2800x, 1900x, and 900x as high as CC, CC, and PDH (respectively)⁴³³. However, PDH exhibited both severe abiotic depletion and ozone depletion, which was propelled by the process' propane feedstock contributions to these categories (94% and 98%, respectively)⁴³³. Furthermore, although SC and CC fared better than CTO in terms of water use, their raw material impacts were considerable; for instance, when looking at the

same metrics of abiotic and ozone depletion potential, naphtha and refinery dry gas drove 66-77% of SC's contributions to these categories, whereas heavy oil accounted for 73% of CC's contributions⁴³³. Nonetheless, an important sustainability aspect to the CC technology was its ability to recover steam from coke combustion, which alone offset 160% of respiratory inorganics, 13% of its water use, and 12% of its acidification impact - though this favourable performance was not reflected across all categories (e.g., ozone depletion, where it is the second most detrimental after PDH)⁴³³. Although this analysis depicts how coal-based MTO is undeniably the most water- and pollution-intensive, propane dehydrogenation shifts the burden towards resource and ozone depletion-related categories, making it challenging to identify which process singlehandedly had the worst overall footprint⁴³³.

In a study covered earlier by Salah et al. 424, a prospective LCA defined a linear olefin production route (or LPR) based on traditional naphtha steam cracking to compare against a waste-to-methanol-to-olefins (WMO) route. Beyond the climate change effects covered earlier, 15 other environmental impact categories were considered which depicted not only circular improvements, but also burden-shifting, measured in terms of probability (percentages)⁴²⁴. For one, WMO illustrated high likelihood of reducing impacts across multiple categories: freshwater ecotoxicity (99%), resource use (100%), land use (87%), and ozone depletion (100%), largely because of the exclusion of naphtha extraction and refining, which are credited for land disturbance, toxic effluents, and fossil resource depletion⁴²⁴. However, WMO was not without its shortcomings; it increased the likelihood of burden-shifting across several categories due to its electricity-intensive nature: acidification (94%), freshwater eutrophication (100%), terrestrial eutrophication (87%), metal/mineral resource use (100%), and particulate matter formation (97%)⁴²⁴. These burdens stem from the global grid mix (2020) - dominated by coal (36% make-up) which emit NOx, SOx, and particulates, in addition to requiring extensive mineral inputs for generation and transmission⁴²⁴. For the remaining six categories - namely, marine eutrophication, human toxicity (carcinogenic and non-carcinogenic), ionising radiation, photochemical oxidant formation, and water use - the results were unclear, with probabilities of burden-shifting between 25-75%, making a firm conclusion across these metrics impossible. Despite this, a low-carbon electricity mix by 2050 would likely omit this notion of burden-shifting, which would make the WMO route a clear sustainable fix across almost all the indicators investigated. Altogether, when aggregating all these performance indicators into one final environmental footprint score. WMO exceeded LPR by 16.8% in 2020 (time of study) and 45.1% by 2050 (future renewable energy grid case), demonstrating that while this circular solution presented many environmental benefits, these advantages could realistically not be realised without grid decarbonisation⁴²⁴.

Centred on comparing prospects of oil-based steam cracking against coal-fuelled MTO, Xiang et al.⁴³⁸ reinforce the striking differences between feedstocks illustrated previously in the context of emissions. Analogous to what was found earlier (for emissions), coal-to-methanol-to-olefins (CMTO) and coke oven gas-based methanol-to-olefins (CGMTO) were the most water-intensive, consuming 44.2 and 55.0 tons of water per ton of olefin,

respectively⁴³⁸. By contrast, natural gas-based MTO (NGMTO) consumed only 27.2 t/t, whereas oil-to-olefins (OTO) had the lowest usage at 22.1 t/t ⁴³⁸. Looking more closely at the indirect water use (associated with energy and feedstock preparation), the demand distribution expressed as a proportion of total water usage among the top three processes was 32.1%, 25.5%, and 21.3%, for CMTO, CGMTO, and NGMTO, respectively - which echoes the earlier idea of accounting for and improving upon upstream process savings⁴³⁸. In the context of this study, geographic misalignment of resources like coal reserves and water exacerbates this impact: if CMTO plants are concentrated in arid regions that are disconnected from a direct water supply, it manifests into a structural water-resource conflict. Thus, steering away from coal-based operations and instead pivoting towards a more diversified olefin production portfolio (e.g., with co-feeding routes or better geographic positioning) could cut average water intensity by 15.8% compared to business as usual. These findings demonstrate how coal-based olefins remain excessive from a consumption standpoint, propelling the need for gas-based alternatives to mitigate water scarcity and regional imbalances⁴³⁸.

Another study discussed by Xiang et al.⁴³⁹ focused on the comparison of feedstocks, depicting the stark contrast in environmental burdens as a byproduct. Yet again, coal-to-olefins (CTO) shouldered a markedly heavier burden in both water and resource consumption in comparison to oil-to-olefins (OTO). For example, the CTO route necessitates 30 t of fresh water per 1 t of olefins produced - 4.2x greater than the water demand of OTO. Furthermore, CTO draws far more heavily on utilities, with 6.0 GJ/t of electricity and 8.8 GJ/t of stem, compared to a mere 0.27 GJ/t and 1.16 GJ/t demanded by OTO, respectively - which points to auxiliary resource requirements beyond direct feedstock burden. As expressed previously, this could pose resource conflicts in water-scarce regions, suggesting that coal-based MTO could worsen resource scarcity unless mitigated in the near-term. To address these coal-backed drawbacks, process-level optimisations (e.g., cooling through air instead of water) and policy intervention could address sustainability bottlenecks in industrial MTO applications⁴³⁹.

6 Future Opportunities

Although the MTO process over SAPO-34 offers a promising route for producing light olefins, challenges such as rapid catalyst deactivation via coke formation, complex reaction mechanisms, and demanding process conditions require innovative solutions to enhance efficiency, selectivity, and scalability. This section outlines key opportunities for future research and development to optimise catalyst longevity, process efficiency, and environmental sustainability, paving the way for next-generation MTO technologies that can realistically cater to the global olefin demand.

One critical area for improvement is that of SAPO-34 catalyst design; given that it is the benchmark MTO catalyst in industry⁴⁴⁰, its synthesis can be further optimised. As covered extensively in this review, one major improvement is that of its crystallite size and morphology - where reductions of crystal size can alleviate the key limitations of diffusion and coke build-up, increasing selectivity and lifetime⁴⁴¹. Given that SAPO-34's cage structure can impose shape-selectivity for light olefins ⁴⁴², engineering hierarchal or nano-sized porosity can alleviate the diffusion limitations of SAPO-34's small 8-ring channels. This allows for the suppression of coke deposition and prolonged catalyst lifetime compared to conventional large crystals, since coke molecules can diffuse out or get confined to smaller domains ^{443,444}. For instance, Guo et al. ⁴⁴⁴ prepared SAPO-34 with a novel aluminium source (pseudoboehmite) with lower Si content and a hierarchal pore structure, resulting in a longer catalytic lifetime than standard SAPO-34 in MTO tests. This approach was paired with the strategy of tuning Si content by optimising the Si/(Al+P) ratio. Balancing activity and stability is key in this regard - as lower Si can improve longevity and boost selectivity, but at the expense of higher temperature⁴⁴⁴. Altogether, enhanced coke resistance is a practical solution as it directly translates into longer operational cycles in industrial reactors⁴⁴⁴. As such, future work should focus on precisely controlling morphology and acid site distribution, given their direct ties to olefin selectivity and catalyst efficiency.

In fluidised bed reactor applications, catalyst regeneration is a potential avenue to mitigate the accumulation of coke (as highlighted in Section 2.2)442, typically through high-temperature air combustion. However, steamassisted regeneration offers a milder alternative (or even a supplement to traditional air/oxygen burning), operating at 400-500 °C to gasify coke into CO, CO₂, and H₂, thereby preserving the catalyst's chabazite framework 445,446. Unlike air-based methods at 600-700 °C, which risk hydrothermal dealumination, Zhao et. al showed that steam regeneration can extend catalyst lifetime by 15-20% by reducing polyaromatic coke formation 140. Another study by Zhou et al.447 proved how partial regeneration of coked SAPO-34 using steam gasification boosted both activity and ethylene selectivity (from 23% for fresh SAPO-34 catalyst to 53% after steam treatment). The occurrence of the latter was attributed to the formation of residual "hydrocarbon pool" coke (mostly methylated benzenes) on the catalyst, which promoted ethylene formation and slowed deactivation, whereas even partial air regeneration left less desirable coke (e.g. oxygenated compounds and naphthalene) that accelerated deactivation⁴⁴⁷. In addition, Liang et al. 445 suggest steam regeneration as a means to both increasing revenue and abating emissions - especially in comparison to conventional air combustion. The authors found that the integration of steam-assisted regeneration improved the catalyst's carbon utilisation rate by ~10% and energy efficiency by ~6%, in addition to exhibiting near net-zero emissions potential⁴⁴⁵. Future research could focus on optimising this potential regeneration for the MTO process⁴⁴⁷. Furthermore, it is important to recall how industrial MTO catalysts are typically spray-dried into millimetre-sized particles (often with a binder like kaolin or alumina) to circulate in fluidised beds⁴⁴⁸. Thus, forthcoming research should also link morphology and binder content of the SAPO-34

particles to their performance and durability since stronger, attrition-resistant particles can reduce catalyst losses over time⁴⁴⁸. What all these insights illuminate is that the deliberate control of the extent of coke removal - rather than catalyst regeneration to a pristine and unadulterated state - may prove most applicable in prolonging catalyst longevity in commercial MTO operations. In addition, integrating dilute oxygen streams in fluidised bed applications could further reduce CO₂ emissions, enhancing environmental sustainability in a largely polluting chemical sector ^{398,431}. On the other hand, recent in-situ nuclear magnetic resonance (NMR) studies also demonstrate how maintaining a modest level of coke on the catalyst (not eliminating it entirely) and co-feeding water during the reaction can significantly preserve catalyst framework and suppress dealumination ⁴⁴². For this purpose, employing in-situ spectroscopic techniques (such as operando infrared or NMR spectroscopy) would provide real-time insights into coke evolution and dynamics, enabling precise process control ⁴⁴⁹. These advancements could significantly reduce operational downtime and improve economic viability of MTO plants, particularly for large-scale fluidised-bed applications.

Another promising direction is hydrogen co-feeding to suppress coke formation ⁹⁸, as highlighted in Section 2.3. By hydrogenating polyaromatic coke precursors, hydrogen can extend SAPO-34's active lifetime by up to 80 hours; though it effectively removes most coke-prone intermediates ⁹⁸, it can often reduce light olefin selectivity due to this alkene hydrogenation ⁹⁸. Corroborating this is the study by Ghavipour et al. ⁴⁵⁰, which captures how the addition of hydrogen extended the time on-stream by ~27%, with only a minor increase in alkane (paraffin) byproducts. Future efforts should focus on designing such catalysts to optimise hydrogenation specificity. To achieve this, kinetic modelling could identify ideal H₂/CH₃OH ratios to balance lifetime extension with selectivity, while density functional theory (DFT) studies could explain hydrogen's interactions with hydrocarbon pool intermediates. By enabling stable operation in fixed-bed reactors - where continuous regeneration is impractical - this approach could enhance MTO's process flexibility and adaptability to diverse feedstock compositions.

With regards to the findings from the earlier sustainability assessment, much of the readily available LCA and techno-economic data on the industrial application of MTO technology is centred on that of coal feedstock ³⁹⁸. From this sustainability analysis, it becomes evident that the four MTO technologies that are presently or will prospectively be employed in industry are the following: "brown" (coal-based), "green" (bio- or waste-based), "blue" (CO₂ point source-based, carbon capture and utilisation), and "purple" (incorporation of carbon capture and storage) ³⁹⁸. With the innumerable cases of coal-powered MTO leading to grave environmental concerns ^{421,433,437–439,451}, alternatives to "business as usual" operations must expediently be developed - particularly when considering how sensitive the coal-to-olefin technology is to national regulatory changes and carbon policies⁴³⁸. In terms of the deployment of CCS solutions to pre-existing coal-MTO technology, this technology is regarded as relatively

mature, though it needs to be complemented by systemic infrastructural changes to be made feasible⁴³⁸. In addition, a study by Xu et al.⁴⁵² emphasises how "brown" solutions may pose a competitive advantage over other methods (like the extensively explored steam cracking, which is largely petroleum-based) in regions that are coal-abundant, since this would reduce reliance on crude oil imports and bolster local economic activity. As such, CCS becomes a key lever in ensuring the sustainable advancement of this technology, since coal's long-term phase-out will need to be rectified by short- to medium-term emissions interventions⁴³⁸. Consequently, "purple" technologies also provide a more inexpensive route to lowering CO₂ emissions than imposing carbon taxes⁴⁵². As for solutions in both CCU (obtaining methanol from CO₂-based sources) and renewable routes (obtaining methanol from biomass-based sources), major leaps need to be made to address technological pitfalls⁴³⁸. Though "green" solutions are expected to remain a marginal segment of the olefin production portfolio, great strides in economic viability could render it competitive with traditional "grey" methods (like naphtha cracking)⁴³⁸. Improvements in gasification and synthesis concepts⁴⁵³ could manifest in a first-of-its-kind demonstration plant within the next decade⁴³⁸. Finally, "blue" (CCU) technologies will be largely dependent on the provision and price of low-carbon electricity - where, if enhanced, could help actualise the several proposed industrial demonstration cases in reality⁴³⁸.

On another note, some researchers have postulated that it is possible to directly convert syngas or even CO₂ into light olefins using bi-functional catalysts ^{454–457} (see Figure 43) - bypassing the intermediate methanol stage altogether in a single reactor. These catalysts combine a metal-based component with a zeolite such as SAPO-34 to achieve relatively high olefin selectivities. This approach is said to eliminate the energy-intensive methanol synthesis step and reduce capital costs - and researchers have made rapid progress in this area^{458–463}. Accelerating this development would present immense advantages to the olefin industry at large - since direct syngas-to-olefins would accommodate for a wide variety of feedstocks (namely, coal, natural gas, and biomass)⁴⁵⁸. However, challenges such as low single-pass conversion (due to thermodynamic limits and the production of CO₂ in the water-gas shift equilibrium) and catalyst stability under operating conditions still remain⁴⁵⁷. Future efforts could focus on developing catalysts with abundant oxygen vacancies or optimised promoters to improve conversion but decrease CO₂ formation⁴⁵⁸. Furthermore, tailoring metal-zeolite interactions or lowering acidity would optimise active site distribution and suppress secondary hydrogenation reactions, such as the formation of methane as opposed to the olefin desired product⁴⁵⁸. Tackling these drawbacks would prove essential to propelling this innovative approach into viable industrial applications.

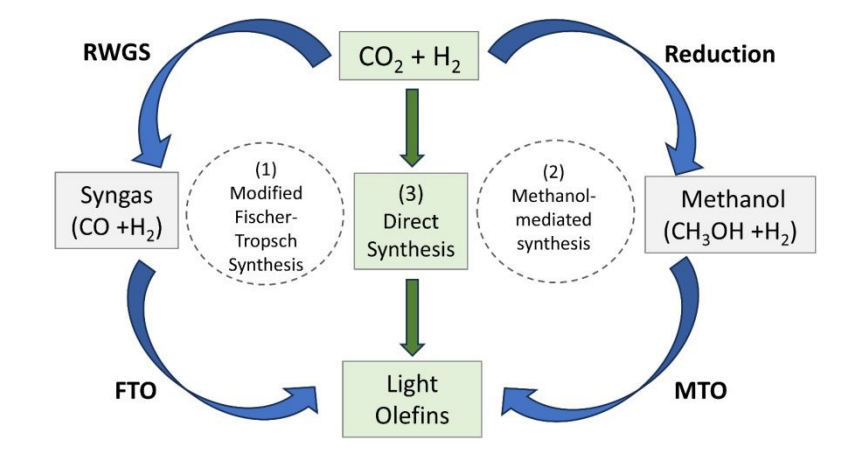


Figure 43 General scheme of the three routes of olefins formation from CO₂: (1) Modified Fischer–Tropsch to Olefins (FTO) via Reverse Water-Gas Shift (RWGS); (2) Methanol to Olefins (MTO); (3) Direct olefin formation from CO₂. Reproduced from reference ⁴⁶⁴ with permission from MDPI, Copyright 2021

Overall, real-world applications of MTO technology have confirmed many of the bottlenecks identified herewith, illustrating which challenges persist in industry and what strategies can be pursued to overcome them. For instance, China's DMTO (Dalian Institute's methanol-to-olefins technology) exemplified how the highly exothermic nature of methanol conversion and rapid SAPO-34 coking necessitate a circulating fluidised-bed reactor with continuous regeneration^{465,466}. This principle was previously emphasised, as fluidised bed technology is a major node of industrial viability for the MTO process at scale. The first commercialised DMTO unit achieved >99% methanol conversion and ~80% light olefin selectivity by using this fixed catalytic cracking style reactor-regenerator design^{465,466}. This configuration also allowed for coke burn-off on SAPO-34 in-situ and maintained near-isothermal operation, which proved superior to the alternative of fixed beds in handling heat removal and deactivation⁴⁶⁵. Industrial implementation also showcased how partial regeneration can occur: rather than burning off the catalyst until it was completely purified, DMTO units typically leave a small hydrocarbon residual on SAPO-34 during regeneration to act as active "hydrocarbon pools." This approach, deployed in commercial units⁴⁶⁵, was found to boost ethylene and total olefin electivity in the following cycle, thereby validating the laboratory-scale notion of the benefits of retaining minor quantities of coke on the catalyst surface.

General industrial applications of MTO point towards its energy- ^{421,428} and water-intensive^{436,467} nature - particularly when considering downstream effects. One key factor contributing to this metric (and, in turn, to operating costs) is that of the refrigeration duty for cryogenic separation⁴⁶⁸. However, advances are being made in prefractionation and absorption techniques to handle the very light components in MTO's product mix (H₂/CH₄) separation - which typically mirrors that of a steam cracker (in that it requires many of the same steps)⁴⁶⁸. One such design study proposed an oil absorption process to remove this residual methane and carbon monoxide, allowing the demethaniser temperature to be raised and bypassing some deep refrigeration steps^{468,469}. Other

technologies like membranes and adsorption are also being considered; to this end, zeolite membranes could selectively permeate olefins over paraffins, potentially de-bottlenecking the C_2/C_3 split and saving energy, such as was the case with the use of metal-organic framework (MOF) adsorbents in the context of MTO purification⁴⁷⁰. As for water management, given the need for resource savings ^{436,467}, researchers are beginning to investigate reuse technologies ⁴⁷¹. This would prove instrumental in resource-challenged, dryer regions⁴³⁸ - whereby wastewater streams can be avoided, and water recovery can simultaneously be attained⁴⁷¹.

7 Conclusion and Outlook

Growing from concept to commercial reality, at present, the influx of research in the topic of the methanol-to-olefin process is catalysed by a need for more sustainable production routes. By enabling the manufacturing of essential petrochemicals, MTO supports energy diversification by opting for alternative feedstocks, thereby reducing reliance on cruel oil (upon which conventional steam cracking relies). Olefins' significance is evidenced by a rise in global demand of around 20% from 2015-2022 for both ethylene and propylene. This steady increase is anticipated to only persist over the next decade, particularly due to the potential of the MTO process as a gateway to a closed-loop carbon cycles, by sourcing methanol into the process from low-carbon or waste-derived feedstocks. Thus, MTO's unique value offering is its ability to convert feedstock flexibility into chemical output that is highly sought after in an increasingly decarbonised sector.

In this literature review, alternative methods to produce light olefins have been presented. Two longstanding frontrunners of light olefin production are thermal cracking and fluid catalytic cracking, though they are widely recognised as being emissions-intensive and low-yielding, respectively. In contrast, the prospects of MTO as a feasible route to sustainable olefin production are quite favourable, those of which are only heightened when paired with the supply of renewable feedstock at the onset. To actualise these, critical parameters and major reactor operating factors such as temperature, *WHSV*, and co-feeding of water and hydrogen are paramount, as illustrated in the main process flow diagram presented in this article.

The development and implementation of the MTO process have taken great leaps in the past few decades. In this article, this was substantiated and chronologically documented in the discussion of MTO reaction mechanisms. Among the numerous proposed schemes, the hydrocarbon pool concept is the most generally agreed-upon, with two key mechanisms which light olefin formation can be attributed to: the side chain mechanism and the expansion-contraction mechanism. One major finding is that preferential behaviour towards one or the other is largely dependent on the acidity of the zeolite catalyst used. Nevertheless, by considering the sheer volume of

proposed reaction routes and their corresponding justifications, there remains the need for studies to be conducted to ascertain which schemes are of primary relevance. A similar consensus arises when examining studies of the process's kinetics. After assessing various proposed kinetic models, it can readily be inferred that some studies disregard the effect of coke formation on the catalyst altogether, which is a primary consideration in the context of performance optimisation. On the other hand, other experiments utilise reaction conditions that are not representative of the industrial application of this process and are therefore not applicable to the scope of this review. Therefore, further documentation and testing must be conducted for a more conclusive assessment.

On the note of catalyst considerations, this review proceeded with the introduction of various materials employed in the MTO process, with SAPO-34 standing out as one of the most viable. To actualise its suitability for this application, various strategies to improve its performance were discussed. Though SAPO-34 is most commonly synthesised by means of the hydrothermal method, other approaches like the dry-gel conversion, ionothermal, ultrasonic, or microwave synthesis methods were explored, offering advantages such as reduced solvent usage, controlled crystallisation, and rapid nucleation. In terms of the template employed during synthesis - though TEAOH is the most prevalent alternative - more inexpensive materials have also been investigated with varying degrees of success, since one opportunity cost of doing so is overall poorer catalytic performance. Therefore, a mixed template approach (with TEAOH followed by a cheaper alternative) offers a competitive edge to capitalise on both benefits: performance and cost-efficiency. On the other hand, silicon content was determined to play a crucial role for selective light olefin production, underscored by a delicate balance of the SiO₂ to Al₂O₃ molar ratio in SAPO-34. Overall, the prevailing consensus is that catalyst morphology of reduced particle size offers enhanced activity and mass transfer properties, thereby proving submicron synthesis to be a viable objective for SAPO-34 development. Various means of attaining hierarchal SAPO-34 synthesis by use of soft or hard templates or posttreatment desilication were also found to be noteworthy paths to overcoming deactivation by coking. In contrast, metal promotion seems to lack reliable analysis on the contribution of secondary metals and their influence on the reaction mechanism, despite numerous claims of its potential to improve the catalyst. This contradictory finding was exacerbated by the antithetical results obtained from different research groups' studies, casting further doubt on the effectiveness of metal promotion overall.

In terms of catalyst use, the spray-dried technique has demonstrated inextricable drawbacks in the fluidised bed application. Catalyst shaping, therefore, paves the way for an open area of research that could substantially improve the economic viability and efficiency of the process. However, instances of in-situ SAPO-34 synthesis over micro-spherical supports still encounter challenges of low loading and proper adhesion. With regards to the

nature of the process itself, current MTO applications have been limited to thermo-catalytic implementation. This presents a pathway for research groups that can try to implement MTO in the context of other viable methods such as electrocatalysis, photocatalysis, homogeneous catalysis, or plasma-based catalysis.

Realising the full potential of MTO in practical applications will require continued innovation focused on both technical viability and environmental sustainability. One core challenge of doing so is the trade-off between catalyst longevity and olefin selectivity - which is where synthesis procedures play an instrumental role in balancing these facets. Alongside catalyst design improvements, optimised process regenerations and co-feeds are on the horizon to address coking issues in industry. In particular, research shows how there is an inextricable link between catalyst structure and performance requirements; these materials must be engineered for reactant conversion and product selectivity, but they must also be robust and regenerable under real-world commercial operating conditions. As a result, recent studies demonstrate the benefit of tuning catalyst morphology, porosity, and acidity to influence reaction pathway and coke dynamics, which can help predict system efficiency and identify any shortcomings. The implication of this is designing catalysts for the MTO process with intention - and with the priority of heightening key performance indicators at the plant-scale.

On the process side, practical bottlenecks will be solved through the continued translation of lab-scale insights to industrial cases. For instance, further development in the context of catalyst regeneration and downstream process innovations must be made. In terms of the former, regeneration can simultaneously reduce energy demand and waste by-products, whereas the latter could improve the overall carbon efficiency of less immediate concerns in the MTO industry. Altogether, auxiliary improvements are critical in terms of making MTO a more competitive route for olefin production.

Finally, the key pillar to overcome current MTO challenges and unlock its full potential as an alternative to traditional olefin production is sustainability. With the basic chemical industry striving for reduced GHG emissions, the ability of MTO to harness renewable feedstocks (and even serve as a carbon sink by integrating CCU-derived sources) uniquely positions this technology as a circular solution frontrunner in its own right. Further assessments will need to be made to both quantify and analyse the current life-cycle environmental detriments and future benefits of transitioning to a low-carbon electricity grid, of improving water and energy use, or of sourcing greener feedstocks. In any of these cases, leveraging SAPO-34 catalyst design in tandem with efficient industry practices will ensure that MTO remains commercially viable and becomes environmentally reliable.

List of Abbreviations

AES - Atomic Emission Spectroscopy

ANN - Artificial Neural Network

BAS - Brønsted Acidic Sites

BETE - Biomass to Ethylene via Ethanol-to-Ethylene

BMTO - Biomass to Olefins via Methanol-to-Olefins

BSE - Back Scattered Electrons

CC - Catalytic Cracking

CCS - Carbon Capture and Storage -

CCU - Carbon Capture and Utilisation -

CFCs - Chlorofluorocarbons -

CFTO - Coal to Olefins via Fischer-Tropsch to Olefins

CGIs - Crystal Growth Inhibitors

CGMTO - Coke Oven Gas based Methanol to Olefins

CHA - Chabazite

CMTO - Coal to Methanol to Olefins

CPP - Catalytic Pyrolytic Process

CTAB - Cetyltrimethylammonium Bromide

CTO - Coal to Olefins

D6R - Double Six Rings

DAC - Direct Air Capture

DEA - Diethylamine

DICP - Dalian Institute of Chemical Physics

View Article Online DOI: 10.1039/D5TA05195A

DME - Dimethyl Ether

DMTO - Dalian Methanol to Olefins

DPA - Dipropylamine

DFT - Density Functional Theory

EDS - Energy Dispersive X-ray Spectroscopy

EMIM - 1-Ethyl 3-Methylimidazolium

ESR - Electron Spin Resonance

FCC - Fluid Catalytic Cracking

FTIR - Fourier Transform Infrared Spectroscopy

FTO - Fischer-Tropsch to Olefins

GC-MS - Gas Chromatography Mass Spectrometry

GHG - Greenhouse Gas

HAADF - High Angle Annular Dark Field

HCP - Hydrocarbon Pool

heptaMB+ - Heptamethylbenzenium Cation

HMB - Hexamethylbenzene

HMMC - Hexamethyl Methylene Cyclohexadiene

ICP - Inductively Coupled Plasma

LAS - Lewis Acidic Sites

LCA - Life Cycle Assessment

LH - Langmuir-Hinshelwood

LMS - Low Medium Silicon Content

LOS - Light Olefin Selectivity

LPG - Liquified Petroleum Gas

LPR - Linear Olefin Production Route

MA - Methylamine

MAS - Magic Angle Spinning

MB - Methylene Blue

MD - Molecular Dynamics

MDOH - Methanol and Dimethyl Ether

ML - Machine Learning

MOF - Metal Organic Framework

MOR - Morpholine

MS - Mass Spectrometry

MTO - Methanol to Olefins

MTG - Methanol to Gasoline

NDE - Nondestructive Evaluation

NGMTO - Natural Gas based Methanol to Olefins

NMR - Nuclear Magnetic Resonance

NMTO - Natural Gas to Olefins via Methanol to Olefins

NMVOC - Non-Methane Volatile Organic Compounds

NSC - Steam Cracking of Conventional Natural Gas

NTO - Natural Gas to Ethylene

OSDA - Organic Structure Directing Agent

OTO - Oil to Ethylene

PDH - Propane Dehydrogenation

PEG - Polyethylene Glycol

PMBs - Polymethylbenzenes

Open Access Article. Published on 22 2025. Downloaded on 30.10.2025 01:47:29.

No This article is licensed under a Creative Commons Attribution-NonCommercial 3.0 Unported Licence.

PMNs - Polymethylnaphthalenes

poly(MN) - Polymethylnaphthalene

polyMBs - Polymethylbenzenes

polyMNs - Polymethylnaphthalenes

PSC - Steam Cracking of Mixed Petroleum

PX - p-Xylene

RVM - Relevance Vector Machine

RWGS - Reverse Water-Gas Shift

SAPO - Silicoaluminophosphate

SC - Steam Cracking

SCR - Selective Catalytic Reduction

SEM - Scanning Electron Microscopy

SEM-EDXS - Scanning Electron Microscopy with Energy Dispersive X Ray Spectroscopy

SSC - Steam Cracking of Shale Gas

TEA - Triethylamine

TEAOH - Tetraethylammonium Hydroxide

TeMB - 1,2,4,6 Tetramethylbenzene

TEM - Transmission Electron Microscopy

TGA - Thermogravimetric Analysis

TMB - 1,2,4 Trimethylbenzene

TOS - Time on Stream

TPD - Temperature Programmed Desorption

TPO - Temperature Programmed Oxidation

UCC - Union Carbide Corporation

UOP	-	Honeywell Universal Oil Products
-----	---	----------------------------------

UV	_	Ultraviolet
UV	_	Omayioici

UVB - Ultraviolet B Radiation

VGO - Vacuum Gas Oil

WHSV - Weight Hourly Space Velocity

WMO - Waste to Methanol to Olefin

XPS - X-Ray photoelectron spectroscopy

XRD - Xray Diffraction

XRF - X-Ray Fluorescence

ZSM - Zeolite Socony Mobil

Open Access Article. Published on 22 2025. Downloaded on 30.10.2025 01:47:29.

Review Article

Author Contributions

Ralph Al Hussami: Conceptualization; Investigation; Methodology; Data curation; Formal analysis; Visualization; Writing - original draft; Validation.

Mohammad Ghavipour: Conceptualization; Investigation; Methodology; Data curation; Formal analysis; Visualization; Writing - original draft; Validation;

Galal Nasser: Conceptualization; Investigation; Methodology; Data curation; Formal analysis; Visualization; Writing - original draft; Validation.

Chasty Duah: Conceptualization; Data curation; Formal analysis; Visualization; Writing - Final draft; Validation.

Shaza Yousef: Conceptualization; Investigation; Data curation; Formal analysis; Visualisation; Writing - original draft; Validation; Permissions & licensing rights acquisition.

Jan Kopyscinski: Funding acquisition; Project administration; Supervision; Writing - review & editing.

Conflicts of interest

There are no conflicts to declare.

Data Availability

No primary research results, software or code have been included, and no new data were generated or analysed as part of this review.

Acknowledgements

The authors would like to acknowledge the financial support from Fonds de recherche du Québec – Nature et technologies (FRQNT - 298262) and via the Centre in Green Chemistry and Catalysis (FRQNT-2020-RS4-265155-CCVC) and Natural Sciences and Engineering Research Council of Canada (NSERC). We also acknowledge Renata Quiñones Busquets for her contributions towards the Reaction Mechanism and Kinetic sections of this literature review.

iceview inticie

References

This article is licensed under a Creative Commons Attribution-NonCommercial 3.0 Unported Licence

- (1) Park, J. W.; Kim, S. J.; Seo, M.; Kim, S. Y.; Sugi, Y.; Seo, G. Product Selectivity and Catalytic Deactivation of MOR Zeolites with Different Acid Site Densities in Methanol-to-Olefin (MTO) Reactions. *Applied Catalysis A: General* **2008**, *349* (1–2), 76–85. https://doi.org/10.1016/J.APCATA.2008.07.006.
- (2) Gholami, Z.; Gholami, F.; Tišler, Z.; Tomas, M.; Vakili, M. A Review on Production of Light Olefins via Fluid Catalytic Cracking. *Energies 2021, Vol. 14, Page 1089* **2021**, *14* (4), 1089. https://doi.org/10.3390/EN14041089.
- (3) Market Research Future. *Light Olefins Market Research Report –Global Forecast to 2030 | MRFR.* https://www.marketresearchfuture.com/reports/light-olefin-market-1037 (accessed 2022-10-19).
- (4) Statista. *Global ethylene demand & capacity 2015-2022* . https://www.statista.com/statistics/1246694/ethylene-demand-capacity-forecast-worldwide/ (accessed 2022-10-19).
- (5) Statista. *Global propylene demand & capacity 2015-2022* . https://www.statista.com/statistics/1246689/propylene-demand-capacity-forecast-worldwide/ (accessed 2022-10-19).
- (6) Rabenhorst, R. *On Purpose What's Driving New Propane Dehydrogenation Projects in North America?* | *RBN Energy*. https://rbnenergy.com/on-purpose-whats-driving-new-propane-dehydrogenation-projects-in-north-america (accessed 2022-10-26).
- (7) Richardson, J. *Petrochemical feedstock purchasing managers: What to think about and what do next Asian Chemical Connections.* https://www.icis.com/asian-chemical-connections/2020/03/petrochemical-feedstock-purchasing-managers-what-to-think-about-and-what-do-next/ (accessed 2022-10-26).
- (8) Yaripour, F.; Shariatinia, Z.; Sahebdelfar, S.; Irandoukht, A. Effect of Boron Incorporation on the Structure, Products Selectivities and Lifetime of H-ZSM-5 Nanocatalyst Designed for Application in Methanol-to-Olefins (MTO) Reaction. *Microporous and Mesoporous Materials* **2015**, *203* (C), 41–53. https://doi.org/10.1016/J.MICROMESO.2014.10.024.
- (9) Akah, A.; Williams, J.; Ghrami, M. An Overview of Light Olefins Production via Steam Enhanced Catalytic Cracking. *Catalysis Surveys from Asia* **2019**, *23* (4), 265–276. https://doi.org/10.1007/s10563-019-09280-6.
- (10) Zacharopoulou, V.; Lemonidou, A. A. Olefins from Biomass Intermediates: A Review. *Catalysts 2018, Vol. 8, Page 2* **2017**, *8* (1), 2. https://doi.org/10.3390/CATAL8010002.
- (11) Samanta, C.; Das, R. K. C3-Based Petrochemicals: Recent Advances in Processes and Catalysts. *Catalysis for Clean Energy and Environmental Sustainability* **2021**, 149–204. https://doi.org/10.1007/978-3-030-65021-6 5.
- (12) Posch, W. Polyolefins. *Applied Plastics Engineering Handbook: Processing and Materials* **2011**, 23–48. https://doi.org/10.1016/B978-1-4377-3514-7.10003-0.
- (13) Britannica. *Steam cracking*. https://www.britannica.com/technology/steam-cracking (accessed 2022-10-27).
- (14) Zimmermann, H.; Walzl, R. Ethylene. *Ullmann's Encyclopedia of Industrial Chemistry* **2009**. https://doi.org/10.1002/14356007.A10_045.PUB3.
- (15) Marco Tagliabue; M. Ferrari; Paolo Pollesel. Petrochemicals and Gas Processing: Increasing Value from Steam Cracker Olefin Streams. **2004**.
- (16) Amghizar, I.; Dedeyne, J. N.; Brown, D. J.; Marin, G. B.; Van Geem, K. M. Sustainable Innovations in Steam Cracking: CO2 Neutral Olefin Production. *Reaction Chemistry & Engineering* **2020**, *5* (2), 239–257. https://doi.org/10.1039/C9RE00398C.
- (17) Akah, A.; Al-Ghrami, M. Maximizing Propylene Production via FCC Technology. *Applied Petrochemical Research 2015 5:4* **2015**, *5* (4), 377–392. https://doi.org/10.1007/S13203-015-0104-3.
- (18) FSC 432: Petroleum Refining;; PennState College of Earth and Mineral Sciences. *Comparison of Products by Type of Hydrocarbon*. https://www.e-education.psu.edu/fsc432/content/comparison-products-type-hydrocarbon (accessed 2022-10-19).
- (19) U.S. Energy Information Administration EIA. *Fluid catalytic cracking is an important step in producing gasoline*. https://www.eia.gov/todayinenergy/detail.php?id=9150 (accessed 2022-10-19).

- (20) MEI. *Fluid Catalytic Cracking*. http://www.maveng.com/index.php/business-streams/industrial/refining/fluid-catalytic-cracking (accessed 2022-10-19).
- (21) Xieqing, W.; Chaogang, X.; Zaiting, L.; Genquan, Z. Catalytic Processes for Light Olefin Production. Practical Advances in Petroleum Processing 2007, 149–168. https://doi.org/10.1007/978-0-387-25789-15.
- Bai, P.; Etim, U. J.; Yan, Z.; Mintova, S.; Zhang, Z.; Zhong, Z.; Gao, X. Fluid Catalytic Cracking (22)Current Recent Discoveries Technology: Status and on Catalyst https://doi.org/10.1080/01614940.2018.1549011 2018, 61 333-405. (3),https://doi.org/10.1080/01614940.2018.1549011.
- (23) Nawaz, Z. Light Alkane Dehydrogenation to Light Olefin Technologies: A Comprehensive Review. *Reviews in Chemical Engineering* **2015**, *31* (5), 413–436. https://doi.org/10.1515/REVCE-2015-0012/XML.
- (24) Nawaz, Z.; Wei, F. Light-Alkane Oxidative Dehydrogenation to Light Olefins over Platinum-Based Sapo-34 Zeolite-Supported Catalyst. *Industrial and Engineering Chemistry Research* **2013**, *52* (1), 346–352. https://doi.org/10.1021/IE301422N/ASSET/IMAGES/LARGE/IE-2012-01422N 0003.JPEG.
- (25) Sattler, J. J. H. B.; Ruiz-Martinez, J.; Santillan-Jimenez, E.; Weckhuysen, B. M. Catalytic Dehydrogenation of Light Alkanes on Metals and Metal Oxides. *Chemical Reviews* **2014**, *114* (20), 10613–10653. https://doi.org/10.1021/CR5002436/ASSET/IMAGES/LARGE/CR-2014-002436 0004.JPEG.
- Luongo, G.; Donat, F.; Krödel, M.; Cormos, C. C.; Müller, C. R. Experimental Data Supported Techno-Economic Assessment of the Oxidative Dehydrogenation of Ethane through Chemical Looping with Oxygen Uncoupling. *Renewable and Sustainable Energy Reviews* **2021**, *149*, 111403. https://doi.org/10.1016/J.RSER.2021.111403.
- (27) Fairuzov, D.; Gerzeliev, I.; Maximov, A.; Naranov, E. Catalytic Dehydrogenation of Ethane: A Mini Review of Recent Advances and Perspective of Chemical Looping Technology. *Catalysts 2021, Vol. 11, Page 833* **2021**, *11* (7), 833. https://doi.org/10.3390/CATAL11070833.
- (28) Li, C.; Wang, G. Dehydrogenation of Light Alkanes to Mono-Olefins. *Chemical Society Reviews* **2021**, *50* (7), 4359–4381. https://doi.org/10.1039/D0CS00983K.
- (29) Asadullah, M.; Ito, S. I.; Kunimori, K.; Yamada, M.; Tomishige, K. Biomass Gasification to Hydrogen and Syngas at Low Temperature: Novel Catalytic System Using Fluidized-Bed Reactor. *Journal of Catalysis* **2002**, *208* (2), 255–259. https://doi.org/10.1006/JCAT.2002.3575.
- (30) Stöcker, M. Methanol-to-Hydrocarbons: Catalytic Materials and Their Behavior. *Microporous and Mesoporous Materials* **1999**, *29* (1–2), 3–48. https://doi.org/10.1016/S1387-1811(98)00319-9.
- (31) Worldometer. World Natural Gas Statistics. https://www.worldometers.info/gas/ (accessed 2022-10-27).
- (32) Makogon, Y. F.; Holditch, S. A.; Makogon, T. Y. Natural Gas-Hydrates A Potential Energy Source for the 21st Century. *Journal of Petroleum Science and Engineering* **2007**, *56* (1–3), 14–31. https://doi.org/10.1016/J.PETROL.2005.10.009.
- (33) Yang, S.; Xu, D.; Xiu, L.; Duan, C.; Pang, B.; Yang, S.; Xu, D.; Xiu, L.; Duan, C.; Pang, B. Composition Characteristics of Gas Hydrate Produced Gas and Pretreatment Research. *Energy and Power Engineering* **2014**, *6* (13), 481–486. https://doi.org/10.4236/EPE.2014.613041.
- (34) Carroll, J. Chapter 11- Additional Topics. *Natural Gas Hydrates* **2020**, 347–360. https://doi.org/10.1016/B978-0-12-821771-9.00011-2.
- (35) Office of Fossil Energy and Carbon Management. *Enhanced Oil Recovery | Department of Energy*. https://www.energy.gov/fecm/science-innovation/oil-gas-research/enhanced-oil-recovery (accessed 2022-10-26).
- (36) RystadEnergy. *Total recoverable oil worldwide is now 9% lower than last year, threatening global energy security.* https://www.rystadenergy.com/news/total-recoverable-oil-worldwide-is-now-9-lower-than-last-year-threatening-global (accessed 2022-10-26).
- (37) Samimi, F.; Hamedi, N.; Rahimpour, M. R. Green Methanol Production Process from Indirect CO2 Conversion: RWGS Reactor versus RWGS Membrane Reactor. *Journal of Environmental Chemical Engineering* **2019**, *7* (1), 102813. https://doi.org/10.1016/J.JECE.2018.102813.

Journal of Materials Chemistry A Accepted Manuscrip

- (38) Chou, C. Y.; Lobo, R. F. Direct Conversion of CO2 into Methanol over Promoted Indium Oxide-Based Catalysts. *Applied Catalysis A: General* **2019**, *583*, 117144. https://doi.org/10.1016/J.APCATA.2019.117144.
- (39) Toyir, J.; Ramírez De La Piscina, P.; Fierro, J. L. G.; Homs, N. Highly Effective Conversion of CO2 to Methanol over Supported and Promoted Copper-Based Catalysts: Influence of Support and Promoter. Applied Catalysis B: Environmental 2001, 29 (3), 207–215. https://doi.org/10.1016/S0926-3373(00)00205-8.
- (40) Wu, Y.; Jiang, Z.; Lu, X.; Liang, Y.; Wang, H. Domino Electroreduction of CO2 to Methanol on a Molecular Catalyst. *Nature 2019 575:7784* 2019, 575 (7784), 639–642. https://doi.org/10.1038/s41586-019-1760-8.
- (41) Olah, G. A. Towards Oil Independence Through Renewable Methanol Chemistry. *Angewandte Chemie International Edition* **2013**, *52* (1), 104–107. https://doi.org/10.1002/ANIE.201204995.
- (42) Carbon Recycling International. *GEORGE OLAH RENEWABLE METHANOL PLANT: FIRST PRODUCTION OF FUEL FROM CO2 AT INDUSTRIAL SCALE*. https://www.carbonrecycling.is/project-goplant (accessed 2022-10-19).
- (43) Borgogna, A.; Iaquaniello, G.; Salladini, A.; Agostini, E.; Boccacci, M.; Borgogna, A.; Iaquaniello, G.; Salladini, A.; Agostini, E.; Boccacci, M. Chemical Carbon and Hydrogen Recycle through Waste Gasification: The Methanol Route. *Gasification* **2021**. https://doi.org/10.5772/INTECHOPEN.98206.
- (44) Enerkem. *Carbon Recycling* | *Advanced Thermochemical Process*. https://enerkem.com/process-technology/carbon-recycling/ (accessed 2022-10-27).
- (45) Statista. *Production of methanol worldwide from 2017 to 2022*. https://www.statista.com/statistics/1323406/methanol-production-worldwide/ (accessed 2022-10-20).
- (46) Statista. *Global methanol demand by application 2021* . https://www.statista.com/statistics/1323424/methanol-demand-worldwide-by-application/ (accessed 2022-11-24).
- (47) Gogate, M. R. Methanol-to-Olefins Process Technology: Current Status and Future Prospects. https://doi.org/10.1080/10916466.2018.1555589 **2019**, 37 (5), 559–565. https://doi.org/10.1080/10916466.2018.1555589.
- (48) Hu, H.; Cao, F.; Ying, W.; Sun, Q.; Fang, D. Study of Coke Behaviour of Catalyst during Methanol-to-Olefins Process Based on a Special TGA Reactor. *Chemical Engineering Journal* **2010**, *160* (2), 770–778. https://doi.org/10.1016/J.CEJ.2010.04.017.
- (49) IZA. *Database of Zeolite Structures*. https://america.iza-structure.org/IZA-SC/framework.php?STC=CHA (accessed 2022-10-18).
- (50) Peng, Q.; Wang, G.; Wang, Z.; Jiang, R.; Wang, D.; Chen, J.; Huang, J. Tuning Hydrocarbon Pool Intermediates by the Acidity of SAPO-34 Catalysts for Improving Methanol-to-Olefins Reaction. *ACS Sustainable Chemistry & Engineering* **2018**, 6 (12), 16867–16875. https://doi.org/10.1021/ACSSUSCHEMENG.8B04210.
- (51) Shen, W.; Li, X.; Wei, Y.; Tian, P.; Deng, F.; Han, X.; Bao, X. A Study of the Acidity of SAPO-34 by Solid-State NMR Spectroscopy. *Microporous and Mesoporous Materials* **2012**, *158*, 19–25. https://doi.org/10.1016/J.MICROMESO.2012.03.013.
- (52) Pastore, H. O.; Coluccia, S.; Marchese, L. POROUS ALUMINOPHOSPHATES: From Molecular Sieves to Designed Acid Catalysts. https://doi.org/10.1146/annurev.matsci.35.103103.120732 2005, 35, 351–395. https://doi.org/10.1146/ANNUREV.MATSCI.35.103103.120732.
- (53) Watanabe, Y.; Koiwai, A.; Takeuchi, H.; Hyodo, S. A.; Noda, S. Multinuclear NMR Studies on the Thermal Stability of SAPO-34. *Journal of Catalysis* **1993**, *143* (2), 430–436. https://doi.org/10.1006/JCAT.1993.1287.
- (54) Yang, L.; Wang, C.; Zhang, L.; Dai, W.; Chu, Y.; Xu, J.; Wu, G.; Gao, M.; Liu, W.; Xu, Z.; Wang, P.; Guan, N.; Dyballa, M.; Ye, M.; Deng, F.; Fan, W.; Li, L. Stabilizing the Framework of SAPO-34 Zeolite toward Long-Term Methanol-to-Olefins Conversion. *Nature Communications 2021 12:1* **2021**, *12* (1), 1–11. https://doi.org/10.1038/s41467-021-24403-2.
- (55) Galadima, A.; Muraza, O. Recent Developments on Silicoaluminates and Silicoaluminophosphates in the Methanol-to-Propylene Reaction: A Mini Review. *Industrial and Engineering Chemistry Research* **2015**,

- 54 (18),4891-4905. https://doi.org/10.1021/ACS.IECR.5B00338/SUPPL FILE/IE5B00338 SI 001.PDF.
- Taheri Najafabadi, A.; Fatemi, S.; Sohrabi, M.; Salmasi, M. Kinetic Modeling and Optimization of the (56)Operating Condition of Mto Process on Sapo-34 Catalyst. Journal of Industrial and Engineering Chemistry **2012**, 18 (1), 29–37. https://doi.org/10.1016/j.jiec.2011.11.088.
- Charghand, M.; Haghighi, M.; Saedy, S.; Aghamohammadi, S. Efficient Hydrothermal Synthesis of (57)Nanostructured SAPO-34 Using Ultrasound Energy: Physicochemical Characterization and Catalytic Performance toward Methanol Conversion to Light Olefins. Advanced Powder Technology 2014, 25 (6), 1728–1736. https://doi.org/10.1016/J.APT.2014.06.022.
- Dai, W.; Wang, X.; Wu, G.; Guan, N.; Hunger, M.; Li, L. Methanol-to-Olefin Conversion on (58)Silicoaluminophosphate Catalysts: Effect of Brønsted Acid Sites and Framework Structures. ACS Catalysis **2011**, I (4), 292–299. https://doi.org/10.1021/CS200016U.
- (59)Pinilla-Herrero, I.; Olsbye, U.; Márquez-Álvarez, C.; Sastre, E. Effect of Framework Topology of SAPO Catalysts on Selectivity and Deactivation Profile in the Methanol-to-Olefins Reaction. Journal of Catalysis **2017**, 352, 191–207. https://doi.org/10.1016/j.jcat.2017.05.008.
- Qi, G.; Xie, Z.; Yang, W.; Zhong, S.; Liu, H.; Zhang, C.; Chen, Q. Behaviors of Coke Deposition on SAPO-(60)34 Catalyst during Methanol Conversion to Light Olefins. Fuel Processing Technology 2007, 88 (5), 437– 441. https://doi.org/10.1016/J.FUPROC.2006.11.008.
- Dai, W.; Wu, G.; Li, L.; Guan, N.; Hunger, M. Mechanisms of the Deactivation of SAPO-34 Materials with (61)Different Crystal Sizes Applied as MTO Catalysts. ACS Catalysis 2013, 3 (4), 588–596. https://doi.org/10.1021/CS400007V.
- (62)Yang, L.; Wang, C.; Zhang, L.; Dai, W.; Chu, Y.; Xu, J.; Wu, G.; Gao, M.; Liu, W.; Xu, Z.; Wang, P.; Guan, N.; Dyballa, M.; Ye, M.; Deng, F.; Fan, W.; Li, L. Stabilizing the Framework of SAPO-34 Zeolite toward Long-Term Methanol-to-Olefins Conversion. Nat Commun 2021, 12 (1), https://doi.org/10.1038/s41467-021-24403-2.
- Sun, T.; Xu, S.; Xiao, D.; Liu, Z.; Li, G.; Zheng, A.; Liu, W.; Xu, Z.; Cao, Y.; Guo, Q.; Wang, N.; Wei, (63)Y.; Liu, Z. Water-Induced Structural Dynamic Process in Molecular Sieves under Mild Hydrothermal Conditions: Ship-in-a-Bottle Strategy for Acidity Identification and Catalyst Modification. Angewandte Chemie International Edition 2020, 59 (46), 20672–20681. https://doi.org/10.1002/anie.202009648.
- (64)Li, Z.; Martínez-Triguero, J.; Yu, J.; Corma, A. Conversion of Methanol to Olefins: Stabilization of Nanosized SAPO-34 by Hydrothermal Treatment. Journal of Catalysis 2015, 329, 379–388. https://doi.org/10.1016/j.jcat.2015.05.025.
- Zhang, C.; Wu, X.; Zhang, Y.; Wang, L.; Jin, Y.; Gao, M.; Ye, M.; Wei, Y.; Liu, Z. Water-Controlled (65)Coking Dynamics during High-Pressure Methanol-to-Olefins Reaction over SAPO-34. ACS Catal. 2025, 15 (3), 1553–1562. https://doi.org/10.1021/acscatal.4c06239.
- (66)Vasconcelos, A. A.; Len, T.; de Oliveira, A. de N.; Costa, A. A. F. da; Souza, A. R. da S.; Costa, C. E. F. da; Luque, R.; Rocha Filho, G. N. da; Noronha, R. C. R.; Nascimento, L. A. S. do. Zeolites: A Theoretical and Practical Approach with Uses in (Bio)Chemical Processes. Applied Sciences 2023, 13 (3), 1897. https://doi.org/10.3390/app13031897.
- Cheng, J.; Han, S.; Ye, Q.; Cheng, S.; Kang, T.; Dai, H. Effects of Hydrothermal Aging at High and Low (67)Temperatures on the Selective Catalytic Reduction of NOx with NH3 over Cu/SAPO-34. Res Chem Intermed 2019, 45 (4), 2023–2044. https://doi.org/10.1007/s11164-018-03712-0.
- Zapata, P. A.; Faria, J.; Ruiz, M. P.; Jentoft, R. E.; Resasco, D. E. Hydrophobic Zeolites for Biofuel (68)Upgrading Reactions at the Liquid-Liquid Interface in Water/Oil Emulsions. J. Am. Chem. Soc. 2012, 134 (20), 8570–8578. https://doi.org/10.1021/ja3015082.
- Prodinger, S.; Derewinski, M. A.; Vjunov, A.; Burton, S. D.; Arslan, I.; Lercher, J. A. Improving Stability (69)of Zeolites in Aqueous Phase via Selective Removal of Structural Defects. J. Am. Chem. Soc. 2016, 138 (13), 4408–4415. https://doi.org/10.1021/jacs.5b12785.
- Guan, B.; Jiang, H.; Peng, X.; Wei, Y.; Liu, Z.; Chen, T.; Lin, H.; Huang, Z. Promotional Effect and (70)Mechanism of the Modification of Ce on the Enhanced NH3-SCR Efficiency and the Low Temperature Hydrothermal Stability over Cu/SAPO-34 Catalysts. Applied Catalysis A: General 2021, 617, 118110. https://doi.org/10.1016/j.apcata.2021.118110.

(71) Web o 07-14 (72) van E

This article is licensed under a Creative Commons Attribution-NonCommercial 3.0 Unported Licence

- Web of Science Core Collection. *Clarivate Analytics*. http://apps.webofknowledge.com/ (accessed 2023-07-14).
- van Eck, N. J.; Waltman, L. Software Survey: VOSviewer, a Computer Program for Bibliometric Mapping. *Scientometrics* **2010**, *84* (2), 523–538. https://doi.org/10.1007/S11192-009-0146-3.
- (73) Chen, J. Q.; Bozzano, A.; Glover, B.; Fuglerud, T.; Kvisle, S. Recent Advancements in Ethylene and Propylene Production Using the UOP/Hydro MTO Process. *Catalysis Today* **2005**, *106* (1–4), 103–107. https://doi.org/10.1016/J.CATTOD.2005.07.178.
- (74) Honeywell UOP. *Olefins*. https://uop.honeywell.com/en/industry-solutions/petrochemicals/olefins (accessed 2023-08-09).
- (75) Cnudde, P.; Demuynck, R.; Vandenbrande, S.; Waroquier, M.; Sastre, G.; Speybroeck, V. Van. Light Olefin Diffusion during the MTO Process on H-SAPO-34: A Complex Interplay of Molecular Factors. *Journal of the American Chemical Society* **2020**, *142* (13), 6007–6017. https://doi.org/10.1021/JACS.9B10249.
- (76) Ghavipour, M.; Al Hussami, R.; Levin, K.; Roy, R.; Kopyscinski, J. SAPO-34 Catalyst: Synthesis Optimization by Template Alteration and In Situ Coke Evolution Analysis in Methanol Conversion to Light Olefins. *Ind. Eng. Chem. Res.* **2023**, *62* (44), 18362–18378. https://doi.org/10.1021/acs.iecr.3c02543.
- (77) Castellanos-Beltran, I. J.; Assima, G. P.; Lavoie, J. M. Effect of Temperature in the Conversion of Methanol to Olefins (MTO) Using an Extruded SAPO-34 Catalyst. *Frontiers of Chemical Science and Engineering* **2018**, *12* (2), 226–238. https://doi.org/10.1007/S11705-018-1709-8.
- (78) Ghavipour, M.; Mehr, A. S.; Wang, Y.; Behbahani, R. M.; Hajimirzaee, S.; Bahrami, K. Investigating the Mixing Sequence and the Si Content in SAPO-34 Synthesis for Selective Conversion of Methanol to Light Olefins Using Morpholine / TEAOH Templates. *RSC Advances* **2016**, *6* (21), 17583–17594. https://doi.org/10.1039/c5ra23432h.
- (79) Taheri Najafabadi, A.; Fatemi, S.; Sohrabi, M.; Salmasi, M. Kinetic Modeling and Optimization of the Operating Condition of MTO Process on SAPO-34 Catalyst. *Journal of Industrial and Engineering Chemistry* **2012**, *18* (1), 29–37. https://doi.org/10.1016/J.JIEC.2011.11.088.
- (80) Wu, X.; Abraha, M. G.; Anthony, R. G. Methanol Conversion on SAPO-34: Reaction Condition for Fixed-Bed Reactor. *Applied Catalysis A: General* **2004**, *260* (1), 63–69. https://doi.org/10.1016/j.apcata.2003.10.011.
- (81) Obrzut, D. L.; Adekkanattu, P. M.; Thundimadathil, J.; Liu, J.; Dubois, D. R.; Guin, J. A. Reducing Methane Formation in Methanol to Olefins Reaction on Metal Impregnated SAPO-34 Molecular Sieve. *Reaction Kinetics and Catalysis Letters* **2003**, *80* (1), 113–121. https://doi.org/10.1023/A:1026088327000.
- (82) Borodina, E.; Sharbini Harun Kamaluddin, H.; Meirer, F.; Mokhtar, M.; Asiri, A. M.; Al-Thabaiti, S. A.; Basahel, S. N.; Ruiz-Martinez, J.; Weckhuysen, B. M. Influence of the Reaction Temperature on the Nature of the Active and Deactivating Species during Methanol-to-Olefins Conversion over H-SAPO-34. *ACS Catalysis* **2017**, *7* (8), 5268–5281. https://doi.org/10.1021/ACSCATAL.7B01497.
- (83) Yuan, X.; Li, H.; Ye, M.; Liu, Z. Kinetic Modeling of Methanol to Olefins Process over SAPO-34 Catalyst Based on the Dual-Cycle Reaction Mechanism. *AIChE Journal* **2019**, *65* (2), 662–674. https://doi.org/10.1002/AIC.16439.
- (84) Zhao, X.; Li, J.; Tian, P.; Wang, L.; Li, X.; Lin, S.; Guo, X.; Liu, Z. Achieving a Superlong Lifetime in the Zeolite-Catalyzed MTO Reaction under High Pressure: Synergistic Effect of Hydrogen and Water. *ACS Catalysis* **2019**, *9* (4), 3017–3025. https://doi.org/10.1021/ACSCATAL.8B04402.
- (85) Álvaro-Muñoz, T.; Márquez-Álvarez, C.; Sastre, E. Use of Different Templates on SAPO-34 Synthesis: Effect on the Acidity and Catalytic Activity in the MTO Reaction. *Catalysis Today* **2012**, *179* (1), 27–34. https://doi.org/10.1016/j.cattod.2011.07.038.
- (86) Taheri Najafabadi, A.; Fatemi, S.; Sohrabi, M.; Salmasi, M. Kinetic Modeling and Optimization of the Operating Condition of MTO Process on SAPO-34 Catalyst. *Journal of Industrial and Engineering Chemistry* **2012**, *18* (1), 29–37. https://doi.org/10.1016/J.JIEC.2011.11.088.
- [87] Jiang, H.; Yuan, L.; Li, D.; Chen, Y. Mathematical Model for the Industrial SMTO Reactor with a SAPO-34 Catalyst. *ACS Omega* **2023**. https://doi.org/10.1021/ACSOMEGA.3C00304.

Open Access Article. Published on 22 2025. Downloaded on 30.10.2025 01:47:29.

(00) II 7 71

- (88) Yang, Z.; Zhang, L.; Zhou, Y.; Wang, H.; Wen, L.; Kianfar, E. Investigation of Effective Parameters on SAPO-34 Nanocatalyst in the Methanol-to-Olefin Conversion Process: A Review. *Reviews in Inorganic Chemistry* **2020**, *40* (3), 91–105. https://doi.org/10.1515/REVIC-2020-0003.
- (89) Marchi, A. J.; Froment, G. F. Catalytic Conversion of Methanol to Light Alkenes on SAPO Molecular Sieves. *Applied Catalysis* **1991**, *71* (1), 139–152. https://doi.org/10.1016/0166-9834(91)85011-J.
- (90) Wilson, S.; Barger, P. The Characteristics of SAPO-34 Which Influence the Conversion of Methanol to Light Olefins. *Microporous and Mesoporous Materials* **1999**, 29 (1–2), 117–126. https://doi.org/10.1016/S1387-1811(98)00325-4.
- (91) Van Niekerk, M. J.; Fletcher, J. C. Q.; O'Connor, C. T. Effect of Catalyst Modification on the Conversion of Methanol to Light Olefins over SAPO-34. *Applied Catalysis A: General* **1996**, *138* (1), 135–145. https://doi.org/10.1016/0926-860X(95)00240-5.
- (92) Wu, X.; Anthony, R. G. Effect of Feed Composition on Methanol Conversion to Light Olefins over SAPO-34. *Applied Catalysis A: General* **2001**, *218* (1–2), 241–250. https://doi.org/10.1016/S0926-860X(01)00651-2.
- (93) De Wispelaere, K.; Wondergem, C. S.; Ensing, B.; Hemelsoet, K.; Meijer, E. J.; Weckhuysen, B. M.; Van Speybroeck, V.; Ruiz-Martínez, J. Insight into the Effect of Water on the Methanol-to-Olefins Conversion in H-SAPO-34 from Molecular Simulations and in Situ Microspectroscopy. *ACS Catalysis* **2016**, *6* (3), 1991–2002. https://doi.org/10.1021/ACSCATAL.5B02139.
- (94) Luo, M.; Fu, Y.; Hu, B.; Wang, D.; Wang, B.; Mao, G. Water Inhibits the Conversion and Coking of Olefins on SAPO-34. *Applied Catalysis A: General* **2019**, *570*, 209–217. https://doi.org/10.1016/J.APCATA.2018.11.017.
- (95) Bahrami, H.; Darian, J. T.; Sedighi, M. Simultaneous Effects of Water, TEAOH and Morpholine on SAPO-34 Synthesis and Its Performance in MTO Process. *Microporous and Mesoporous Materials* **2018**, *261*, 111–118. https://doi.org/10.1016/J.MICROMESO.2017.11.011.
- (96) Arora, S. S.; Nieskens, D. L. S.; Malek, A.; Bhan, A. Lifetime Improvement in Methanol-to-Olefins Catalysis over Chabazite Materials by High-Pressure H2 Co-Feeds. *Nature Catalysis* **2018**, *I* (9), 666–672. https://doi.org/10.1038/s41929-018-0125-2.
- (97) Shi, Z.; Neurock, M.; Bhan, A. Methanol-to-Olefins Catalysis on HSSZ-13 and HSAPO-34 and Its Relationship to Acid Strength. *ACS Catalysis* **2021**, *11* (3), 1222–1232. https://doi.org/10.1021/ACSCATAL.0C04011.
- (98) Deluca, M.; Janes, C.; Hibbitts, D. Contrasting Arene, Alkene, Diene, and Formaldehyde Hydrogenation in H-ZSM-5, H-SSZ-13, and H-SAPO-34 Frameworks during MTO. *ACS Catalysis* **2020**, *10* (8), 4593–4607. https://doi.org/10.1021/ACSCATAL.9B04529/SUPPL_FILE/CS9B04529_SI_002.ZIP.
- (99) Shi, Z.; Bhan, A. Methanol-to-Olefins Catalysis on Window-Cage Type Zeolites/Zeotypes with Syngas Co-Feeds: Understanding Syngas-to-Olefins Chemistry. *Journal of Catalysis* **2022**, *413*, 913–922. https://doi.org/10.1016/J.JCAT.2022.07.035.
- (100) Chen, D.; Grønvold, A.; Moljord, K.; Holmen, A. Methanol Conversion to Light Olefins over SAPO-34: Reaction Network and Deactivation Kinetics. *Industrial and Engineering Chemistry Research* **2007**, *46* (12), 4116–4123. https://doi.org/10.1021/IE0610748.
- (101) Pop, G.; Bozga, G.; Ganea, R.; Natu, N. Methanol Conversion to Dimethyl Ether over H-SAPO-34 Catalyst. *Industrial and Engineering Chemistry Research* **2009**, 48 (15), 7065–7071. https://doi.org/10.1021/IE900532Y.
- (102) Masih, D.; Rohani, S.; Kondo, J. N.; Tatsumi, T. Low-Temperature Methanol Dehydration to Dimethyl Ether over Various Small-Pore Zeolites. *Applied Catalysis B: Environmental* **2017**, *217*, 247–255. https://doi.org/10.1016/J.APCATB.2017.05.089.
- (103) Ghavipour, M.; Behbahani, R. M.; Rostami, R. B.; Lemraski, A. S. Methanol/Dimethyl Ether to Light Olefins over SAPO-34: Comprehensive Comparison of the Products Distribution and Catalyst Performance. *Journal of Natural Gas Science and Engineering* **2014**, *21*, 532–539. https://doi.org/10.1016/J.JNGSE.2014.09.015.
- (104) Spivey, J. J.; Froment, G. F.; Dehertog, W. J. H.; Marchi, A. J. Zeolite Catalysis in the Conversion of Methanol into Olefins. *Catalysis* **1992**, 1–64. https://doi.org/10.1039/9781847553218-00001.

Open Access Article. Published on 22 2025. Downloaded on 30.10.2025 01:47:29.

(105) Olah, G. A.; Doggweiler, H.; Felberg, J. D.; Frohlich, S.; Grdina, M. J.; Karpeles, R.; Keumi, T.; Inaba, S. ichi; Ip, W. M.; Lammertsma, K.; Salem, G.; Tabor, D. C. Onium Ylide Chemistry. 1. Bifunctional Acid-Base-Catalyzed Conversion of Heterosubstituted Methanes into Ethylene and Derived Hydrocarbons. The Onium Ylide Mechanism of the C1 → C2 Conversion. *Journal of the American Chemical Society* **1984**, 106 (7), 2143–2149. https://doi.org/10.1021/JA00319A039.

- (106) Sayed, M. B. Comments on the Mechanism of MTG/HZSM-5 Conversion. *Journal of the Chemical Society, Faraday Transactions 1: Physical Chemistry in Condensed Phases* **1987**, *83* (6), 1771–1778. https://doi.org/10.1039/F19878301771.
- (107) Olah, G. A.; Doggweiler, H.; Felberg, J. D. Onium Ylide Chemistry. 2. Methylenedialkyloxonium Ylides. *Journal of Organic Chemistry* **1984**, 49 (12), 2112–2116. https://doi.org/10.1021/JO00186A006/ASSET/JO00186A006.FP.PNG V03.
- (108) Chang, C. D.; Silvestri, A. J. The Conversion of Methanol and Other O-Compounds to Hydrocarbons over Zeolite Catalysts. *Journal of Catalysis* **1977**, *47* (2), 249–259. https://doi.org/10.1016/0021-9517(77)90172-5.
- (109) Swabb, E. A.; Gates, B. C. Diffusion, Reaction, and Fouling in H-Mordenite Crystallites. The Catalytic Dehydration of Methanol. *Industrial and Engineering Chemistry Fundamentals* **1972**, *11* (4), 540–545. https://doi.org/10.1021/I160044A018.
- (110) Chang, C. D.; Chu, C. T. W. On the Mechanism of Hydrocarbon Formation from Methanol over Zeolite Catalysts: Evidence for Carbene Intermediacy. *Journal of Catalysis* **1982**, 74 (1), 203–206. https://doi.org/10.1016/0021-9517(82)90026-4.
- (111) Yoshio Ono*; Tomoyuki Mori. Mechanism of Methanol Conversion into Hydrocarbons over ZSM-5 Zeolite. *J. Chem. SOC., Faraday Trans. I* **1981**, 77, 2209–2221.
- (112) Kagi, D. In Re: Mechanism of Conversion of Methanol over ZSM-5 Catalyst. *Journal of Catalysis* **1981**, 69 (1), 242–243. https://doi.org/10.1016/0021-9517(81)90154-8.
- (113) Nagy, J. B.; Gilson, J. P.; Derouane, E. G. A 13C-N.M.R. Investigation of the Conversion of Methanol on H-ZSM-5 in the Presence of Carbon Monoxide. *Journal of Molecular Catalysis* **1979**, *5* (5), 393–397. https://doi.org/10.1016/0304-5102(79)80015-2.
- (114) Smith, R. D.; Futrell, J. H. Evidence for Complex Formation in the Reactions of CH+3 and CD+3 with CH3OH, CD3OD, and C2H5OH. *Chemical Physics Letters* **1976**, 41 (1), 64–67. https://doi.org/10.1016/0009-2614(76)85248-7.
- (115) Chang, C. D.; Hellring, S. D.; Pearson, J. A. On the Existence and Role of Free Radicals in Methanol Conversion to Hydrocarbons over HZSM-5: I. Inhibition by NO. *Journal of Catalysis* **1989**, *115* (1), 282–285. https://doi.org/10.1016/0021-9517(89)90030-4.
- (116) Clarke, J. K. A.; Darcy, R.; Hegarty, B. F.; O'donoghue, E.; Amir-Ebrahimi, V.; Rooney, J. J. Free Radicals in Dimethyl Ether on H-ZSM-5 Zeolite. A Novel Dimension of Heterogeneous Catalysis. *J. CHEM. SOC., CHEM. COMMUN* **1986**.
- (117) Zatorski, W.; Krzyzanowski, S. Conversion of Methanol to Hydrocarbons over Natural Mordenite. *Acta Phys. Chem.* **1978**, *29*, 347–356.
- (118) Peng, C.; Wang, H.; Hu, P. Theoretical Insights into How the First C–C Bond Forms in the Methanol-to-Olefin Process Catalysed by HSAPO-34. *Physical Chemistry Chemical Physics* **2016**, *18* (21), 14495–14502. https://doi.org/10.1039/C5CP08029K.
- (119) Haw, J. F.; Song, W.; Marcus, D. M.; Nicholas, J. B. The Mechanism of Methanol to Hydrocarbon Catalysis. *Accounts of Chemical Research* **2003**, *36* (5), 317–326. https://doi.org/10.1021/ar0200060.
- (120) B. Minova, I.; Bühl, M.; K. Matam, S.; A. Catlow, C. R.; D. Frogley, M.; Cinque, G.; A. Wright, P.; F. Howe, R. Carbene-like Reactivity of Methoxy Groups in a Single Crystal SAPO-34 MTO Catalyst. **2022**. https://doi.org/10.1039/D1CY02361F.
- (121) Dahl, I. M.; Kolboe, S. On the Reaction Mechanism for Hydrocarbon Formation from Methanol over SAPO-34: I. Isotopic Labeling Studies of the Co-Reaction of Ethene and Methanol. *Journal of Catalysis* **1994**, *149* (2), 458–464. https://doi.org/10.1006/JCAT.1994.1312.
- (122) Dahl, I. M.; Kolboe, S. On the Reaction Mechanism for Propene Formation in the MTO Reaction over SAPO-34. *Catalysis Letters* 1993 20:3 1993, 20 (3), 329–336. https://doi.org/10.1007/BF00769305.

- (123) Bjørgen, M.; Olsbye, U.; Kolboe, S. Coke Precursor Formation and Zeolite Deactivation: Mechanistic Insights from Hexamethylbenzene Conversion. *Journal of Catalysis* **2003**, *215* (1), 30–44. https://doi.org/10.1016/S0021-9517(02)00050-7.
- (124) Olsbye, U.; Bjørgen, M.; Svelle, S.; Lillerud, K. P.; Kolboe, S. Mechanistic Insight into the Methanol-to-Hydrocarbons Reaction. *Catalysis Today* **2005**, *106* (1–4), 108–111. https://doi.org/10.1016/J.CATTOD.2005.07.135.
- (125) Lesthaeghe, D.; Horré, A.; Waroquier, M.; Marin, G. B.; Van Speybroeck, V. Theoretical Insights on Methylbenzene Side-Chain Growth in ZSM-5 Zeolites for Methanol-to-Olefin Conversion. *Chemistry A European Journal* **2009**, *15* (41), 10803–10808. https://doi.org/10.1002/CHEM.200901723.
- (126) Arstad, B.; Nicholas, J. B.; Haw, J. F. Theoretical Study of the Methylbenzene Side-Chain Hydrocarbon Pool Mechanism in Methanol to Olefin Catalysis. *Journal of the American Chemical Society* **2004**, *126* (9), 2991–3001. https://doi.org/10.1021/JA035923J.
- (127) Dai, W.; Wang, C.; Dyballa, M.; Wu, G.; Guan, N.; Li, L.; Xie, Z.; Hunger, M. Understanding the Early Stages of the Methanol-to-Olefin Conversion on H-SAPO-34. *ACS Catalysis* **2014**, *5* (1), 317–326. https://doi.org/10.1021/CS5015749.
- (128) Zhou, J.; Gao, M.; Zhang, J.; Liu, W.; Zhang, T.; Li, H.; Xu, Z.; Ye, M.; Liu, Z. Directed Transforming of Coke to Active Intermediates in Methanol-to-Olefins Catalyst to Boost Light Olefins Selectivity. *Nature Communications* 2021 12:1 2021, 12 (1), 1–11. https://doi.org/10.1038/s41467-020-20193-1.
- (129) Wang, W.; Buchholz, A.; Seiler, M.; Hunger, M. Evidence for an Initiation of the Methanol-to-Olefin Process by Reactive Surface Methoxy Groups on Acidic Zeolite Catalysts. *Journal of the American Chemical Society* **2003**, *125* (49), 15260–15267. https://doi.org/10.1021/JA0304244.
- (130) Li, J.; Wei, Z.; Chen, Y.; Jing, B.; He, Y.; Dong, M.; Jiao, H.; Li, X.; Qin, Z.; Wang, J.; Fan, W. A Route to Form Initial Hydrocarbon Pool Species in Methanol Conversion to Olefins over Zeolites. *Journal of Catalysis* **2014**, *317*, 277–283. https://doi.org/10.1016/J.JCAT.2014.05.015.
- (131) Peng, Q.; Wang, G.; Wang, Z.; Jiang, R.; Wang, D.; Chen, J.; Huang, J. Tuning Hydrocarbon Pool Intermediates by the Acidity of SAPO-34 Catalysts for Improving Methanol-to-Olefins Reaction. *ACS Sustainable Chemistry & Engineering* **2018**, 6 (12), 16867–16875. https://doi.org/10.1021/ACSSUSCHEMENG.8B04210.
- (132) Zhou, J.; Gao, M.; Zhang, J.; Liu, W.; Zhang, T.; Li, H.; Xu, Z.; Ye, M.; Liu, Z. Directed Transforming of Coke to Active Intermediates in Methanol-to-Olefins Catalyst to Boost Light Olefins Selectivity. *Nature Communications* 2021 12:1 2021, 12 (1), 1–11. https://doi.org/10.1038/s41467-020-20193-1.
- (133) Wang, S.; Chen, Y.; Wei, Z.; Qin, Z.; Liang, T.; Dong, M.; Li, J.; Fan, W.; Wang, J. Evolution of Aromatic Species in Supercages and Its Effect on the Conversion of Methanol to Olefins over H-MCM-22 Zeolite: A Density Functional Theory Study. *Journal of Physical Chemistry C* **2016**, *120* (49), 27964–27979. https://doi.org/10.1021/acs.jpcc.6b08154.
- (134) Mole, T.; Bett, G.; Seddon, D. Conversion of Methanol to Hydrocarbons over ZSM-5 Zeolite: An Examination of the Role of Aromatic Hydrocarbons Using 13carbon- and Deuterium-Labeled Feeds. *Journal of Catalysis* **1983**, *84* (2), 435–445. https://doi.org/10.1016/0021-9517(83)90014-3.
- (135) Fečík, M.; Plessow, P. N.; Studt, F. Theoretical Investigation of the Side-Chain Mechanism of the MTO Process over H-SSZ-13 Using DFT and Ab Initio Calculations. *Catalysis Science & Technology* **2021**, *11* (11), 3826–3833. https://doi.org/10.1039/D1CY00433F.
- (136) Chen, Y.; Wang, S.; Wei, Z.; Li, J.; Dong, M.; Qin, Z.; Wang, J.; Fan, W. Unraveling the Relationship between Zeolite Structure and MTO Product Distribution by Theoretical Study of the Reaction Mechanism. *Journal of Physical Chemistry C* **2021**, *125* (48), 26472–26483. https://doi.org/10.1021/ACS.JPCC.1C07692.
- (137) Sullivan, R. F.; Egan, C. J.; Langlois, G. E.; Sieg, R. P. A New Reaction That Occurs in the Hydrocracking of Certain Aromatic Hydrocarbons. *Journal of the American Chemical Society* **1961**, *83* (5), 1156–1160. https://doi.org/10.1021/JA01466A036/ASSET/JA01466A036.FP.PNG V03.
- (138) Ferri, P.; Li, C.; Paris, C.; Vidal-Moya, A.; Moliner, M.; Boronat, M.; Corma, A. Chemical and Structural Parameter Connecting Cavity Architecture, Confined Hydrocarbon Pool Species, and MTO Product Selectivity in Small-Pore Cage-Based Zeolites. *ACS Catalysis* **2019**, *9* (12), 11542–11551. https://doi.org/10.1021/ACSCATAL.9B04588.

This article is licensed under a Creative Commons Attribution-NonCommercial 3.0 Unported Licence.

- (139) Bjørgen, M.; Olsbye, U.; Petersen, D.; Kolboe, S. The Methanol-to-Hydrocarbons Reaction: Insight into the Reaction Mechanism from [12C]Benzene and [13C]Methanol Coreactions over Zeolite H-Beta. *Journal of Catalysis* **2004**, *221* (1), 1–10. https://doi.org/10.1016/S0021-9517(03)00284-7.
- (140) Sayed, M. B. Comments on the Mechanism of MTG/HZSM-5 Conversion. *J. Chem. Soc., Faraday Trans. I* **1987**, *83* (6), 1771. https://doi.org/10.1039/f19878301771.
- (141) Olah, G. A.; Doggweiler, H.; Felberg, J. D.; Frohlich, S.; Grdina, M. J.; Karpeles, R.; Keumi, T.; Inaba, S.; Ip, W. M.; Lammertsma, K.; Salem, G.; Tabor, D. Onium Ylide Chemistry. 1. Bifunctional Acid-Base-Catalyzed Conversion of Heterosubstituted Methanes into Ethylene and Derived Hydrocarbons. The Onium Ylide Mechanism of the C1 .Fwdarw. C2 Conversion. *J. Am. Chem. Soc.* **1984**, *106* (7), 2143–2149. https://doi.org/10.1021/ja00319a039.
- (142) Chang, C. On the Mechanism of Hydrocarbon Formation from Methanol over Zeolite Catalysts: Evidence for Carbene Intermediacy. *Journal of Catalysis* **1982**, 74 (1), 203–206. https://doi.org/10.1016/0021-9517(82)90026-4.
- (143) Nagy, J. B.; Gilson, J. P.; Derouane, E. G. A 13C-N.M.R. Investigation of the Conversion of Methanol on H-ZSM-5 in the Presence of Carbon Monoxide. *Journal of Molecular Catalysis* **1979**, *5* (5), 393–397. https://doi.org/10.1016/0304-5102(79)80015-2.
- (144) Lesthaeghe, D.; Horré, A.; Waroquier, M.; Marin, G. B.; Van Speybroeck, V. Theoretical Insights on Methylbenzene Side-Chain Growth in ZSM-5 Zeolites for Methanol-to-Olefin Conversion. *Chemistry A European Journal* **2009**, *15* (41), 10803–10808. https://doi.org/10.1002/chem.200901723.
- (145) Clarke, J. K. A.; Darcy, R.; Hegarty, B. F.; O'Donoghue, E.; Amir-Ebrahimi, V.; Rooney, J. J. Free Radicals in Dimethyl Ether on H-ZSM-5 Zeolite. A Novel Dimension of Heterogeneous Catalysis. *J. Chem. Soc., Chem. Commun.* **1986**, No. 5, 425. https://doi.org/10.1039/c39860000425.
- (146) Ke, J.; Hu, W.-D.; Du, Y.-J.; Wang, Y.-D.; Wang, C.-M.; Xie, Z.-K. Microkinetic Simulations of Methanol-to-Olefin Conversion in H-SAPO-34: Dynamic Distribution and Evolution of the Hydrocarbon Pool and Implications for Catalytic Performance. *ACS Catal.* **2023**, *13* (13), 8642–8661. https://doi.org/10.1021/acscatal.3c02140.
- (147) Mole, T.; Bett, G.; Seddon, D. Conversion of Methanol to Hydrocarbons over ZSM-5 Zeolite: An Examination of the Role of Aromatic Hydrocarbons Using %arbon- and Deuterium-Labeled Feeds'.
- (148) Li, J.; Wei, Y.; Liu, G.; Qi, Y.; Tian, P.; Li, B.; He, Y.; Liu, Z. Comparative Study of MTO Conversion over SAPO-34, H-ZSM-5 and H-ZSM-22: Correlating Catalytic Performance and Reaction Mechanism to Zeolite Topology. *Catalysis Today* **2011**, *171* (1), 221–228. https://doi.org/10.1016/j.cattod.2011.02.027.
- (149) Gong, X.; Jiang, S.; Dikhtiarenko, A.; Nastase, S. A. F.; Abou-Hamad, E.; Ye, Y.; Zhou, H.; You, X.; Khairova, R.; Patarroyo, J.; Cavallo, L.; Gascon, J.; Chowdhury, A. D. The Paradoxical Influence of Hydrothermally Treated Zeolites on the Hydrocarbon Pool Mechanism. *Angewandte Chemie International Edition* **2025**, *64* (2), e202414724. https://doi.org/10.1002/anie.202414724.
- (150) Yu, B.; Lou, C.; Zhang, W.; Xu, S.; Han, J.; Yu, Z.; Wei, Y.; Liu, Z. Insight into the Dual Cycle Mechanism of Methanol-to-Olefins Reaction over SAPO-34 Molecular Sieve by Isotopic Tracer Studies. *Chem. Res. Chin. Univ.* **2020**, *36* (6), 1203–1208. https://doi.org/10.1007/s40242-020-0216-x.
- (151) Peng, Q.; Wang, G.; Wang, Z.; Jiang, R.; Wang, D.; Chen, J.; Huang, J. Tuning Hydrocarbon Pool Intermediates by the Acidity of SAPO-34 Catalysts for Improving Methanol-to-Olefins Reaction. *ACS Sustainable Chemistry & Engineering* **2018**, 6 (12), 16867–16875. https://doi.org/10.1021/ACSSUSCHEMENG.8B04210.
- (152) Enss, A. E.; Plessow, P. N.; Studt, F. Theoretical Investigation of the Paring Mechanism of the MTO Process in Different Zeolites. *Journal of Catalysis* **2024**, *432*, 115363. https://doi.org/10.1016/j.jcat.2024.115363.
- (153) Taheri Najafabadi, A.; Fatemi, S.; Sohrabi, M.; Salmasi, M. Kinetic Modeling and Optimization of the Operating Condition of Mto Process on Sapo-34 Catalyst. *Journal of Industrial and Engineering Chemistry* **2012**, *18* (1), 29–37. https://doi.org/10.1016/j.jiec.2011.11.088.
- (154) Obrzut, D. L.; Adekkanattu, P. M.; Thundimadathil, J.; Liu, J.; Dubois, D. R.; Guin, J. A. Reducing Methane Formation in Methanol to Olefins Reaction on Metal Impregnated SAPO-34 Molecular Sieve. *Reaction Kinetics and Catalysis Letters* **2003**, *80* (1), 113–121. https://doi.org/10.1023/A:1026088327000.

(155) Castellanos-Beltran, I. J.; Assima, G. P.; Lavoie, J. M. Effect of Temperature in the Conversion of Methanol to Olefins (MTO) Using an Extruded SAPO-34 Catalyst. Frontiers of Chemical Science and Engineering **2018**, 12 (2), 226–238. https://doi.org/10.1007/S11705-018-1709-8.

- (156) Borodina, E.; Sharbini Harun Kamaluddin, H.; Meirer, F.; Mokhtar, M.; Asiri, A. M.; Al-Thabaiti, S. A.; Basahel, S. N.; Ruiz-Martinez, J.; Weckhuysen, B. M. Influence of the Reaction Temperature on the Nature of the Active and Deactivating Species during Methanol-to-Olefins Conversion over H-SAPO-34. ACS Catalysis 2017, 7 (8), 5268–5281. https://doi.org/10.1021/ACSCATAL.7B01497.
- (157) Ke, J.; Hu, W.-D.; Du, Y.-J.; Wang, Y.-D.; Wang, C.-M.; Xie, Z.-K. Microkinetic Simulations of Methanolto-Olefin Conversion in H-SAPO-34: Dynamic Distribution and Evolution of the Hydrocarbon Pool and Performance. **Implications** for Catalytic ACS Catal. 2023, 13 (13),https://doi.org/10.1021/acscatal.3c02140.
- (158) (PDF) Durable and Highly Selective Tungsten-Substituted MFI Metallosilicate Catalysts for the Methanolto-Propylene Process by Designing a Novel Feed-Supply Technique. ResearchGate 2025. https://doi.org/10.1016/j.crci.2018.01.001.
- (159) Bjørgen, M.; Olsbye, U.; Kolboe, S. Coke Precursor Formation and Zeolite Deactivation: Mechanistic Insights from Hexamethylbenzene Conversion. Journal of Catalysis 2003, 215 (1), 30-44. https://doi.org/10.1016/S0021-9517(02)00050-7.
- (160) Ghavipour, M.; J. Goncalves, T.; Hussami, R. A.; Roy, R.; Siahrostami, S.; Kopyscinski, J. Uncovering the Role of Lewis and Brønsted Acid Sites in Perforated SAPO-34 with an Enhanced Lifetime in Methanol Conversion to Light Olefins. New Journal of Chemistry 2023, 47 (34), 15907–15921. https://doi.org/10.1039/D3NJ02514D.
- (161) Fatourehchi, N.; Sohrabi, M.; Royaee, S. J.; Mirarefin, S. M. Preparation of SAPO-34 Catalyst and Presentation of a Kinetic Model for Methanol to Olefin Process (MTO). Chemical Engineering Research and Design **2011**, 89 (6), 811–816. https://doi.org/10.1016/j.cherd.2010.10.007.
- (162) Hu, H.; Ying, W.; Fang, D. Reaction and Deactivation Kinetics of Methanol-to-Olefins Process Based on a Special TGA Reactor. Journal of Natural Gas Chemistry 2010, 19 (4), https://doi.org/10.1016/S1003-9953(09)60097-9.
- (163) Bos, A. N. R.; Tromp, P. J. J.; Akse, H. N. Conversion of Methanol to Lower Olefins. Kinetic Modeling, Reactor Simulation, and Selection. Ind. Eng. Chem. Res 1995, 34, 3808–3816.
- (164) Yuan, X.; Li, H.; Ye, M.; Liu, Z. Comparative Study of MTO Kinetics over SAPO-34 Catalyst in Fixed Fluidized Engineering 329. Bed Reactors. Chemical Journal 2017. 35–44. https://doi.org/10.1016/J.CEJ.2017.04.041.
- (165) Gayubo, A. G.; Aguayo, A. T.; Sánchez Del Campo, A. E.; Tarrío, A. M.; Bilbao, J. Kinetic Modeling of Methanol Transformation into Olefins on a SAPO-34 Catalyst. Industrial and Engineering Chemistry Research 2000, 39 (2), 292–300. https://doi.org/10.1021/ie990188z.
- (166) Lee, M. K.; Kim, J.; Ryu, J. H.; Yoon, Y. S.; Kim, C. U.; Jeong, S. Y.; Lee, I. B. Modeling of Reaction and Deactivation Kinetics in Methanol-to-Olefins Reaction on SAPO-34. Industrial and Engineering Chemistry Research 2019. 58 (29),13227-13238. https://doi.org/10.1021/ACS.IECR.9B01940/ASSET/IMAGES/MEDIUM/IE-2019-01940S M025.GIF.
- (167) Mousavi, S. H.; Fatemi, S.; Razavian, M. Kinetic Modeling of the Methanol to Olefins Process in the Presence of Hierarchical SAPO-34 Catalyst: Parameter Estimation, Effect of Reaction Conditions and Lifetime Prediction. Reaction Kinetics, Mechanisms and Catalysis 2017, 122 (2), 1245-1264. https://doi.org/10.1007/S11144-017-1266-Z/TABLES/6.
- (168) Azarhoosh, M. J.; Halladj, R.; Askari, S. Presenting a New Kinetic Model for Methanol to Light Olefins Reactions over a Hierarchical SAPO-34 Catalyst Using the Langmuir-Hinshelwood-Hougen-Watson Mechanism. Journal of Physics: Condensed Matter 2017, 29 (42), 425202. https://doi.org/10.1088/1361-648X/AA85F0.
- (169) An, H.; Li, H.; Zhou, J.; Zhang, J.; Zhang, T.; Ye, M.; Liu, Z. Kinetics of Steam Regeneration of SAPO-34 Zeolite Catalyst in Methanol-to-Olefins(MTO) Process. Chinese Journal of Chemical Engineering **2021**. https://doi.org/10.1016/J.CJCHE.2021.07.009.

Journal of Materials Chemistry A Accepted Manuscrip

- (170) Zhao, J.; Zhou, J.; Ye, M.; Liu, Z. Kinetic Study on Air Regeneration of Industrial Methanol-to-Olefin Catalyst. Industrial and Engineering Chemistry Research 2020, 59 (26), 11953–11961. https://doi.org/10.1021/ACS.IECR.0C00153/ASSET/IMAGES/LARGE/IE0C00153 0007.JPEG.
- (171) Hejazi, B.; Shabany, N. Kinetic Modeling of Methanol-to-Olefins Process over SAPO-34 Catalysts in a Dual Fluidized Bed Reactor-Regenerator. Chemical Engineering Research and Design 2022, 179, 374-387. https://doi.org/10.1016/J.CHERD.2022.01.037.
- (172) Taheri Najafabadi, A.; Fatemi, S.; Sohrabi, M.; Salmasi, M. Kinetic Modeling and Optimization of the Operating Condition of MTO Process on SAPO-34 Catalyst. Journal of Industrial and Engineering Chemistry **2012**, 18 (1), 29–37. https://doi.org/10.1016/j.jiec.2011.11.088.
- (173) Fatourehchi, N.; Sohrabi, M.; Royaee, S. J.; Mirarefin, S. M. Preparation of SAPO-34 Catalyst and Presentation of a Kinetic Model for Methanol to Olefin Process (MTO). Chemical Engineering Research and Design 2011, 89 (6), 811–816. https://doi.org/10.1016/j.cherd.2010.10.007.
- (174) Gayubo, A. G.; Aguayo, A. T.; Sánchez del Campo, A. E.; Tarrío, A. M.; Bilbao, J. Kinetic Modeling of Methanol Transformation into Olefins on a SAPO-34 Catalyst. Ind. Eng. Chem. Res. 2000, 39 (2), 292-300. https://doi.org/10.1021/ie990188z.
- (175) Hu, H.; Ying, W.; Fang, D. Reaction and Deactivation Kinetics of Methanol-to-Olefins Process Based on Special TGA Reactor. Journal of Natural Gas Chemistry 2010, 19 (4), https://doi.org/10.1016/S1003-9953(09)60097-9.
- (176) Yuan, X.; Li, H.; Ye, M.; Liu, Z. Comparative Study of MTO Kinetics over SAPO-34 Catalyst in Fixed Fluidized Reactors. Chemical Engineering Journal 2017, Bed https://doi.org/10.1016/j.cej.2017.04.041.
- Chen, D.; Grønvold, A.; Moljord, K.; Holmen, A. Methanol Conversion to Light Olefins over SAPO-34: Reaction Network and Deactivation Kinetics. Ind. Eng. Chem. Res. 2007, 46 (12), 4116-4123. https://doi.org/10.1021/ie0610748.
- (178) Bos, A. N. R.; Tromp, P. J. J.; Akse, H. N. Conversion of Methanol to Lower Olefins. Kinetic Modeling, Reactor Simulation, and Selection. Ind. Eng. Chem. Res. 1995, 34 (11), https://doi.org/10.1021/ie00038a018.
- (179) Lee, M.-K.; Kim, J.; Ryu, J.-H.; Yoon, Y.-S.; Kim, C.-U.; Jeong, S.-Y.; Lee, I.-B. Modeling of Reaction and Deactivation Kinetics in Methanol-to-Olefins Reaction on SAPO-34. Ind. Eng. Chem. Res. 2019, 58 (29), 13227–13238. https://doi.org/10.1021/acs.iecr.9b01940.
- (180) Azarhoosh, M. J.; Halladi, R.; Askari, S. Presenting a New Kinetic Model for Methanol to Light Olefins Reactions over a Hierarchical SAPO-34 Catalyst Using the Langmuir-Hinshelwood-Hougen-Watson Mechanism. J. Phys.: Condens. Matter 2017, 29 (42), 425202. https://doi.org/10.1088/1361-648X/aa85f0.
- (181) Mousavi, S. H.; Fatemi, S.; Razavian, M. Kinetic Modeling of the Methanol to Olefins Process in the Presence of Hierarchical SAPO-34 Catalyst: Parameter Estimation, Effect of Reaction Conditions and Lifetime Prediction. Reac Kinet Mech Cat 2017, 122 (2), 1245–1264. https://doi.org/10.1007/s11144-017-
- (182) Fatourehchi, N.; Sohrabi, M.; Royaee, S. J.; Mirarefin, S. M. Preparation of SAPO-34 Catalyst and Presentation of a Kinetic Model for Methanol to Olefin Process (MTO). Chemical Engineering Research and Design 2011, 89 (6), 811–816. https://doi.org/10.1016/j.cherd.2010.10.007.
- (183) Yuan, X.; Li, H.; Ye, M.; Liu, Z. Kinetic Modeling of Methanol to Olefins Process over SAPO-34 Catalyst Based on the Dual-Cycle Reaction Mechanism. AIChE Journal 2019, 65 (2), 662-674. https://doi.org/10.1002/aic.16439.
- (184) Wang, C.; Wang, W.; Sun, Y.; Pan, Y.; Feng, S. Hybrid Modeling of Methanol to Olefin Reaction Kinetics Based on the Artificial Neural Network. Ind. Eng. Chem. Res. 2024, 63 (12), 5065-5077. https://doi.org/10.1021/acs.iecr.3c04190.
- (185) Wang, Z.; Wang, L.; Yuan, Z.; Chen, B. Data-Driven Optimal Operation of the Industrial Methanol to Olefin Process Based on Relevance Vector Machine. Chinese Journal of Chemical Engineering 2021, 34, 106–115. https://doi.org/10.1016/j.cjche.2020.09.040.
- (186) Gao, M.; Li, H.; Yang, M.; Zhou, J.; Yuan, X.; Tian, P.; Ye, M.; Liu, Z. A Modeling Study on Reaction and Diffusion in MTO Process over SAPO-34 Zeolites. Chemical Engineering Journal 2019, 377, 119668. https://doi.org/10.1016/j.cej.2018.08.054.

- (187) Cnudde, P.; Demuynck, R.; Vandenbrande, S.; Waroquier, M.; Sastre, G.; Speybroeck, V. V. Light Olefin Diffusion during the MTO Process on H-SAPO-34: A Complex Interplay of Molecular Factors. J. Am. Chem. Soc. 2020, 142 (13), 6007–6017. https://doi.org/10.1021/jacs.9b10249.
- (188) Gao, M.; Li, H.; Liu, W.; Xu, Z.; Peng, S.; Yang, M.; Ye, M.; Liu, Z. Imaging Spatiotemporal Evolution of Molecules and Active Sites in Zeolite Catalyst during Methanol-to-Olefins Reaction. Nat Commun 2020, 11 (1), 3641. https://doi.org/10.1038/s41467-020-17355-6.
- (189) Rui, P.; Wang, B.; Chen, F.; Xiang, Y.; Yang, J.; Guo, T.; Wu, Z.; Liao, W.; Shu, X. The Hydrothermal Synthesis of Hierarchical SAPO-34 with Improved MTO Performance. New Journal of Chemistry 2021, 45 (25), 11093–11100. https://doi.org/10.1039/D1NJ01066B.
- (190) Tan, J.; Liu, Z.; Bao, X.; Liu, X.; Han, X.; He, C.; Zhai, R. Crystallization and Si Incorporation Mechanisms SAPO-34. *Microporous* and Mesoporous *Materials* 2002. 53 https://doi.org/10.1016/S1387-1811(02)00329-3.
- (191) Ashtekar, S.; Chilukuri, S. V. V.; Chakrabarty, D. K. Small-Pore Molecular Sieves SAPO-34 and SAPO-44 with Chabazite Structure: A Study of Silicon Incorporation. Journal of Physical Chemistry 1994, 98 (18), 4878–4883. https://doi.org/10.1021/J100069A018.
- (192) Sastre, G.; Lewis, D. W.; Richard, C.; Catlow, A. Modeling of Silicon Substitution in SAPO-5 and SAPO-34 Molecular Sieves. Journal of Physical Chemistry B 1997, 101 (27), https://doi.org/10.1021/JP963736K.
- (193) Yuan, D.; Xing, A.; Miao, P.; Sun, Q.; Cui, L.; Wang, H.; Ma, L.; Chiang, F. K.; Kong, J. Assembly of Sub-Crystals on the Macroscale and Construction of Composite Building Units on the Microscale for Chemistry Journal 2018. SAPO-34. Asian 13 (20),3063-3072. https://doi.org/10.1002/ASIA.201801069.
- Sutrisno, A.; Lucier, B. E. G.; Zhang, L.; Ding, L.; Chu, Y.; Zheng, A.; Huang, Y. Inspecting the Structure and Formation of Molecular Sieve SAPO-34 via 17O Solid-State NMR Spectroscopy. Journal of Physical Chemistry C 2018, 122 (13), 7260–7277. https://doi.org/10.1021/ACS.JPCC.8B00746.
- (195) Cnudde, P.; Demuynck, R.; Vandenbrande, S.; Waroquier, M.; Sastre, G.; Speybroeck, V. Van. Light Olefin Diffusion during the MTO Process on H-SAPO-34: A Complex Interplay of Molecular Factors. Chemical 2020, 142 (13),6007-6017. Journal of the American Society https://doi.org/10.1021/JACS.9B10249.
- (196) Lin, S.; Li, J.; Sharma, R. P.; Yu, J.; Xu, R. Fabrication of SAPO-34 Crystals with Different Morphologies by Microwave Heating. Topics in Catalysis 2010, 53 (19–20), 1304–1310. https://doi.org/10.1007/s11244-010-9588-3.
- (197) Zhao, L.; Yang, G.; Hu, H.; Sun, Y.; Ma, Z.; Peng, P.; Ng, E. P.; Tian, P.; Guo, H.; Svetlana, M. SAPO-34 Crystals with Nanosheet Morphology Synthesized by Pyrophosphoric Acid as New Phosphorus Source. and Mesoporous Materials 2022, 333. 111753. https://doi.org/10.1016/J.MICROMESO.2022.111753.
- (198) Carreon, M. A.; Li, S.; Falconer, J. L.; Noble, R. D. SAPO-34 Seeds and Membranes Prepared Using Multiple Structure Directing Agents. Advanced Materials 2008. 20 (4),729–732. https://doi.org/10.1002/ADMA.200701280.
- (199) Enhancing the Stability of Methanol-to-Olefins Reaction Catalyzed by SAPO-34 Zeolite in the Presence of CO2Oxygen-Vacancy-Rich *ZnCeZrOx* ACS Catalysis. https://pubs.acs.org/doi/full/10.1021/acscatal.3c04707 (accessed 2025-09-24).
- (200) Controlling the SAPO-34 Particle Size to Enhance Reaction-Diffusion Behavior for Improving Catalytic the MTO Reaction Industrial & Engineering Chemistry https://pubs.acs.org/doi/full/10.1021/acs.iecr.3c00555 (accessed 2025-09-24).
- (201) Setting up In2O3-ZrO2/SAPO-34 Catalyst for Improving Olefin Production via Hydrogenation of CO2/CO Mixtures. https://www.mdpi.com/2073-4344/13/7/1101 (accessed 2025-09-24).
- (202) Theoretical study of the influence of H-SAPO-34 modified with Zn2+ on the formation of butadiene -ScienceDirect. https://www.sciencedirect.com/science/article/pii/S0009250923002087 (accessed 2025-09-
- (203) Sun, Q.; Xie, Z.; Yu, J. The State-of-the-Art Synthetic Strategies for SAPO-34 Zeolite Catalysts in Methanol-to-Olefin Conversion. Natl Sci Rev 2018, 5 (4), 542–558. https://doi.org/10.1093/nsr/nwx103.

- (204) Zhang, W.; Lin, S.; Wei, Y.; Tian, P.; Ye, M.; Liu, Z. Cavity-Controlled Methanol Conversion over Zeolite Catalysts. Natl Sci Rev 2023, 10 (9), nwad120. https://doi.org/10.1093/nsr/nwad120.
- (205) Jiang, S.; Zhou, H.; Zhang, X.; Zhou, X.; Chowdhury, A. D. Assessing the Effects of Dealumination and Bifunctionalization on 8-Membered Ring Zeolite/Zeo-Type Materials in the Methanol-to-Olefin Catalytic Process. Catal. Sci. Technol. 2024, 14 (12), 3346–3363. https://doi.org/10.1039/D4CY00110A.
- (206) Shen, W.; Li, X.; Wei, Y.; Tian, P.; Deng, F.; Han, X.; Bao, X. A Study of the Acidity of SAPO-34 by Solid-State NMR Spectroscopy. Microporous and Mesoporous Materials 2012, 158, 19–25. https://doi.org/10.1016/j.micromeso.2012.03.013.
- (207) Li, J.; Wei, Y.; Liu, G.; Qi, Y.; Tian, P.; Li, B.; He, Y.; Liu, Z. Comparative Study of MTO Conversion over SAPO-34, H-ZSM-5 and H-ZSM-22: Correlating Catalytic Performance and Reaction Mechanism to Zeolite Topology. Catalysis Today 2011, 171 (1), 221–228. https://doi.org/10.1016/j.cattod.2011.02.027.
- (208) Qi, G.; Xie, Z.; Yang, W.; Zhong, S.; Liu, H.; Zhang, C.; Chen, Q. Behaviors of Coke Deposition on SAPO-34 Catalyst during Methanol Conversion to Light Olefins. Fuel Processing Technology 2007, 88 (5), 437– 441. https://doi.org/10.1016/j.fuproc.2006.11.008.
- (209) Huang, Y.; Ma, H.; Xu, Z.; Qian, W.; Zhang, H.; Ying, W. Utilization of SAPO-18 or SAPO-35 in the Bifunctional Catalyst for the Direct Conversion of Syngas to Light Olefins. RSC Adv. 2021, 11 (23), 13876— 13884. https://doi.org/10.1039/D1RA02087K.
- (210) Castellanos-Beltran, I. J.; Assima, G. P.; Lavoie, J.-M. Effect of Temperature in the Conversion of Methanol to Olefins (MTO) Using an Extruded SAPO-34 Catalyst. Front. Chem. Sci. Eng. 2018, 12 (2), 226–238. https://doi.org/10.1007/s11705-018-1709-8.
- (211) Müller, S.; Liu, Y.; Vishnuvarthan, M.; Sun, X.; van Veen, A. C.; Haller, G. L.; Sanchez-Sanchez, M.; Lercher, J. A. Coke Formation and Deactivation Pathways on H-ZSM-5 in the Conversion of Methanol to Olefins. Journal of Catalysis 2015, 325, 48–59. https://doi.org/10.1016/j.jcat.2015.02.013.
- (212) Yang, L.; Wang, C.; Zhang, L.; Dai, W.; Chu, Y.; Xu, J.; Wu, G.; Gao, M.; Liu, W.; Xu, Z.; Wang, P.; Guan, N.; Dyballa, M.; Ye, M.; Deng, F.; Fan, W.; Li, L. Stabilizing the Framework of SAPO-34 Zeolite toward Long-Term Methanol-to-Olefins Conversion. Nat Commun 2021, https://doi.org/10.1038/s41467-021-24403-2.
- (213) Li, L.; Cui, X.; Li, J.; Wang, J. Synthesis of SAPO-34/ZSM-5 Composite and Its Catalytic Performance in the Conversion of Methanol to Hydrocarbons. J. Braz. Chem. Soc. 2015, 26, 290-296. https://doi.org/10.5935/0103-5053.20140279.
- Akhgar, S.; Towfighi, J.; Hamidzadeh, M. MTO Performance over Seed-Assisted SAPO-34 Zeolites Synthesized by Reducing Template Consumption. Journal of Materials Research and Technology 2020, 9 (6), 12126–12136. https://doi.org/10.1016/J.JMRT.2020.08.067.
- (215) Sun, Q.; Wang, N.; Bai, R.; Chen, G.; Shi, Z.; Zou, Y.; Yu, J. Mesoporogen-Free Synthesis of Hierarchical SAPO-34 with Low Template Consumption and Excellent Methanol-to-Olefin Conversion. *ChemSusChem* **2018**, 11 (21), 3812–3820. https://doi.org/10.1002/CSSC.201801486.
- (216) Valizadeh, B.; Askari, S.; Halladj, R.; Haghmoradi, A. Effect of Synthesis Conditions on Selective Formation of SAPO-5 and SAPO-34. Synthesis and Reactivity in Inorganic, Metal-Organic, and Nano-Metal Chemistry 2013, 44 (1), 79–83. https://doi.org/10.1080/15533174.2013.768646.
- (217) Thommes, M.; Kaneko, K.; Neimark, A. V.; Olivier, J. P.; Rodriguez-Reinoso, F.; Rouquerol, J.; Sing, K. S. W. Physisorption of Gases, with Special Reference to the Evaluation of Surface Area and Pore Size Distribution (IUPAC Technical Report). Pure and Applied Chemistry 2015, 87 (9-10), 1051-1069. https://doi.org/10.1515/PAC-2014-1117.
- (218) Chen, X.; Xi, D.; Sun, Q.; Wang, N.; Dai, Z.; Fan, D.; Valtchev, V.; Yu, J. A Top-down Approach to Hierarchical SAPO-34 Zeolites with **Improved** Selectivity **2016**. https://doi.org/10.1016/j.micromeso.2016.07.045.
- (219) Yang, H.; Liu, Z.; Gao, H.; Xie, Z. Synthesis and Catalytic Performances of Hierarchical SAPO-34 Monolith. Journal of Materials Chemistry 2010, 20 (16), 3227–3231. https://doi.org/10.1039/b924736j.
- (220)Gong, J.; Tong, F.; Ji, X.; Zeng, C.; Wang, C.; Lv, Y.; Zhang, L. Hollow SAPO-34 Cubes with Hierarchically Organized Internal Structure. Crystal Growth and Design 2014, 14 (8), 3857–3863. https://doi.org/10.1021/CG500382W.

- (221) Wu, L.; Liu, Z.; Xia, L.; Qiu, M.; Liu, X.; Zhu, H.; Sun, Y. Effect of SAPO-34 Molecular Sieve Morphology on Methanol to Olefins Performance. *Cuihua Xuebao/Chinese Journal of Catalysis* **2013**, *34* (7), 1348–1356. https://doi.org/10.1016/s1872-2067(12)60575-0.
- (222) Sun, C.; Wang, Y.; Zhao, A.; Wang, X.; Wang, C.; Zhang, X.; Wang, Z.; Zhao, J.; Zhao, T. Synthesis of Nano-Sized SAPO-34 with Morpholine-Treated Micrometer-Seeds and Their Catalytic Performance in Methanol-to-Olefin Reactions. *Applied Catalysis A: General* **2020**, *589*, 117314. https://doi.org/10.1016/J.APCATA.2019.117314.
- (223) Van Heyden, H.; Mintova, S.; Bein, T. Nanosized SAPO-34 Synthesized from Colloidal Solutions. *Chemistry of Materials* **2008**, *20* (9), 2956–2963. https://doi.org/10.1021/cm703541w.
- (224) Lee, Y. J.; Baek, S. C.; Jun, K. W. Methanol Conversion on SAPO-34 Catalysts Prepared by Mixed Template Method. *Applied Catalysis A: General* **2007**, *329*, 130–136. https://doi.org/10.1016/j.apcata.2007.06.034.
- (225) Yang, H.; Miao, P.; Sun, Q.; Zhang, Y.; Tian, D. Dual Templating Fabrication of Hollow SAPO-34 Molecular Sieves for Enhanced MTO Catalytic Activity and Selectivity. *Crystal Research and Technology* **2019**, *54* (2), 1800132. https://doi.org/10.1002/CRAT.201800132.
- (226) Mazzoli, A.; Favoni, O. Particle Size, Size Distribution and Morphological Evaluation of Airborne Dust Particles of Diverse Woods by Scanning Electron Microscopy and Image Processing Program. *Powder Technology* **2012**, *225*, 65–71. https://doi.org/10.1016/J.POWTEC.2012.03.033.
- (227) Charghand, M.; Haghighi, M.; Aghamohammadi, S. The Beneficial Use of Ultrasound in Synthesis of Nanostructured Ce-Doped SAPO-34 Used in Methanol Conversion to Light Olefins. *Ultrasonics Sonochemistry* **2014**, *21* (5), 1827–1838. https://doi.org/10.1016/J.ULTSONCH.2014.03.011.
- (228) Inkson, B. J. Scanning Electron Microscopy (SEM) and Transmission Electron Microscopy (TEM) for Materials Characterization. *Materials Characterization Using Nondestructive Evaluation (NDE) Methods* **2016**, 17–43. https://doi.org/10.1016/B978-0-08-100040-3.00002-X.
- (229) Gu, Y.; Chen, P.; Wang, X.; Lyu, Y.; Liu, W.; Liu, X.; Yan, Z. Active Sites and Induction Period of Fe/ZSM-5 Catalyst in Methane Dehydroaromatization. *ACS Catalysis* **2021**, *11* (12), 6771–6786. https://doi.org/10.1021/ACSCATAL.1C01467.
- (230) Sena, F. C.; De Souza, B. F.; De Almeida, N. C.; Cardoso, J. S.; Fernandes, L. D. Influence of Framework Composition over SAPO-34 and MeAPSO-34 Acidity. *Applied Catalysis A: General* **2011**, *406* (1–2), 59–62. https://doi.org/10.1016/J.APCATA.2011.08.010.
- (231) Sedighi, M.; Ghasemi, M.; Sadeqzadeh, M.; Hadi, M. Thorough Study of the Effect of Metal-Incorporated SAPO-34 Molecular Sieves on Catalytic Performances in MTO Process. *Powder Technology* **2016**, *291*, 131–139. https://doi.org/10.1016/J.POWTEC.2015.11.066.
- (232) Akhoundzadeh, H.; Taghizadeh, M.; Sharifi Pajaie, H. Synthesis of Highly Selective and Stable Mesoporous Ni–Ce/SAPO-34 Nanocatalyst for Methanol-to-Olefin Reaction: Role of Polar Aprotic N,N-Dimethylformamide Solvent. *Particuology* **2018**, 40, 113–122. https://doi.org/10.1016/j.partic.2017.11.004.
- (233) Hashemi, F.; Taghizadeh, M.; Rami, M. D. Polyoxometalate Modified SAPO-34: A Highly Stable and Selective Catalyst for Methanol Conversion to Light Olefins. *Microporous and Mesoporous Materials* **2020**, *295*, 109970. https://doi.org/10.1016/J.MICROMESO.2019.109970.
- (234) Kline, W. E.; Scott Fogler, H. Dissolution of Silicate Minerals by Hydrofluoric Acid. *ACS Publications* **1981**, *23* (120), 141.
- (235) Chen, X.; Jiang, R.; Zhou, Z.; Wang, X. Synthesis of SAPO-34 Zeolite from Laponite and Its Application in the MTO Reaction. *European Journal of Inorganic Chemistry* **2020**, *2020* (22), 2170–2176. https://doi.org/10.1002/EJIC.202000183.
- (236) Lee, S. U.; Lee, Y. J.; Kim, J. R.; Jeong, K. E.; Jeong, S. Y. Cobalt-Isomorphous Substituted SAPO-34 via Milling and Recrystallization for Enhanced Catalytic Lifetime toward Methanol-to-Olefin Reaction. *Journal of Industrial and Engineering Chemistry* **2019**, *79*, 443–451. https://doi.org/10.1016/J.JIEC.2019.07.020.
- (237) Zhong, J.; Han, J.; Wei, Y.; Xu, S.; Sun, T.; Guo, X.; Song, C.; Liu, Z. Enhancing Ethylene Selectivity in MTO Reaction by Incorporating Metal Species in the Cavity of SAPO-34 Catalysts. *Chinese Journal of Catalysis* **2018**, *39* (11), 1821–1831. https://doi.org/10.1016/S1872-2067(18)63141-9.

Journal of Materials Chemistry A Accepted Manuscrip

This article is licensed under a Creative Commons Attribution-NonCommercial 3.0 Unported Licence.

- (238) Zhong, J.; Han, J.; Wei, Y.; Xu, S.; Sun, T.; Guo, X.; Song, C.; Liu, Z. The Template-Assisted Zinc Ion Incorporation in SAPO-34 and the Enhanced Ethylene Selectivity in MTO Reaction. Journal of Energy Chemistry 2019, 32, 174–181. https://doi.org/10.1016/J.JECHEM.2018.07.017.
- (239) Yao, J.; Jiao, J.; Liu, R.; Zha, F.; Guo, X.; Tang, X.; Tian, H.; Chang, Y. Template-Assisted Preparation of Metal-Modified SAPO-34 Molecular Sieves for the Catalysis of Methanol-to-Olefins. Korean Journal of Chemical Engineering 2021, 38 (7), 1381–1393. https://doi.org/10.1007/S11814-021-0793-5.
- (240) Salmasi, M.; Fatemi, S.; Najafabadi, A. T. Improvement of Light Olefins Selectivity and Catalyst Lifetime in MTO Reaction; Using Ni and Mg-Modified SAPO-34 Synthesized by Combination of Two Templates. Journal Industrial and Engineering Chemistry 2011, 17 (4),755-761. https://doi.org/10.1016/J.JIEC.2011.05.031.
- (241) Lee, S. U.; Lee, Y. J.; Kim, J. R.; Jeong, K. E.; Jeong, S. Y. Cobalt-Isomorphous Substituted SAPO-34 via Milling and Recrystallization for Enhanced Catalytic Lifetime toward Methanol-to-Olefin Reaction. 79, Journal Industrial and Engineering Chemistry 2019, 443-451. of https://doi.org/10.1016/J.JIEC.2019.07.020.
- (242) Huang, H.; Wang, H.; Zhu, H.; Zhang, S.; Zhang, Q.; Li, C. Enhanced Ethene to Propene Ratio over Zn-Modified SAPO-34 Zeolites in Methanol-to-Olefin Reaction. Catalysis Science & Technology 2019, 9 (9), 2203–2210. https://doi.org/10.1039/C9CY00335E.
- (243) Li, Z.; Martínez-Triguero, J.; Yu, J.; Corma, A. Conversion of Methanol to Olefins: Stabilization of Nanosized SAPO-34 by Hydrothermal Treatment. Journal of Catalysis 2015, 329, 379–388. https://doi.org/10.1016/J.JCAT.2015.05.025.
- (244) Ashtekar, S.; Chilukuri, S. V. V.; Chakrabarty, D. K. Small-Pore Molecular Sieves SAPO-34 and SAPO-44 with Chabazite Structure: A Study of Silicon Incorporation. Journal of Physical Chemistry 1994, 98 (18), 4878–4883. https://doi.org/10.1021/J100069A018.
- (245) Anderson, M. W.; Sulikowski, B.; Barrie, P. J.; Klinowski, J. In Situ Solid-State NMR Studies of the Catalytic Conversion of Methanol on the Molecular Sieve SAPO-34. *Journal of Physical Chemistry* **1990**, 94 (7), 2730–2734. https://doi.org/10.1021/J100370A002.
- (246) Tan, J.; Liu, Z.; Bao, X.; Liu, X.; Han, X.; He, C.; Zhai, R. Crystallization and Si Incorporation Mechanisms SAPO-34. *Microporous* and Mesoporous Materials 2002. 53 (1-3),97-108.https://doi.org/10.1016/S1387-1811(02)00329-3.
- (247) Álvaro-Muñoz, T.; Márquez-Álvarez, C.; Sastre, E. Use of Different Templates on SAPO-34 Synthesis: Effect on the Acidity and Catalytic Activity in the MTO Reaction. Catalysis Today 2012, 179 (1), 27–34. https://doi.org/10.1016/J.CATTOD.2011.07.038.
- (248) Zhu, Q.; Kondo, J. N.; Ohnuma, R.; Kubota, Y.; Yamaguchi, M.; Tatsumi, T. The Study of Methanol-to-Olefin over Proton Type Aluminosilicate CHA Zeolites. *Microporous and Mesoporous Materials* 2008, 112 (1-3), 153–161. https://doi.org/10.1016/J.MICROMESO.2007.09.026.
- (249) Wilson, S.; Barger, P. The Characteristics of SAPO-34 Which Influence the Conversion of Methanol to Olefins. *Microporous* and Mesoporous Materials 1999. (1-2),https://doi.org/10.1016/S1387-1811(98)00325-4.
- (250) Gong, F.; Wang, X.; Wang, P.; Xuan, L.; Li, Z.; Zhu, Y. Facile Synthesis of SAPO-34 with Excellent Methanol-to-Olefin Activity in a Short Time via a Conventional Hydrothermal Method. New Journal of Chemistry 2020, 44 (25), 10410–10417. https://doi.org/10.1039/D0NJ01550D.
- (251) Blackwell, C. S.; Patton, R. L. Aluminum-27 and Phosphorus-31 Nuclear Magnetic Resonance Studies of Aluminophosphate Molecular Sieves. Journal of Physical Chemistry 1984, 88 (25), 6135–6139. https://doi.org/10.1021/J150669A016.
- (252) Yao, J.; Tian, H.; Zha, F.; Ma, S.; Tang, X.; Chang, Y.; Guo, X. Regulating the Size and Acidity of SAPO-34 Zeolites Using Dual Templates to Enhance the Selectivity of Light Olefins in MTO. New Journal of Chemistry 2021, 45 (26), 11812–11822. https://doi.org/10.1039/D1NJ01845K.
- (253) Jin, W.; Wang, B.; Tuo, P.; Li, C.; Li, L.; Zhao, H.; Gao, X.; Shen, B. Selective Desilication, Mesopores Formation, and MTO Reaction Enhancement via Citric Acid Treatment of Zeolite SAPO-34. Industrial Engineering Chemistry Research 57 4231-4236. 2018. (12),https://doi.org/10.1021/ACS.IECR.8B00632.

- (254) Chen, X.; Vicente, A.; Qin, Z.; Ruaux, V.; Gilson, J. P.; Valtchev, V. The Preparation of Hierarchical SAPO-34 Crystals via Post-Synthesis Fluoride Etching. *Chemical Communications* **2016**, *52* (17), 3512–3515. https://doi.org/10.1039/C5CC09498D.
- (255) Yakimov, A. V.; Ravi, M.; Verel, R.; Sushkevich, V. L.; Van Bokhoven, J. A.; Copéret, C. Structure and Framework Association of Lewis Acid Sites in MOR Zeolite. *Journal of the American Chemical Society* **2022**, 144 (23), 10377–10385. https://doi.org/10.1021/JACS.2C02212/ASSET/IMAGES/LARGE/JA2C02212 0004.JPEG.
- (256) Prakash, A. M.; Unnikrishnan, S. Synthesis of SAPO-34: High Silicon Incorporation in the Presence of Morpholine as Template. *Journal of the Chemical Society, Faraday Transactions* **1994**, *90* (15), 2291–2296. https://doi.org/10.1039/FT9949002291.
- (257) Zibrowius, B.; Löffler, E.; Hunger, M. Multinuclear MAS n.m.r. and i.r. Spectroscopic Study of Silicon Incorporation into SAPO-5, SAPO-31, and SAPO-34 Molecular Sieves. *Zeolites* **1992**, *12* (2), 167–174. https://doi.org/10.1016/0144-2449(92)90079-5.
- (258) Gao, S.; Xu, S.; Wei, Y.; Qiao, Q.; Xu, Z.; Wu, X.; Zhang, M.; He, Y.; Xu, S.; Liu, Z. Insight into the Deactivation Mode of Methanol-to-Olefins Conversion over SAPO-34: Coke, Diffusion, and Acidic Site Accessibility. *Journal of Catalysis* **2018**, *367*, 306–314. https://doi.org/10.1016/J.JCAT.2018.09.010.
- (259) Guisnet, M.; Magnoux, P. Organic Chemistry of Coke Formation. *Applied Catalysis A: General* **2001**, *212* (1–2), 83–96. https://doi.org/10.1016/S0926-860X(00)00845-0.
- (260) Haw, J. F.; Song, W.; Marcus, D. M.; Nicholas, J. B. The Mechanism of Methanol to Hydrocarbon Catalysis. *Accounts of Chemical Research* **2003**, *36* (5), 317–326. https://doi.org/10.1021/AR020006O.
- (261) Yu, B.; Zhang, W.; Wei, Y.; Wu, X.; Sun, T.; Fan, B.; Xu, S.; Liu, Z. Capture and Identification of Coke Precursors to Elucidate the Deactivation Route of the Methanol-to-Olefin Process over H-SAPO-34. *Chemical Communications* **2020**, *56* (58), 8063–8066. https://doi.org/10.1039/D0CC02408B.
- (262) Li, Y.; Huang, Y.; Guo, J.; Zhang, M.; Wang, D.; Wei, F.; Wang, Y. Hierarchical SAPO-34/18 Zeolite with Low Acid Site Density for Converting Methanol to Olefins. *Catalysis Today* **2014**, *233*, 2–7. https://doi.org/10.1016/J.CATTOD.2014.03.038.
- (263) Chen, D.; Moljord, K.; Fuglerud, T.; Holmen, A. The Effect of Crystal Size of SAPO-34 on the Selectivity and Deactivation of the MTO Reaction. *Microporous and Mesoporous Materials* **1999**, *29* (1–2), 191–203. https://doi.org/10.1016/S1387-1811(98)00331-X.
- (264) Askari, S.; Halladj, R.; Sohrabi, M. Methanol Conversion to Light Olefins over Sonochemically Prepared SAPO-34 Nanocatalyst. *Microporous and Mesoporous Materials* **2012**, *163*, 334–342. https://doi.org/10.1016/J.MICROMESO.2012.07.041.
- (265) Dai, W.; Wu, G.; Li, L.; Guan, N.; Hunger, M. Mechanisms of the Deactivation of SAPO-34 Materials with Different Crystal Sizes Applied as MTO Catalysts. *ACS Catalysis* **2013**, *3* (4), 588–596. https://doi.org/10.1021/CS400007V.
- (266) Peng, Q.; Wang, G.; Wang, Z.; Jiang, R.; Wang, D.; Chen, J.; Huang, J. Tuning Hydrocarbon Pool Intermediates by the Acidity of SAPO-34 Catalysts for Improving Methanol-to-Olefins Reaction. *ACS Sustainable Chemistry & Engineering* **2018**, 6 (12), 16867–16875. https://doi.org/10.1021/ACSSUSCHEMENG.8B04210.
- (267) Lee, K. Y.; Chae, H. J.; Jeong, S. Y.; Seo, G. Effect of Crystallite Size of SAPO-34 Catalysts on Their Induction Period and Deactivation in Methanol-to-Olefin Reactions. *Applied Catalysis A: General* **2009**, 369 (1–2), 60–66. https://doi.org/10.1016/j.apcata.2009.08.033.
- (268) Ren, S.; Liu, G.; Wu, X.; Chen, X.; Wu, M.; Zeng, G.; Liu, Z.; Sun, Y. Enhanced MTO Performance over Acid Treated Hierarchical SAPO-34. *Chinese Journal of Catalysis* **2017**, *38* (1), 123–130. https://doi.org/10.1016/S1872-2067(16)62557-3.
- (269) Yang, G.; Wei, Y.; Xu, S.; Chen, J.; Li, J.; Liu, Z.; Yu, J.; Xu, R. Nanosize-Enhanced Lifetime of SAPO-34 Catalysts in Methanol-to-Olefin Reactions. *Journal of Physical Chemistry C* **2013**, *117* (16), 8214–8222. https://doi.org/10.1021/JP312857P.
- (270) Zhao, X.; Li, J.; Tian, P.; Wang, L.; Li, X.; Lin, S.; Guo, X.; Liu, Z. Achieving a Superlong Lifetime in the Zeolite-Catalyzed MTO Reaction under High Pressure: Synergistic Effect of Hydrogen and Water. **2019**. https://doi.org/10.1021/acscatal.8b04402.

Journal of Materials Chemistry A Accepted Manuscrip

View Article Online DOI: 10.1039/D5TA05195A

Journal of Materials Chemistry A

This article is licensed under a Creative Commons Attribution-NonCommercial 3.0 Unported Licence.

- (271) Izadbakhsh, A.; Farhadi, F.; Khorasheh, F.; Sahebdelfar, S.; Asadi, M.; Feng, Y. Z. Effect of SAPO-34's Composition on Its Physico-Chemical Properties and Deactivation in MTO Process. Applied Catalysis A: General 2009, 364 (1–2), 48–56. https://doi.org/10.1016/j.apcata.2009.05.022.
- (272) Wang, C.; Yang, M.; Tian, P.; Xu, S.; Yang, Y.; Wang, D.; Yuan, Y.; Liu, Z. Dual Template-Directed Synthesis of SAPO-34 Nanosheet Assemblies with Improved Stability in the Methanol to Olefins Reaction. Journal of Materials Chemistry A 2015, 3 (10), 5608-5616. https://doi.org/10.1039/c4ta06124a.
- (273) Guo, L.; Zhu, W.; Xing, A.; Li, F.; Guo, Z. Morphology Control of SAPO-34 and Its Catalytic Performance for Methanol to Olefin Reaction. New Journal of Chemistry 2022, 46 (11), 5171-5175. https://doi.org/10.1039/D2NJ00336H.
- (274) Wang, P.; Lv, A.; Hu, J.; Xu, J.; Lu, G. The Synthesis of SAPO-34 with Mixed Template and Its Catalytic Performance for Methanol to Olefins Reaction. *Microporous and Mesoporous Materials* **2012**, 152, 178– 184. https://doi.org/10.1016/J.MICROMESO.2011.11.037.
- (275) Sedighi, M.; Bahrami, H.; Towfighi Darian, J. Thorough Investigation of Varying Template Combinations on SAPO-34 Synthesis, Catalytic Activity and Stability in the Methanol Conversion to Light Olefin. RSC Advances **2014**, 4 (91), 49762–49769. https://doi.org/10.1039/C4RA08607D.
- Borade, R. B.; Clearfield, A. A Comparative Study of Acidic Properties of SAPO-5, -11, -34 and -37 Molecular Sieves. Journal of Molecular Catalysis 1994, 88 (2), 249–265. https://doi.org/10.1016/0304-5102(93)E0262-F.
- (277) Martins, G. V. A.; Berlier, G.; Bisio, C.; Coluccia, S.; Pastore, H. O.; Marchese, L. Quantification of Brønsted Acid Sites in Microporous Catalysts by a Combined FTIR and NH3-TPD Study. Journal of Physical Chemistry C 2008, 112 (18), 7193–7200. https://doi.org/10.1021/jp710613q.
- (278) Lok, B. M.; Messina, C. A.; Patton, R. L.; Gajek, R. T.; Cannan, T. R.; Flanigen, E. M. Crystalline Silicoaluminophosphates. US4440871A, April 3, 1984. https://patents.google.com/patent/US4440871A/en (accessed 2024-09-09).
- (279) Yu, W.; Wu, X.; Cheng, B.; Tao, T.; Min, X.; Mi, R.; Huang, Z.; Fang, M.; Liu, Y. Synthesis and Applications of SAPO-34 Molecular Sieves. Chemistry – A European Journal 2022, 28 (11). https://doi.org/10.1002/CHEM.202102787.
- (280) Izadbakhsh, A.; Farhadi, F.; Khorasheh, F.; Sahebdelfar, S.; Asadi, M.; Yan, Z. F. Key Parameters in Hydrothermal Synthesis and Characterization of Low Silicon Content SAPO-34 Molecular Sieve. (1-2),*Microporous* and Mesoporous Materials 2009. 1-7.https://doi.org/10.1016/J.MICROMESO.2008.12.009.
- (281) Li, Z.-H.; Li, X.-F.; Di, C.-Y.; Dou, T.; Chen, S.-L. A Green and Cost-Effective Synthesis of Hierarchical SAPO-34 through Dry Gel Conversion and Its Performance in a Methanol-to-Olefin Reaction. *Ind. Eng.* Chem. Res. 2021, 60 (43), 15380–15390. https://doi.org/10.1021/acs.iecr.1c02782.
- (282) Wang, P.; Yang, D.; Hu, J.; Xu, J.; Lu, G. Synthesis of SAPO-34 with Small and Tunable Crystallite Size by Two-Step Hydrothermal Crystallization and Its Catalytic Performance for MTO Reaction. Catalysis Today 2013, 212, 62.e1-62.e8. https://doi.org/10.1016/j.cattod.2012.08.027.
- (283) Han, L.; Yan, X.; Guo, L.; Duan, Y.; Wang, Z.; Lu, T.; Xu, J.; Zhan, Y.; Wang, J. Ionothermal Synthesis of Triclinic SAPO-34 Zeolites. Catalysts 2021, 11 (5), 616. https://doi.org/10.3390/catal11050616.
- (284) Askari, S.; Halladj, R. Ultrasonic Pretreatment for Hydrothermal Synthesis of SAPO-34 Nanocrystals. Ultrasonics Sonochemistry 2012, 19 (3), 554–559. https://doi.org/10.1016/J.ULTSONCH.2011.09.006.
- (285) Álvaro-Muñoz, T.; Sastre, E.; Márquez-Álvarez, C. Microwave-Assisted Synthesis of Plate-like SAPO-34 Nanocrystals with Increased Catalyst Lifetime in the Methanol-to-Olefin Reaction. Catalysis Science & Technology **2014**, 4 (12), 4330–4339. https://doi.org/10.1039/C4CY00775A.
- (286) Hirota, Y.; Murata, K.; Tanaka, S.; Nishiyama, N.; Egashira, Y.; Ueyama, K. Dry Gel Conversion Synthesis of SAPO-34 Nanocrystals. Materials Chemistry and Physics 2010, 123 (2-3), 507-509. https://doi.org/10.1016/j.matchemphys.2010.05.005.
- (287) Dumitriu, E.; Azzouz, A.; Hulea, V.; Lutic, D.; Kessler, H. Synthesis, Characterization and Catalytic Activity of SAPO-34 Obtained with Piperidine as Templating Agent. Microporous Materials 1997, 10 (1– 3), 1–12. https://doi.org/10.1016/S0927-6513(96)00107-1.

Open Access Article. Published on 22 2025. Downloaded on 30.10.2025 01:47:29.

(288) Doan, T.; Nguyen, K.; Dam, P.; Huyen Vuong, T.; Thang Le, M.; Pham Thanh, H. Synthesis of SAPO-34 Using Different Combinations of Organic Structure-Directing Agents. *Journal of Chemistry* **2019**. https://doi.org/10.1155/2019/6197527.

(289) Liu, P.; Ren, J.; Sun, Y. Influence of Template on Si Distribution of SAPO-11 and Their Performance for n-Paraffin Isomerization. *Microporous and Mesoporous Materials* **2008**, *114* (1–3), 365–372. https://doi.org/10.1016/J.MICROMESO.2008.01.022.

- (290) Lee, Y. J.; Baek, S. C.; Jun, K. W. Methanol Conversion on SAPO-34 Catalysts Prepared by Mixed Template Method. *Applied Catalysis A: General* **2007**, *329*, 130–136. https://doi.org/10.1016/J.APCATA.2007.06.034.
- (291) Rostami, R. B.; Ghavipour, M.; Behbahani, R. M.; Aghajafari, A. Improvement of SAPO-34 Performance in MTO Reaction by Utilizing Mixed-Template Catalyst Synthesis Method. *Journal of Natural Gas Science and Engineering* **2014**, *20*, 312–318. https://doi.org/10.1016/J.JNGSE.2014.07.015.
- (292) Najafi, N.; Askari, S.; Halladj, R. Hydrothermal Synthesis of Nanosized SAPO-34 Molecular Sieves by Different Combinations of Multi Templates. *Powder Technology* **2014**, *254*, 324–330. https://doi.org/10.1016/J.POWTEC.2014.01.037.
- (293) Ye, L.; Cao, F.; Ying, W.; Fang, D.; Sun, Q. Effect of Different TEAOH/DEA Combinations on SAPO-34's Synthesis and Catalytic Performance. *Journal of Porous Materials* **2010**, *18* (2), 225–232. https://doi.org/10.1007/s10934-010-9374-4.
- (294) Wang, P.; Lv, A.; Hu, J.; Xu, J.; Lu, G. The Synthesis of SAPO-34 with Mixed Template and Its Catalytic Performance for Methanol to Olefins Reaction. *Microporous and Mesoporous Materials* **2012**, *152*, 178–184. https://doi.org/10.1016/j.micromeso.2011.11.037.
- (295) Álvaro-Muñoz, T.; Márquez-Álvarez, C.; Sastre, E. Effect of Silicon Content on the Catalytic Behavior of Chabazite Type Silicoaluminophosphate in the Transformation of Methanol to Short Chain Olefins. *Catalysis Today* **2013**, *213*, 219–225. https://doi.org/10.1016/J.CATTOD.2013.04.031.
- (296) Xing, A.; Yuan, D.; Tian, D.; Sun, Q. Controlling Acidity and External Surface Morphology of SAPO-34 and Its Improved Performance for Methanol to Olefins Reaction. *Microporous and Mesoporous Materials* **2019**, *288*. https://doi.org/10.1016/j.micromeso.2019.109562.
- (297) Amoozegar, A.; Haghighi, M.; Aghamohammadi, S. Enhancement of Catalytic Properties and Lifetime of Nanostructured SAPO-34 by La Isomorphous Substitution and Alteration of Si/Al Ratio Used in Methanol Conversion to Light Olefins. *RSC Advances* **2016**, *6* (56), 51024–51036. https://doi.org/10.1039/C6RA02664H.
- (298) Pinilla-Herrero, I.; Olsbye, U.; Márquez-Álvarez, C.; Sastre, E. Effect of Framework Topology of SAPO Catalysts on Selectivity and Deactivation Profile in the Methanol-to-Olefins Reaction. *Journal of Catalysis* **2017**, *352*, 191–207. https://doi.org/10.1016/j.jcat.2017.05.008.
- (299) Sun, Q.; Ma, Y.; Wang, N.; Li, X.; Xi, D.; Xu, J.; Deng, F.; Yoon, K. B.; Oleynikov, P.; Terasaki, O.; Yu, J. High Performance Nanosheet-like Silicoaluminophosphate Molecular Sieves: Synthesis, 3D EDT Structural Analysis and MTO Catalytic Studies †. **2014**. https://doi.org/10.1039/c4ta03419h.
- (300) Xu, L.; Du, A.; Wei, Y.; Wang, Y.; Yu, Z.; He, Y.; Zhang, X.; Liu, Z. Synthesis of SAPO-34 with Only Si(4Al) Species: Effect of Si Contents on Si Incorporation Mechanism and Si Coordination Environment of SAPO-34. *Microporous and Mesoporous Materials* **2008**, *115* (3), 332–337. https://doi.org/10.1016/j.micromeso.2008.02.001.
- (301) Izadbakhsh, A.; Farhadi, F.; Khorasheh, F.; Sahebdelfar, S.; Asadi, M.; Feng, Y. Z. Effect of SAPO-34's Composition on Its Physico-Chemical Properties and Deactivation in MTO Process. *Applied Catalysis A: General* **2009**, *364* (1–2), 48–56. https://doi.org/10.1016/J.APCATA.2009.05.022.
- (302) Rahimi, K.; Towfighi, J.; Sedighi, M.; Masoumi, S.; Kooshki, Z. The Effects of SiO2/Al2O3 and H2O/Al2O3 Molar Ratios on SAPO-34 Catalysts in Methanol to Olefins (MTO) Process Using Experimental Design. *Journal of Industrial and Engineering Chemistry* **2016**, *35*, 123–131. https://doi.org/10.1016/J.JIEC.2015.12.015.
- (303) Barthomeuf, D. Topological Model for the Compared Acidity of SAPOs and SiAl Zeolites. *Zeolites* **1994**, *14* (6), 394–401. https://doi.org/10.1016/0144-2449(94)90164-3.

- (304) Yang, G.; Wei, Y.; Xu, S.; Chen, J.; Li, J.; Liu, Z.; Yu, J.; Xu, R. Nanosize-Enhanced Lifetime of SAPO-34 Catalysts in Methanol-to-Olefin Reactions. *Journal of Physical Chemistry C* **2013**, *117* (16), 8214–8222. https://doi.org/10.1021/JP312857P.
- (305) Nasser, G. A.; Muraza, O.; Nishitoba, T.; Malaibari, Z.; Yamani, Z. H.; Al-Shammari, T. K.; Yokoi, T. Microwave-Assisted Hydrothermal Synthesis of CHA Zeolite for Methanol-to-Olefins Reaction. *Industrial and Engineering Chemistry Research* **2019**, *58* (1), 60–68. https://doi.org/10.1021/ACS.IECR.8B04401.
- (306) Chen, G.; Sun, Q.; Yu, J. Nanoseed-Assisted Synthesis of Nano-Sized SAPO-34 Zeolites Using Morpholine as the Sole Template with Superior MTO Performance. *Chemical Communications* **2017**, *53* (100), 13328–13331. https://doi.org/10.1039/C7CC07508A.
- (307) Zhang, Y.; Ding, H.; Li, L.; Zhu, K.; Liu, J. Generating Nanocrystalline SAPO-34 through Bead-Milling and Porogen-Assisted Recrystallization: Structural Evolution and Catalytic Consequence in Dimethyl Ether-to-Olefin Conversion. *Applied Catalysis A: General* **2022**, *632*, 118483. https://doi.org/10.1016/J.APCATA.2022.118483.
- (308) Xiao, X.; Xu, Z.; Wang, P.; Liu, X.; Fan, X.; Kong, L.; Xie, Z.; Zhao, Z. Solvent-Free Synthesis of Sapo-34 Zeolite with Tunable Sio2/Al2o3 Ratios for Efficient Catalytic Cracking of 1-Butene. *Catalysts* **2021**, *11* (7), 835. https://doi.org/10.3390/CATAL11070835.
- (309) Charghand, M.; Haghighi, M.; Saedy, S.; Aghamohammadi, S. Efficient Hydrothermal Synthesis of Nanostructured SAPO-34 Using Ultrasound Energy: Physicochemical Characterization and Catalytic Performance toward Methanol Conversion to Light Olefins. *Advanced Powder Technology* **2014**, *25* (6), 1728–1736. https://doi.org/10.1016/J.APT.2014.06.022.
- (310) Bakhtiar, S. U. H.; Wang, X.; Ali, S.; Yuan, F.; Li, Z.; Zhu, Y. CTAB-Assisted Size Controlled Synthesis of SAPO-34 and Its Contribution toward MTO Performance. *Dalton Transactions* **2018**, *47* (29), 9861–9870. https://doi.org/10.1039/C8DT01811A.
- (311) Shalmani, F. M.; Halladj, R.; Askari, S. Effect of Contributing Factors on Microwave-Assisted Hydrothermal Synthesis of Nanosized SAPO-34 Molecular Sieves. *Powder Technology* **2012**, *221*, 395–402. https://doi.org/10.1016/J.POWTEC.2012.01.036.
- (312) Álvaro-Muñoz, T.; Sastre, E.; Márquez-Álvarez, C. Microwave-Assisted Synthesis of Plate-like SAPO-34 Nanocrystals with Increased Catalyst Lifetime in the Methanol-to-Olefin Reaction. *Catalysis Science & Technology* **2014**, *4* (12), 4330–4339. https://doi.org/10.1039/C4CY00775A.
- (313) Ranjbaran Lodrijeh, S.; Askari, S.; Halladj, R. Seeding-Induced Nano-Sized SAPO-34 Synthesis with Superior MTO Performance: Energy-Efficient Approach with Highly Reduced OSDA Consumption. *Powder Technology* **2021**, *389*, 383–391. https://doi.org/10.1016/J.POWTEC.2021.05.042.
- (314) Sun, Q.; Wang, N.; Guo, G.; Yu, J. Ultrafast Synthesis of Nano-Sized Zeolite SAPO-34 with Excellent MTO Catalytic Performance. *Chemical Communications* **2015**, *51* (91), 16397–16400. https://doi.org/10.1039/C5CC07343J.
- (315) Sun, Q.; Wang, N.; Bai, R.; Chen, X.; Yu, J. Seeding Induced Nano-Sized Hierarchical SAPO-34 Zeolites: Cost-Effective Synthesis and Superior MTO Performance. *Journal of Materials Chemistry A* **2016**, *4* (39), 14978–14982. https://doi.org/10.1039/c6ta06613e.
- (316) Wang, X.; Li, Z.; Gong, F.; Ma, M.; Zhu, Y. Synthesis of SAPO-34 with Modifying Si Distribution by Seed-Assisted Method and Its Excellent Catalytic Performance for Methanol to Olefins. *Molecular Catalysis* **2021**, *499*, 111312. https://doi.org/10.1016/J.MCAT.2020.111312.
- (317) Lee, S. U.; Lee, Y. J.; Kim, J. R.; Jeong, K. E.; Jeong, S. Y. Cobalt-Isomorphous Substituted SAPO-34 via Milling and Recrystallization for Enhanced Catalytic Lifetime toward Methanol-to-Olefin Reaction. *Journal of Industrial and Engineering Chemistry* **2019**, *79*, 443–451. https://doi.org/10.1016/J.JIEC.2019.07.020.
- (318) Yang, M.; Tian, P.; Wang, C.; Yuan, Y.; Yang, Y.; Xu, S.; He, Y.; Liu, Z. A Top-down Approach to Prepare Silicoaluminophosphate Molecular Sieve Nanocrystals with Improved Catalytic Activity. *Chemical Communications* **2014**, *50* (15), 1845–1847. https://doi.org/10.1039/C3CC48264B.
- (319) Meng, X.; Wu, Q.; Chen, F.; Xiao, F. S. Solvent-Free Synthesis of Zeolite Catalysts. *Science China Chemistry* **2015**, *58* (1), 6–13. https://doi.org/10.1007/S11426-014-5252-2.

- (320) Di, C. Y.; Li, X. F.; Wang, P.; Li, Z. H.; Fan, B. Bin; Dou, T. Green and Efficient Dry Gel Conversion Synthesis of SAPO-34 Catalyst with Plate-like Morphology. *Petroleum Science* **2017**, *14* (1), 203–213. https://doi.org/10.1007/S12182-016-0145-Y.
- (321) Askari, S.; Sedighi, Z.; Halladj, R. Rapid Synthesis of SAPO-34 Nanocatalyst by Dry Gel Conversion Method Templated with Morphline: Investigating the Effects of Experimental Parameters. *Microporous and Mesoporous Materials* **2014**, *197*, 229–236. https://doi.org/10.1016/J.MICROMESO.2014.06.028.
- (322) Li, M.; Wang, Y.; Bai, L.; Chang, N.; Nan, G.; Hu, D.; Zhang, Y.; Wei, W. Solvent-Free Synthesis of SAPO-34 Nanocrystals with Reduced Template Consumption for Methanol-to-Olefins Process. *Applied Catalysis A: General* **2017**, *531*, 203–211. https://doi.org/10.1016/j.apcata.2016.11.005.
- (323) Askari, S.; Halladj, R.; Sohrabi, M. Methanol Conversion to Light Olefins over Sonochemically Prepared SAPO-34 Nanocatalyst. *Microporous and Mesoporous Materials* **2012**, *163*, 334–342. https://doi.org/10.1016/j.micromeso.2012.07.041.
- (324) Askari, S.; Halladj, R. Ultrasonic Pretreatment for Hydrothermal Synthesis of SAPO-34 Nanocrystals. *Ultrasonics Sonochemistry* **2012**, *19* (3), 554–559. https://doi.org/10.1016/J.ULTSONCH.2011.09.006.
- (325) Venna, S. R.; Carreon, M. A. Synthesis of SAPO-34 Crystals in the Presence of Crystal Growth Inhibitors. *Journal of Physical Chemistry B* **2008**, *112* (51), 16261–16265. https://doi.org/10.1021/JP809316S.
- (326) Solvent-Free Synthesis of Silicoaluminophosphate Zeolites Jin 2013 Angewandte Chemie International Edition Wiley Online Library. https://onlinelibrary.wiley.com/doi/10.1002/anie.201302672 (accessed 2024-10-31).
- (327) Zheng, J.; Zhang, W.; Liu, Z.; Huo, Q.; Zhu, K.; Zhou, X.; Yuan, W. Unraveling the Non-Classic Crystallization of SAPO-34 in a Dry Gel System towards Controlling Meso-Structure with the Assistance of Growth Inhibitor: Growth Mechanism, Hierarchical Structure Control and Catalytic Properties. *Microporous and Mesoporous Materials* **2016**, *225*, 74–87. https://doi.org/10.1016/j.micromeso.2015.12.007.
- (328) He, Y. R.; Zhu, Y. L.; Duan, Y.; Zhang, M.; Jiang, J. Green Route to Grow Hierarchical SAPO-34 Crystal with Excellent Catalytic Performance in Methanol to Olefin Reaction. *Crystal Growth and Design* **2020**, 20 (1), 17–23. https://doi.org/10.1021/acs.cgd.9b01257.
- (329) Yang, B.; Zhao, P.; Ma, J.; Li, R. Synthesis of Hierarchical SAPO-34 Nanocrystals with Improved Catalytic Performance for Methanol to Olefins. *Chemical Physics Letters* **2016**, *665*, 59–63. https://doi.org/10.1016/j.cplett.2016.10.052.
- (330) Zhu, Y. L.; Dai, H.; Duan, Y.; Chen, Q.; Zhang, M. Excellent Methanol to Olefin Performance of SAPO-34 Crystal Deriving from the Mixed Micropore, Mesopore, and Macropore Architecture. *Crystal Growth and Design* **2020**, *20* (4), 2623–2631. https://doi.org/10.1021/ACS.CGD.0C00002.
- (331) Zheng, T.; Liu, H.; He, P.; Zhang, R.; Meng, X.; Xu, C.; Liu, H.; Yue, Y.; Liu, Z. Post Synthesis of Hierarchical SAPO-34 via Citric Acid Etching: Mechanism of Selective Desilication. *Microporous and Mesoporous Materials* **2022**, *335*, 111798. https://doi.org/10.1016/J.MICROMESO.2022.111798.
- (332) Chen, X.; Vicente, A.; Qin, Z.; Ruaux, V.; Gilson, J. P.; Valtchev, V. The Preparation of Hierarchical SAPO-34 Crystals via Post-Synthesis Fluoride Etching. *Chemical Communications* **2016**, *52* (17), 3512–3515. https://doi.org/10.1039/C5CC09498D.
- (333) Liu, X.; Ren, S.; Zeng, G.; Liu, G.; Wu, P.; Wang, G.; Chen, X.; Liu, Z.; Sun, Y. Coke Suppression in MTO over Hierarchical SAPO-34 Zeolites. *RSC Advances* **2016**, *6* (34), 28787–28791. https://doi.org/10.1039/c6ra02282k.
- (334) Du, S.; Chen, X.; Sun, Q.; Wang, N.; Jia, M.; Valtchev, V.; Yu, J. A Non-Chemically Selective Top-down Approach towards the Preparation of Hierarchical TS-1 Zeolites with Improved Oxidative Desulfurization Catalytic Performance. *Chemical Communications* **2016**, *52* (17), 3580–3583. https://doi.org/10.1039/C5CC10232D.
- (335) Varzaneh, A. Z.; Towfighi, J.; Sahebdelfar, S.; Bahrami, H. Carbon Nanotube Templated Synthesis of Hierarchical SAPO-34 Catalysts with Different Structure Directing Agents for Catalytic Conversion of Methanol to Light Olefins. *Journal of Analytical and Applied Pyrolysis* **2016**, *121*, 11–23. https://doi.org/10.1016/j.jaap.2016.06.007.

Journal of Materials Chemistry A Accepted Manuscrip

This article is licensed under a Creative Commons Attribution-NonCommercial 3.0 Unported Licence.

- (336) Sun, Q.; Wang, N.; Xi, D.; Yang, M.; Yu, J. Organosilane Surfactant-Directed Synthesis of Hierarchical Porous SAPO-34 Catalysts with Excellent MTO Performance. Chemical Communications 2014, 50 (49), 6502–6505. https://doi.org/10.1039/c4cc02050b.
- (337) Schmidt, F.; Paasch, S.; Brunner, E.; Kaskel, S. Carbon Templated SAPO-34 with Improved Adsorption Kinetics and Catalytic Performance in the MTO-Reaction. Microporous and Mesoporous Materials 2012, 164, 214–221. https://doi.org/10.1016/j.micromeso.2012.04.045.
- (338) Cui, Y.; Zhang, O.; He, J.; Wang, Y.; Wei, F. Pore-Structure-Mediated Hierarchical SAPO-34: Facile Synthesis, Tunable Nanostructure, and Catalysis Applications for the Conversion of Dimethyl Ether into Olefins. Particuology 2013, 11 (4), 468–474. https://doi.org/10.1016/j.partic.2012.12.009.
- (339) Sun, Q.; Wang, N.; Guo, G.; Chen, X.; Yu, J. Synthesis of Tri-Level Hierarchical SAPO-34 Zeolite with Intracrystalline Micro-Meso-Macroporosity Showing Superior MTO Performance. Journal of Materials Chemistry A 2015, 3 (39), 19783–19789. https://doi.org/10.1039/C5TA04642D.
- (340) Karimi, H.; Towfighi, J.; Akhgar, S. Synthesis of Hierarchical SAPO-34 Zeolites with Tuned Mesopore Structure for Methanol to Olefins (MTO) Reaction Using Polyethylene Glycol as a Soft Template. *Journal* of Sol-Gel Science and Technology 2021, 100 (2), 286–298. https://doi.org/10.1007/S10971-021-05585-Z.
- Wang, Y.; Wang, Z.; Sun, C.; Chen, H.; Li, H.; Li, H. Performance of Methanol-to-Olefins Catalytic Reactions by the Addition of PEG in the Synthesis of SAPO-34. Transactions of Tianjin University 2017, 23 (6), 501–510. https://doi.org/10.1007/S12209-017-0065-Y.
- (342) Mousavi, S. H.; Fatemi, S.; Razavian, M. Synthesis and Stability Evaluation of Hierarchical Silicoaluminophosphates with Different Structural Frameworks in the Methanol to Olefins Process. Particuology 2018, 37, 43–53. https://doi.org/10.1016/J.PARTIC.2017.06.004.
- (343) Verboekend, D.; Milina, M.; Pérez-Ramírez, J. Hierarchical Silicoaluminophosphates by Postsynthetic Modification: Influence of Topology, Composition, and Silicon Distribution. Chemistry of Materials 2014, 26 (15), 4552–4562. https://doi.org/10.1021/CM501774S.
- (344) Varzaneh, A. Z.; Towfighi, J.; Sahebdelfar, S. Carbon Nanotube Templated Synthesis of Metal Containing Hierarchical SAPO-34 Catalysts: Impact of the Preparation Method and Metal Avidities in the MTO 1-12.Reaction. Microporous and Mesoporous *Materials* 2016. *236*. https://doi.org/10.1016/j.micromeso.2016.08.027.
- (345) Lu, J.; Wang, X.; Li, H. Catalytic Conversion of Methanol to Olefins over Rare Earth (La, Y) Modified SAPO-34. Reaction Kinetics and Catalysis Letters 2009, 97 (2), 255-261. https://doi.org/10.1007/s11144-009-0046-9.
- (346) Mirza, K.; Ghadiri, M.; Haghighi, M.; Afghan, A. Hydrothermal Synthesize of Modified Fe, Ag and K-SAPO-34 Nanostructured Catalysts Used in Methanol Conversion to Light Olefins. Microporous and Mesoporous Materials 2018, 260, 155–165. https://doi.org/10.1016/J.MICROMESO.2017.10.045.
- Salih, H. A.; Muraza, O.; Abussaud, B.; Al-Shammari, T. K.; Yokoi, T. Catalytic Enhancement of SAPO-34 for Methanol Conversion to Light Olefins Using in Situ Metal Incorporation. 2018. https://doi.org/10.1021/acs.iecr.7b04549.
- (348) Salmasi, M.; Fatemi, S.; Najafabadi, A. T. Improvement of Light Olefins Selectivity and Catalyst Lifetime in MTO Reaction; Using Ni and Mg-Modified SAPO-34 Synthesized by Combination of Two Templates. Journal Industrial and Engineering Chemistry 2011, https://doi.org/10.1016/J.JIEC.2011.05.031.
- (349) Dubois, D. R.; Obrzut, D. L.; Liu, J.; Thundimadathil, J.; Adekkanattu, P. M.; Guin, J. A.; Punnoose, A.; Seehra, M. S. Conversion of Methanol to Olefins over Cobalt-, Manganese- and Nickel-Incorporated SAPO-34 Molecular Sieves. Fuel Processing Technology 2003, 83 (1-3 SPEC.), 203–218. https://doi.org/10.1016/S0378-3820(03)00069-9.
- (350) Aghaei, E.; Haghighi, M. Hydrothermal Synthesis of Nanostructured Ce-SAPO-34: High-Performance and Long-Lifetime Catalyst with Various Ceria Contents for Methanol to Light Olefins Conversion. *Microporous* and Mesoporous Materials 2018, 270, 227–240. https://doi.org/10.1016/J.MICROMESO.2018.05.011.
- (351) Hu, X.; Yuan, L.; Cheng, S.; Luo, J.; Sun, H.; Li, S.; Li, L.; Wang, C. GeAPSO-34 Molecular Sieves: Synthesis, Characterization and Methanol-to-Olefins Performance. Catalysis Communications 2019, 123, 38–43. https://doi.org/10.1016/j.catcom.2019.02.007.

This article is licensed under a Creative Commons Attribution-NonCommercial 3.0 Unported Licence Open Access Article. Published on 22 2025. Downloaded on 30.10.2025 01:47:29.

- (352) Kang, M. Methanol Conversion on Metal-Incorporated SAPO-34s (MeAPSO-34s). *Journal of Molecular* Catalysis A: Chemical 2000, 160 (2), 437–444. https://doi.org/10.1016/S1381-1169(00)00281-8.
- (353) Huang, H.; Yu, M.; Zhang, Q.; Li, C. Mechanistic Study on the Effect of ZnO on Methanol Conversion SAPO-34 Zeolite. Catalysis **Communications** 2020. 137. 105932. https://doi.org/10.1016/J.CATCOM.2020.105932.
- Chae, H. J.; Park, S. S.; Shin, Y. H.; Park, M. B. Synthesis and Characterization of Nanocrystalline TiAPSO-34 Catalysts and Their Performance in the Conversion of Methanol to Light Olefins. *Microporous* and Mesoporous Materials 2018, 259, 60–66. https://doi.org/10.1016/j.micromeso.2017.09.035.
- (355) Sadeghpour, P.; Haghighi, M. Incorporation of Mono and Bimetallic MnNi into SAPO-34 Framework Used in Conversion of Methanol to Ethylene and Propylene: Alteration of Acidic Properties and Catalytic Performance. Asia-Pacific Journal of Chemical Engineering 2018. https://doi.org/10.1002/APJ.2163.
- (356) Huang, F.; Cao, J.; Wang, L.; Wang, X.; Liu, F. Enhanced Catalytic Behavior for Methanol to Lower Olefins over SAPO-34 Composited with ZrO2. Chemical Engineering Journal 2020, 380. https://doi.org/10.1016/J.CEJ.2019.122626.
- Sun, C.; Wang, Y.; Wang, Z.; Chen, H.; Wang, X.; Li, H.; Sun, L.; Fan, C.; Wang, C.; Zhang, X. Fabrication of Hierarchical ZnSAPO-34 by Alkali Treatment with Improved Catalytic Performance in the Methanol-21 to-Olefin Reaction. **Comptes** Rendus Chimie 2018, (1),61-70.https://doi.org/10.1016/j.crci.2017.11.006.
- (358) Inui, T.; Kang, M. Reliable Procedure for the Synthesis of Ni-SAPO-34 as a Highly Selective Catalyst for Methanol to Ethylene Conversion. Applied Catalysis A: General 1997, 164 (1-2), 211-223. https://doi.org/10.1016/S0926-860X(97)00172-5.
- (359) Obrzut, D. L.; Adekkanattu, P. M.; Thundimadathil, J.; Liu, J.; Dubois, D. R.; Guin, J. A. Reducing Methane Formation in Methanol to Olefins Reaction on Metal Impregnated SAPO-34 Molecular Sieve. Reaction Kinetics and Catalysis Letters **2003**, 80 (1), 113–121. https://doi.org/10.1023/A:1026088327000.
- (360) Fujimoto, Y.; Shu, Y.; Miyake, K.; Uchida, Y.; Nishiyama, N. SAPO-34 Zeolite Nanocrystals Coated with ZrO2as Catalysts for Methanol-to-Olefin Conversion. ACS Applied Nano Materials 2021, 4 (8), 8321– 8327. https://doi.org/10.1021/acsanm.1c01511.
- (361) Ghavipour, M.; Hussami, R. A.; Nasser, G.; Kopyscinski, J. Can Metal Promotion of SAPO-34 Genuinely Improve Its Catalytic Performance in Methanol Conversion to Light Olefins Reaction? https://doi.org/10.1002/cphc.202400357.
- (362) Abbasi, A.; Darian, J. T.; Pourmand, M.; Yazd, M. S. Mechanistic Insights into Coke Suppression and Enhanced Olefin Selectivity in Mixed Metal Oxide-Modified SAPO-34 for High-Performance Methanol-Engineering to-Olefins Catalysis. Chemical Journal Advances 2025, 22. https://doi.org/10.1016/j.ceja.2025.100745.
- (363) Sun, G.; Grace, J. R. The Effect of Particle Size Distribution on the Performance of a Catalytic Fluidized Bed Reactor. Chemical Engineering Science 1990, 45 (8), 2187–2194. https://doi.org/10.1016/0009-2509(90)80094-U.
- (364) Wang, P.; Lv, A.; Hu, J.; Xu, J.; Lu, G. In Situ Synthesis of SAPO-34 Grown onto Fully Calcined Kaolin Microspheres and Its Catalytic Properties for the MTO Reaction. *Industrial and Engineering Chemistry* Research 2011, 50 (17), 9989–9997. https://doi.org/10.1021/ie201060u.
- (365) Zhu, J.; Cui, Y.; Nawaz, Z.; Wang, Y.; Wei, F. In Situ Synthesis of SAPO-34 Zeolites in Kaolin Microspheres for a Fluidized Methanol or Dimethyl Ether to Olefins Process. Chinese Journal of Chemical Engineering 2010, 18 (6), 979–987. https://doi.org/10.1016/S1004-9541(09)60156-7.
- (366) Zhou, H.; Wang, Y.; Wei, F.; Wang, D.; Wang, Z. In Situ Synthesis of SAPO-34 Crystals Grown onto α-Al2O3 Sphere Supports as the Catalyst for the Fluidized Bed Conversion of Dimethyl Ether to Olefins. Applied Catalysis A: General 2008, 341 (1-2), 112-118. https://doi.org/10.1016/j.apcata.2008.02.030.
- (367) Zhang, L.; Liu, H.; Yue, Y.; Olsbye, U.; Bao, X. Design and in Situ Synthesis of Hierarchical SAPO-34@kaolin Composites as Catalysts for Methanol to Olefins. Catalysis Science & Technology 2019, 9 (22), 6438–6451. https://doi.org/10.1039/C9CY01663E.

Journal of Materials Chemistry A Accepted Manuscrip

View Article Online DOI: 10.1039/D5TA05195A

Journal of Materials Chemistry A

Review Article

This article is licensed under a Creative Commons Attribution-NonCommercial 3.0 Unported Licence.

- (368) Ghavipour, M.; Kopyscinski, J. Direct Growth of SAPO-34 Crystals on y-Al2O3 Microspheres: A Designated Catalyst for Fluidized-Bed Reactors of Methanol Conversion to Light Olefins. Catalysis Today **2024**, 437, 114784. https://doi.org/10.1016/j.cattod.2024.114784.
- (369) Tian, P.; Wei, Y.; Ye, M.; Liu, Z. Methanol to Olefins (MTO): From Fundamentals to Commercialization. ACS Catal. 2015, 5 (3), 1922–1938. https://doi.org/10.1021/acscatal.5b00007.
- ppPLUS. ppPLUS. https://portfolio-pplus.com (accessed 2025-08-07).
- (371) Doan, T.; Nguyen, K.; Dam, P.; Huyen Vuong, T.; Thang Le, M.; Pham Thanh, H. Synthesis of SAPO-34 Using Different Combinations of Organic Structure-Directing Agents. Journal of Chemistry 2019. https://doi.org/10.1155/2019/6197527.
- (372) Zhang, Y.; Ren, Z.; Wang, Y.; Deng, Y.; Li, J. Synthesis of Small-Sized SAPO-34 Crystals with Varying Template Combinations for the Conversion of Methanol to Olefins. Catalysts 2018, 8 (12), 570. https://doi.org/10.3390/catal8120570.
- (373) Akhgar, S.; Towfighi, J.; Hamidzadeh, M. MTO Performance over Seed-Assisted SAPO-34 Zeolites Synthesized by Reducing Template Consumption. Journal of Materials Research and Technology 2020, 9 (6), 12126–12136. https://doi.org/10.1016/J.JMRT.2020.08.067.
- Akhgar, S.; Towfighi, J.; Hamidzadeh, M. Investigation of Synthesis Time and Type of Seed along with Reduction of Template Consumption in the Preparation of SAPO-34 Catalyst and Its Performance in the MTO Reaction. **2020**. https://doi.org/10.1039/D0RA05673A.
- (375) Zhang, L.; Yao, J.; Zeng, C.; Xu, N. Combinatorial Synthesis of SAPO-34 via Vapor-Phase Transport. **2003**. https://doi.org/10.1039/B305915D.
- (376) Hirota, Y.; Murata, K.; Tanaka, S.; Nishiyama, N.; Egashira, Y.; Ueyama, K. Dry Gel Conversion Synthesis of SAPO-34 Nanocrystals. Materials Chemistry and Physics 2010, 123 (2-3), 507-509. https://doi.org/10.1016/j.matchemphys.2010.05.005.
- (377) Askari, S.; Sedighi, Z.; Halladj, R. Rapid Synthesis of SAPO-34 Nanocatalyst by Dry Gel Conversion Method Templated with Morphline: Investigating the Effects of Experimental Parameters. *Microporous* and Mesoporous Materials 2014, 197, 229–236. https://doi.org/10.1016/J.MICROMESO.2014.06.028.
- (378) Li, Y.; Huang, Y.; Guo, J.; Zhang, M.; Wang, D.; Wei, F.; Wang, Y. Hierarchical SAPO-34/18 Zeolite with Low Acid Site Density for Converting Methanol to Olefins. Catalysis Today 2014, 233, 2-7. https://doi.org/10.1016/J.CATTOD.2014.03.038.
- (379) Parnham, E. R.; Morris, R. E. 1-Alkyl-3-Methyl Imidazolium Bromide Ionic Liquids in the Ionothermal Synthesis of Aluminium Phosphate Molecular Sieves. Chem. Mater. 2006, 18 (20), 4882–4887. https://doi.org/10.1021/cm0615929.
- (380) Sánchez-Sánchez, M.; Romero, Á. A.; Pinilla-Herrero, I.; Sastre, E. Ionothermal Preparation of Triclinic SAPO-34 and Its Catalytic Performance in the MTO Process. Catalysis Today 2017, 296, 239–246. https://doi.org/10.1016/j.cattod.2017.04.065.
- (381) Nasser, G. A.; Sanhoob, M. A.; Bakare, I. A.; Alyassir, N.; Vyas, M.; Malibari, Z.; Yamani, Z. H.; Muraza, O. Green In-Situ Incorporation of Metals in Chabazite (CHA) Zeolite. Microporous and Mesoporous Materials **2021**, 326, 111375. https://doi.org/10.1016/j.micromeso.2021.111375.
- (382) Nasser, G. A.; Al-Qadri, A. A.; Jamil, A. K.; Bakare, I. A.; Sanhoob, M. A.; Muraza, O.; Yamani, Z. H.; Yokoi, T.; Saleem, Q.; Alsewdan, D. Conversion of Methanol to Olefins over Modified OSDA-Free CHA Zeolite Catalyst. Ind. Eng. Chem. Res. 2021, 60 (33),12189–12199. https://doi.org/10.1021/acs.iecr.1c01633.
- (383) MURAZA, O.; NASSER, G. A.; MALAIBARI, Z. O.; SHAMMARI, T. K. A.; MAYANK, V. M.; Yamani, Z. SDA-Free Synthesis of Chabazite (CHA) Zeolite and Uses Thereof, US11247911B2, February 15, 2022. https://patents.google.com/patent/US11247911B2/en (accessed 2024-04-26).
- (384) Nasser, G. A.; Muraza, O.; Nishitoba, T.; Malaibari, Z.; Al-Shammari, T. K.; Yokoi, T. OSDA-Free Chabazite (CHA) Zeolite Synthesized in the Presence of Fluoride for Selective Methanol-to-Olefins. 277-285. *Microporous* and Mesoporous Materials 2019, 274, https://doi.org/10.1016/j.micromeso.2018.07.020.
- (385) Liu, T.; Li, X.; Curnow, O. J.; Choi, J.; Yip, A. C. K. Advancing Zeolite Design via Ionic Liquid Templating Approach. https://doi.org/10.1039/D5CE00253B.

- (386) Lin, S.; Li, J.; Sharma, R. P.; Yu, J.; Xu, R. Fabrication of SAPO-34 Crystals with Different Morphologies by Microwave Heating. *Topics in Catalysis* **2010**, *53* (19–20), 1304–1310. https://doi.org/10.1007/s11244-010-9588-3.
- (387) Yang, G.; Wei, Y.; Xu, S.; Chen, J.; Li, J.; Liu, Z.; Yu, J.; Xu, R. Nanosize-Enhanced Lifetime of SAPO-34 Catalysts in Methanol-to-Olefin Reactions. *Journal of Physical Chemistry C* **2013**, *117* (16), 8214–8222. https://doi.org/10.1021/JP312857P.
- (388) Sedighi, M.; Ghasemi, M.; Sadeqzadeh, M.; Hadi, M. Thorough Study of the Effect of Metal-Incorporated SAPO-34 Molecular Sieves on Catalytic Performances in MTO Process. *Powder Technology* **2016**, *291*, 131–139. https://doi.org/10.1016/J.POWTEC.2015.11.066.
- (389) Tian, S.; Ji, S.; Lü, D.; Bai, B.; Sun, Q. Preparation of Modified Ce-SAPO-34 Catalysts and Their Catalytic Performances of Methanol to Olefins. *Journal of Energy Chemistry* **2013**, *22* (4), 605–609. https://doi.org/10.1016/S2095-4956(13)60079-0.
- (390) Fan, J.; Ning, P.; Wang, Y.; Song, Z.; Liu, X.; Wang, H.; Wang, J.; Wang, L.; Zhang, Q. Significant Promoting Effect of Ce or La on the Hydrothermal Stability of Cu-SAPO-34 Catalyst for NH3-SCR Reaction. *Chemical Engineering Journal* **2019**, *369*, 908–919. https://doi.org/10.1016/j.cej.2019.03.049.
- (391) Ghavipour, M.; Al Hussami, R.; Nasser, G.; Kopyscinski, J. Can Metal Promotion of SAPO-34 Genuinely Improve Its Catalytic Performance in Methanol Conversion to Light Olefins Reaction? *ChemPhysChem n/a* (n/a), e202400357. https://doi.org/10.1002/cphc.202400357.
- (392) Karch, J. A.; Reynolds, T. M. Attrition Resistant MTO Catalyst. US7309679B2, December 18, 2007. https://patents.google.com/patent/US7309679B2/en (accessed 2025-08-07).
- (393) Aghamohammadi, S.; Haghighi, M.; Ebrahimi, A. Fabrication of Attrition-Resistant Nanostructured Catalyst by Spray Dryer for Methanol to Light Olefins Reaction in a Fluid Bed Reactor and Coke Formation. *Microporous and Mesoporous Materials* **2019**, 279, 371–386. https://doi.org/10.1016/j.micromeso.2019.01.017.
- (394) Kim, M.; Chae, H.-J.; Kim, T.-W.; Jeong, K.-E.; Kim, C.-U.; Jeong, S.-Y. Attrition Resistance and Catalytic Performance of Spray-Dried SAPO-34 Catalyst for MTO Process: Effect of Catalyst Phase and Acidic Solution. *Journal of Industrial and Engineering Chemistry* **2011**, *17* (3), 621–627. https://doi.org/10.1016/j.jiec.2011.05.009.
- (395) Akbari, A.; Salehibai, S. Y. Impact of Cs and Ni Promotion on Attrition Resistance and Catalytic Performance of Formulated Spray-Dried SAPO-34 in Fluidized-Bed MTO Conversion. *Powder Technology* **2025**, *465*, 121316. https://doi.org/10.1016/j.powtec.2025.121316.
- (396) Di, C. Y.; Li, X. F.; Wang, P.; Li, Z. H.; Fan, B.; Dou, T. Green and Efficient Dry Gel Conversion Synthesis of SAPO-34 Catalyst with Plate-like Morphology. *Petroleum Science* **2017**, *14* (1), 203–213. https://doi.org/10.1007/S12182-016-0145-Y.
- (397) Malehmirchegini, L.; Chapman, A. J. Strategies for Achieving Carbon Neutrality within the Chemical Industry. *Renewable and Sustainable Energy Reviews* **2025**, *217*, 115762. https://doi.org/10.1016/j.rser.2025.115762.
- (398) Reznichenko, A.; Harlin, A. Next Generation of Polyolefin Plastics: Improving Sustainability with Existing and Novel Feedstock Base. *SN Appl. Sci.* **2022**, *4* (4), 108. https://doi.org/10.1007/s42452-022-04991-4.
- (399) Ren, T.; Patel, M. K.; Blok, K. Steam Cracking and Methane to Olefins: Energy Use, CO2 Emissions and Production Costs. *Energy* **2008**, *33* (5), 817–833. https://doi.org/10.1016/j.energy.2008.01.002.
- (400) Zhao, Z.; Chong, K.; Jiang, J.; Wilson, K.; Zhang, X.; Wang, F. Low-Carbon Roadmap of Chemical Production: A Case Study of Ethylene in China. *Renewable and Sustainable Energy Reviews* **2018**, *97*, 580–591. https://doi.org/10.1016/j.rser.2018.08.008.
- (401) von Rosing, M. CO2 Reduction (Scopes 1-2-3) and How to Go about It. In *The Sustainability Handbook, Volume 1*; von Rosing, M., Ed.; Elsevier, 2025; pp 103–114. https://doi.org/10.1016/B978-0-323-90110-9.00011-8.
- (402) Borthakur, P. P.; Borthakur, B. The Role of Industrial Catalysts in Accelerating the Renewable Energy Transition. *Chemistry Proceedings* **2025**, *17* (1), 6. https://doi.org/10.3390/chemproc2025017006.
- (403) Xiang, D.; Yang, S.; Liu, X.; Mai, Z.; Qian, Y. Techno-Economic Performance of the Coal-to-Olefins Process with CCS. *Chemical Engineering Journal* **2014**, 240, 45–54. https://doi.org/10.1016/j.cej.2013.11.051.

- (404) Wang, Y.; Hao, Y.; Hou, Y.; Quan, Q.; Li, Y. Optimizing Scope 3 Emissions in the Automotive Manufacturing Industry: A Multidisciplinary Approach. Carbon Res. https://doi.org/10.1007/s44246-024-00131-2.
- (405) Miskolczi, N.; Juzsakova, T.; Sója, J. Preparation and Application of Metal Loaded ZSM-5 and y-Zeolite Catalysts for Thermo-Catalytic Pyrolysis of Real End of Life Vehicle Plastics Waste. *Journal of the Energy Institute* **2019**, *92* (1), 118–127. https://doi.org/10.1016/j.joei.2017.10.017.
- (406) Quosay, A.; Reem, A. Exploring the Rainbow of Hydrogen Technology; A Path to Sustainable Energy and Climate Resilience. https://doi.org/10.13140/RG.2.2.31394.34243.
- (407) Keller, F.; Lee, R. P.; Meyer, B. Life Cycle Assessment of Global Warming Potential, Resource Depletion and Acidification Potential of Fossil, Renewable and Secondary Feedstock for Olefin Production in Germany. Journal of Cleaner Production 2020. 250. https://doi.org/10.1016/j.jclepro.2019.119484.
- (408) Flores-Granobles, M.; Saeys, M. Quantitative Analysis of CO2 Emissions Reduction Potential of Alternative Light Olefins Production Processes. Green Chem. 2023, 25 (16), 6459–6471. https://doi.org/10.1039/D3GC01237A.
- Tillman, A.-M.; Ekvall, T.; Baumann, H.; Rydberg, T. Choice of System Boundaries in Life Cycle Assessment. Journal of Cleaner Production 1994, 2 (1), 21–29. https://doi.org/10.1016/0959-6526(94)90021-3.
- (410) Frischknecht, R.; Rebitzer, G. The Ecoinvent Database System: A Comprehensive Web-Based LCA Database. Journal of Cleaner **Production** 2005. 13 (13),https://doi.org/10.1016/j.jclepro.2005.05.002.
- (411) Zhao, Z.; Liu, Y.; Wang, F.; Li, X.; Deng, S.; Xu, J.; Wei, W.; Wang, F. Life Cycle Assessment of Primary Energy Demand and Greenhouse Gas (GHG) Emissions of Four Propylene Production Pathways in China. Journal of Cleaner Production 2017, 163, 285–292. https://doi.org/10.1016/j.jclepro.2015.12.099.
- (412) Lv, L.; Song, G.; Zhao, X.; Chen, J. Environmental Burdens of China's Propylene Manufacturing: Comparative Life-Cycle Assessment and Scenario Analysis. Science of The Total Environment 2021, 799, 149451. https://doi.org/10.1016/j.scitotenv.2021.149451.
- (413) Li, Z.; Ahman, M.; Nilsson, L. J.; Bauer, F. Towards Carbon Neutrality: Transition Pathways for the Chinese Ethylene Industry. Renewable and Sustainable Energy Reviews 2024, 199, 114540. https://doi.org/10.1016/j.rser.2024.114540.
- (414) Zhang, O.; Hu, S.; Chen, D. A Comparison between Coal-to-Olefins and Oil-Based Ethylene in China: An Economic and Environmental Prospective. Journal of Cleaner Production 2017, 165, 1351-1360. https://doi.org/10.1016/j.jclepro.2017.06.229.
- (415) Xiang, D.; Yang, S.; Li, X.; Qian, Y. Life Cycle Assessment of Energy Consumption and GHG Emissions of Olefins Production from Alternative Resources in China. Energy Conversion and Management 2015, 90, 12–20. https://doi.org/10.1016/j.enconman.2014.11.007.
- (416) Chen, Q.; Lv, M.; Wang, D.; Tang, Z.; Wei, W.; Sun, Y. Eco-Efficiency Assessment for Global Warming Potential of Ethylene Production Processes: A Case Study of China. Journal of Cleaner Production 2017, 142, 3109–3116. https://doi.org/10.1016/j.jclepro.2016.10.156.
- (417) Man, Y.; Yang, S.; Qian, Y. An Integrated Process of Coke-Oven Gas Tri-Reforming and Coal to Methanol with High Carbon Utilization and Energy Efficiency. In Computer Aided Chemical Engineering; Kravanja, Z., Bogatai, M., Eds.; 26 European Symposium on Computer Aided Process Engineering; Elsevier, 2016; Vol. 38, pp 775–780. https://doi.org/10.1016/B978-0-444-63428-3.50134-X.
- (418) Man, Y.; Yang, S.; Zhang, J.; Qian, Y. Conceptual Design of Coke-Oven Gas Assisted Coal to Olefins Process for High Energy Efficiency and Low CO2 Emission. Applied Energy 2014, 133, 197–205. https://doi.org/10.1016/j.apenergy.2014.07.105.
- (419) Yang, S.; Yang, Q.; Man, Y.; Xiang, D.; Qian, Y. Conceptual Design and Analysis of a Natural Gas Assisted Coal-to-Olefins Process for CO2 Reuse. Ind. Eng. Chem. Res. 2013, 52 (40), 14406–14414. https://doi.org/10.1021/ie401937k.
- (420) Yu, Y.; Chen, D.; Zhu, B.; Hu, S. Eco-Efficiency Trends in China, 1978–2010: Decoupling Environmental Pressure **Ecological Indicators** 2013. 24, 177–184. from Economic Growth. https://doi.org/10.1016/j.ecolind.2012.06.007.

(421) Zhao, Z.; Liu, Y.; Wang, F.; Li, X.; Deng, S.; Xu, J.; Wei, W.; Wang, F. Life Cycle Assessment of Primary Energy Demand and Greenhouse Gas (GHG) Emissions of Four Propylene Production Pathways in China. *Journal of Cleaner Production* **2017**, *163*, 285–292. https://doi.org/10.1016/j.jclepro.2015.12.099.

- (422) Tsiropoulos, I.; Faaij, A. P. C.; Lundquist, L.; Schenker, U.; Briois, J. F.; Patel, M. K. Life Cycle Impact Assessment of Bio-Based Plastics from Sugarcane Ethanol. *Journal of Cleaner Production* **2015**, *90*, 114–127. https://doi.org/10.1016/j.jclepro.2014.11.071.
- (423) Muñoz, I.; Flury, K.; Jungbluth, N.; Rigarlsford, G.; i Canals, L. M.; King, H. Life Cycle Assessment of Bio-Based Ethanol Produced from Different Agricultural Feedstocks. *Int J Life Cycle Assess* **2014**, *19* (1), 109–119. https://doi.org/10.1007/s11367-013-0613-1.
- (424) Environmental Benefits of Circular Ethylene Production from Polymer Waste | ACS Sustainable Chemistry & Engineering. https://pubs.acs.org/doi/10.1021/acssuschemeng.4c04241 (accessed 2025-09-25).
- (425) Cuevas-Castillo, G. A.; Michailos, S.; Akram, M.; Hughes, K.; Ingham, D.; Pourkashanian, M. Techno Economic and Life Cycle Assessment of Olefin Production through CO2 Hydrogenation within the Powerto-X Concept. *Journal of Cleaner Production* **2024**, *469*, 143143. https://doi.org/10.1016/j.jclepro.2024.143143.
- (426) Salah, C.; Istrate, R.; Bjørn, A.; Tulus, V.; Pérez-Ramírez, J.; Guillén-Gosálbez, G. Environmental Benefits of Circular Ethylene Production from Polymer Waste. *ACS Sustainable Chem. Eng.* **2024**, *12* (37), 13897–13906. https://doi.org/10.1021/acssuschemeng.4c04241.
- (427) Li, Z.; Åhman, M.; Nilsson, L. J.; Bauer, F. Towards Carbon Neutrality: Transition Pathways for the Chinese Ethylene Industry. *Renewable and Sustainable Energy Reviews* **2024**, *199*, 114540. https://doi.org/10.1016/j.rser.2024.114540.
- (428) Quantitative analysis of CO2 emissions reduction potential of alternative light olefins production processes Green Chemistry (RSC Publishing). https://pubs.rsc.org/en/content/articlelanding/2023/gc/d3gc01237a (accessed 2025-09-25).
- (429) Jones, M. P.; Krexner, T.; Bismarck, A. Repurposing Fischer-Tropsch and Natural Gas as Bridging Technologies for the Energy Revolution. *Energy Conversion and Management* **2022**, *267*, 115882. https://doi.org/10.1016/j.enconman.2022.115882.
- (430) Malehmirchegini, L.; Chapman, A. J. Strategies for Achieving Carbon Neutrality within the Chemical Industry. *Renewable and Sustainable Energy Reviews* **2025**, *217*, 115762. https://doi.org/10.1016/j.rser.2025.115762.
- (431) Ren, T.; Patel, M. K.; Blok, K. Steam Cracking and Methane to Olefins: Energy Use, CO2 Emissions and Production Costs. *Energy* **2008**, *33* (5), 817–833. https://doi.org/10.1016/j.energy.2008.01.002.
- (432) Ren, T.; Patel, M.; Blok, K. Olefins from Conventional and Heavy Feedstocks: Energy Use in Steam Cracking and Alternative Processes. *Energy* **2006**, *31* (4), 425–451. https://doi.org/10.1016/j.energy.2005.04.001.
- (433) Lv, L.; Song, G.; Zhao, X.; Chen, J. Environmental Burdens of China's Propylene Manufacturing: Comparative Life-Cycle Assessment and Scenario Analysis. *Science of The Total Environment* **2021**, 799, 149451. https://doi.org/10.1016/j.scitotenv.2021.149451.
- (434) Gorman, W.; Kemp, J. M.; Rand, J.; Seel, J.; Wiser, R.; Manderlink, N.; Kahrl, F.; Porter, K.; Cotton, W. Grid Connection Barriers to Renewable Energy Deployment in the United States. *Joule* **2025**, *9* (2), 101791. https://doi.org/10.1016/j.joule.2024.11.008.
- (435) Hauschild, M. Z.; Huijbregts, M. A. J. Introducing Life Cycle Impact Assessment. In *Life Cycle Impact Assessment*; Hauschild, M. Z., Huijbregts, M. A. J., Eds.; Springer Netherlands: Dordrecht, 2015; pp 1–16. https://doi.org/10.1007/978-94-017-9744-3_1.
- (436) Zhang, Q.; Hu, S.; Chen, D. A Comparison between Coal-to-Olefins and Oil-Based Ethylene in China: An Economic and Environmental Prospective. *Journal of Cleaner Production* **2017**, *165*, 1351–1360. https://doi.org/10.1016/j.jclepro.2017.06.229.
- (437) Chen, Q.; Lv, M.; Wang, D.; Tang, Z.; Wei, W.; Sun, Y. Eco-Efficiency Assessment for Global Warming Potential of Ethylene Production Processes: A Case Study of China. *Journal of Cleaner Production* **2017**, *142*, 3109–3116. https://doi.org/10.1016/j.jclepro.2016.10.156.

Journal of Materials Chemistry A Accepted Manuscrip

View Article Online

Journal of Materials Chemistry A

Review Article

This article is licensed under a Creative Commons Attribution-NonCommercial 3.0 Unported Licence.

- (438) Xiang, D.; Qian, Y.; Man, Y.; Yang, S. Techno-Economic Analysis of the Coal-to-Olefins Process in Oil-to-Olefins Comparison with the Process. Applied Energy 2014, https://doi.org/10.1016/j.apenergy.2013.08.013.
- (439) Xiang, D.; Gao, L.; Liu, X.; Guo, C.; Yang, S.; Qian, Y. Water Consumption Analysis of Olefins Production from Alternative Resources in China. Journal of Cleaner Production 2016, 139, 146-156. https://doi.org/10.1016/j.jclepro.2016.08.031.
- (440) Jiang, S.; Zhou, H.; Zhang, X.; Zhou, X.; Chowdhury, A. D. Assessing the Effects of Dealumination and Bifunctionalization on 8-Membered Ring Zeolite/Zeo-Type Materials in the Methanol-to-Olefin Catalytic Process. Catal. Sci. Technol. 2024, 14 (12), 3346–3363. https://doi.org/10.1039/D4CY00110A.
- (441) Yao, J.; Tian, H.; Zha, F.; Ma, S.; Tang, X.; Chang, Y.; Guo, X. Regulating the Size and Acidity of SAPO-34 Zeolites Using Dual Templates to Enhance the Selectivity of Light Olefins in MTO. New Journal of Chemistry 2021, 45 (26), 11812–11822. https://doi.org/10.1039/D1NJ01845K.
- (442) Yang, L.; Wang, C.; Zhang, L.; Dai, W.; Chu, Y.; Xu, J.; Wu, G.; Gao, M.; Liu, W.; Xu, Z.; Wang, P.; Guan, N.; Dyballa, M.; Ye, M.; Deng, F.; Fan, W.; Li, L. Stabilizing the Framework of SAPO-34 Zeolite toward Long-Term Methanol-to-Olefins Conversion. Nat Commun 2021, 12 https://doi.org/10.1038/s41467-021-24403-2.
- (443) Abbasi, A.; Darian, J. T.; Emami, M. J.; Yazd, M. S. Mechanistic Insights into Coke Suppression in the Methanol-to-Olefins Process via CeO2 Doping to SAPO-34. RSC Adv. 2025, 15 (37), 30312–30325. https://doi.org/10.1039/D5RA04614A.
- (444) Guo, L.; Xing, A.; Zhu, W.; Li, F.; Guo, Z. Enhanced Methanol-to-Olefins (MTO) Performance over SAPO-34 Molecular Sieves Synthesized Using Novel Sources of Silicon and Aluminium. Clean En 2022, 6 (3), 528–533. https://doi.org/10.1093/ce/zkac031.
- (445) Liang, J.; Liu, D.; Xu, S.; Ye, M. Modeling and Analysis of Air Combustion and Steam Regeneration in Methanol to Olefins Processes. Chinese Journal of Chemical Engineering 2024, 66, 94-103. https://doi.org/10.1016/j.cjche.2023.09.007.
- (446) Zhou, J.; Gao, M.; Zhang, J.; Liu, W.; Zhang, T.; Li, H.; Xu, Z.; Ye, M.; Liu, Z. Directed Transforming of Coke to Active Intermediates in Methanol-to-Olefins Catalyst to Boost Light Olefins Selectivity. Nature Communications 2021 12:1 2021, 12 (1), 1–11. https://doi.org/10.1038/s41467-020-20193-1.
- (447) Zhou, J.; Zhang, J.; Zhi, Y.; Zhao, J.; Zhang, T.; Ye, M.; Liu, Z. Partial Regeneration of the Spent SAPO-34 Catalyst in the Methanol-to-Olefins Process via Steam Gasification. *Ind. Eng. Chem. Res.* **2018**, *57* (51), 17338–17347. https://doi.org/10.1021/acs.iecr.8b04181.
- (448) Akbari, A.; Salehibai, S. Y. Impact of Cs and Ni Promotion on Attrition Resistance and Catalytic Performance of Formulated Spray-Dried SAPO-34 in Fluidized-Bed MTO Conversion. Powder Technology 2025, 465, 121316. https://doi.org/10.1016/j.powtec.2025.121316.
- (449) Jiang, H.; Yuan, L.; Li, D.; Chen, Y. Mathematical Model for the Industrial SMTO Reactor with a SAPO-34 Catalyst. ACS Omega 2023, 8 (10), 9630–9643. https://doi.org/10.1021/acsomega.3c00304.
- (450) Ghavipour, M.; Al Hussami, R.; Nasser, G.; Kopyscinski, J. Can Metal Promotion of SAPO-34 Genuinely Improve Its Catalytic Performance in Methanol Conversion to Light Olefins Reaction? ChemPhysChem **2024**, 25 (24), e202400357. https://doi.org/10.1002/cphc.202400357.
- (451) Zhao, Z.; Chong, K.; Jiang, J.; Wilson, K.; Zhang, X.; Wang, F. Low-Carbon Roadmap of Chemical Production: A Case Study of Ethylene in China. Renewable and Sustainable Energy Reviews 2018, 97, 580–591. https://doi.org/10.1016/j.rser.2018.08.008.
- (452) Xu, Z.; Fang, C.; Ma, T. Analysis of China's Olefin Industry Using a System Optimization Model Considering Technological Learning and Energy Consumption Reduction. *Energy* **2020**, *191*, 116462. https://doi.org/10.1016/j.energy.2019.116462.
- (453) Hannula, I. Co-Production of Synthetic Fuels and District Heat from Biomass Residues, Carbon Dioxide and Electricity: Performance and Cost Analysis. Biomass and Bioenergy 2015, 74, 26-46. https://doi.org/10.1016/j.biombioe.2015.01.006.
- (454) Mahmoudi, E.; Sayyah, A.; Farhoudi, S.; Bahranifard, Z.; Behmenyar, G.; Turan, A. Z.; Delibas, N.; Niaei, A. Advances in Catalysts for Direct Syngas Conversion to Light Olefins: A Review of Mechanistic and Performance Insights. Utilization 102893. Journal of CO22024, 86, https://doi.org/10.1016/j.jcou.2024.102893.

This article is licensed under a Creative Commons Attribution-NonCommercial 3.0 Unported Licence. Open Access Article. Published on 22 2025. Downloaded on 30.10.2025 01:47:29.

- (455) Huang, Y.; Ma, H.; Xu, Z.; Qian, W.; Zhang, H.; Ying, W. Direct Conversion of Syngas to Light Olefins over a ZnCrOx + H-SSZ-13 Bifunctional Catalyst. ACS Omega 2021, 6 (16), 10953-10962. https://doi.org/10.1021/acsomega.1c00751.
- (456) Zhang, P.; Meng, F.; Li, X.; Yang, L.; Ma, P.; Li, Z. Excellent Selectivity for Direct Conversion of Syngas to Light Olefins over a Mn-Ga Oxide and SAPO-34 Bifunctional Catalyst. Catal. Sci. Technol. 2019, 9 (20), 5577–5581. https://doi.org/10.1039/C9CY01348B.
- (457) Wang, Y.; Liu, S.; Wang, J.; Liu, F.; Ma, J.; Yao, M.; Geng, S.; Cao, J.; Li, Z. Direct Conversion of Carbon Dioxide into Light Olefins over ZnZrOx/ZSM-5@n-ZrO2 Tandem Catalyst. Fuel 2024, 357, 129727. https://doi.org/10.1016/j.fuel.2023.129727.
- (458) Su, J.; Zhou, H.; Liu, S.; Wang, C.; Jiao, W.; Wang, Y.; Liu, C.; Ye, Y.; Zhang, L.; Zhao, Y.; Liu, H.; Wang, D.; Yang, W.; Xie, Z.; He, M. Syngas to Light Olefins Conversion with High Olefin/Paraffin Ratio ZnCrOx/AlPO-18 Bifunctional Catalysts. Nat Commun 2019, https://doi.org/10.1038/s41467-019-09336-1.
- (459) Yang, J.; Pan, X.; Jiao, F.; Li, J.; Bao, X. Direct Conversion of Syngas to Aromatics. Chem. Commun. **2017**, *53* (81), 11146–11149. https://doi.org/10.1039/C7CC04768A.
- Cheng, K.; Gu, B.; Liu, X.; Kang, J.; Zhang, Q.; Wang, Y. Direct and Highly Selective Conversion of Synthesis Gas into Lower Olefins: Design of a Bifunctional Catalyst Combining Methanol Synthesis and Carbon-Carbon Coupling. Angewandte Chemie International Edition 2016, 55 (15), 4725-4728. https://doi.org/10.1002/anie.201601208.
- (461) Direct transformation of syngas to lower olefins synthesis over hybrid Zn–Al2O3/SAPO-34 catalysts New Journal of Chemistry (RSC Publishing). https://pubs.rsc.org/en/content/articlelanding/2018/nj/c7nj04734g (accessed 2025-09-25).
- (462) Role of Manganese Oxide in Syngas Conversion to Light Olefins | ACS Catalysis. https://pubs.acs.org/doi/10.1021/acscatal.7b00221 (accessed 2025-09-25).
- (463) Su, J.; Wang, D.; Wang, Y.; Zhou, H.; Liu, C.; Liu, S.; Wang, C.; Yang, W.; Xie, Z.; He, M. Direct Conversion of Syngas into Light Olefins over Zirconium-Doped Indium(III) Oxide and SAPO-34 Bifunctional Catalysts: Design of Oxide Component and Construction of Reaction Network. ChemCatChem 2018, 10 (7), 1536–1541. https://doi.org/10.1002/cctc.201702054.
- (464) Pawelec, B.; Guil-López, R.; Mota, N.; Fierro, J. L. G.; Navarro Yerga, R. M. Catalysts for the Conversion of CO2 to Low Molecular Weight Olefins—A Review. *Materials* **2021**, 14 (22), 6952. https://doi.org/10.3390/ma14226952.
- (465) Ye, M.; Tian, P.; Liu, Z. DMTO: A Sustainable Methanol-to-Olefins Technology. *Engineering* **2021**, 7(1), 17–21. https://doi.org/10.1016/j.eng.2020.12.001.
- (466) Sun, Q.; Xie, Z.; Yu, J. The State-of-the-Art Synthetic Strategies for SAPO-34 Zeolite Catalysts in Methanol-to-Olefin Conversion. National Science Review 2018. https://doi.org/10.1093/NSR/NWX103.
- (467) Xiang, D.; Gao, L.; Liu, X.; Guo, C.; Yang, S.; Qian, Y. Water Consumption Analysis of Olefins Production from Alternative Resources in China. Journal of Cleaner Production 2016, 139, 146-156. https://doi.org/10.1016/j.jclepro.2016.08.031.
- (468) Han, X.; Li, N.; She, Y.; Feng, J.; Liu, H.; Liu, G.; Zhang, Z. Simultaneous Integration of the Methanol-to-Olefin Separation Process and Heat Exchanger Network Based on Bi-Level Optimization. *Processes* 2024, 12 (5), 897. https://doi.org/10.3390/pr12050897.
- (469) Reyniers, P. A.; Vandewalle, L. A.; Saerens, S.; de Smedt, P.; Marin, G. B.; Van Geem, K. M. Techno-Economic Analysis of an Absorption Based Methanol to Olefins Recovery Section. Applied Thermal Engineering 2017, 115, 477–490. https://doi.org/10.1016/j.applthermaleng.2016.12.124.
- (470) Tang, B.; Yu, X.; Liu, Y. Metal-Organic Frameworks for Purification of Methanol-to-Olefin (MTO) Products. Dalton Trans. 2025, 54 (29), 11141–11149. https://doi.org/10.1039/D5DT01117E.
- (471) Liu, B.; Ma, H.; Huang, Q.; Chen, J.; Huang, Y.; Huang, H.; Wei, Q.; Wang, H.; Lv, W. Internal Reuse of Methanol-to-Olefin Wastewater Based on Micro-Channel Separation Coupling Hydrocyclone Environmental 118791. Regeneration. Journal of Management 2023. *345*. https://doi.org/10.1016/j.jenvman.2023.118791.

Journal of Materials Chemistry A Accepted Manuscrip